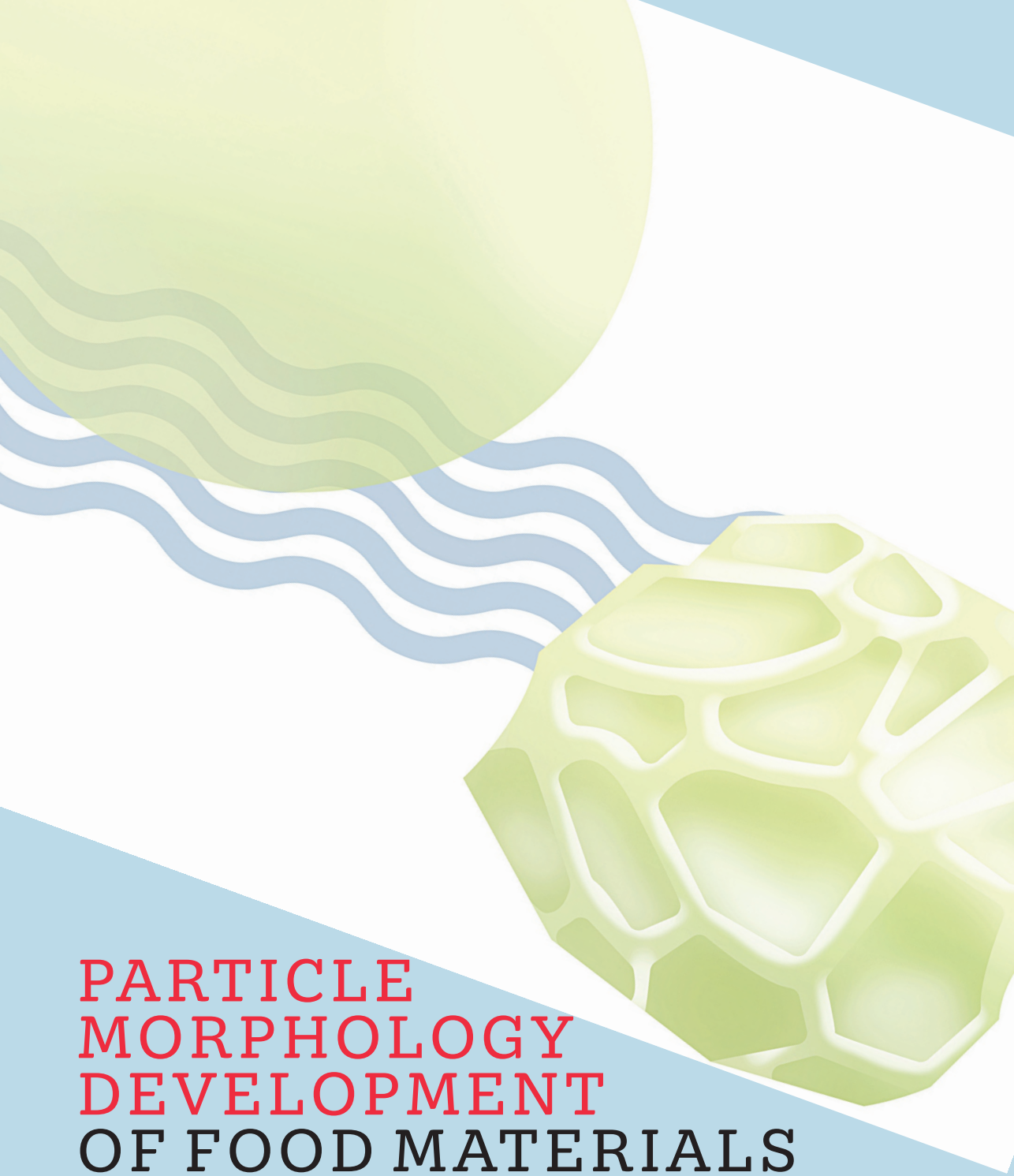

PARTICLE MORPHOLOGY DEVELOPMENT OF FOOD MATERIALS DURING DRYING

ISABEL SIEMONS

Propositions

1. Knowledge of a material's rheological behaviour is essential for predicting its morphology development during droplet drying.

   (this thesis)

2. Moisture diffusivity in glassy foods is still an enigma.

   (this thesis)

3. Construction of master curves gives understanding of rheological data even if it fails to describe the data.

4. Confronting students early during their education with failure of experiments and rejection of hypotheses will help them to become better scientists.

5. The term "identical twins" is misleading.

6. The Japanese "Wabi-Sabi" philosophy for finding beauty in imperfection should be taught in school to promote mental health and environmental sustainability.

Propositions belonging to the thesis entitled

Particle morphology development of food materials during drying

Isabel Siemons

Wageningen, 16 December 2021

Particle morphology development of food materials during drying

Isabel Siemons

Thesis committee

Promotors

Dr Maarten A.I. Schutyser

Associate professor, Laboratory of Food Process Engineering

Wageningen University & Research

Prof. Dr Ruud G.M. van der Sman

Special professor, Modelling in Food Materials Engineering

Wageningen University & Research

Co-promotor

Prof. Dr Remko M. Boom

Professor of Food Process Engineering

Wageningen University & Research

Other members

Prof. Dr Jasper van der Gucht, Wageningen University & Research

Dr Albert T. Poortinga, Eindhoven University of Technology

Dr Nan Fu, Suzhou University, China

Dr Kevin N. van Koerten, Nizo Food Research, Ede

This research was conducted under the auspices of the Graduate School VLAG (Advanced studies in Food Technology, Agrobiotechnology, Nutrition and Health Sciences)

Particle morphology development of food materials during drying

Isabel Siemons

Thesis

submitted in fulfilment of the requirements for the degree of doctor

at Wageningen University

by the authority of the Rector Magnificus,

Prof. Dr A.P.J. Mol,

in the presence of the

Thesis Committee appointed by the Academic Board

to be defended in public

on Thursday 16 December 2021

at 11 a.m. in the Aula.

Isabel Siemons

Particle morphology development of food materials during drying

196 pages

PhD thesis, Wageningen University, Wageningen, the Netherlands (2021)

With references, with summary in English

ISBN: 978-94-6395-997-1

DOI: 10.18174/554101

Contents

Chapter 1

Introduction and thesis outline

1.1. General introduction

Drying refers to the process of removing water or another solvent from a material by evaporation. The process is not only applied to achieve the desired end-product but also enables preservation, efficient handling and transportation. Many dryer types have been reported in literature and are used in the drying of solutions, slurries, pastes, particulate solids or sheets (Mujumdar, 2015; Ratti, 2001). The most prominent dryers, covering over 85% of all industrial dryers, are convective with either hot air or combustion gases as heat transfer medium (Mujumdar, 2015). Among the convection drying technologies, spray drying is a widespread technique used to transform a liquid feed into powder particles by contacting an atomized feed with a hot drying gas (Masters, 1985). Spray drying results in powders with long shelf lives, which can easily be transported and readily reconstituted. The industrial application of spray drying began already in the 1920s with milk and detergents (Keshani et al., 2015). Over the years, spray drying evolved as an industrial drying technology with a wide range of applications in the food, pharmaceutical and chemical industries (Fu et al., 2020; Fu, Woo, Chen, et al., 2012; Vehring, 2008). The array of spray-dried products has extended in recent years owing to the many advantages of the technique, including its high production capacity and fast drying rate, controllable continuous mode of operation, applicability to heat-sensitive materials and its suitability for drying various types of feedstocks (Filková & Mujumdar, 1995). Despite the advantages and widespread use of spray dryers, it is still difficult to predict and thus control the quality of the powder that is produced. This is caused for a substantial part by the limited understanding of the particle formation process (Vicente et al., 2013). The desired product quality is usually attained by inefficient trial-and-error approaches that need to be repeated for different products and spray drying systems. The lack of understanding and limited scope for control of the particle formation process negatively affects the operational efficiency of spray dryers, for instance due to fouling and suboptimal production capacity. This may lead to higher energy costs than necessary and may result in significant material losses when the final powder fails to meet the desired quality specifications. Hence, understanding the particle formation process is considered key for improving the operation efficiency, with possible energy and material savings, while achieving the desired powder quality.

During spray drying, droplets generated by atomization of the liquid feed are converted into powder particles with a particular size, surface composition and morphology depending on

both the feed properties and the process parameters. The properties of the primary particles are also the basis for the properties of agglomerates, which are porous secondary particles often generated by joining primary particles via collisions during spray drying (Palzer, 2005). The properties of the agglomerated powder largely define the powder performance, including the bulk density, flowability, stability, dispersion and dissolution behaviour (Dhanalakshmi et al., 2011; Fu et al., 2020). Considering that the primary particles constitute the agglomerated particles and accordingly determine the bulk properties of the final powder, it would be desired to predict and control the properties of the primary particles, such as the morphology (Bumiller et al., 2002; Fu, Woo, Chen, et al., 2012; Sadek, Schuck, et al., 2015; Takeiti et al., 2008; Walton, 2000). To create a free-flowing powder, for example, particles should ideally be smooth and spherical with little or no surface distortions, while irregular particles will not be free-flowing and have a higher bulk density (Both et al., 2020; Walton, 2000). Spherically shaped and porous powder particles may have superior wetting, dispersibility and solubility properties (Sadek et al., 2014; Selvamuthukumaran, 2019). Morphological control of primary particles from spray drying is also essential for peroral, pulmonary or nasal delivery of pharmaceuticals. For example, low density or hollow particles can be advantageous for pulmonary drug delivery as they improve the dispersibility and the delivery efficiency by lowering the aerodynamic diameter of particles (Vehring, 2008). The control of the morphology development during drying is also believed to be critical for the controlled release and protection of active ingredients or retention of volatile substances, like flavours (Hecht & King, 2000; Nandiyanto & Okuyama, 2011; Vehring, 2008).

For successfully adapting the primary particle morphology during spray drying towards desired applications, a sound understanding of key factors governing the morphology development during drying is required. In practice, many system parameters have been found to influence particle morphology. These include the gas temperature, gas and feed injection rates, the shape of the nozzle and the physicochemical properties of the material (Boel et al., 2020; Both et al., 2020; Sadek, Pauchard, et al., 2015; Vehring et al., 2007). Despite the obtained insights in parameters affecting the morphology, there is still a lack of coherent understanding of the physical effects responsible for the morphology evolution. A thorough understanding of these effects and subsequent predictive modelling are crucial next steps to advance particle morphology engineering during drying.

Given that the morphology of the primary particles is at the basis of the properties of a powder formed from these particles or from aggregates that may be formed from these primary particles, we will focus on the development of the morphology of the primary particles during spray drying. The following sections of this chapter provide background information on the morphology development of these primary droplets during drying. In section 1.2 the principles of morphology development will be discussed with a focus on skin formation. Approaches to studying the morphology development during drying are discussed in section 1.3. Here, single droplet drying is highlighted as an important research technique for obtaining real-time information on morphology development during drying. Finally, in section 1.4 the research objective and an outline of the thesis are provided.

1.2. Morphology development

During spray drying, water or another solvent is evaporated from the droplets. The result is that dry particles are generated with different shapes and internal structures, i.e. different morphologies. In the past decade, interest has increased in finding effective strategies to tailor the morphology of particles during spray drying, especially when there is a need to control for easy powder handling and desired powder bulk properties (Giorgiutti-Dauphiné & Pauchard, 2018). Therefore, efforts to understand and accordingly steer the morphology development during spray drying have been made in various fields; including food (Both, Nuzzo, et al., 2018; Bouman et al., 2016; Griesing et al., 2016; Rogers et al., 2012; Sadek, Pauchard, et al., 2015; Wu et al., 2014), pharmaceutical (Boel et al., 2020; Vehring, 2008; Vicente et al., 2013) and chemical/nano-industry (Iskandar et al., 2003; Nandiyanto & Okuyama, 2011).

The morphology development of a droplet depends on the solidification mechanism during drying, which is directly influenced by both the composition and the process parameters. In literature, one often discriminates the type of solidification mechanism initiated based on comparing the diffusion rate of the solutes with the radial velocity of the receding droplet surface, which is often described with the non-dimensional Péclet number (Archer et al., 2020; Boel et al., 2020; Both, 2019; Bouman et al., 2016; Sadek, Schuck, et al., 2015; Vehring et al., 2007; Vicente et al., 2013). The Péclet number is defined as the ratio of the evaporation rate and the solute diffusion coefficient. As long as the diffusive transport of the solute away from the droplet surface to the droplet centre is fast relative to the rate of evaporation (Pe « 1), the droplet shrinks isotropically and solutes diffuse inward, yielding a

solid and dense particle (Fig. 1.1). During most droplet drying processes, however, the evaporation rate remains large while diffusion rates go down at some point (Pe » 1). In this case, there is insufficient time for redistribution of the solutes by diffusion within the droplet, resulting in large concentration gradients between the droplet's surface and centre. The surface becomes enriched in solutes leading eventually to a semi-solid layer referred to as "skin" (Fig. 1.1). Most organic materials, including many food formulations, are skin forming materials (Walton, 2000). Besides skin forming materials, crystalline and agglomerate materials also exist, but these are usually produced from inorganic compounds. The vast majority of morphology research has been concerned with the study of skin forming materials, as is the case in this thesis.

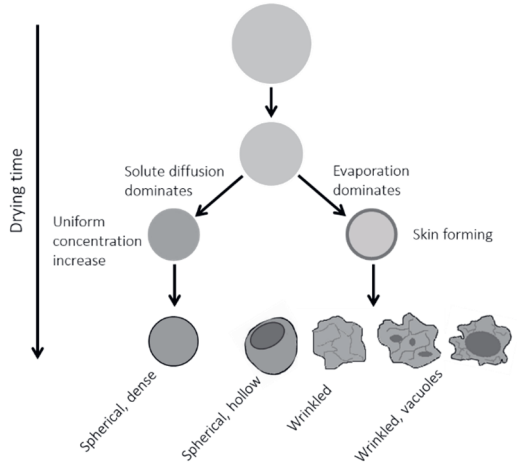

Figure 1.1. Schematic illustration of the common types of morphologies developed based on the solidification mechanism. When the diffusive transport is dominating during drying (i.e. Pe « 1) it likely results in a dense and solid particle (left path). If, however, evaporation predominates (i.e. Pe » 1), a skin is formed and different morphologies may arise (right path).

From the onset of skin formation, the morphology of the droplet can change considerably depending on the process conditions and material properties. The spherical droplet may for instance develop into a smooth and hollow particle or a more irregular particle with dents and possibly a vacuole or multiple vacuoles (Fig. 1.1). As soon as the skin develops some degree of solidity, or sometimes one refers to elasticity, further evaporation will result in the accumulation of internal stresses. This elasticity may arise when a gel or glass is formed due to for example entanglements or jamming of molecules (van der Sman, 2012b). The stresses emerge from pressure differences generated during drying and changes in the material

properties due to drying or phase transformations (Vehring, 2008). To illustrate, during drying of colloidal dispersions, capillary stresses develop as menisci form between the colloidal particles during solvent evaporation (Lintingre et al., 2016). Besides, compressive/shrinkage stresses develop during continuing evaporation of solvent from the core of the drop through the skin. The final particle morphology developed is said to be governed by the skin's reaction to these stresses (Giorgiutti-Dauphiné & Pauchard, 2018; Sadek, Pauchard, et al., 2015). Depending on how the skin properties, including rheological properties and shell thickness, evolve with the drying time, different mechanical instabilities occur to relieve the stresses acting on the skin, including cavitation, buckling, cracking, or wrinkling (Both, 2019; Bouman et al., 2016; Du et al., 2020; Giorgiutti-Dauphiné & Pauchard, 2018; Lintingre et al., 2016; Sadek et al., 2013; Tsapis et al., 2005; Zhang et al., 2014). If, for instance, a skin has enough structural strength early during drying, it will not deform considerably during the time scale of drying, hence resisting most surface distortions and retaining its spherical shape. Softer skins will gradually deform over time to relieve the drying stresses, which may result in for example wrinkling, folding or creasing (Du et al., 2020; Li et al., 2011).

The development of the rheological properties and the thickness of the skin during the drying process depends on the material properties and the drying conditions (Boel et al., 2020; Giorgiutti-Dauphiné & Pauchard, 2018). Sadek et al. (2015a) studied the mechanical properties of milk protein skins after drying. They demonstrated with whey proteins, which are sometimes compared with rigid colloids, a brittle plastic skin layer was formed yielding smooth, spherical, hollow and fractured particles. The hollow structure is the consequence of an under-pressure which is developed in the droplet during drying and causes cavitation or sometimes named vacuole formation (Bouman et al., 2016). For casein micelles on the other hand, which may be viewed as soft, deformable colloids, a ductile elastic skin was formed resulting in twisted and wrinkled particles. The effect of changing the composition of mixtures of protein and carbohydrate was studied by Both et al. (2018a), who found that a high concentration of proteins yielded smooth and hollow particles, whereas particles with more carbohydrate (maltodextrin) were wrinkled and contained small vacuoles. They concluded in a later report that in the case of high ratios of whey proteins, jamming of whey proteins in the skin occurs during drying, resulting in an elastic skin yielding a smooth and spherical particle (Both, Tersteeg, Boom, et al., 2019). Besides the solute composition, the

solute concentration is also important for the skin properties developed. Bouman et al. (2016) showed for whey proteins that lower initial concentrations resulted in more wrinkled particles, while higher concentrations yielded smooth and hollow particles. Similarly, Rogers et al. (2012) found more extensive buckling at low initial concentrations. This is probably related to the thickness of the skin at the moment that it develops structural rigidity.

Since the formation of a skin results from the balance between diffusion and evaporation rate (i.e. Péclet number), the drying conditions, like the temperature, relative humidity and droplet size also affect the skin properties and the resulting particle morphology. Generally, higher temperatures lead to rapid evaporation and rapid skin formation, whereas lower temperatures give slower evaporation and allow the diffusional redistribution of the components depending on their characteristics (e.g. molecular weight and surface activity) (Sadek, Schuck, et al., 2015). The eventual skin properties may differ depending on this redistribution, affecting the final morphology of the particle. Both et al. (2018a) for instance obtained more hollow particles after single droplet drying at low temperatures, whereas particles dried at higher temperatures tended to become wrinkled with a fixed ratio of maltodextrins and whey proteins. With confocal Raman microscopy, they showed that different drying temperatures result in different distributions of the components in the skin, where low temperatures promote phase separation causing whey proteins to dominate the skin properties and hence the morphology development.

The initial droplet size has similar effects on the eventual distribution and morphology development during single droplet drying. Droplets with larger initial diameter have a smaller surface-area-to-volume ratio and dry at a lower relative rate. Since they take longer to dry at similar process conditions than smaller droplets, there is more time for redistribution of the components and skin formation occurs later in the drying process (Both, 2019). Therefore, the larger droplets will develop a thicker skin (Gouaou et al., 2019). This effect of the droplet size on the eventual skin properties should especially be considered when comparing single droplet drying and spray drying as the droplet sizes are typically much larger for single droplet drying techniques. For this reason, it is important that the droplets studied in isolation should be as small as possible, and ideally similar to those generated in a spray dryer, resulting in more comparable drying rates and Péclet numbers (section 1.3).

Next to the drying temperature and the droplet sizes, the relative humidity of the vapour phase affects the properties of the skin formed and the deformations occurring (Pauchard & Allain,

2003). All the aforementioned studies indicate that we should understand skin formation and the developed skin properties as a combined function of the material properties and the process conditions. This will involve measuring, predicting and mechanistically understanding the skin formation dynamics not after, but during drying.

1.3. Studying particle morphology

In industrial practice, spray drying processes are often optimised via experiments and subsequent statistical analysis of process and formulation parameters with the produced powder characteristics, including the morphology (Dobry et al., 2009). Spray drying processing parameters and/or feed properties may be systematically changed and produced morphologies are subsequently studied after spray drying, employing microscopy (Alamilla-Beltrán et al., 2005; Both et al., 2020; Littringer et al., 2013; Paramita et al., 2010; Walton & Mumford, 1999). Although this empirical approach is useful for deducing relevant parameters for the final morphology, it does not allow for conclusions about conditions outside the range of those used during the experiments, and may therefore lead to suboptimal operation. Mechanistic understanding will however enable us to draw general conclusions, even if they are outside the direct range of experimental study. For this, we however need direct observation of the particle morphology evolution during the drying process itself.

Studying the morphology development in a spray dryer is virtually impossible as droplets show a wide size distribution and trajectories upon atomization, while the fast-drying kinetics (~ seconds) complicates recording the dynamics (Adhikari et al., 2000; Sadek, Schuck, et al., 2015). Additionally, probing the relevant processing parameters for morphology development *in situ* may be cumbersome at a large scale, and performing experiments at larger scales may become costly and may generate significant waste. These issues have resulted in the development of single droplet drying techniques as a better-controlled version of the spray drying process itself, allowing for continuous tracking of a single droplet during drying under controlled conditions that resemble to any extent possible those found in spray dryers (Fu, Woo, Chen, et al., 2012).

Single droplet drying was originally developed to study the evaporation of pure liquid droplets by Fuchs (1934), Frossling (1938) and Langstroth et al. (1950). These studies were later extended by Ranz and Marshall (1952) to solutions, suspensions and pastes. In recent years, single droplet drying has been used to establish insight on the effect of multiple

parameters during droplet drying on morphology development, including formulation, droplet size, initial solids concentration, drying air temperature and speed and air humidity (Both, 2019; Fu, Woo, Chen, et al., 2012; Schutyser et al., 2018). Several experimental techniques for studying single droplet drying have been developed for this purpose, including free-flying, pendant, sessile and acoustic/aerodynamic levitation. The morphology development during drying is typically tracked by cameras or microscopic techniques and dried particles can be further characterized for their morphology with for example scanning electron microscopy, (cryo-) transmission electron microscopy, X-ray diffraction, confocal Raman microscopy or X-ray tomography (Boel et al., 2020; Both, 2019). In this thesis a novel sessile single droplet dryer is introduced, enabling drying of droplets with smaller initial droplet sizes than can be obtained using most existing sessile single droplet drying techniques (i.e. with a minimum of 200 µm instead of typically mm range) (Foerster et al., 2016). As discussed earlier, this is important for allowing better comparison to industrial-scale spray dryers. The technique consists of depositing a droplet on a hydrophobic surface placed inside a drying chamber where the drying conditions are controlled (Fig. 1.2). The hydrophobic surface is required to fix its location and at the same time retain an almost spherical droplet shape. This drying technique is well capable of following the morphology development during drying as the droplet remains in the focal plane of the camera throughout the drying process. With the drying videos recorded, it is then possible to obtain an indirect indication for the inception of the skin (i.e. locking point) and to follow the subsequent mechanical instabilities taking place.

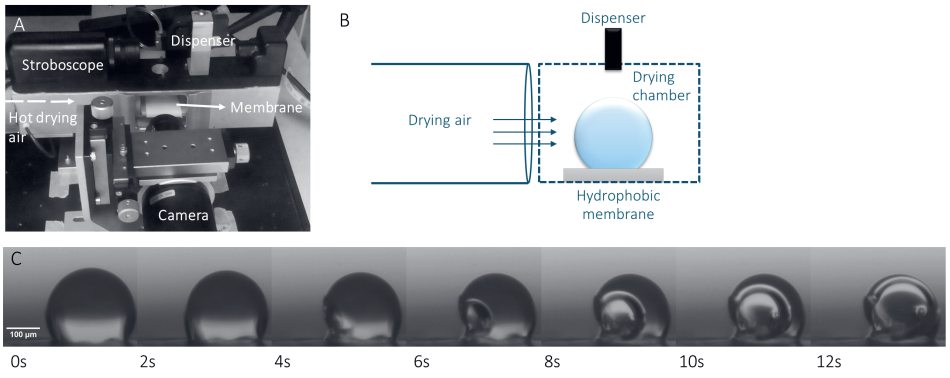

Figure 1.2. Sessile single droplet drying, with (A) an overview of the novel sessile single droplet drying set-up presented in this thesis, (B) a schematic illustration of the sessile single droplet technique, (C) a time-lapse of a drying maltodextrin droplet with an initial dry matter content of 30% (w/w), dried with hot air of 90 °C and an air velocity of 0.3 m/s.

The single droplet drying process is frequently used to interpret the morphology development during industrial spray drying, though it is undoubtedly a simplified, idealized version of the spray drying process. For instance, many single droplet drying techniques dry droplets with larger droplet diameter when compared to the size ranges achieved during spray drying (i.e. mm instead of ~10-100 μm), resulting in an increased drying time (i.e. minutes instead of seconds) and a different balance between evaporation and diffusion (Boel et al., 2020; Fu, Woo, & Chen, 2012; Sadek, Schuck, et al., 2015). In addition, heat and mass transfer can be different from spray drying due to the design of the drying device, which can be the case for pendant and sessile droplet drying (Perdana, Fox, Schutyser, et al., 2013). Besides, during spray drying, different droplets experience different drying trajectories through the spray dryer, which probably include droplet-droplet and droplet-drying chamber wall collisions. Despite the differences between the single drop drying and spray drying process, literature has frequently shown that overall the industrial spray-dried particle morphologies could be deduced from those generated with single droplet drying (Both et al., 2020; El-Sayed et al., 1990; Fu, Woo, Moo, et al., 2012; Nuzzo et al., 2017; Schiffter & Lee, 2007; Ullum et al., 2010; Walton & Mumford, 1999). This implies that, within limitations, it is possible to use single droplet drying as a technique to study and predict the morphology of spray-dried powders without performing expensive industrial spray drying trials. Additionally, drying of a single droplet under controlled conditions is valuable for providing real-time information on the mechanisms of drying that give rise to the morphologies, including shrinkage behaviour of droplets, skin formation, and mechanical instabilities occurring, such as cavitation and wrinkling. Once the observations during single droplet drying are complemented with particle analysis after drying and other experiments that facilitate insights on the drying behaviour of materials, a theoretical framework can be designed to fill the gap in knowledge regarding the particle morphology and engineering thereof. Besides this, models simulating droplet morphology evolution are also expected to contribute to an improved understanding of morphology development during drying, albeit still in their infancy. Handscomb and Kraft (2010) were the first to construct a modelling framework simulating the structural evolution of droplets following shell formation. The framework combined a core droplet description with a number of structural sub-models. They developed criteria for picking the appropriate sub-model, allowing simulation of structural evolution as influenced by changing droplet composition and drying conditions. They used the framework to simulate the drying of droplet colloidal silica and combined the results from the

simulations to produce a morphology map linking the suspended particle size to the dried-particle morphology. Du et al. (2020) also developed a model for the morphology development of a soft matter droplet based on a pseudo-dynamic analysis. They were able to construct morphology maps, linking the final morphology to elastic length, gel layer thickness and weight loss. It is expected that eventually morphological models will be developed that have a sound coupling between rheology and drying, where the parameters of the model are tuned by comparison to for instance single droplet drying and rheology experiments.

1.4. Objective and outline of the thesis

On the basis of the discussion above, the overall objective of this thesis is to relate the fundamental properties of the drying materials to the dynamics and skin properties of drying single droplets. To do this, we aim to predict the skin properties during drying and the final particle morphology, from the rheological properties of the constituents depending on concentration and change in temperature. The insights obtained in this work may offer a route towards multi-scale understanding and better control of spray drying processes.

To achieve our goals, different experimental techniques and models are combined. Given the primary interest in foods, the focus will be on components that are relevant for foods, such as maltodextrins, whey proteins, caseins and probiotics. In the following paragraphs, the content of the chapters of this thesis is summarized (Fig. 1.3).

In **Chapter 2** the viscosity profiles as function of the concentration of maltodextrins, whey proteins and their mixtures are measured and described with well-known viscosity models. Whey proteins follow the Krieger-Dougherty relation for dispersions of hard-spheres, while the viscosity of maltodextrins can be described with a combination of the Spurlin-Martin-Tennent and Williams-Landel-Ferry theories. The viscosity data are linked to observations during single droplet drying.

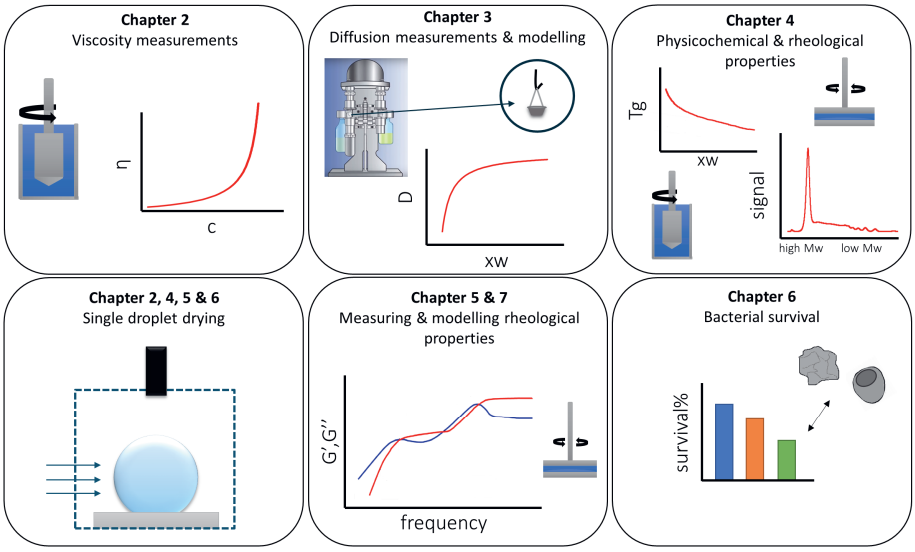

Figure 1.3. Schematic overview of the thesis content including chapter division.

Chapter 3 focuses on the moisture diffusivity during drying of concentrated protein and carbohydrate systems. An accurate description of the moisture diffusivity supports modelling the single droplet drying process. Diffusion data for the different food matrices are obtained from thin film drying combined with gravimetric analysis in a dynamic vapour sorption analyser. Obtained experimental moisture diffusivities are compared to theoretical diffusion models, including the Darken relation for the mutual diffusivity and the free-volume theory for the self-diffusivity of moisture.

In **Chapter 4** a new sessile single droplet dryer is employed which is specifically designed for studying the morphology development of sessile single droplets closer to the droplet sizes generated during spray drying. The novel system uses a piezoelectric dispenser capable of dispensing small droplets at relatively high initial dry matter contents. With this single droplet drying technique, the morphology development of maltodextrins varying in dextrose equivalence (DE) is investigated. Molecular weights, glass transition temperatures and rheological properties of the different maltodextrins are used to explain the evolution of the structure of different particles.

Chapter 5 continues with a more detailed characterisation of the rheological behaviour of concentrated maltodextrins varying in DE. For this, rheological master curves are constructed with superposition principles, which map the rheological behaviour of maltodextrins at

various temperatures and concentrations in a single plot, covering a very wide range of conditions. Master curves are described with a model for transient or entangled networks. Rheological data are linked to droplet drying based on modelling of temperature and moisture evolution using an effective diffusion model validated with sessile single droplet drying experiments.

In **Chapter 6** we assess if morphology development may be important for protecting heat-sensitive components. More specifically, we investigate if morphology development can be related to the survival of probiotic *Lactobacillus plantarum* WCFS1 after drying. Different drying matrices varying in physicochemical properties have been selected that result in different particle morphologies.

Finally, in **Chapter 7** we first provide a general discussion of the main findings of Chapters 2-6. To put the main findings into a broader perspective we then investigate the rheology of concentrated globular whey proteins as an important protein model system and accordingly test the applicability of superposition principles for explaining the morphology evolution during drying. We compare the results for whey proteins and maltodextrins and attempt to establish a mechanistic explanation for the morphology development. Additionally, pilot-scale spray drying experiments are performed to verify whether and how the conclusions from single droplet drying can be translated to the results obtained at large scale. Finally, the chapter will provide some thoughts for future research.

Chapter 2

The role of viscosity in morphology development during single droplet drying

This chapter has been published as Both, E.M., Siemons, I., Boom, R.M., Schutyser, M.A.I. The role of viscosity in morphology development during single droplet drying. *Food Hydrocolloids.* **2019**, *94*. https://doi.org/10.1016/j.foodhyd.2019.03.023.

2.1. Abstract

Particle morphology influences the final quality of a powdered product. However, the mechanisms behind morphology formation are not completely understood yet. In this study particle morphology is linked to rheological properties of the concentrated liquid formulations at high concentration. Shear rate sweeps showed jamming of the whey proteins at concentrations of ~50% (w/w), whereas maltodextrins remained fluid up to concentrations of ~70% (w/w). The morphology development of the latter components during single droplet drying could be influenced by altering the initial droplet size and dry matter content. If droplets had a high initial dry matter (50% (w/w) morphology development started immediately, and the formed morphology could be explained by the rheological behaviour of the mixture at that concentration. This indicated that measuring the rheological properties at high concentrations can provide insight in morphology development. Gaining insight on morphology development will eventually lead to higher quality powdered products.

2.2. Introduction

Spray drying is a widely used process to convert liquid formulations into powder to facilitate transport and extend their shelf-life. During drying not only water is removed, but the powder will also attain a particular morphology, which is related to quality parameters such as flowability (Fu, Huck, Makein et al., 2012) and reconstitution behaviour (Takeiti et al., 2008). The morphology development during spray drying of droplets can be followed using single droplet drying, imposing controlled and monitored conditions (Schutyser et al., 2018). The use of single droplet drying to mimic spray drying has been extensively discussed in reviews (Fu, Woo, Chen, et al., 2012; Sadek, Schuck, et al., 2015; Schutyser et al., 2018). Although the drying rate during single droplet drying experiments is lower (especially due to difference in droplet size) compared to spray drying, the particle morphologies observed are representative for spray-dried particles (Nuzzo et al., 2015; Sadek et al., 2014; Sadek et al., 2016). Some studies report more pronounced morphologies in single droplet drying, while the overall appearance is similar (Nuzzo et al., 2017). This shows that single droplet drying experiments are meaningful for mimicking and studying spray drying processes.

In a previous study on single droplet drying of solutions containing whey protein (WP) and maltodextrin DE12 (MD) we already concluded that the typical morphology varies from particles with a wrinkled surface and small internal vacuoles, to particles with a smooth surface and a large internal vacuole (Both, Karlina, et al., 2018; Bouman et al., 2016). This morphology could be influenced by altering the drying conditions, which was explained by the combination of the drying rate and the subsequent different skin properties. Depending on the composition, conditions could be identified at which lowering the drying temperature created a transition from wrinkled towards smooth particles. In the current research we will extend this work by investigating the effect of the dry matter content and droplet size on the morphology development, at the conditions identified previously.

To understand the morphology development, it is important to gain better insight on the rheological properties of the formed skin. During drying, solutes in the droplet become increasingly concentrated at the droplet surface, which leads to the formation of a viscoelastic skin (Vehring et al., 2007). The rheological properties of the skin contribute to particle morphology development; however, measurement of these properties in-line is very challenging or virtually impossible. Instead, bulk rheological properties of the solutions may be assessed, e.g. viscosity or viscoelastic properties. The viscosity of highly concentrated

solutions has been measured for several model systems (e.g. Avaltroni et al., 2004; Brownsey et al., 2003; Dahbi et al., 2010; Haene and Liederkerke, 1996; Parker et al., 2005) and for whey proteins has been related to morphology by Sadek et al. (2013). The relationship between viscoelastic properties and morphology has not yet been much explored, except for two recent studies via indentation of 5 mm thick dried films (Sadek, Pauchard, et al., 2015), and via oscillatory droplet tensiometry (Andersson et al., 2018). Therefore, in this study we aim to understand the morphology development by analysis of the viscous behaviour of mixed formulations at increasing concentrations. This can contribute to better understanding of the morphology development during spray drying, and with that facilitate the production of powders with a higher quality and lower environmental impact.

2.3. Materials and methods

2.3.1. Materials

Solutions of whey protein isolate (94% protein, Friesland Campina, The Netherlands) and maltodextrin with a dextrose equivalent of 12 (Roquette, France) were made with varying mass ratios: 100:0, 75:25, 50:50, 25:75 and 0:100 (WP:MD on a dry basis) and varying dry matter content: 20, 30, 40 and 50% (w/w). First, the whey protein was dissolved in demineralized water and stirred overnight at 4 °C to ensure complete hydration. Next, the maltodextrin was added to this solution and stirred for 30 min at room temperature. The solutions used in single droplet drying (SDD) were made with a dry matter content of 30, 40 or 50% (w/w), with mass ratios of 25:75 or 50:50 (WP:MD), where the 40 and 50% (w/w) solutions were deaerated for 20 min to remove entrapped air in an ultrasonic bath (5210E-DTH, Branson, USA). The solutions used in rheology could not all be dissolved at the targeted dry matter content, due to the higher protein content and/or dry matter content than the samples used in SDD. Therefore, all solutions were first made at 20% (w/w) and subsequently concentrated using a rotational evaporator at 70 mBar and 50 °C. Following this procedure, we ensured that all components remained in solution.

2.3.2. Sessile single droplet drying

The morphology development during the drying of solutions was studied with a sessile droplet drying platform (Fig. 2.1) that was further developed from the platform that was previously described by Perdana et al. (2011). A pneumatic micro-dispenser (Nordson Engineering Dispensing, USA) deposited a droplet on a hydrophobic membrane

(Polypropylene, Akzo Nobel Faser Ag., the Netherlands) in the focus of a CCD camera (µEye 1480ME, Imaging Development systems GMBH, Germany). The droplet was dried with dry, hot air at 60 °C (25:75 WP:MD) or 70 °C (50:50 WP:MD), which are the transition conditions as identified in Both et al. (2018a) with a velocity of 0.3 m/s, and a relative humidity of ~1%. The initial droplet radii varied between 300 and 700 µm and the initial dry matter content was 30, 40 or 50% (w/w). The 40 and 50% (w/w) solutions were deaerated for 20 min to remove entrapped air in an ultrasonic bath (5210E-DTH, Branson, USA). The data analysis is based on 4 replicates. The initial droplet size, final droplet size and locking point size were determined from the recorded movie with ImageJ (National Institute of Health, USA). The scale was determined by correlating the number of pixels of the needle to its actual size, which is 225 µm. The locking point was defined as the first visual deviation from the original spherical droplet shape.

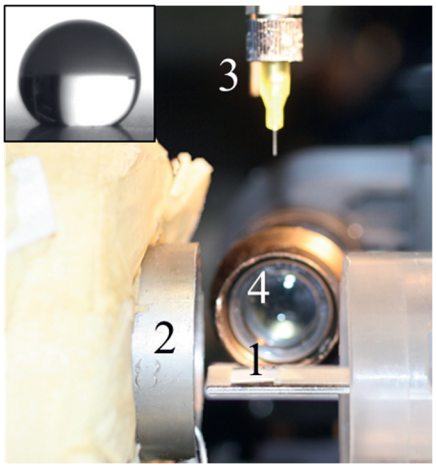

Figure 2.1. Sessile single droplet drying platform, with (1) sample holder with hydrophobic membrane, (2) insulated air tunnel, (3) robotic dispenser with needle tip, (4) µEye camera. The insert shows a droplet on the hydrophobic membrane.

2.3.3. Rheology measurements

The rheological experiments were carried out with a strain-controlled rheometer (MCR 502, Anton Paar). A shear rate sweep was performed using a concentric cup geometry (CC17, 16,660 mm x 24,858 mm (width x height), Anton Paar) at 20 °C. The shear rate was logarithmically increased from 0.1 to 100 s^{-1}, with 15 measuring points with durations that decreased logarithmically from 300 to 1 s. Subsequently, the procedure was reversed, i.e. from 100 to 0.1 s^{-1} with 15 measurement points and logarithmically increasing durations of

1 to 300 s. With this procedure the absence of loading history and sample fracture were verified. Samples of varying dry matter content were measured in duplicate; once including the reversed procedure, and once without the reversed procedure. A rotational temperature sweep was performed at a constant shear rate of 50 s^{-1} using a cone-plate geometry (CP50-4, Anton Paar) with a diameter of 25 mm and 4.000° angle. Samples had a dry matter content of 40% (w/w) and the sample temperature was linearly increased from 15 °C to 90 °C with a ramp of 2.5 °C·min^{-1}, with 121 measuring points and a duration of 15 s per point. Paraffin oil was used to avoid any undesired evaporation from the samples during the temperature sweep.

2.3.4. Describing the relation between viscosity and concentration

Maltodextrin DE12

The viscosity profile upon concentration of a polymer solution can be described with a series of universal relations. In the semi-dilute regime the combination of the empirical Spurlin-Martin-Tennent's (SMT) model combined with the Mark-Houwink relation has been shown to describe the viscosity of maltodextrin solutions (Avaltroni et al., 2004; Spurlin et al., 1946), being random coil polymers. The intrinsic viscosity of a polymer solution $[\eta]$ can be described with the Mark-Houwink relation:

$$[\eta] = kM_v{}^{\alpha} \qquad 2.1$$

With M_v the viscosity-averaged molecular weight (10,000 g·mol^{-1} for the maltodextrin used), and k and α constants related to the degree of molecular expansion at 20 °C, thus the polymer backbone stiffness and polymer-solvent interactions. For maltodextrin, (Avaltroni et al., 2004) found that k and α are $2.43 \cdot 10^{-3}$ (dl·g^{-1}) and 0.337 (-). These parameters are the input parameters for the SMT model, which is based upon the Huggins model:

$$\eta_{sp} = [\eta]ce^{k_H[\eta]c} \qquad 2.2$$

With η_{sp} the specific viscosity $\eta_{sp} = \eta_{eff}^{SMT}/\eta_{water} - 1$ (-), c the concentration (g·dl^{-1}), $[\eta]$ the intrinsic viscosity (dl·g^{-1}), and k_H the Huggins parameter. The effective viscosity (η_{eff}) is the dynamic viscosity (Pa·s). The Huggins parameter k_H, was in this study used as a fitting parameter and in earlier studies estimated to be 1.34±0.20 or 1.2 (-) for maltodextrins (Avaltroni et al., 2004; van der Sman & Meinders, 2013). An average density was used in

the semi dilute regime (20 – 40% w/w) to convert the weight fraction x_{md} (% w/w) to concentration c (g·dl^{-1}), namely 1150 kg·m^{-3} which corresponds to a 30% (w/w) solution.

In the concentrated regime, the viscosity of a polymer solution is governed by the amount of free volume. Williams, Landel and Ferry developed a free volume model (WLF) which relates the viscosity of a polymer solution at a specific temperature to the viscosity at the glass transition temperature (Williams et al., 1955):

$$\log\left(\frac{\eta_{eff}^{WLF}}{\eta_g}\right) = -\frac{C_1(T - T_g)}{C_2 + T - T_g} \tag{2.3}$$

With η_g the universal viscosity at the glass transition ~10^{11} Pa·s, the universal parameters $C_1 = 17.4$ and $C_2 = 51.6$ K (Anese et al., 1996; Soesanto & Williams, 1981), and the glass transition temperature T_g which can be described by the Couchman-Karasz theory (Couchman & Karasz, 1978):

$$T_g = \frac{x_w \Delta C_{p,w} T_{g,w} + x_{md} \Delta C_{p,s} T_{g,s}}{x_w \Delta C_{p,w} + x_{md} \Delta C_{p,s}} \tag{2.4}$$

With $x_w = 1 - x_{md}$ the mass fraction of water, $T_{g,w}$ the glass transition of water (134 K), $\Delta C_{p,w}$the change in specific heat capacity at the glass transition of water (1.92 J·g^{-1}·K^{-1}), $T_{g,s}$ the glass transition of maltodextrin DE12 (450 K), $\Delta C_{p,s}$ the change in specific heat capacity at the glass transition of maltodextrin DE12 (0.426 J·g^{-1}·K^{-1}) (Avaltroni et al., 2004; van der Sman & Meinders, 2011).

The SMT model is applicable to systems with low concentrations, while the WLF equation is only valid for higher concentrations. Thus we need to combine these two models if we want describe the full range of concentrations. We combine the two model equations using an ordinary smoothed step function:

$$\eta_{eff,md} = \left(1 - \left(\frac{1}{1 + e^{-\frac{x_{md} - b}{t}}}\right)\right)\eta_{eff}^{SMT} + \left(\frac{1}{1 + e^{-\frac{x_{md} - b}{t}}}\right)\eta_{eff}^{WLF} \tag{2.5}$$

With b and t as fitting parameters, where b represents the transition point from η_{eff}^{SMT} to η_{eff}^{WLF}, and t is a measure of the abruptness of the transition, where a larger t provides a smoother transition.

Whey protein and mixtures of whey protein and maltodextrin

Globular proteins such as whey proteins do not exhibit the same rheological behaviour as random coil polymers, such as maltodextrins. Whey protein solutions may be considered to behave as hard-sphere dispersions upon concentrating (Loveday et al., 2007), and therefore the viscosity can be described by the Krieger-Dougherty relation (KD), which describes the viscosity as a function of the volume fraction of the protein (ϕ):

$$\frac{\eta_{eff,wpi}}{\eta_{medium}} = \left(1 - \frac{\phi}{\phi_{max}}\right)^{-[\eta]\phi_{max}} \qquad 2.6$$

With ϕ_{max} the maximum packing density and $[\eta]$ the intrinsic viscosity. The volume fraction of protein was calculated from the weight fraction multiplied with the voluminosity: $\varphi = x_{wpi} \cdot q$. The voluminosity of whey protein is estimated 1.5 mL·g^{-1} (Walstra et al., 1984) and assumed constant at varying concentration. For whey protein solutions the viscosity of water is used as η_{medium}, whereas for mixed systems the viscosity of the maltodextrin solution was used. Furthermore, in mixed systems a modified weight fraction was used for both maltodextrin and whey protein: $x_{mod,i} = x_i/(x_i + x_{H_2O})$. By using a modified fraction it is assumed that the presence of another component has no effect on the viscosity of the component modelled.

2.4. Results and discussion

As drying is essentially a concentration process, we first discuss the effect of concentration on the viscosity of maltodextrin and whey protein mixtures (section 2.4.1 and 2.4.2). Subsequently we will address the effect of temperature for the same mixtures (section 2.4.3). Our observations are then related to the particle morphology development during spray drying (section 2.4.4).

2.4.1. Effect of concentration on viscosity of maltodextrin and whey protein solutions

The viscosity of maltodextrins, whey proteins and mixtures thereof was Newtonian in the measured shear rate range for all compositions (Fig. A.2.1). The experimental data for the effective viscosity of maltodextrins as a function of concentration and the proposed models are shown in Fig. 2.2. At lower concentrations (<40% w/w), the effective viscosity follows the prediction by the Spurlin-Martin-Tennent (SMT) theory quite closely (Eqn. 2.1 and 2.2). Avaltroni et al. (2004) already showed that the SMT-model gives fair estimations of the

viscosity of (semi-)dilute maltodextrin mixtures (from 1-50% w/w) with different dextrose equivalent (Avaltroni et al., 2004). The Huggins parameter (k_H) is influenced by the molecular architecture of the glucose homopolymer, and was found to be 1.34 or 1.2 (-) for maltodextrin in previous work (Avaltroni et al., 2004; van der Sman & Meinders, 2013). Linear regression on the current data resulted in a value of 1.23±0.02 (-), in line with expectation. Generally, a Huggins parameter value >1 indicates a poor solvent quality. This is underlying the general tendency of carbohydrate polymers to aggregate (Avaltroni et al., 2004). Upon increasing the concentration (>40% w/w), the polymer-polymer association becomes more pronounced and maltodextrins are expected to form a percolating network via hydrogen bonding, increasing the mechanical stability of the solution (Molinero et al., 2003). Therefore, the SMT theory cannot predict the viscosity of concentrated solutions.

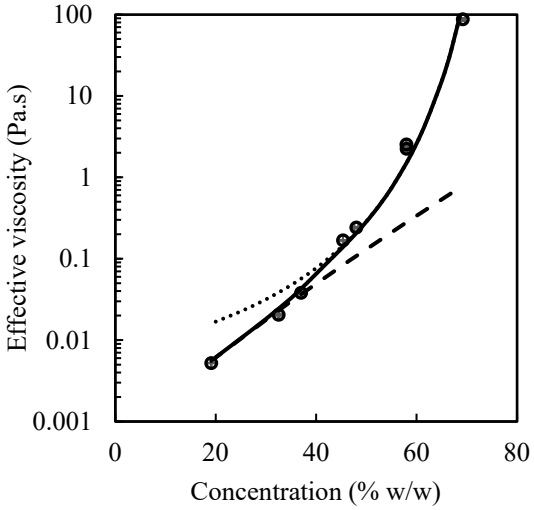

Figure 2.2. Viscosity of maltodextrin solutions at 20 °C as a function of concentration, with (○) *experimental data,* (- -) *SMT model,* (···) *WLF model,* (−) *Smoothed step function.*

For higher concentrated solutions the Williams-Landel-Ferry (WLF) theory is better suitable to describe the viscosity of polymers (Williams et al., 1955). This theory can be used to predict the viscosity depending on temperature and the concentration (Eqn. 2.3 and 2.4). From Fig. 2.2 we can conclude that the effective viscosity of highly concentrated (>40% w/w) maltodextrin solutions was well described by the WLF theory. To illustrate, the WLF model was able to accurately describe the rheological behaviour of starch hydrolysates in a concentration range between 60 and 85% (w/w) and for temperatures ranging between 20 °C and 80 °C (Haene & Liederkerke, 1996), and Sopade et al. (2003) showed that the WLF

theory could also more accurately describe the temperature dependency of the viscosity of honey when compared to Arrhenius, Vogel-Tamman-Fulcher and power-law models (Sopade et al., 2002). In general, the WLF theory should not be applied much below the Tg or at very low viscosity levels (<10 Pa·s). However, Haene and Liederkerke (1996) showed that for starch hydrolysis products, the theory could be applied down to viscosity levels of 0.1 Pa·s. Also here we find that the theory can be applied for maltodextrins down to ~0.1 Pa·s (Fig. 2.2). The viscosity of the maltodextrin solution over the whole range of concentrations can be described by combining the SMT and the WLF theory using a smoothed step function approach (Eqn. 2.5), with $b = 0.45$ and $t = 0.03$ as the fitting parameters. This generalized equation can aid in for instance predicting the self-diffusivity of maltodextrins following the generalized Stokes-Einstein equation (van der Sman & Meinders, 2013).

The effective viscosity of whey protein can be described using the commonly applied Krieger-Dougherty relation for dispersions of hard-spheres (Fig. 2.3, Eqn. 2.6). This relation assumes that there is a steady state between individual spherical particles and cooperatively moving packets of particles that are constantly formed and dissociated (Loveday et al., 2007). The KD model has already been shown before to describe the viscosity of β-lactoglobulin, which is the major protein present in whey protein isolate (deWit & Klarenbeek, 1984; Loveday et al., 2007). Applying this model to the data presented here, the intrinsic viscosity and maximum packing density of the protein were found to be 4.92 ± 0.41 ($dl \cdot g^{-1}$) and 0.79 ± 0.03 (-), respectively. These values are substantially higher than the theoretical values of 2.5 and 0.62, respectively, for monodisperse, completely rigid spheres (Dörr et al., 2013). However, Loveday et al. found that pure β-lactoglobulin dispersions already have an intrinsic viscosity of 3.6 and a maximum packing density of 0.71 (Loveday et al., 2007). The increased packing density for β-lactoglobulin dispersions may be explained by the formation of dimers. Their shape can be approximated by prolate ellipsoids, which form a denser packing than spheres (Donev et al., 2004; Parker et al., 2005). In the case of our whey protein dispersions, the packing density is even further increased as it is a mixture of differently sized, shaped and charged molecules, which will allow even denser packing.

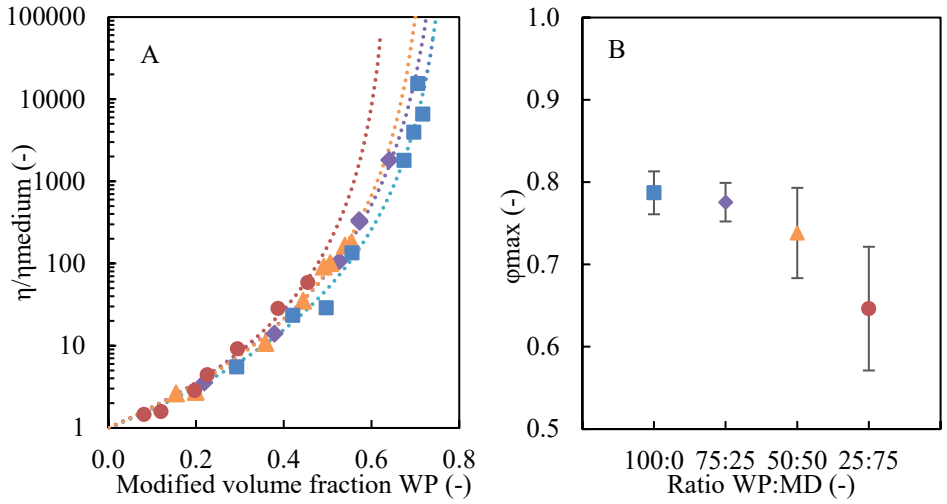

Figure 2.3. (A) η/η_{medium} as a function of modified volume fraction whey protein and composition, where the colour of the line of the KD model fit is similar to the corresponding symbol of the experimental data. (B) the maximum packing density from KD as a function of composition. With (■) whey protein, (◆) 75:25 WP:MD, (▲) 50:50 WP:MD, (●) 25:75 WP:MD.

2.4.2. Effect of concentration on viscosity of maltodextrin - whey protein mixtures

The viscosity of the mixed maltodextrin-whey protein solutions was analysed using KD. In the analysis, the viscosity of the medium was described as the viscosity of the modified weight fraction maltodextrin using the SMT/WLF theory and the KD model was fitted on the basis of the modified volume fraction of whey protein (Fig. 2.3, Eqn. 2.6). This approach provided a good fit for 75:25 (WP:MD) with a similar maximum packing density as for pure whey protein. However, when the mixtures were higher in maltodextrin, the modified volume fractions of whey protein and the η/η_{medium} were much lower, which resulted in higher uncertainty of the fitted maximum packing density. Furthermore, the fitted ϕ_{max} of the whey proteins decreased with increasing maltodextrin content (Fig. 2.3B), showing that the presence of maltodextrin influences the packing and jamming of the whey proteins. This implicates that the whey protein solutions high in maltodextrin do not undergo jamming upon concentration, simply because the fraction maltodextrin is too high. This is also illustrated in Fig. 2.4, where the viscosity is plotted against the concentration. Here the jamming of the whey proteins in the 100:0 and 75:25 (WP:MD) is clearly visible from the asymptote around ~50% (w/w), whereas the solutions higher in maltodextrin have a gradual slope even at high concentration.

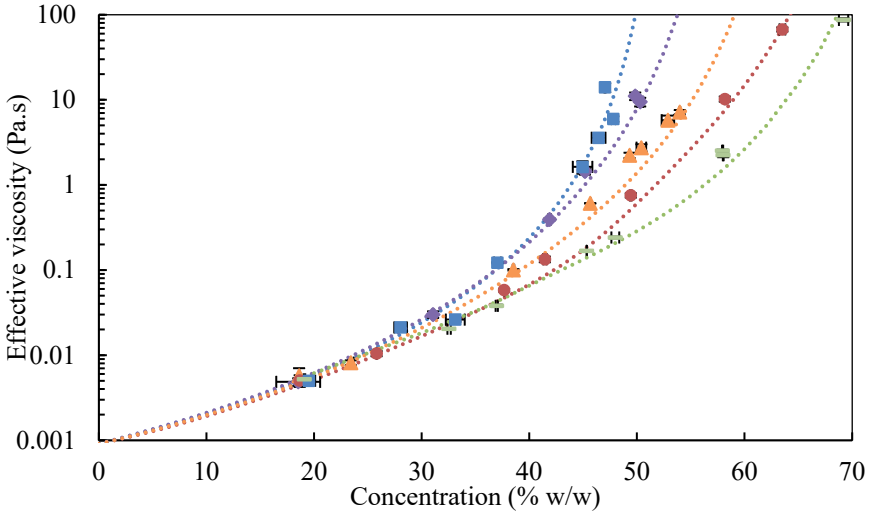

Figure 2.4. Viscosity of maltodextrin, whey protein and mixtures thereof as a function of concentration. The colour of the line of the model fit is similar to the corresponding symbol of the experimental data. With (-) maltodextrin, (■) whey protein, (◆) 75:25 WP:MD, (▲) 50:50 WP:MD, (●) 25:75 WP:MD.

2.4.3. Effect of temperature on viscosity of maltodextrin – whey protein mixtures

The viscosity is influenced by the concentration and the temperature. While initially the droplet temperature settles at the wet bulb temperature, after reaching a critical moisture content the droplet temperature starts to increase while at the same time the skin is being formed. This may lead to a reduction in viscosity, which again can influence the skin formation and thus the morphology development. To assess the temperature dependency, solutions of 40% (w/w) were heated from 15 °C to 90 °C at a constant shear rate (Fig. 2.5A). The results showed that the influence of the temperature on the viscosity of whey protein solutions was smaller than for maltodextrin solutions. The viscosity of maltodextrin solutions at 50 °C was reduced by a factor 4 compared to the viscosity at 15 °C, whereas the viscosity of whey protein was reduced by a factor 3. At high temperatures the viscosity increased again, in the case of whey protein this was around 58 °C. This may be related to denaturation of whey proteins, which usually starts around 63-65 °C. Sugars can delay protein denaturation (M. A. Haque et al., 2015), which explains that the temperature at which denaturation occurs shifts to higher temperatures with higher maltodextrin content (Fig. 2.5B). In the mixture 75:25 (WP:MD) the maltodextrin apparently is not able to delay the protein denaturation, which may be possibly aligned with the limited effect of the maltodextrin on the jamming of whey proteins (Fig. 2.4).

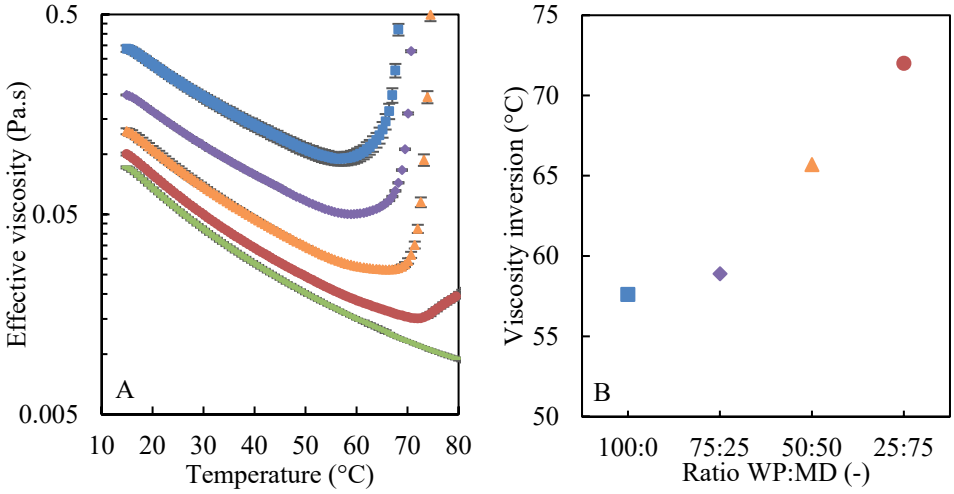

Figure 2.5. (A) Viscosity of maltodextrin, whey protein and mixtures thereof as a function of temperature, and (B) Temperature at viscosity inversion as a function of ratio WP:MD. With (-) maltodextrin, (■) whey protein, (◆) 75:25 WP:MD, (▲) 50:50 WP:MD, (●) 25:75 WP:MD. The temperatures indicate the temperature at the viscosity inversion.

2.4.4. Morphology development during single droplet drying

As discussed in the introduction, solutions of mixtures were dried around their transition conditions, because at these conditions, small variations of the drying conditions will cause large differences in morphology. Fig. 2.6 demonstrates that on this transition, the same drying conditions can either result in a smooth, hollow particle, or in a denser, wrinkled particle. In Fig. 2.6A a time series of a drying droplet forming a smooth and hollow morphology is shown. The drying started at a constant drying rate (Both, Karlina, et al., 2018), while slowly the concentration of components at the surface increased and a skin was formed. When the skin thickened, the morphology started to develop at the so-called locking point. Afterwards, the droplets formed a vacuole which rapidly grew until the droplet was hollow. In Fig. 2.6B a droplet was dried under the same conditions. The initial drying was similar, but after the locking point a different morphology was formed: the skin was pulled in from multiple sides leading to a fully wrinkled particle surface.

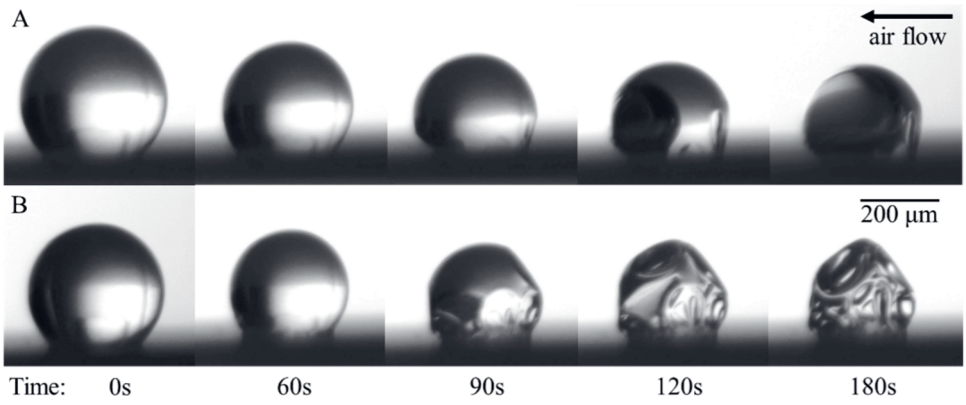

Figure 2.6. Time series of droplets dried under similar conditions yielding different morphologies, with (A) vacuole formation and (B) wrinkling. Specific conditions: 25:75 (WP:MD), T_{air}: 60 °C, R_0: 370 µm, DM_0: 30% (w/w). Air flow is from right to left, as indicated by an arrow.

Subsequently, droplet drying experiments were carried out at varying initial size and initial dry matter content at the transition conditions. The effect of both parameters on the final particle morphology is shown in Fig. 2.7A (25:75 WP:MD) and Fig. 2.7B (50:50 WP:MD). The morphology of droplets with an initial dry matter content of 30% (w/w) showed a clear effect of the droplet size; larger droplets tended to result in a smooth and hollow morphology, while smaller droplets were more likely to result in wrinkled particles. The droplets with an initial radius of 370 µm (25:75) and 390 µm (50:50) were dried at the transition conditions, which provided particles showing either hollow of more wrinkled morphology. Increasing the initial dry matter content to 40% or 50% (w/w), yielded wrinkled particles regardless of the initial size.

The onset of morphology development, the so-called locking point, provides information on the skin formation. Therefore, the locking point time (Fig. 2.8A) and the size at the locking point (Fig. 2.8B) were determined for these samples, to identify the effect of both initial size and initial dry matter content. The droplets with composition 25:75 (WP:MD) showed a later locking point time, and therefore a smaller normalized radius (R/R_0) at the locking point than the 50:50 mixture, due to the lower drying temperature. Generally, larger droplets had a later locking point, but the normalized radius (R/R_0) was independent of the initial size. Increasing the dry matter content from 30% to 40% (w/w) decreased the locking point time approximately by half, while further increasing to 50% (w/w) only slightly lowered the locking point time. The same effect was visible for the radius at the locking point: at 30%

(w/w) it is ~88% of the initial radius, whereas for 40% and 50% (w/w) it lies around ~96%. These small differences between the 40 and 50% (w/w) samples suggest that only a small amount of water needs to be evaporated before the skin reaches a sufficiently high strength and the morphology starts to form.

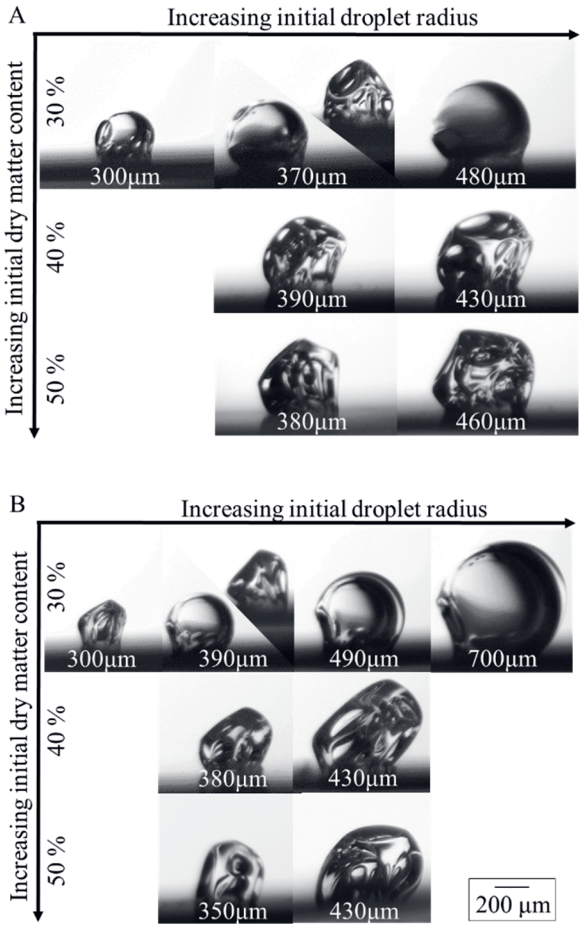

Figure 2.7. Final particle morphology of dried droplets, with different composition: (A) 25:75 (WP:MD) at T_{air} 60 °C and (B) 50:50 (WP:MD) at T_{air} 70 °C, and varying initial dry matter content (vertical) and initial droplet radius (horizontal). The radius given corresponds to the initial droplet radius.

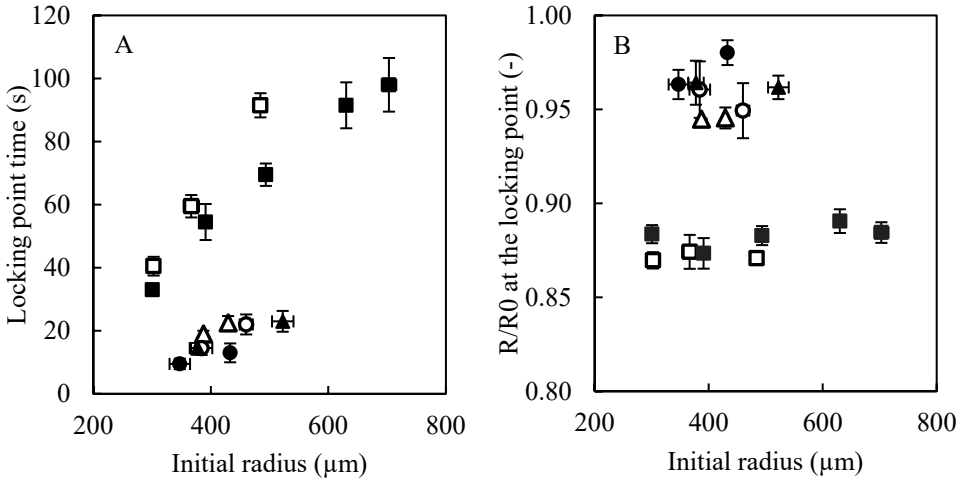

Figure 2.8.(A) Locking point time and (B) normalized radius (R/R_0) at the locking point of drying droplets as a function of initial droplet size, with varying composition (□,△,○ WP:MD 25:75; ■,▲,● WP:MD 50:50), and varying initial dry matter content (■,□: 30% (w/w); ▲,△: 40% (w/w); ●,○: 50% (w/w)). The droplets with the composition of WP:MD 25:75 were dried at 60 °C and WP:MD 50:50 were dried at 70 °C.

A critical phenomenon for morphology development is the formation of a skin at the droplet surface. During drying water evaporates from the surface of the droplet, leading to an increase of concentration of molecules near the surface. If the diffusion rate of the molecules away from the surface is slower than the evaporation rate, a skin is formed that gradually increases in thickness during further drying (Vehring et al., 2007). At a certain skin consistency, the skin will no longer be able to shrink to compensate the volume reduction due to water evaporation. However, water evaporation still continues, and therefore the internal pressure decreases and as a result stresses are building up to deform the droplet skin (Sugiyama et al., 2006). Therefore, the skin consistency determines the type of morphology. A rigid, jammed skin cannot easily deform, and the internal pressure continues to decline until a local weak point in the skin will collapse. This creates a defect and initiates a large vacuole to be formed. A viscous and deformable skin can continuously deform leading to a wrinkled particle. The skin strength depends on the rheological properties of the system, i.e. whey protein and maltodextrin DE12 solutions will behave differently upon concentration. Whey proteins act as a 'hard-spheres' and therefore jamming will occur at sufficiently high concentrations. Maltodextrin, on the other hand, will slowly increase in viscosity and only undergo glass transition upon cooling. When advancing towards the glass transition, water diffusion rates will decrease and thus drying will slow down, which allows more time for the skin to deform.

These different responses were clearly observed in the rheology measurements (Fig. 2.4). For whey protein jamming occurred at a concentration above ~50% (w/w), forming a rigid skin and subsequent vacuole formation. Maltodextrin solutions were still fluid when concentrated to 70% (w/w), leading to the formation of a weak skin and therefore a wrinkled morphology.

The locking point analysis of the drying droplets (Fig. 2.8) showed that for droplets with an initial dry matter content of 50% (w/w) locking occurs almost instantly. Therefore, this dry matter content can be regarded as a critical concentration in morphology development, and rheological testing at this concentration can provide valuable insights. Mixtures with a 75:25 (WP:MD) ratio are close to maximum packing at this concentration and are expected to form a rigid skin, which was shown in previous research for drying temperatures ranging from 40 to 90 °C (Both, Karlina, et al., 2018). The mixtures with a 50:50 or 25:75 (WP:MD) are not close to maximum packing, and will thus form a weak skin, which may be expected to lead to a wrinkled morphology. However, as showed in Fig. 2.7 vacuole formation was observed during the drying of droplets with a large initial radius (>35 μm at 30% dm). Due to the slow drying, phase separation may occur, leading to whey protein enriched zones. This could provide rigidity to the skin, leading to the formation of hollow particles. Although phase separation was not measured here, it has been previously observed for droplets dried under similar conditions (Both, Karlina, et al., 2018; Nuzzo et al., 2015), and is therefore the most likely phenomenon behind the effect of droplet size on morphology. Phase separation may either be entropically induced liquid-liquid phase separation, or be caused by denaturation of the protein (see Fig. 2.5), depending on the conditions during drying, especially on the temperature. Furthermore, whey protein is a surface-active component and has a higher molecular weight than maltodextrin. It is therefore likely that relatively more whey protein is present at the air-water interface than maltodextrin (Fäldt et al., 1993; Meerdink & van't Riet, 1995).

2.5. Conclusions

The rheological properties of concentrated aqueous solutions of whey protein isolate and DE12 maltodextrin were investigated and related to the development of distinct particle morphology during drying of single droplets of the same mixtures. The viscosity increase of the mixed whey protein and maltodextrin as function of concentration and temperature was described with various models. Subsequent droplet drying experiments revealed that morphology development of the whey protein-maltodextrin solutions could be well related to the rheological behaviour of the mixtures. The droplets were expected to form wrinkled morphologies, as the viscosity increased only moderately even at high concentrations. However, the morphology appeared highly dependent on drying time, where the 'slower' dried droplets were more likely to form a smooth and hollow morphology. Therefore, it was assumed that phase separation occurred, leading to whey protein enriched zones. If skin formation occurs faster than phase separation, maltodextrin will dominate morphology development and a wrinkled morphology develops.

Rheological analysis of the concentrated mixed systems assisted in gaining insight in morphology development, since the viscosity at high concentration could act as an indicator for morphology of the tested components. Combining single droplet drying with rheology extends the possibilities of interpretation of single droplet drying observations. A wider range of components should be tested to analyse if rheological behaviour at high concentrations can be used as an indicator for morphology development. For example, the viscosity profile of micellar caseins gave a good explanation for the formed morphology (Dahbi et al., 2010; Sadek et al., 2016). Also in the case of lactose, the very low viscosity at high concentrations can explain the later locking and the formation of a collapsed morphology (Both, Nuzzo, et al., 2018). In future work therefore the relationship between rheology and morphology should be investigated for a wider range of component mixtures, and at higher dry matter contents.

2.6. Appendix

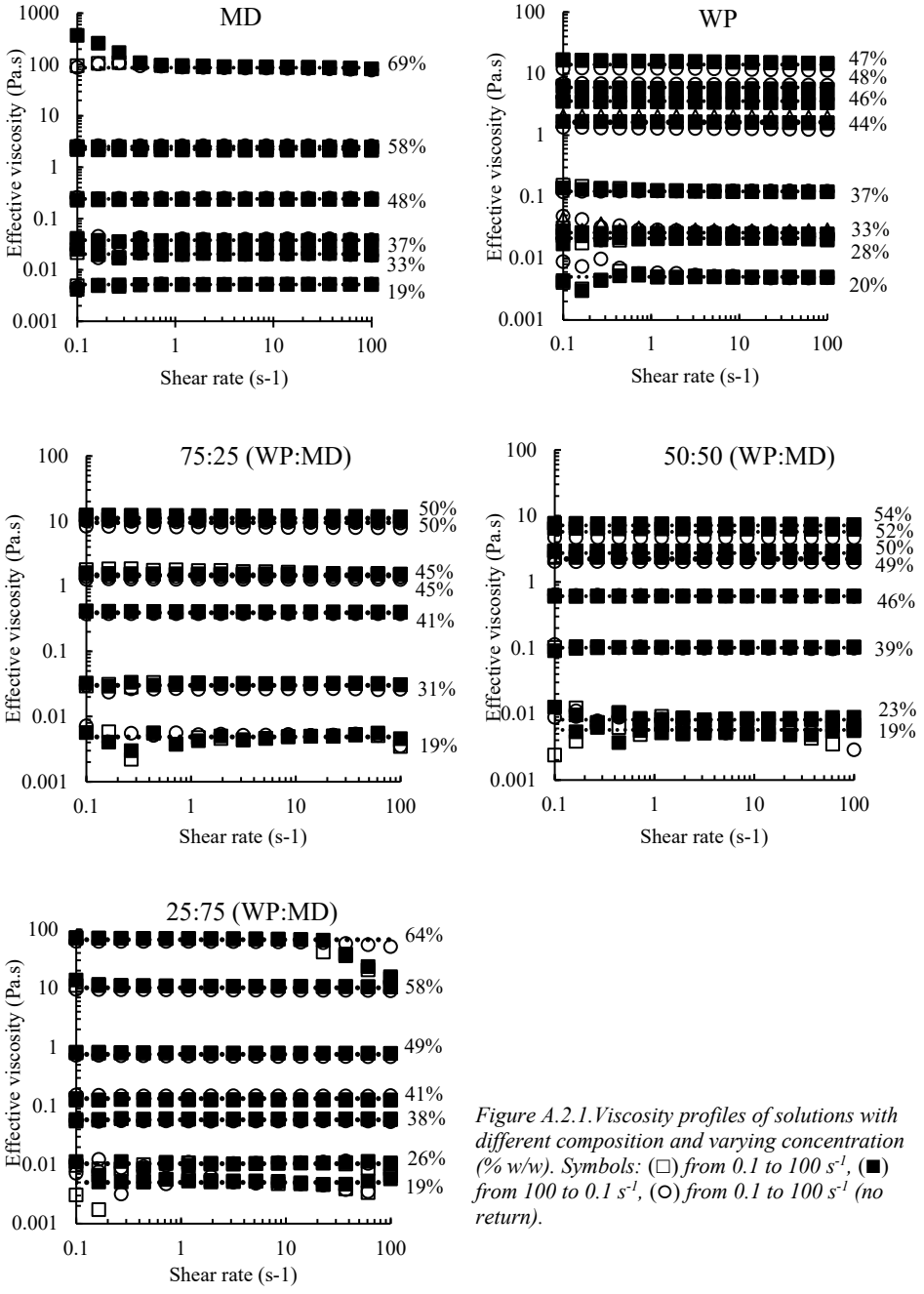

Figure A.2.1.Viscosity profiles of solutions with different composition and varying concentration (% w/w). Symbols: (□) from 0.1 to 100 s^{-1}, (■) from 100 to 0.1 s^{-1}, (○) from 0.1 to 100 s^{-1} (no return).

Chapter 3

Moisture diffusivity in concentrated and dry protein – carbohydrate films

This chapter has been published as Siemons, I., Boom, R.M., van der Sman, R.G.M., Schutyser, M.A.I. Moisture diffusivity in concentrated and dry protein-carbohydrate films. *Food Hydrocolloids.* **2019**, *97*. https://doi.org/10.1016/j.foodhyd.2019.105219.

3.1. Abstract

Understanding moisture diffusivity behaviour over a wide range of moisture contents is pivotal for optimising drying operations. Generally, data on moisture diffusivity are scarce and the effect of matrix composition on moisture diffusivity at relevant temperature for drying processes is not yet well described. In this paper moisture diffusivity in protein-carbohydrate films is systematically investigated for a wide range of moisture contents at 80 °C. Diffusion data are obtained from controlled thin film drying experiments following the regular regime method and compared to theoretical models. Moisture diffusivity for binary maltodextrin-water and whey protein-water systems appeared similar and were reasonably well described with the Darken relation. Diffusivity was lower for casein-water systems at moisture contents above 0.12 kg water/kg, which may be explained by compartmentalization of water in the casein micelles. At low moisture contents all binary systems showed universal behaviour, which may be explained by random coil behaviour leading to similar water-molecule interactions. This behaviour could be well described by free-volume theory. In mixed systems of proteins and carbohydrates moisture diffusivity appeared strongly influenced by the presence of casein, probably due to their high voluminosity. Finally, it was surprisingly observed that diffusivity in multicomponent systems decreased sharply at lower water contents when compared to binary systems. This might be explained by a denser molecular packed system in the dry regime for multicomponent systems or water trapping by protein-carbohydrate complexes.

3.2. Introduction

Diffusion of water is ubiquitous in many natural and industrial processes. It is a critical phenomenon for designing drying operations in food, pharma and chemical industries as it determines process efficiency and affects product quality (Chen, 2007; Labuza & Hyman, 1998; Malafronte et al., 2015; Thirunathan et al., 2017). Most drying processes are diffusion-limited and accurate description of moisture diffusivity can support the improvement of critical drying applications, such as the encapsulation of probiotics and bioactive ingredients (He, 2006; Schutyser et al., 2012). Ideally, the moisture diffusivity for such applications is known as a function of water content and temperature.

Limited data on moisture diffusivity over a wide range of water contents and temperatures are available. Particularly for multi-component food matrices, there is a wide variation of the reported diffusivity values due to the complexity of foods and different methods of measurement (Mittal, 1999). The most important techniques to assess moisture diffusion include nuclear magnetic resonance (NMR) spectroscopy (Malafronte et al., 2015; Marcone et al., 2013), magnetic resonance imaging (MRI) (Chen, 2007; Ghosh et al., 2002) and gravimetric methods (Ferrari et al., 1989; Perdana, van der Sman, et al., 2014; Räderer et al., 2002; Thirunathan et al., 2017).

Perdana et al. (2014b) employed the regular regime method to extract moisture diffusivity from thin film drying experiments in a dynamic vapour sorption (DVS) analyser. The DVS analyser allows drying at different temperatures and provides accurate weight measurements at short time intervals. With this method, moisture diffusivity can be determined over a large range of moisture contents at the film temperature. The method was evaluated for its potential to obtain diffusivities for different carbohydrates and their mixtures, which are frequently applied to encapsulate active ingredients. The moisture diffusivities in the different carbohydrate systems were found to exhibit similar behaviour with varying moisture content. The latter was attributed to the fact that carbohydrates have very similar repeating molecular groups, which result in the same water molecule-carbohydrate interactions and thus result in a similar water self-diffusivity. Additionally, experimental diffusivities were found comparable to model predictions from theory via the Darken relation combined with the generalized Stokes-Einstein relation for solute self-diffusivity and the free-volume theory for water self-diffusivity (Perdana, van der Sman, et al., 2014; van der Sman & Meinders, 2013).

In practice many product formulations that are dried consist of proteins or a combination of proteins and carbohydrates, such as with skim milk. Colsenet et al. (2005) and Mariette et al. (2002) already studied water diffusion with NMR spectroscopy in whey protein and casein dispersions at varying concentrations and at ambient temperature. Malafronte et al. (2015) evaluated effective moisture diffusivity in skim milk during drying over a large range of moisture contents and temperatures (from 50 to 90 °C) by combining NMR and direct parameter estimation. However, to the best of our knowledge, studies that systematically investigate the effect of the composition on moisture diffusivity for more complex matrices are lacking. Especially, there is lack of knowledge on diffusion behaviour of water at low moisture content and elevated temperature, which are relevant parameters to drying processes. Therefore, the objective of the present work is to quantify diffusivity in concentrated protein and carbohydrate systems. Thin film drying experiments were carried out in a DVS system and experimental diffusivities were compared to theoretical models. First, different binary systems were evaluated, including maltodextrin-water, whey protein-water and casein-water systems. Second, we evaluated ternary systems of mixtures of maltodextrins and whey proteins or caseins. Finally, skim milk was investigated as a practical, but even more relevant matrix.

3.3. Materials and methods

3.3.1. Materials

Binary solutions

Protein stock solutions were prepared by adding whey protein isolate (94% protein, Friesland Campina, The Netherlands) or micellar casein (Cas, 88% protein, Friesland Campina, The Netherlands) to demineralised water, and stirring overnight at 4 °C to ensure complete hydration. Carbohydrate stock solutions were prepared by adding maltodextrin with a dextrose equivalent of 12 (MD12, Roquette, France) to demineralised water and stirring for 30 min. The whey protein and maltodextrin solutions had a dry matter concentration of 20% (w/w) and the casein solutions had a dry matter concentration of 10% (w/w).

Complex matrices

The stock solutions were mixed in various mass ratios and subsequently mixed for 30 min. Skim milk (Arla Food Ingredients, Denmark) was slowly dissolved in demineralised water at 50 °C. Subsequently, the solution was stirred for 60 min at 45 °C to ensure complete dissolution. The final mixtures had a dry matter concentration of 10% (w/w) or 20% (w/w).

3.3.2. Dynamic vapour sorption analysis of a drying thin film

The prepared solutions were cast in an aluminium cup to create a film of 8 x 8 mm with a thickness of ~1 mm. Before the maltodextrin solutions could be tested, ~1-1.5% (w/w) agar powder (Sigma Aldrich, USA) was added and subsequently the mixture was allowed to boil for a maximum of 30 s in a microwave oven. After boiling, the maltodextrin mixture was cast in the aluminium cup and the solution was slowly cooled down to solidify at room temperature. Agar was added to the pure maltodextrin formulations to suppress convective flow in the film (Räderer et al., 2002). Earlier studies indicated that the agar had negligible effect on the moisture diffusivity (Coumans, 2000; Yamamoto, 1999). Agar was not added to formulations with protein as their higher viscosity already suppressed internal convective flow.

The thin film drying experiments were performed in a dynamic vapour sorption (DVS) system (Surface Measurement System, England). The slightly adapted drying procedure originally developed by Perdana et al. (2014b) was used. The thin film was first dried at 80 °C for 24 h. Next, the drying air temperature was increased to 120 °C for 24 h to obtain the final dry matter in the sample. After this, the air temperature was re-adjusted to 80 °C. During drying at 80 °C, the mass of the film was recorded each 3 s and during drying at 120 °C every 15s. The relative humidity of the drying air was set at 0.0% and the air flow applied was 7 cm/min.

The mutual diffusivities were calculated adopting the regular regime method as described by Perdana et al. (2014b). This regular regime approach was already verified by Perdana et al. (2014b) by checking the effect of the initial drying conditions, i.e. mass transport in the drying air was not limiting and the initial water content had only limited influence on the measured diffusivities. To calculate the desorption rate in the regular regime we varied the densities of the systems based on the composition and these are summarized in Table 3.1.

Table 3.1. The selected densities for the matrices tested.

Component	ρ (kg·m^{-3})	Reference
Maltodextrin	1550	(van der Sman & Meinders, 2013)
Whey protein	1350	(Akkerman, 1992; Buma, 1965)
Casein	1265	(De Kruif et al., 2012)
Skim milk	1036	(Sherbon, 1988)

3.3.3. Modelling the mutual diffusivity of water in binary systems

The mutual diffusivity of water in binary systems was described by following the generalised Darken relation (Darken, 1948; Krishna & Van Baten, 2005; Perdana, van der Sman, et al., 2014; van der Sman & Meinders, 2013):

$$D = \left(\phi_j D_{i,self} + \phi_i D_{j,self}\right) Q \tag{3.1}$$

In which D is the mutual diffusivity (m^2/s) of component i in a $i-j$ system, $D_{i,self}$ and $D_{j,self}$ (m^2/s) are the self-diffusivities of components i and j, respectively. ϕ is the volume fraction (m^3/m^3) and Q (-) is the thermodynamic factor, which is related to the derivative of the themodynamic potential. We have used the volume fraction instead of the molar fraction as was already proposed by Krishna and Van Baten (2005).

The thermodynamic factor can be written following the Flory-Huggins free energy function:

$$Q = 1 - 2\chi\phi_j(1-\phi_j) \tag{3.2}$$

Where χ (-) is the Flory-Huggins interaction parameter between solvent and solute components, which is assumed to be composition dependent. The interaction parameter follows (van der Sman & Meinders, 2011):

$$\chi_{p,w} = \chi^1_{p,w} - (\chi^1_{p,w} - \chi^0_{p,w})(1-\phi_p)^n \tag{3.3}$$

$\chi^1_{p,w}$ is the interaction parameter of a nearly dry biopolymer ($\phi_p \approx 1$) and $\chi^0_{p,w}$ is the interaction parameter of a fully hydrated biopolymer ($\phi_p \approx 0$). For all the components we take $\phi_p \to 0$, then $\chi^0_{p,w} = 0.5$, indicating that water is a theta solvent under dilute conditions and when $\phi_p \to 1$, $\chi_{p,w} = \chi^1_{p,w} \approx 0.8$ for maltodextrins (van der Sman & Meinders, 2011). For whey proteins a value of $\chi^1_{p,w}$ = 1.8 is assumed and for caseins $\chi^1_{p,w}$ = 1.4, taking into account (partial) denaturation of proteins at the elevated temperatures which leads to

exposure of hydrophobic groups (van der Sman, 2015). The value of the exponent was chosen $n = 2$, which is taken from van der Sman (2015), and also used in other approximations of the Pincus-deGennes-Tanaka theory (Baulin & Halperin, 2002; Dormidontova, 2002).

For a maltodextrin-water system, the self-diffusion of carbohydrate molecules is predicted using the generalized Stokes-Einstein relation:

$$D_{s,self} = \frac{kT}{6\pi r_H \eta_{eff}} \tag{3.4}$$

In which k is the Boltzmann constant, T (K) the temperature, r_H (m) the hydrodynamic radius of the molecules, and η_{eff} (Pa·s) is the effective viscosity. The hydrodynamic radius is calculated from the degree of polymerization of maltodextrin DE12 following the Mark-Houwink relation (Scholte et al., 1984):

$$r_H = \frac{a_u}{DP^{-0.49}} \tag{3.5}$$

DP is the degree of polymerization, $DP = 111.11/DE$ (Dokic et al., 1998).The hard-sphere radius of a monomeric subunit a_u (m) follows (Perdana, van der Sman, et al., 2014):

$$a_u = \left(\frac{M_u}{4/3\pi N_a \rho_s}\right)^{1/3} \tag{3.6}$$

In which M_u is the molecular weight of the monomeric anhydroglucose unit, N_a the number of Avogadro and ρ_s the density of maltodextrin, fixed at 1550 kg/m^3.

The effective viscosity of the maltodextrin DE12-water system is calculated by combining Spurlin-Martin-Tennent's (SMT) model and the Williams, Landel and Ferry free volume model (WLF) by using an smoothed step function (Both, Siemons, et al., 2019):

$$\eta_{eff,md} = \left(1 - \left(\frac{1}{1 + e^{-\frac{x_{md} - b}{t}}}\right)\right)\eta_{eff}^{SMT} + \left(\frac{1}{1 + e^{-\frac{x_{md} - b}{t}}}\right)\eta_{eff}^{WLF} \tag{3.7}$$

x_{md} is the mass fraction of maltodextrin (% w/w), b and t are fitting parameters, where b =0.45 represents the transition point from η_{eff}^{SMT} the effective viscosity as determined by SMT to $\phi\eta_{eff}^{WLF}$ the effective viscosity as determined by WLF. t is a measure of the abruptness of the transition, where t =0.03 was used as proposed by Both et al. (2019a).

The self-diffusion coefficient of whey protein was described by taking the concentration dependence of the self-diffusion coefficient of Brownian spherical particles as described by (Nesmelova et al., 2002):

$$D/D_0 = \frac{1-9\varphi/32}{1+H(\varphi)+(\varphi/\varphi_0)/(1-\varphi/\varphi_0)^2} \quad 3.8$$

Where D_0 (m^2/s) is the Stokes-Einstein relation, in which η (Pa·s) is the viscosity of pure water and r_H is taken 3.5 nm (Kristiansen et al., 1998), $\varphi_0 \approx 0.5718$ is the concentration of dense packing of spheres, and $H(\varphi)$ is calculated as follows:

$$H(\varphi) = \frac{2b^2}{(1-b)} - \frac{c}{(1+2c)} - \frac{bc(2+c)}{(1+c)(1-b+c)} \quad 3.9$$

$$b = \left(\frac{9\varphi}{8}\right)^{\frac{1}{2}} \text{ and } c = \frac{11\varphi}{16}$$

The volume fraction φ is calculated using the following relation:

$$\varphi = 1/(1 + \frac{v1}{v2}\frac{x1}{1-x1}) \quad 3.10$$

In which $x1$ is the weight fraction of water in solution, and $v1 = 10^{-3}$ m^3/kg and $v2 = 0.75 \cdot 10^{-3}$ m^3/kg are the specific volumes of water and protein, respectively (Colsenet et al., 2005). We assume that the partial volumes of the components remain constant.

The casein self-diffusivity was predicted using an empirical equation proposed by Speedy (1987) and Salami et al. (2013), in which caseins behave as hard-spheres below the close packing limit and as soft particles above this limit:

$$D = D_0(1 - \frac{\varphi}{0.571})(1 + \varphi^2(1.459 - 11.04\varphi^2)) \quad 3.11$$

In which D_0= 2·10^{-11} m^2/s and φ is the volume fraction occupied by the hard-spheres.

The self-diffusion coefficient of water in a maltodextrin system is predicted using the free-volume theory based on the work of Vrentas & Duda (1977):

$$D_{w,self} = D_0 exp\left(-\frac{E}{RT}\right) exp\left[\frac{-(m_w\tilde{V}_w^* + m_s\xi\tilde{V}_s^*)}{m_w\left(\frac{\hat{V}_{FH,w}}{\gamma_w}\right) + m_s\left(\frac{\hat{V}_{FH,s}}{\gamma_s}\right)}\right] \quad 3.12$$

$$\hat{V}_{FH,w} = K_{1w}(K_{2w} - T_{g,w} + T) \quad 3.13$$

$$\hat{V}_{FH,s} = K_{1s}(K_{2s} - T_{g,s} + T) \quad 3.14$$

$$D_{w,self} = D_0 exp\left(-\frac{E}{RT}\right) exp\left[\frac{-(m_w\tilde{V}_w^* + m_s\xi\tilde{V}_s^*)}{m_w\left(\frac{K_{1w}}{\gamma}\right)(K_{2w} - T_{g,w} + T) + m_s\left(\frac{K_{1s}}{\gamma}\right)(K_{2s} - T_{g,s} + T)}\right] \quad 3.15$$

With D_0=1.48·10^{-7} is the pre-exponential factor (m^2/s), E the energy to overcome the attractive forces from neighbouring molecules, 2.34 (kJ/mol), R the gas constant (J/mol.K), T the temperature (K), $\tilde{V}^*$ the specific critical free volume (m^3/kg), ξ the ratio of solvent and polymer jumping units. With K_{1w}, K_{2w}, K_{1s}, K_{2s} the free volume parameters (m^3/kg.K and K respectively), T_g the glass transition temperature, and γ the overlap factor for shared free volume (between 0.5 and 1). Table 3.2 shows the parameters used for a maltodextrin system as was proposed by Perdana et al. (2014b) and van der Sman and Meinders (2013). The free volume parameters for maltodextrin-water system are listed in Table 3.2.

Table 3.2. Free volume parameters for water and carbohydrates.

Free volume parameters	Water	Carbohydrates
$\tilde{V}^*$ (m^3/kg)	9.10·10^{-4}	5.90·10^{-4}
T_g (K)	136	347
ξ (-)	-	0.79
K_1/ (m^3/kg ·K)	1.945·10^{-6}	0.336·10^{-6}
K_2 (K)	-19.73	69.21

For the self-diffusion coefficient of water in a whey protein and casein system, the ratio of the solvent and solute jumping units (ξ), and the specific critical free volume of the protein ($\tilde{V}_s^*$) are unknown. Similarly, the free volume contribution of the protein ($\hat{V}_{FH,s}$) is unknown. These parameters were obtained by fitting the free volume theory to the moisture diffusivity measured below 0.15 kg water/kg.

3.4. Results and discussion

3.4.1. Modelling of moisture diffusivity in binary systems

The experimental data and predicted mutual moisture diffusivity for a maltodextrin-water, whey protein-water and casein-water systems are shown in Fig. 3.1. Perdana et al. (2014b) showed that experimental diffusivities for various carbohydrate systems could be well described by the generalised Darken relation, using the Stokes-Einstein relation for the solute self-diffusivity and the free-volume theory for the water self-diffusivity based on the work of Vrentas and Duda (1977). In this study, a similar modelling approach was applied for a maltodextrin-water system, but extended with the Spurlin-Martin-Tennent (SMT) and Williams-Landel-Ferry (WLF) theories to describe viscosity (Both, Siemons, et al., 2019). In Fig. 3.1A we observe that the calculated mutual diffusivity for a maltodextrin-water system is close to the experimental data over a wide range of moisture contents. In the range of moisture contents between 0.04 kg water/kg and 0.2 kg water/kg the free-volume theory gives a better estimation of the measured mutual moisture diffusivity than the Darken relation. The latter is in agreement with the work of van der Sman and Meinders (2013), who showed that diffusion of water in concentrated systems of simple sugars and glucose homopolymers is well described by the solvent self-diffusivity as predicted by the free volume theory.

The mutual diffusivity in protein-water systems was modelled using a similar approach (Fig. 3.1B and C). The self-diffusivities of whey proteins and casein are concentration dependent. For whey proteins we made use of the assumption that whey proteins behave as Brownian spherical particles (Nesmelova et al., 2002; Tokuyama & Oppenheim, 1995), assuming that the particle diffusion follows the classic theory of Brownian motion. For micellar casein, we proposed the empirical equation by Speedy (1987), which was later validated by Salami et al. (2013). Because former self-diffusivity models are no longer valid in low moisture regimes, we assume that whey proteins are effectively immobilized below 0.36 kg water/kg and caseins are immobilized below 0.55 kg water/kg.

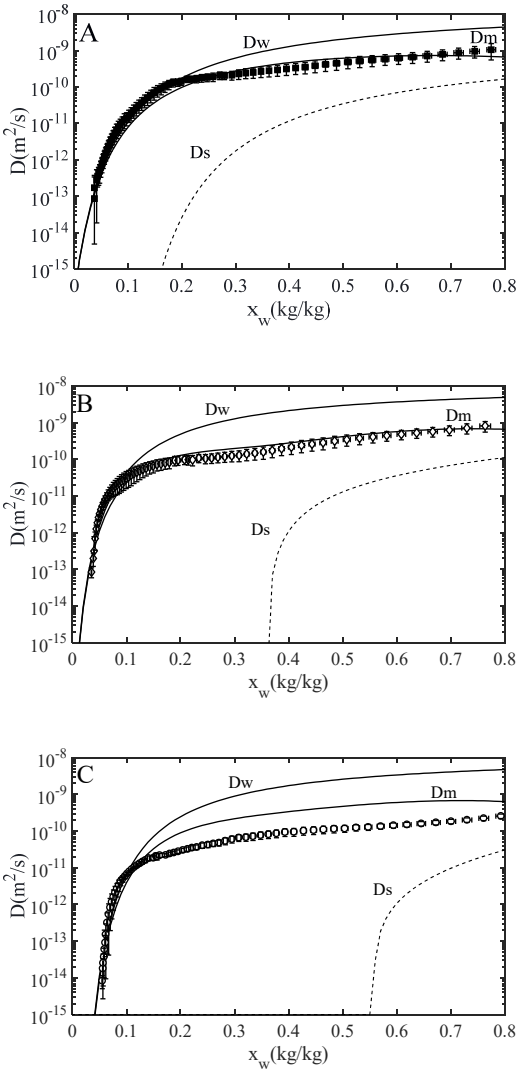

Figure 3.1. Mutual diffusivity of water in a maltodextrin-water system (■), (B) in a whey protein-water system (◇), and (C) in a casein-water system (○) at 80 °C determined at an air flow of 7 cm/min (n ≥2). Lines represent the predictions of the mutual moisture diffusivity using Darken relation (-, Dm), the water self-diffusivity (-, Dw), and the solute self-diffusivity (--, Ds).

The water self-diffusivity for protein systems was also described by the free volume theory (Fig. 3.1B and C). This was done as it was shown that the Vrentas-Duda free-volume theory could be applied to predict the water self-diffusion in different thermodynamically complex systems, including biopolymers, sugars, polyols and gelatin (van der Sman & Meinders, 2013; Yapel et al., 1994). The wider applicability of this theory may be explained by the fact that the interactions of these different components with water is similar; via hydrogen bonding. For prediction of the water self-diffusion in protein systems, we fitted the ratio of the solvent and solute jumping units (ξ), the specific critical free volume of the protein ($\tilde{V}_s^*$)

($\tilde{V}_s^* \xi = 2.91 \cdot 10^{-4}$ m^3/kg for whey protein, $3.16 \cdot 10^{-4}$ m^3/kg for casein and for comparison $4.66 \cdot 10^{-4}$ m^3/kg for carbohydrates). We also fitted the free volume contribution of the protein ($\hat{V}_{FH,s}$) ($\frac{\hat{V}_{FH,s}}{\gamma_s} = 1.20 \cdot 10^{-5}$ m^3/kg for whey protein, $3.67 \cdot 10^{-6}$ m^3/kg for casein and for comparison $2.36 \cdot 10^{-5}$ m^3/kg for carbohydrates). Adjustment of these parameters is proposed due to exposure of hydrophobic domains of proteins in the intermediate to dry moisture-regime (Brindle & Krochta, 2008; Dauphas et al., 2005). This phenomenon is expected to affect the hydrogen-bonded network and associated free volume.

The calculated mutual diffusivity in a whey protein system using the Darken relation was in agreement with the experimentally determined mutual diffusion (Fig. 3.1B). However, the mutual diffusivity calculated for casein was above the measured values for a moisture regime between ~0.12 and 0.8 kg water/kg (Fig. 3.1C). The differences observed between the theoretical calculations and measured diffusivity for casein systems may be explained by skin formation. Micellar caseins absorb at the air-water interface (Sadek et al., 2014) and jam when their concentration reaches a critical level with dramatic increase of viscosity. According to Dahbi et al. (2010) this critical concentration is already at 18.5% (w/w) casein. Therefore, a skin will be formed rapidly upon concentration, which is probably still permeable to water but reduces moisture diffusivity as would be predicted by theory.

3.4.2. Binary systems compared

For comparison of the mutual water diffusivities in the binary systems we plotted the measured mutual diffusivities of the systems in Fig. 3.2. The mutual diffusivities in a maltodextrin-water system and a whey protein-water system are similar at higher moisture contents (≥0.5 kg water/kg), whereas the mutual diffusivity in a casein matrix is clearly lower. As discussed earlier, this lower mutual diffusivity may be explained by the low critical casein concentration of ~18.5% (w/w) (Fig. 3.3) (Dahbi et al., 2010). At this concentration the micelles are highly swollen and tightly packed (Bouchoux et al., 2012), which does not allow for large water mobility over distances larger than the size of the micelles; the water is likely compartmentalised into the separate micelles.

Below a moisture content of 0.15 kg water/kg, the diffusion of water showed universal behaviour for the different matrices (Fig. 3.2). We hypothesize that in this regime proteins partly lose their conformation due to concentration effects or heat induced denaturation during our drying experiments (Horne, 2008; Vasbinder & De Kruif, 2003). Bouchoux et al.

(2010) indicated that upon concentration some parts of the casein micelles readily collapse, while other micelles are pushed closer together. Whey proteins such as β-lactoglobulins start to dissociate into monomers above 40 °C and can further lose conformation due to heat denaturation (deWit & Klarenbeek, 1984). If proteins lose their (meso)structure, they behave as random coils similar to maltodextrin molecules (Atkins & De Paula, 2010; Avaltroni et al., 2004; Tanford, 1968). This all together results in similar water-molecule interactions and therefore almost similar diffusivities.

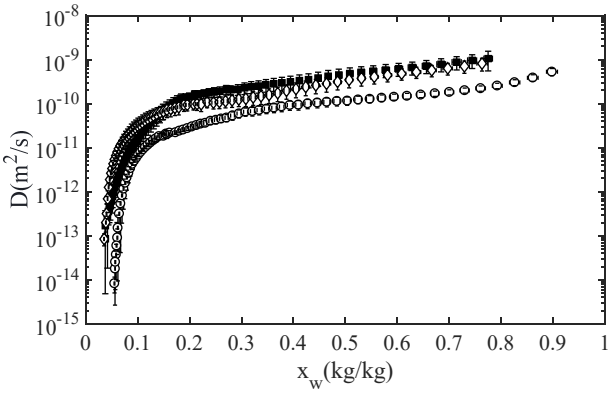

Figure 3.2. Experimentally determined moisture diffusivity at 80 °C for a maltodextrin-water mixture (■)*, whey protein-water system* (◇) *and a micellar casein-water system* (○) *(n ≥2).*

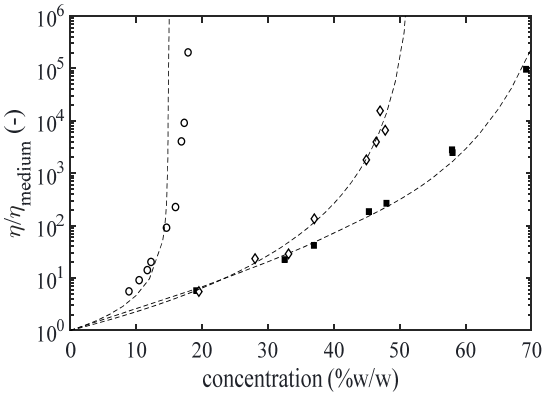

Figure 3.3. Viscosity profile of casein (○) *as function of concentration as obtained by Dahbi et al. (2010), maltodextrin* (■) *and whey protein* (◇) *solutions as a function of concentration (Both, Siemons, et al., 2019; Dahbi et al., 2010). The dashed lines are the predicted viscosities as reported by Dahbi et al. (2010) for caseins and Both et al. (2019a) for maltodextrins and whey proteins.*

3.4.3. Moisture diffusion in complex matrices

Moisture diffusion was also studied in ternary and complex, and practical systems (Fig. 3.4). The moisture diffusivity in a mixture of whey proteins and maltodextrins (1:1 mass ratio) was observed close to the moisture diffusivity in binary systems of the individual components between moisture contents 0.5 to 0.7 kg water/kg (Fig. 3.4A). From 0.3 to 0.5 kg water/kg the diffusivity of the mixed system followed the diffusivity of a binary whey protein-water system. Below 0.08 kg water/kg, the water diffusion in the mixed maltodextrin-whey protein system decreased faster than expected based on the theory.

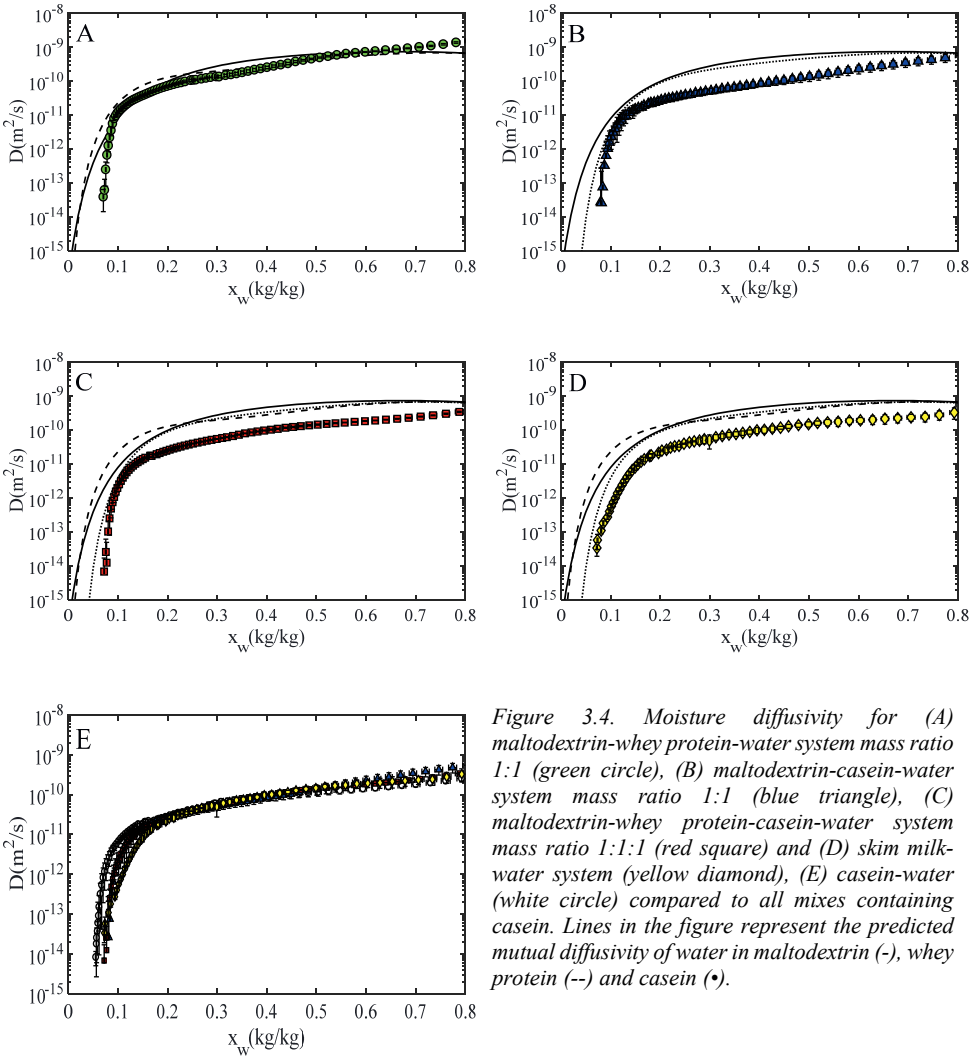

Figure 3.4. Moisture diffusivity for (A) maltodextrin-whey protein-water system mass ratio 1:1 (green circle), (B) maltodextrin-casein-water system mass ratio 1:1 (blue triangle), (C) maltodextrin-whey protein-casein-water system mass ratio 1:1:1 (red square) and (D) skim milk-water system (yellow diamond), (E) casein-water (white circle) compared to all mixes containing casein. Lines in the figure represent the predicted mutual diffusivity of water in maltodextrin (-), whey protein (--) and casein (•).

In general casein dictates the diffusive behaviour of water in the tested matrices (Fig. 3.4B, C, D and E); when casein was mixed with maltodextrin or with maltodextrin and whey proteins, we observed a diffusivity curve closely following the diffusivity as measured in a casein system (Fig. 3.4E). Skim milk, containing ~30% (w/w) casein and 5% (w/w) whey protein (Karlsson et al., 2005), also showed a diffusivity curve close to that for a pure casein system (Fig. 3.4E). Interestingly, other macromolecules present in the system besides caseins had little influence on the mutual diffusivity measured. This dominant effect of casein on mutual diffusivity could be due to the higher voluminosity (m^3/kg of dry component) of caseins (~$3.9 \cdot 10^{-3}$ m^3/kg) as compared to that of whey proteins (~$1.5 \cdot 10^{-3}$ m^3/kg) and carbohydrates (~$0.6 \cdot 10^{-3}$ m^3/kg) (McSweeney & Fox, 2009; Townrow et al., 2010; Walstra, 1979). The higher voluminosity implicates that there are stronger interactions of water with micellar caseins as compared to the other components, resulting in a diffusivity dominated by caseins.

Based on the observation that the moisture diffusivity in concentrated binary systems showed uniform behaviour (section 3.4.2), it was expected that the water diffusivities in concentrated multicomponent systems was similar. However, the moisture diffusivity curves of multicomponent systems with proteins decreased more sharply at lower moisture content (Fig. 3.4). This phenomenon was not observed by Perdana et al. (2014b) when comparing the mutual diffusivity of water in ternary carbohydrate systems to that in binary systems. Therefore, we further examined the effect of protein-carbohydrate ratio on mutual diffusivity in concentrated ternary systems (Fig. 3.5).

The mutual diffusivities for a 25:75 whey protein-maltodextrin (WP:MD) system was close to the mutual diffusivity for a 50:50 WP:MD system (Fig. 3.5A). Similarly, in Fig. 3.5B one can observe that the mutual diffusivity for 25:75 casein-maltodextrin (Cas:MD) system is analogous to that of the 50:50 Cas:MD system. Mixtures containing only 10% (w/w) protein showed diffusivity curves close to the diffusivities measured for binary systems. These results indicated that decreasing protein concentrations in mixed systems of proteins and maltodextrins results in higher diffusivities at low moisture contents (i.e. the diffusivity curves shift to the left). This might imply that the addition of proteins to carbohydrate systems results in more dense random molecular packing in the dry regime (i.e. glassy state), where most of the free volume holes are filled, concomitantly decreasing moisture diffusivity (Ubbink, 2016). However, this argument can only be confirmed if one further examines the

sizes of the free volume holes as function of moisture content for the different systems tested. Positron annihilation lifetime spectroscopy (PALS) might be a promising technique to quantify the size distribution of the free volume holes in the matrix (Cangialosi et al., 2003; Ubbink, 2016). Alternatively, the more sharp decrease observed for multicomponent systems might be explained by water trapping due to the formation of a denser skin or due to promoted protein-carbohydrate interactions (Soltanizadeh et al., 2014). Overall, it would be interesting to further investigate anomalous properties of water in concentrated multicomponent systems. Townrow et al. (2010) suggest that infrared spectroscopy, pressure-volume-temperature (PVT) analysis, nuclear magnetic resonance spectroscopy, electron spin resonance spectroscopy, and neutron scattering might be suitable techniques to study the latter.

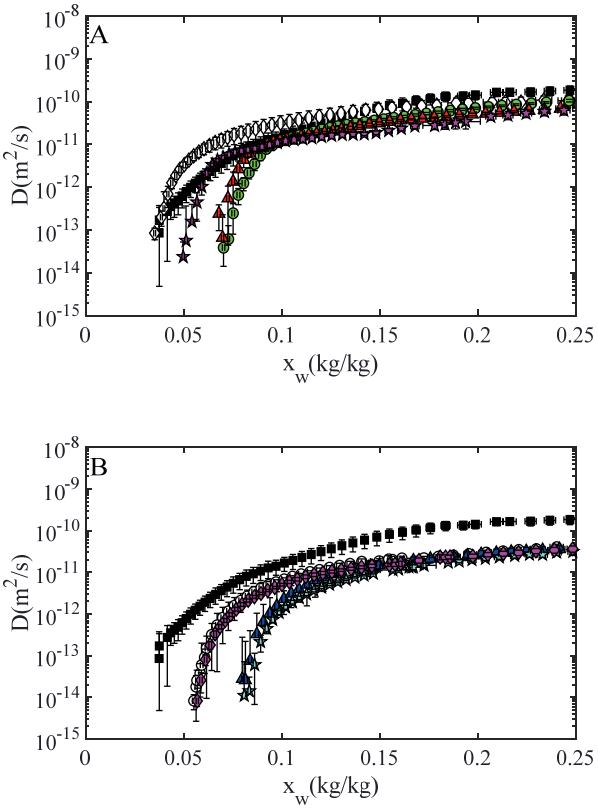

Figure 3.5. (A) Moisture diffusivity in whey protein-maltodextrin systems for mass ratio 0:100 (black square), 10:90 (magenta star), 25:75 (red triangle), 50:50 (green circle), 100:0 (white diamond). (B) Moisture diffusivities casein-maltodextrin systems mass ratio 0:100 (black square), 10:90 (magenta diamond), 25:75 (cyan star), 50:50 (blue triangle) and 100:0 (white circle) for moisture contents below 0.25 kg water/kg.

3.5. Conclusions

Thin film drying combined with gravimetric analysis was used to obtain mutual moisture diffusivities for different food matrices adopting the regular regime method. Model predictions of the moisture diffusivity using the Darken relation captured the trends in experimental data reasonably well for maltodextrin-water and whey protein-water systems. Diffusion of water in concentrated binary systems (≤0.15 kg water/kg) was showing quite universal behaviour. Universal behaviour in the dry regime was attributed to random coil behaviour, resulting in similar interaction with water and accordingly similar diffusivities. The Darken relation overestimated the moisture diffusion in a casein-water system for moisture contents above ~0.12 kg water/kg. The reason behind this discrepancy was explained by jamming of the surface-active micelles upon concentrating, resulting in the formation of a dense skin, and consequently a decreased diffusivity as compared to prediction from theory. Comparison of the binary systems revealed similar diffusivities for maltodextrin systems and whey protein systems at higher moisture contents (≥0.5 kg water/kg), whereas mutual diffusivity for casein was lower. Probably the latter is due to compartmentalization of water in micelles, reducing water mobility. To obtain a more in-depth understanding of moisture diffusion in complex matrices during drying, we examined diffusion in complex mixed systems and skim milk. Moisture diffusion curves for complex system showed that the presence of casein greatly influenced the moisture diffusive behaviour, which may be due to the high voluminosity of caseins. In addition, it was found that moisture diffusivity curves of multicomponent systems decreased more sharply at lower water content when compared to binary systems. This phenomenon may be attributed to a denser random molecular packing in the dry regime, filling most of the free volume holes, and consequently a lower moisture diffusivity. Alternatively, skin formation or formation of protein-carbohydrate complexes might result in water trapping. Further studies aiming at the analysis of the molecular structure of mixed protein and carbohydrate matrices in the glassy state can potentially verify the mechanism behind the sharper decrease in diffusivity found.

3.6. Appendix

Table A.3.1. Overview of parameters.

Parameter	Definition	Additional information
D	Mutual diffusion coefficient of water in solute (m^2 s^{-1})	▪ Experimentally obtained after thin film drying in this work by applying regular regime approach. For calculations one is referred to Perdana et al. (2014b) ▪ Theoretical description was obtained by the generalised Darken relation (Darken, 1948; Krishna & Van Baten, 2005)
ϕ	Volume fraction (m^3 m^{-3})	
Q	Thermodynamic factor for diffusion coefficient (-)	▪ Calculated by the Flory-Huggins free energy function
$\chi^1_{p,w}$	Flory-Huggins interaction parameter of a nearly dry biopolymer (-)	▪ 0.8 for maltodextrins (van der Sman & Meinders, 2011) ▪ 1.8 for whey proteins ▪ 1.4 for caseins (van der Sman, 2015)
$\chi^0_{p,w}$	Flory-Huggins interaction parameter of a fully hydrated biopolymer (-)	▪ 0.5 for all biopolymers (van der Sman, 2015)
k	Boltzmann constant	
r_H	Hydrodynamic radius (m)	▪ Calculated following Mark-Houwink relation for maltodextrin (Scholte et al., 1984) ▪ Whey proteins, 3.5nm (Kristiansen et al., 1998)
a_u	Hard-sphere radius of monomeric unit (m)	▪ 0.36nm calculated
DP	Degree of polymerisation of carbohydrate molecule (-)	▪ 111.11/DE (Dokic et al., 1998)
M_u	Molecular weight of the monomeric anhydroglucose unit (g $mole^{-1}$)	
ρ_s	Density (kg m^{-3})	▪ 1550 for maltodextrins (van der Sman & Meinders, 2013) ▪ 1350 for whey proteins (Akkerman, 1992; Buma, 1965) ▪ 1265 (De Kruif et al., 2012) ▪ 1036 (Sherbon, 1988)
η_{eff}	Effective viscosity (Pa·s)	▪ Calculated for maltodextrins by combining Spurlin-Martin-Tennent's (SMT) model and the Williams, Landel and Ferry free volume model. For calculations one is referred to Both et al. (2019a)

D_0	Pre-exponential diffusion factor ($m^2\ s^{-1}$)	▪ $2 \cdot 10^{-11}$ $m^2\ s^{-1}$ was selected for caseins (Salami et al., 2013) ▪ $1.48 \cdot 10^{-7}$ $m^2\ s^{-1}$ was used for Vrentas-Duda equation as determined by Perdana et al. (2014b)
E	Energy to overcome the attractive force from neighbouring molecule to enable molecule diffusion ($J\ mol^{-1}$)	▪ 2.34 $kJ\ mol^{-1}$ was used for Vrentas-Duda equation as determined by Perdana et al. (2014b)
$\hat{V}^*$	Specific critical free volume ($m3\ kg^{-1}$)	▪ For water $9.10 \cdot 10^{-4}$ $m3\ kg^{-1}$ (van der Sman & Meinders, 2013) ▪ For carbohydrates $5.90 \cdot 10^{-4}$ $m3\ kg^{-1}$ (van der Sman & Meinders, 2013) ▪ For whey proteins and caseins we obtained a combined value by fitting the theory to moisture diffusivity measured below 0.15 kg water/kg
ξ	Ratio of solvent and polymer jumping units (–)	▪ 0.79 for carbohydrates (van der Sman & Meinders, 2013) ▪ For whey proteins and caseins we obtained a combined value by fitting the theory to moisture diffusivity measured below 0.15 kg water/kg
K_1	Free volume parameter (m^3/kg ·K)	▪ For water $1.945 \cdot 10^{-6}$ m^3/kg ·K (van der Sman & Meinders, 2013) ▪ For carbohydrates $0.336 \cdot 10^{-6}$ m^3/kg ·K (van der Sman & Meinders, 2013) ▪ For whey proteins and caseins we obtained a combined value by fitting the theory to moisture diffusivity measured below 0.15 kg water/kg
K_2	Free volume parameter (K)	▪ For water -19.73 K (van der Sman & Meinders, 2013) ▪ For carbohydrates 69.21 K (van der Sman & Meinders, 2013) ▪ For whey proteins and caseins we obtained a combined value by fitting the theory to moisture diffusivity measured below 0.15 kg water/kg
T_g	Glass transition temperature (K)	▪ For water 136 K (van der Sman & Meinders, 2013) ▪ For carbohydrates 347 K (van der Sman & Meinders, 2013) ▪ For whey proteins and caseins we obtained a combined value by fitting the theory to moisture diffusivity measured below 0.15 kg water/kg
γ	Overlap factor for shared free volume (-)	▪ 0.6 for maltodextrin ▪ For whey proteins and caseins we obtained a combined value by fitting the theory to moisture diffusivity measured below 0.15 kg water/kg

Chapter 4

Dextrose equivalence of maltodextrins determines particle morphology development during single sessile droplet drying

This chapter has been published as Siemons, I., Politiek, R.G.A., Boom, R.M., van der Sman, R.G.M., Schutyser, M.A.I. Dextrose equivalence of maltodextrins determines particle morphology development during single sessile droplet drying. *Food Research International.* **2020**, *131*. https://doi.org/10.1016/j.foodres.2020.108988.

4.1. Abstract

Particle morphology development during spray drying is critical to powder properties. The aim of this study was to investigate whether the dextrose equivalence (DE) of maltodextrins can be used as an indicator for the final particle morphology. Maltodextrins were characterized on glass transition temperature (T_g) and viscosity, where low DE-value maltodextrins exhibited higher T_g and viscosity than high DE maltodextrins (≥21). A new custom-built sessile single droplet dryer was used to analyse morphology development of minute maltodextrin droplets (R_0 ~100 μm) at 60 °C and 90 °C. Droplets with low DE showed early skin formation (2–5 s) and developed smoothly shaped particles with large cavities. Rheology on low DE maltodextrin films at dry matter of 82% (w/w) suggested that drying droplets acquired elasticity after locking providing resistance against surface compression. After locking morphology development is probably halted as the glassy state is approached. On the contrary, rheology on high DE maltodextrin (≥21) films at dry matter of 93% (w/w) suggested that drying droplets with high DE developed viscous skins, which are susceptible to surface deformations, leading to wrinkling, folding or creasing particle morphologies. The results demonstrated that DE-value may be used as an indicator for particle morphology development when interpreted in view of the process conditions.

4.2. Introduction

Drying of fluids, containing for example polymers and colloids, has gained great interest during the last decade (Both, Nuzzo, et al., 2018; Fu, Woo, & Chen, 2012; Giorgiutti-Dauphiné & Pauchard, 2018; Lintingre, Lequeux, Talini, & Tsapis, 2016; Meng, Doi, & Ouyang, 2014; Sadek, Pauchard, et al., 2015). Droplets of these fluids acquire different morphologies according to the material properties and conditions applied during formation. In turn the morphology affects the dried powder properties, including reconstitution behaviour and flowability (Takeiti et al., 2008; Walton & Mumford, 1999). Therefore, a sound understanding of morphology development during drying is necessary to control and steer final powder properties.

During spray drying, the solutes accumulate below the droplet's surface, due to rapid solvent evaporation. Eventually, this accumulation leads to the formation of a "skin" that has at least some characteristics of a solid (Pauchard & Allain, 2003; Vehring, 2008). The physicochemical and mechanical characteristics of this skin significantly affect particle structure evolution towards its final morphology. Interactions of these aspects with drying conditions will result in morphological characteristics such as surface wrinkling and/or the formation of cavities. A closer study of these surface instabilities may be done via drying of single droplets under well-controlled and monitored conditions (Fu, Woo, Chen, et al., 2012; Sadek, Schuck, et al., 2015; Schutyser et al., 2018). For example, Pauchard and Allain (2003) studied buckling instabilities of colloidal particle suspensions and polymer solutions using sessile single droplet drying. They concluded that buckling requires a permeable, somewhat rigid skin which may still bend under the pressure of solvent evaporation. Sadek et al. (2014) and (2015a) studied wrinkling phenomena exploiting single droplet drying of colloidal casein suspensions. Droplet surface wrinkling was explained by the capacity of micelles to reduce their voluminosity as soft spheres in jamming conditions, resulting in a ductile elastic skin layer susceptible to surface distortion. Vacuole formation during drying of whey protein droplets was well described by Bouman et al. (2016) and Both et al. (2018a) and requires a rigid skin that resists bending, but still allows permeation of the solvent.

Physical effects responsible for the formation of different morphologies have been mostly studied with colloidal suspensions. Many spray-dried powders include carbohydrates, varying from simple sugars or disaccharides to polydisperse carbohydrate oligomers and polymers (Ubbink et al., 2008). Among the carbohydrates, maltodextrins are particularly

used in spray drying as drying aids and can serve as encapsulation agents for bioactive ingredients (Adhikari et al., 2004; Renzetti et al., 2012). Typically, maltodextrins are obtained from starch polymers by acid hydrolysis, enzymatic hydrolysis, or a combination of both and are characterized by their dextrose equivalent (DE), being the fraction of hydrolysed glucoside bonds (Loret et al., 2004). Maltodextrins with different DE-values have different properties (Takeiti et al., 2008). Dokic et al. (1998), for instance showed a linear relation between viscosity and the DE-value of a maltodextrin. Others found a linear correlation between the DE-value and glass transition temperature (Avaltroni et al., 2004; Levine & Slade, 1986; Roos & Karel, 1991), which is in line with the well-known Fox-Flory equation (Fox & Flory, 1950).

In this specific study we investigate whether the DE of maltodextrins can also be used as an indicator for the final powder particle morphology. For this purpose, we investigated five different maltodextrins varying in DE. First, characteristics such as the molecular weight distributions, viscosities and glass transition temperatures as function of the maltodextrin concentration were measured. We hypothesize that especially the rheological characteristics at high concentrations can provide deeper insight in morphology development. Therefore, we also evaluated the rheological properties of maltodextrins at high concentrations using thin film rheology on high dry matter thin films (Both, Tersteeg, et al., 2019).

Morphology development during drying was analysed using a new sessile single droplet drying system, where we make use of a piezoelectric dispenser capable of dispensing small droplets (180-220 μm) at relatively high initial dry matter contents (30% (w/w)). We developed this system as most previously available sessile single droplet dryers relied on droplets larger than those relevant for spray drying. It is known that droplet size influences morphology development (Both, Siemons, et al., 2019); therefore, we make use of a new system allowing the study of much smaller droplets, closer to the range of those in spray drying.

4.3. Materials and methods

4.3.1. Materials

All maltodextrins originate from corn-starch and were obtained from Roquette Frères (Lestrem, France). The following dextrose equivalents (DE) were used: DE5; DE12; DE21; DE29 and DE38. Solutions were prepared by adding the maltodextrins powders to demineralized water and stirring for at least 30 min until the solution was transparent. The final solutions had different dry matter concentrations depending on the experiment performed.

4.3.2. Molecular weight distribution

Molecular weight distributions of the different maltodextrins were determined by High Performance Liquid Chromatography (HPLC) using a Shodex KS-803 8.0 × 300 (mm) IDxLength+Guard column. The column is operated at 50 °C and connected to a refractive index (RI) detector (Shodex RI-501). Milli-Q water was used as eluent with a flow rate of 1 mL/min.

4.3.3. Glass transition temperature

Differential scanning calorimetry (DSC) experiments were performed to determine the glass transition temperature (T_g) of maltodextrins as function of their moisture content. The water content in powders was increased by a cold mixing procedure as described by Ruan et al. (1999), where a known amount of distilled water was frozen in liquid nitrogen in a mortar and the obtained ice crystals were ground into fine ice powder. Liquid nitrogen and appropriate amounts of maltodextrin powder were then added to the ice powder in the mortar and mixed by using the pestle. The mixture was stored in a fridge at 4 °C for at least 24 h to ensure homogeneous distribution of the moisture before the DSC measurements.

The prepared samples (10-20 mg) were hermetically sealed in a DSC aluminium pan and introduced to a Pyris Diamond DSC (Perkin-Elmer, DSC 8000, Norwalk, USA). An empty pan was used as a reference. The pans were first equilibrated for 1 min at the lowest temperature of the selected DSC run (at least 30 °C below the expected T_g), after which a heating ramp followed with either 1 °C/min or 5 °C/min to the highest temperature (at least 30 °C above the expected T_g) of the DSC run to provide a good resolution of the transition. The pans were then equilibrated at the highest temperature of the selected run for 1 min and subsequently the sample was cooled at a rate of 10 °C/min to the lowest temperature of the

selected run. The heating cycle was then repeated. The settings of the run were estimated based on the measured T_g values for different maltodextrins at varying moisture content as reported by Avaltroni et al. (2004) and Castro et al. (2016). Obtained DSC thermograms were analysed using software interfaced with the DSC, and the T_g was determined from the onset point of the change in heat flow observed at the second heating ramp. All measurements were done in duplicate for each condition and the T_g values were averaged.

The experimental data were fitted with a combination of the Couchman-Karasz and Fox-Flory (Roos & Karel, 1991; van der Sman & Meinders, 2011). The Couchman-Karasz relation states:

$$T_g = \frac{y_w \Delta C_{p,w} T_{g,w} + y_s \Delta C_{p,s} T_{g,s}}{y_w \Delta C_{p,w} + y_s \Delta C_{p,s}} \quad 4.1$$

Here y_i is the mass fraction ($i = w, s$ for water and solute), $T_{g,i}$ is the glass transition temperature for the pure component ($T_{g,w}$ =139 K), $\Delta C_{p,i}$ is the change in the specific heat at the glass transition. For $\Delta C_{p,w}$ a value of 1.91 kJ/kg·K was used. The $\Delta C_{p,s}$ was considered similar for all maltodextrins at 0.426 kJ/ kg·K (Haene & Liederkerke, 1996; van der Sman & Meinders, 2011).

The glass transition of the anhydrous material, $T_{g,s}$, can be described by the Fox-Flory relation:

$$T_{g,s} = T_{g,s}^{\infty} - \frac{a_{FF}}{M} \quad 4.2$$

$T_{g,s}^{\infty}$ (K) is the glass transition temperature for polymers with an infinite polymer chain length, a_{FF} (K·g/mol) is a constant and M= $162 * \left(\frac{111.11}{DE}\right) + 18$ is the molecular weight of the polymer (Dokic et al., 1998). Combining the Couchman-Karasz and the Fox-Flory relations provides the following equation:

$$T_g = \frac{y_w \Delta C_{p,w} T_{g,w} + y_s \Delta C_{p,s} (T_{g,s}^{\infty} - \frac{a_{FF}}{M})}{y_w \Delta C_{p,w} + y_s \Delta C_{p,s}} \quad 4.3$$

which simultaneously describes the effects of the water content and the molecular weight of the maltodextrin on the glass transition temperature. Equation 4.3 was fitted to the experimental data to obtain the $T_{g,s}^{\infty}$ and the a_{FF} parameters.

4.3.4. Rheology measurements

The rheological properties were investigated with a strain-controlled rheometer (MCR 502, Anton Paar). For viscosity measurements, solutions were first prepared at 20% (w/w) dry matter and subsequently concentrated using a rotational evaporator at 70 mBar at 50 °C as described by Both et al. (2019a). A shear rate sweep was performed using a concentric cup geometry (CC17, 16,660 mm x 24,858 mm (width x height), Anton Paar). The shear rate was logarithmically increased from 0.1 to 100 s^{-1}, with 15 measuring points with duration decreasing logarithmically from 300 to 1 s. Subsequently, the procedure was reversed, i.e. from 100 to 0.1 s^{-1} with 15 measurement points and logarithmically increasing duration of 1 to 300 s. Samples of varying dry matter content were measured in duplicate; once including the reversed procedure, and once without the reversed procedure.

Amplitude and frequency sweeps were performed on thin films using a parallel-plate geometry at 50 °C as was described by Both et al. (2019b). Thin films were prepared with an initial dry matter of 30-60% (w/w), followed by an equilibration step in a climate chamber (Memmert, Germany) at 50 °C for three days (Table A.4.1). Amplitude sweeps were performed to determine the extent of the linear viscoelastic regime. We tested a strain range of 0.1% to 100% at an angular frequency of 10 $rad \cdot s^{-1}$ with the normal force constant at 1 N. Frequency sweeps were subsequently performed at a shear strain of 0.05%. Data points (20) were collected over an angular frequency range of 0.01-100%. Measurements were done in duplicate or more.

4.3.5. Single droplet drying

Morphology development of maltodextrin solutions (30% (w/w) dry matter) during drying was studied using a novel sessile single droplet drying platform (Fig. 4.1). The droplet was dispensed by a PipeJet® NanoDispenser (BioFluidix, Germany) using 200-S PipeJet® Pipes (BioFluidix, Germany) on a hydrophobic membrane to retain the spherical shape (contact angle of the single droplet >100°) of the droplet (PF3010 Polytetrafluoroethylene membrane, pore size 25-35 µm, porosity 55-60%, thickness 1 ± 0.25 mm) (Polyfluor Plastics BV, The Netherlands). The dispensing was controlled to obtain a desired droplet volume using BioFluidix Control Software V2.9 connected to a stroboscope (BioFluidix, Germany).

Droplets were dried in heated air (RH = 0%) at 60 °C or 90 °C and a flow velocity of 0.3 m/s using an insulated air feed tunnel as was originally designed by Perdana et al. (2011). Deposited droplets had an initial radius (R_0) of 100 µm ± 15 µm and were followed for a

minimum of 20 s drying time w.r.t. their size and shape using a Monochrome USB 3.0 Camera (Edmund Optics, Germany) with a VZM™ 1000 Zoom Imaging Lens (Edmund Optics, Japan) at a frame rate of 35 fps. The obtained sequences were analysed for the initial droplet size and locking points via image analysis using Image J software (National Institute of Health, USA). The locking point, which represents the onset of morphology development, was defined as the first visual observation of shape deviation of the drying sessile droplet during video analysis. At this point, the spherical shape of the droplet becomes distorted and shows first signs of cavity formation/denting. For all the formulations dried, experiments were performed at least in triplicate at both 60 °C and 90 °C. Thus, all image and data analyses correspond minimally to triplicates.

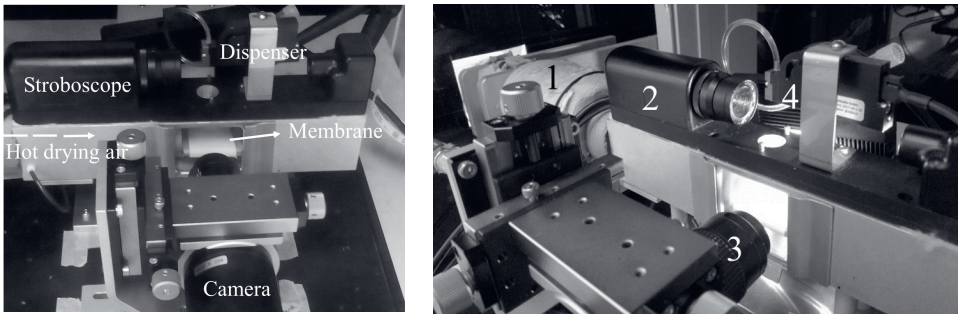

Figure 4.1. Sessile single droplet drying setup. Left picture provides a front view of the setup. The right picture shows (1) the insulated air tunnel, (2) the stroboscope, (3) the camera, (4) the PipeJet dispenser.

After drying, particles were studied using scanning electron microscopy (SEM). For SEM analysis, samples were fixed on the sample holder using carbon adhesive tabs. SEM images were taken at 5 kV, 3.7 pA, using a Phenom G2 Pure SEM (Thermo Fischer Scientific, The Netherlands). For all droplets a full image and a topographic image were made by a high sensitivity backscatter electron detector (Thermo Fischer Scientific, The Netherlands). Again, all analyses were performed in triplicate.

4.4. Results and discussion

4.4.1. Physicochemical properties

Higher DE-values have lower number average molecular weight (Rong et al., 2009). However, low DE-value maltodextrins in particular, represent a blend of saccharides with a broad molecular weight distribution (Chronakis, 1998). The molecular weight distribution influences for example the viscosity and glass transition temperature, parameters relevant to drying behaviour (Avaltroni et al., 2004; Castro et al., 2016). Therefore, we determined the molecular weight distribution of the maltodextrins (Fig. 4.2).

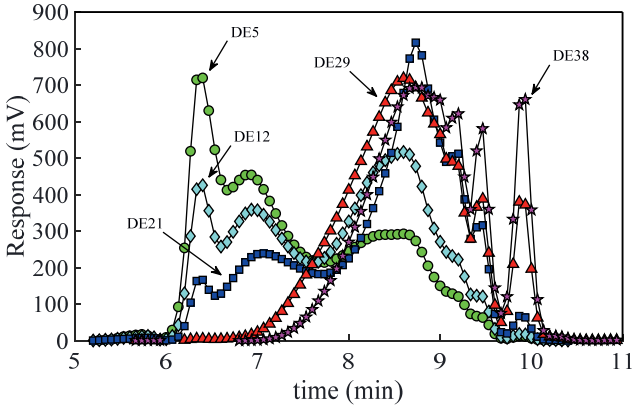

Figure 4.2. Molecular weight distribution for maltodextrin DE5 (circles), DE12 (diamonds), DE21 (squares), DE29 (triangles) and DE38 (stars). Molecules with higher molecular weight elute first, followed by low molecular weight components.

Maltodextrins DE5, DE12 and DE21 showed a broader distribution of molecular weights, with first elution peaks between 6 and 7 min and additional peaks after 8 min (Fig. 4.2). This broader distribution was also identified by Castro et al. (2016) for maltodextrins DE6, DE12, DE17 and DE19. The first peaks in Fig. 4.2 for DE5, DE12 and DE21 correspond to higher molecular weight polymers. Maltodextrins DE5 and DE12 showed higher peaks around 6 to 7 min than maltodextrin DE21, indicating that they contained a larger fraction of high molecular weight polysaccharides. Maltodextrin DE21, however, consisted of a larger fraction low molecular weight oligo-saccharides than maltodextrins DE5 and DE12 as can be observed from the higher peaks after 8 min. Overall, the molecular weight distribution of the analysed maltodextrins turned out to be narrower as DE-value increased, where maltodextrins DE29 and DE38 consisted mostly of low molecular weight sugars.

In addition to the molecular weight distribution, glass transition temperatures and viscosities for the different maltodextrins were measured as function of water content (Fig. 4.3 and 4.4). The latter was done as these are critical physicochemical parameters characterizing the functionality and the structure of a matrix during the drying process (Avaltroni et al., 2004; Palzer, 2010). We first measured and modelled glass transition temperatures as function of water content for the different maltodextrins (Fig. 4.3). In agreement with literature, increasing glass transition temperatures were obtained for decreasing DE-values at a given dry matter content (Dokic et al., 1998). We fitted the measured glass transition temperatures by combining Couchman-Karasz and Fox-Flory (Eqn. 4.3), where all measured data points were included to estimate $T_{g,s}^{\infty}$ and a_{FF}. The optimum parameters $T_{g,s}^{\infty}$ and the constant a_{FF} were found to be 460 ± 5 K and $54.8 \cdot 10^3 \pm 0.41 \cdot 10^3$ K·g/mol, respectively. The values of $T_{g,s}^{\infty}$ and a_{FF} were close to literature values found: 450 K for fructans and 475 K for glucose-based polysaccharides (van der Sman, 2013) and $53 \cdot 10^3$ K·g/mol for various types of maltodextrins (Avaltroni et al., 2004). From Fig. 4.3 it can be observed that the fitted equation is in agreement with the experimental data. For maltodextrins DE29 and DE38, more deviations between theory and experiments can be observed as these contain higher amounts of glucoses (van der Sman & Meinders, 2011). This is related to the Fox-Flory equation, which more accurately describes glass transition for polymers at intermediate and high molecular weight (Novikov & Rössler, 2013; van der Sman & Meinders, 2011).

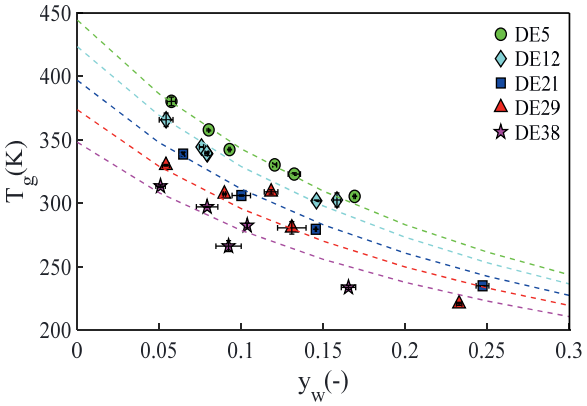

Figure 4.3. Glass transition temperature (T_g) measured for maltodextrins as function of water content of the sample. Dotted lines are the model predictions (green: DE5, cyan: DE12, blue: DE21, red: DE29, magenta: DE38).

In addition, viscosity was measured as function of concentration (Fig. 4.4A). All the shear stress-shear rate flow curves indicated Newtonian behaviour. From Fig. 4.4A it can be observed that maltodextrin DE5 had the highest viscosity upon concentration among the different DE samples, which was in line with our expectations based on the work of Avaltroni et al. (2004). Maltodextrins DE21, DE29 and DE38 showed quite similar viscosities upon concentration, which could be due to comparable molecular weight distributions (Fig. 4.2).

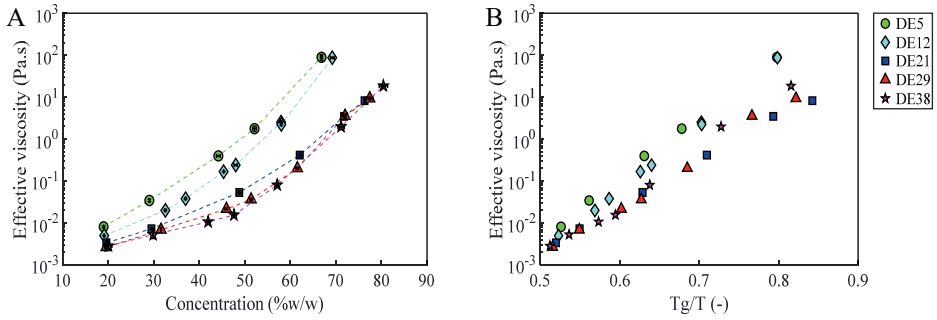

Figure 4.4. (A) Viscosity of maltodextrins as function of concentration (% (w/w)). Dotted lines are drawn to guide the eye. (B) Viscosity as function of T_g/T (-). Viscosities are measured in duplicate at 20 °C. T_g was calculated by Eqn. 4.3 based on the moisture content of the sample.

Additionally, we plotted the viscosity of the samples as function of T_g/T as it was demonstrated already that viscosity of various carbohydrate solutions is governed by the ratio of T_g/T (Dupas-Langlet et al., 2019; van der Sman & Mauer, 2019; van der Sman & Meinders, 2013; Williams et al., 1955). T_g values were computed using the Fox-Flory and Couchman-Karasz equation (Eqn. 4.3). Fig. 4.4B suggests indeed that the viscosity of maltodextrin solutions scales with T_g/T, where a steeper increase in viscosity as function of T_g/T was obtained for low DE-value maltodextrins.

4.4.2. Skin formation

Single droplets of maltodextrin solutions were dried at 60 °C and 90 °C to study the effect of DE-value on particle morphology development. Fig. 4.5 shows two time series of drying droplets as examples. An overview of all the time series collected at both drying air temperatures are presented in Fig. A.4.1 and Fig. A.4.2. Initially, a period of ideal drying was observed where mass transfer is externally limited and the droplet remains more or less spherical (Both, Karlina, et al., 2018). In this first drying period, the evaporation rate was observed to be similar for all different DE-values (data not shown), which is in agreement

with the findings of Both et al. (2018a). As the evaporation of water progresses, solutes accumulate at the droplet surface, resulting in a local increase of the viscosity near the droplet surface, which develops into a semi-solid thin layer referred to as a "skin". It is expected that all droplets eventually form a skin layer as the dimensionless Péclet number (ratio of the drying rate and the solute diffusivity in the droplet) quickly becomes >1 during our drying experiments (Vehring et al., 2007). The critical concentration at which this skin starts to influence the drying process is sometimes called "locking point" and can be considered the onset of the development of the morphology (Both, Karlina, et al., 2018; Tran, Avila-Acevedo, & Tsotsas, 2016).

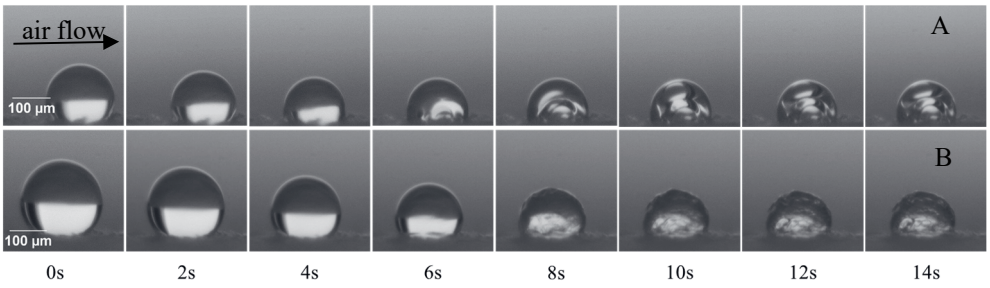

Figure 4.5. Morphology developments in time for (A) maltodextrin DE5 and (B) maltodextrin DE38. The droplets were dried at 60 °C and the air flow (0.3 m/s) came from the left side as indicated by the arrow.

We used the drop evolution images to analyse the relation between the locking points and the DE-value of the maltodextrins (Fig. 4.6A). Earlier locking points were obtained at higher drying air temperature as in agreement with Tran et al. (2016) and Both et al. (2018a) and explained by faster drying. Additionally, faster locking was observed for maltodextrin DE5 droplets than higher DE-value droplets dried at both drying air temperatures. This finding coincided with the observation that maltodextrin DE5 had the highest viscosity upon concentration among the different DE matrices (Fig. 4.4A), therefore it is likely that skin formation occurred earlier in the drying process. The normalized radius at the locking point as function of DE-value for both drying air temperatures is provided in Fig. 4.6B. A larger normalized radius was obtained at the locking point for lower DE-values (Fig. 4.6B). Faster locking at larger normalized radius for low DE-value droplets is supported by the work of Sugiyama et al. (2006), where it was observed that single droplets of high molecular weight components deformed earlier in the drying process, while they were still large, as opposed to droplets of low molecular weight components that deformed later during drying when they

were smaller. It should be noted from Fig. 4.6 that the drying air temperature influenced the locking point time, however, it did not affect the normalized radius at the start of morphology development; the relative size of the droplet at the onset of morphology development is temperature independent. This finding is in agreement with the work of Lin and Chen (2004), where they demonstrated that the drying air temperature had only little effect on the droplet diameter change during drying of 30% (w/w) initial solids droplets.

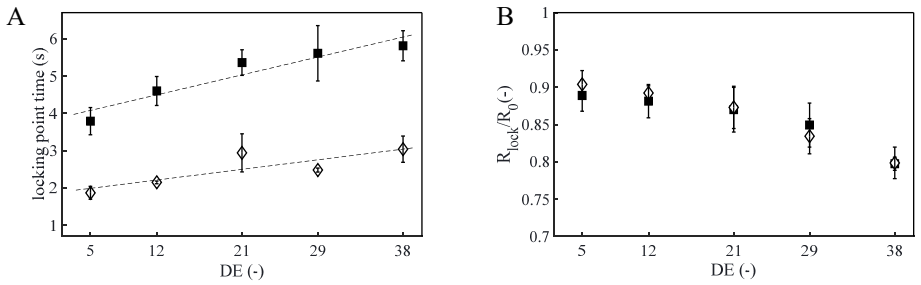

Figure 4.6. Droplets were dried at 60 °C (squares) and 90 °C (diamonds) (A) Locking point time as function of DE-value. Dotted lines are drawn to guide the eye. (B) Normalized radius (Rlock/R_0) at the locking point of the droplets as function of DE-value.

4.4.3. Rheological properties of maltodextrins at high concentrations

From the locking point on, different particle structures develop, which is greatly affected by the stability of the skin formed (Both, Tersteeg, et al., 2019; Pauchard & Allain, 2003; Sadek, Pauchard, et al., 2015). According to Pauchard and Allain (2003), skin stability is determined by both mechanical characteristics and by physicochemical properties of the system and their according time and space dependencies. Both et al. (2019b) demonstrated that oscillatory frequency sweep tests on equilibrated thin films at high dry matter concentrations can provide information on the resistance against deformation of the material studied. This information can then be linked to deformation of the droplets during drying. Therefore, we prepared partially dried thin films (≥80% (w/w) dry matter) and measured the frequency dependence of the loss and storage modulus in the frequency range of 0.01-100 rad/s (Fig. 4.7).

In Fig. 4.7A we compare the rheological response of thin maltodextrin DE5 and DE12 films at dry matter of 82% (w/w). At 82% (w/w) dry matter, maltodextrin DE12 films exhibit typical features of viscoelastic behaviour of polymers (Sperling, 2001; Sunthar, 2012). At low frequency the response was viscous and followed by a cross-over to a broad plateau region. This plateau region, where G' dominates over G'', is typically associated with

rubbery material and was already observed by Both et al. (2019b). For maltodextrin DE5 at 82% (w/w), G'' dominates of G' in the entire range of frequencies investigated, which implies viscous behaviour for DE5 at this dry matter. However, based on the rheological response of DE12, the molecular weight distribution (Fig. 4.2), the higher T_g and accordingly higher viscosity values found for maltodextrin DE5 (Fig. 4.3 and 4.4), we hypothesize that maltodextrin DE5 at this dry matter is in a transition region towards glassy behaviour. This was confirmed when we prepared thin maltodextrin DE5 films at dry matter content 90% (w/w). These films showed cracks on the surface, consistent with glass behaviour (Gianfrancesco et al., 2012). Beyond the angular frequencies measured here, G' will again dominate G'' as the maltodextrins are virtually immobile and thus exhibit glassy behaviour.

For the lower molecular weight maltodextrins DE21, DE29 and DE38, we were able to prepare thin films at a dry matter content of 93% (w/w). These films did not exhibit a rubbery region as the smaller sugar molecules cannot entangle. Fig. 4.7B shows viscous behaviour for the thin films of DE21, 29 and 38 at dry matter of 93% (w/w). These high value DE maltodextrins will likely exhibit only glassy behaviour at even higher dry matter contents (≥93% (w/w)).

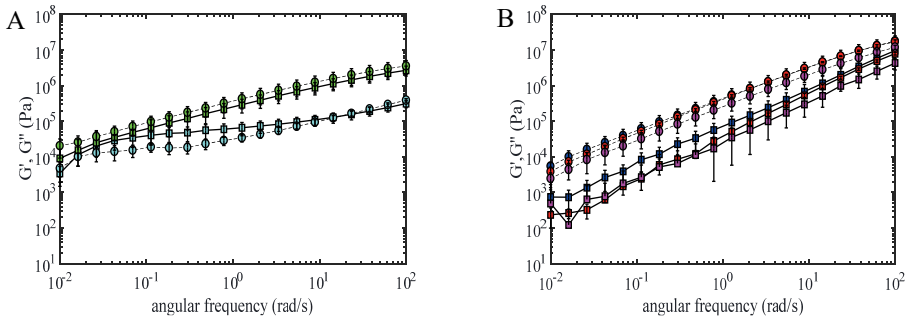

Figure 4.7. Storage and loss moduli (squares and circles, respectively) as a function of the angular frequency for (A) maltodextrins DE5 and DE12 (green: DE5, cyan: DE12) measured at 82% (w/w) dry matter, 0.54 mm thick; (B) maltodextrins DE21, DE29 and DE38 (blue: DE21, red: DE29, magenta: DE38) at 93% (w/w), 0.62 mm thick.

4.4.4. Final particle morphologies

An overview of the final morphologies as obtained after single droplet drying at both drying air temperatures is provided in a morphology diagram (Fig. 4.8). Generally, low DE-values resulted in smoothly shaped particles with large cavities, whereas higher DE-values showed more surface irregularities during drying and ultimately wrinkled particle morphologies

could be observed. Maltodextrin DE5 at drying air temperatures of 60 °C and 90 °C and maltodextrin DE12 at 60 °C formed smooth particles with large internal cavities and little or no surface distortions. These hollow particles with smooth surfaces were also observed after single droplet drying of unhydrolyzed starch solutions with 30% (w/w) initial dry matter at 80 °C and 140 °C (Gouaou et al., 2016). Maltodextrin DE12 showed a transition from a smooth surface after drying at 60 °C to a more dented structure after drying at 90 °C; hence, DE12 was just in between two regimes. A similar dented structure was previously observed by Both et al. (2018b) for sessile single droplet drying of maltodextrin DE12 at 90 °C (R_0 of ~550 µm). Dented morphologies were also observed for maltodextrins DE21, DE29 and DE38 at both drying air temperatures. Maltodextrins DE21 and DE29 showed very similar denting patterns; yet, for DE29 coarser edges were observed using scanning electron microscopy (Fig. 4.8 SEM column). Maltodextrin DE38 had a smoother and more furrowed pattern, with sometimes a few large indentations.

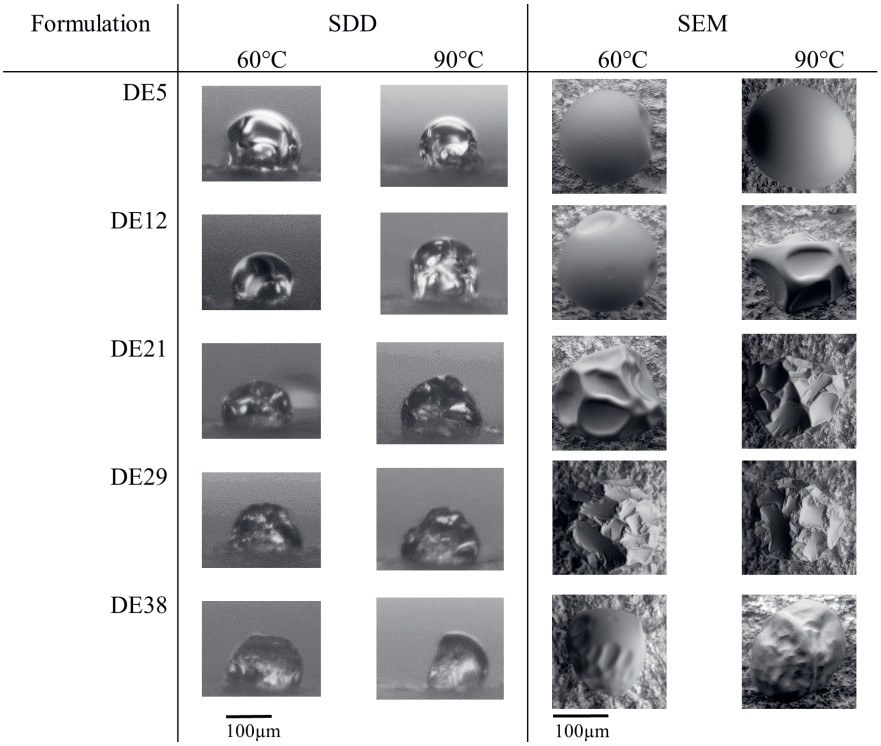

Figure 4.8. Final particle morphologies for the different maltodextrins when dried at 60 °C and 90 °C with a velocity of 0.3 m/s for droplets with R_0=100 ± 15 µm. Column named SDD shows the morphologies collected by the camera of the single droplet drying setup. Column SEM shows the scanning electron images of dried particles, note that these images are not necessarily the same droplets as shown in the SDD column. Scale bars are provided for the separate columns.

From locking onward, the temperature of the droplet will increase as shown in Fig. 4.9 (Ziaee et al., 2019). After locking, the temperature will gradually converge to the drying air temperature. We suspect that at this time, the skin stability will dictate the final morphology developed. If then the droplet temperature is in close proximity to its surface glass transition temperature, molecular motions are largely restricted to short-range rotational motions and vibrations, and droplet skins have adequate strength to resist most surface stresses developed during drying. Here, we expect that the morphology development is halted. These expectations are to some extent in line with the work of Werner et al. (2008), who concluded that mechanical stresses developed in droplet skins are related to the proximity of the surface to its glass transition.

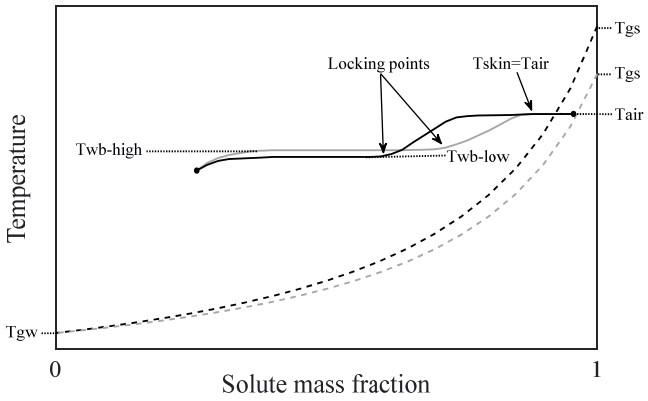

Figure 4.9. Schematic diagram showing the droplet temperature (Low DE: black solid line and high DE: grey solid line) during single droplet drying. Glass transition curves of the skin as function of solute mass fraction are drawn (Low DE: black dashed line, high DE: grey dashed line). When the droplet skin temperature is in close proximity to its surface glass transition temperature, morphology development is halted. T_{gw} and T_{gs} are the glass transition temperatures of the water and dry solute, respectively. Wet bulb temperature (Low DE: Twb-low and high DE: Twb-high) and temperature of the drying air (Tair) are indicated. Droplet temperature profiles differ for low and high DE maltodextrins as assumed based on locking point analysis and sorption isotherms (van der Sman & Meinders, 2011).

Low DE-value maltodextrins

The maltodextrins DE5 and DE12 dried at both drying air temperatures, developed a skin at an earlier stage than droplets with higher DE maltodextrins, which was explained by the steeper increase in viscosities upon concentration (Section 4.4.1). After locking, these droplets remained fairly spherical and developed large cavities (Fig. A.4.1 and A.4.2). The smooth particles obtained after drying, suggest that for these droplets a critical skin stability is reached relatively early in the drying process, close to the locking point. These stable skins

cannot deform on the timescales of the drying process and thus can withstand the internal stresses that are developed during drying. The spherical form of the droplet is therefore retained, and buckling instabilities are almost lacking (Giorgiutti-Dauphiné & Pauchard, 2018).

We suspect that this smooth and hollow morphology may be explained by the acquired skin elasticity soon after locking, resulting in skins that are more stable against surface stressed developed. The acquired elasticity can be confirmed by the observation of a broad rubbery plateau region for DE12 thin films at 82% (w/w) dry matter (Fig. 4.7A). Maltodextrin DE5 probably develop elastic skins earlier in the drying process than DE12, which is in agreement with Fig. 4.7A. The elasticity likely results from physical entanglement ($c > c^*$) due to the large fraction high molecular weight polysaccharides present, but there is also a chance it might result from retrogradation at lower temperatures (Sobolewska-Zielińska & Fortuna, 2010; Sperling, 2001). This elastic skin still allows for water evaporation, which makes the maltodextrin DE5 and DE12 droplets amenable to the formation of cavities. As water evaporates, the elastic skin is compressed, resulting in an increase in the elastic energy of deformation, which is reduced again by the formation of a cavity (Meng et al., 2014). Ultimately, the elastic skin approaches the glassy state, which happens earlier for maltodextrin DE5 droplets than DE12 droplets (Fig. 4.3).

It should be noted that maltodextrin DE12 droplets dried at 90 °C resulted in dented particles. The latter could be the consequence of a delayed glass transition; a higher drying air temperature could have resulted in an increase in the droplet temperature, consequently postponing transition to the glassy state. Therefore, it could be that DE12 skins at 90 °C exhibit rubbery behaviour for a longer drying time as compared to DE5 at 60 °C and 90 °C, and DE12 at 60 °C, possibly resulting in more surface instabilities. Thus, faster transition from elastic/rubbery to glassy skins may even further decrease the surface instabilities observed after drying.

High DE-value maltodextrins

Maltodextrins consisting of short oligomers and small sugars do not develop any form of elasticity shortly after locking. These droplets increase slowly in viscosity upon concentration, and after locking their skins will not be sufficiently stable to withstand stresses exerted on the droplet surface, leading to deformation of the surface. The latter was confirmed

by thin film rheology, where at a dry matter content of 93% (w/w), films with maltodextrin DE21, DE29 and DE38 still exhibited viscous behaviour (Fig. 4.7B). Most likely, skin stability is only obtained when the droplet surface approaches the glassy state (Fig. 4.9).

The final morphologies obtained here for maltodextrins with higher DE-values are well in line with the work of Li et al. (2011), who investigated surface wrinkling patterns on a core-shell soft sphere. Li et al. (2012) found that the morphological instability of a soft material can be divided into three distinct phenotypes: wrinkling, folding and creasing. Initially, during early stage of drying the sphere shrinks isotropically. During drying, the shrinkage of the soft sphere exceeds a critical value and the sphere will buckle and form a regular pattern of pentagons and hexagons to release the circumferential compression within the shell. This pattern is comparable to the final morphologies we here observe with maltodextrin DE12 at 90 °C and maltodextrin DE21 at 60 °C.

With further shrinking of the droplet, the phenotype changes from a wrinkling pattern to a folding pattern as some of the polygons merge with their neighbours, while others form troughs; such a pattern may be related to the morphologies obtained with maltodextrin DE21 at 90 °C and maltodextrin DE29 at 60 and 90 °C. When the troughs that are formed deepen and the ridges become sharper, eventually a labyrinthine topography is formed, which resembles the final morphologies that we obtained with maltodextrin DE38 at 90 °C. This type of morphology could be referred to as “creasing”, which is formed when an initial soft and smooth surface forms ridges or sulci.

4.5. Conclusions

Particle morphology development during spray drying is critical to the final powder properties. Maltodextrins are frequently spray-dried and can develop both a hollow sphere morphology and a wrinkled or creased morphology. Here we have investigated whether the dextrose equivalence (DE) of maltodextrins can be used as an indicator for the final powder particle morphology. To investigate this in detail, we employed a newly designed sessile single droplet dryer.

Low DE maltodextrins (≤12) are only slightly hydrolysed and have a broad molecular weight distribution. They exhibit higher glass transition temperatures and viscosities than high DE maltodextrins (≥21) consisting mostly of oligosaccharides. We showed that the viscosity of

maltodextrins can be described by the ratio of glass transition temperature to the system temperature T_g/T.

Morphology development with solutions of low DE maltodextrins starts relatively early in the drying process. We hypothesize that the skins of droplets with low DE maltodextrins show significant elasticity after locking. Thus, these are able to withstand surface compression, leading to smooth particles having cavities. These low DE-value maltodextrin skins approach the glassy state slightly later, halting morphology development. In contrast, high DE droplet skins do not develop significant elasticity after locking and these skins become mostly viscous, allowing deformation due to surface compression, leading to wrinkling, folding or creasing, depending on the viscosity during deformation.

Our results demonstrate that the DE-value is a critical parameter of the particle morphology, when it is interpreted in the context of process conditions. There is a direct link between the rheological properties at high concentrations and morphology development of powder particles. In the future, it would be worthwhile to further investigate the rheology of maltodextrins in the vicinity of the glass transition temperature. This will eventually allow better prediction of the morphology, which can then be used to predict powder properties such as flowability and rehydration behaviour. Key results of our study are summarized in Fig. 4.10.

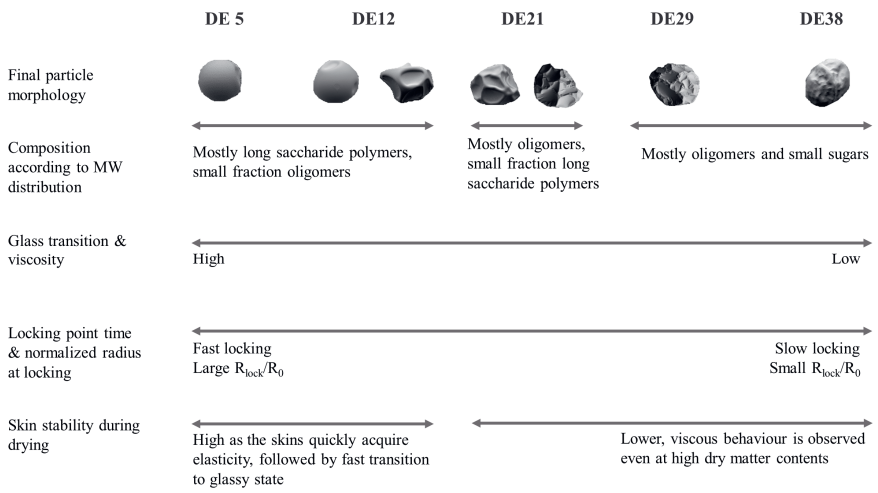

Figure 4.10. Summary of results relating to the final particle morphologies.

4.6. Appendix

Table A.4.1. Thin films for rheology measurements were prepared by partial drying of the solutions in an oven set at 80 °C, followed by an equilibration step in a climate chamber. Sample volumes, oven times and relative humidity (RH) of the climate chamber are indicated. NA indicates no partial drying in an oven was required before equilibration in the climate chamber. Average dry matter contents and thickness are provided.

	Sample preparation			Sample properties	
DE	Volume (mL)	Oven time (min)	RH (%)	D.M. % (w/w)	Thickness (mm)
5	6	115	82-85	82±0.5	0.62±0.11
12	6-7	115	85	82±0.3	0.45±0.01
21	4.5-5	NA	65	93±0.5	0.62±0.05
29	5	NA	55	94±0.2	0.61±0.04
38	5	NA	50	93±0.3	0.65±0.04

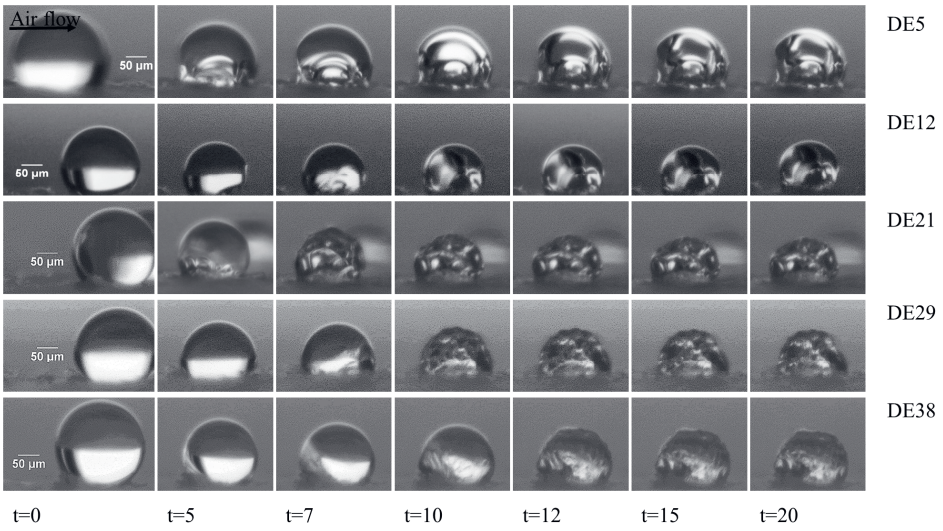

Figure A.4.1. Morphology development in time (s) for maltodextrins dried at 60 °C. The air flow (0.3 m/s) came from the left side as indicated by the arrow. R_0= 100 ± 15 µm.

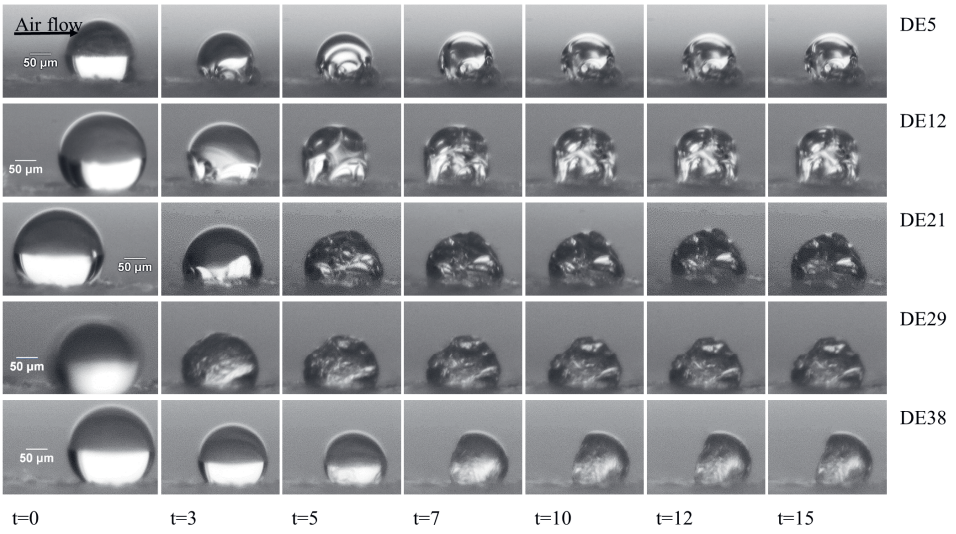

Figure A.4.2. Morphology development in time (s) for maltodextrins dried at 90 °C. The air flow (0.3 m/s) came from the left side as indicated by the arrow. R_0= 100 ± 15 µm.

Chapter 5

Rheological behaviour of concentrated maltodextrins describes skin formation and morphology development during droplet drying

This chapter has been submitted as Siemons, I., Veser, J., Boom, R.M., Schutyser, M.A.I., van der Sman, R.G.M. Rheological behaviour of concentrated maltodextrins describes skin formation and morphology development during droplet drying.

5.1. Abstract

We have studied the rheological behaviour of concentrated maltodextrins varying in dextrose equivalence value (DE) over a range of temperatures (≤70 °C) and concentrations (≥62% (w/w) solids) using small amplitude oscillatory experiments. Rheological data could be mapped onto master curves for storage and loss modulus as described with a model for transient or entangled polymeric networks. Maltodextrins DE5 and DE12 showed a rubber-to-glass transition, where the rubber-like behaviour is hypothesised to be the consequence of physical entanglements at sufficiently high concentrations of polysaccharides. Maltodextrins DE21 and DE38 mostly consisting of small sugars and oligomers exhibited viscous behaviour over a large range of frequencies and only at high frequencies the onset of a cross-over was visible which could signify the vicinity of the glass transition. An effective diffusion drying model validated with sessile single droplet drying experiments was coupled to rheological models to estimate rheological behaviour of the skin formed at the surface of the droplet during drying. The predicted rheological properties of the skin could be related to the occurrence of mechanical instabilities later during drying, including cavitation for elastic skins and wrinkling for viscous skins. Insight in rheological behaviour at high concentrations may therefore offer help in predicting the morphology of droplets generated with spray drying.

5.2. Introduction

The rheological behaviour of concentrated food systems is of importance for the design and optimisation of both processes and product properties. Examples of operations that involve materials that are concentrated in carbohydrates and/or proteins are extrusion, coating, evaporation and spray drying. In spray drying, the rheological behaviour of the concentrated feed solution is critical for the atomization into fine droplets, but also influences the particle structure evolution and agglomeration behaviour during drying, concomitantly co-determining the final powder properties (Both, Siemons, et al., 2019; Finotello, et al., 2017; Porfirio et al., 2020; Ubbink & Dupas-Langlet, 2020).

Various investigations studied the rheological behaviour of concentrated systems to provide better mechanistic insight of skin formation and subsequent morphology development during spray drying (Both, Siemons, et al., 2019; Le Floch-Fouéré et al., 2019; Sadek, Pauchard, et al., 2015; Sugiyama et al., 2006). For this, studies employed single droplet drying under controlled conditions to mimic the spray drying environment. For skin forming materials, the emergence of the rheological properties of the skin that is forming at the surface of the droplet during drying is hypothesised to be critical to the formation of wrinkles and/or cavities, and accordingly to the final particle morphology (Du et al., 2020; Wang & Cai, 2015). For example, cavity formation during drying of droplets consisting of colloidal dispersions or polymer solutions is suggested to be the result of the formation of an elastic skin that still allows for moisture evaporation (Bouman et al., 2016). The continued moisture evaporation through the skin and the resulting reduction of volume of the droplet, causes the skin to be compressed, followed by an increase in the elastic energy of deformation and a resulting lower pressure inside the droplet. The elastic compression is then reduced by the formation of a cavity to comply with the pressure reduction, rather than further shrinkage (Meng et al., 2014). Wrinkling phenomena may occur when droplet skins are thin and do not develop significant elasticity, allowing deformation due to surface compression (Du et al., 2020; Siemons et al., 2020). Wrinkling may in fact be followed by cavitation depending on elastic properties of the skin and the skin thickness developed during drying (Du et al., 2020).

In our previous study, we employed small amplitude oscillatory shear (SAOS) on concentrated thin maltodextrin films, which provided valuable rheological data that could be related to morphology development of maltodextrins during single droplet drying (Both, Tersteeg, et al., 2019; Siemons et al., 2020). However, rheology experiments were only

performed for films at one concentration and with a fixed temperature. As moisture content and temperature are continuously evolving during drying, it is important to assess the rheological behaviour over a wider range of concentrations and temperatures.

The rheology that needs to be investigated for drying spans a large range of conditions, to allow this, superposition principles may be used to connect the influences of time (frequency), temperature and concentration. To do this, one can study the frequency-dependent properties of materials, including storage (G') and loss (G'') modulus. The time-temperature superposition principle (TTSP) then poses, that the effects of time and temperature are related and can be combined in a master curve showing rheological behaviour covering a broad range of frequencies (Dealy & Plazek, 2009). For constructing a master curve, rheological data for one temperature and frequency are translated to the equivalent response at a different temperature by multiplying the frequency with a temperature-dependent shift factor (Dealy & Plazek, 2009; Kasapis, 2001). Several researchers already showed for various concentrated carbohydrate systems that master curves using TTSP can be constructed (De Freitas et al., 2015; Kasapis, 2001; Palzer, 2010; Tsoga et al., 1999). In more recent work by van der Sman et al. (2021), it was demonstrated for concentrated polysaccharides that the superposition principle could be extended to different frequencies, temperatures and concentrations, using the glass transition temperature divided by the temperature (T_g/T) as scaling parameter. The master curves constructed in the latter work partially resembled the universal master curve for entangled polymers (Groot & Agterof, 1995; Sperling, 2001), showing three zones: a rubbery plateau zone, a transition zone from rubber-like to glass-like behaviour and a glassy zone.

Here, we study the effects of time (frequency), temperature and concentration on the rheological behaviour of concentrated maltodextrins varying in dextrose equivalence value using SAOS testing. We constructed master curves, which map the rheological behaviour of maltodextrins at various temperatures and concentrations in a single plot. Master curves were described with a model for transient or entangled networks (Marin & Graessley, 1977). Horizontal shift factors, incorporating both the effect of temperature and concentration were collected. Finally, to discuss the added value of the obtained rheological insights, we discuss how the rheological behaviour can be connected to morphology development during drying. The latter was done on the basis of modelling of the temperature and moisture evolution

during droplet drying, using an effective diffusion drying model validated with sessile single droplet drying experiments.

5.3. Materials and methods

5.3.1. Materials

Maltodextrins with dextrose equivalence (DE) 5, 12, 21 and 38 were purchased from Roquette Frères (Lestrem, France). Solutions were prepared at a dry matter concentration of 30% (w/w) by adding maltodextrin powder to demineralized water and stirring for at least 30 min until the solution was transparent.

5.3.2. Preparation of concentrated samples and thin films

Concentrated maltodextrin samples were prepared by rotary evaporation or thin film preparation (Both, Siemons, et al., 2019; Both, Tersteeg, et al., 2019; Siemons et al., 2020). Rotary evaporation was performed to reach intermediate concentrations (~62-85% (w/w) solids depending on DE), while thin films were prepared to reach higher concentrations close to the glassy state (~80-95% (w/w) solids depending on DE).

The rotational evaporator (RC900, KNF, Germany) was operated at 30-70 mBar at 50-70 °C to concentrate 30% (w/w) maltodextrin solutions. Concentrated solutions were deaerated for 10 min to remove the entrapped air in an ultrasonic bath (5210E-DTH, Branson, USA). Thin maltodextrin films were prepared with an initial dry matter of 30-60% (w/w), followed by an equilibration step in a climate chamber (Memmert, Germany) at 50 °C for three days as was described by Siemons et al. (2020). The thin films varied in dry matter concentration depending on the set relative humidity of the climate chamber (Table A.5.1).

5.3.3. Small amplitude oscillatory shear testing

Small amplitude oscillatory shear (SAOS) was used to determine the linear viscoelastic (LVE) properties of concentrated maltodextrin systems using a MCR 502 Rheometer (Anton Paar, Austria). Thin film rheology measurements were performed using a parallel plate geometry with a ribbed probe with a diameter of 25 mm, 1 N force control. Maltodextrins concentrated with rotary evaporation were tested with stainless steel cone plate geometry with a diameter of 50 mm. A thin layer of paraffin oil was applied on the edge of the sample in order to prevent moisture loss during the measurements. Samples were allowed to rest and equilibrate for 15 min before testing. Amplitude sweeps were performed to determine the

extent of the LVE region with a shear strain range of 0.01-100.00% with constant angular frequency set at 1 rad/s for thin films and 10 rad/s for rotary evaporation samples. For frequency sweep tests a frequency range of 0.1-100 rad/s was used at fixed strains within the LVE region. Tests were carried out with a temperature range below 70 °C. An overview of all SAOS data is given in the supplementary data (Fig. S.5.1-S.5.6).

5.3.4. Constructing master curves

Master curves for G' and G'' were constructed in an iterative manner using a customized Python algorithm developed by van der Sman et al. (2021). The algorithm aims to match SAOS data at different temperatures and concentrations to the Marin-Graessley (MG) model for transient/entangled networks (Marin & Graessley, 1977). In this model the complex compliance ($J^* = 1/G^*$ and $G^* = G' + iG''$ with $i = \sqrt{-1}$) is given by:

$$J^*(\omega) = J_\infty \left[1 + \frac{1}{i\omega\tau_M} + \frac{k_p}{1 + \left(i\omega\tau_p\right)^p} + \frac{k_\alpha}{1 + (i\omega\tau_\alpha)^\alpha} \right] \quad 5.1$$

Where J_∞ (Pa^{-1}) is the compliance in the glassy regime ($J_\infty = \frac{1}{G_\infty}$), the first two terms of equation 1 represent Maxwell (viscoelastic) relaxation, the third term modifies the response in the plateau zone and the last term represents the α-relaxation (segmental relaxation). The latter two terms are expressions following a Cole-Cole type relaxation model. τ_M (s) is the relaxation time of the Maxwell relaxation mode, τ_p (s) is a characteristic relaxation time and τ_α (s) is the relaxation time of the α-relaxation. k_p and k_α (-) are related to the amplitudes in the plateau and transition zones, respectively. The scaling exponent α determines the shape of the curve in the transition zone, exponent p influences the shape of the curve in the plateau zone.

For matching SAOS data to the MG model, a method of least squares was used:

$$L_2 = \sum_i w_1 \left[\log\left(G'_{ref,i}(w_{ref})\right) - \log\left(G'_{new,i}(\omega \cdot a_T)\right) \right]^2 + w_2 \left[\log\left(G''_{ref,i}(w_{ref})\right) - \log\left(G''_{new,i}(\omega \cdot a_T)\right) \right]^2 \quad 5.2$$

$G_{ref,i}$ represents the reference master curve of the MG model, and $G_{new,i}$ represents the experimental data with frequencies shifted by horizontal shift factor a_T ($\omega \cdot a_T = w_{ref}$). w_1 and w_2 are weight factors, which we have chosen as $w_1/w_2 \approx 2$.

Horizontal shift factors a_T used to minimize the distance between the reference master curve of the MG model and experimental data were stored as a function of temperature divided by glass transition temperature (T_g/T). T_g was estimated as function of moisture content using the Couchmann-Karasz model (Couchman & Karasz, 1978):

$$T_g = \frac{y_w \Delta C_{p,w} T_{g,w} + y_s \Delta C_{p,s} T_{g,s}}{y_w \Delta C_{p,w} + y_s \Delta C_{p,s}} \quad 5.3$$

Here y_i is the mass fraction ($i = w, s$ for water and solute), $T_{g,i}$ is the glass transition temperature for the pure component ($T_{g,w} = 139$ K), $\Delta C_{p,i}$ is the change in the specific heat at the glass transition ($\Delta C_{p,w} = 1.91$ kJ/kg·K, $\Delta C_{p,s} = 0.42$ kJ/kg·K) (van der Sman & Meinders, 2011, 2013).

The glass transition of the anhydrous maltodextrin, $T_{g,s}$, can be described by the Flory-Fox relation (Avaltroni et al., 2004; Fox & Flory, 1950; Roos & Karel, 1991; Sman & Meinders, 2011):

$$T_{g,s} = T_{g,s}^{\infty} - \frac{a_{FF}}{M} \quad 5.4$$

$T_{g,s}^{\infty}$ (K) is the glass transition temperature for polymers with an infinite polymer chain length ($T_{g,s}^{\infty} = 475$ K), $a_{FF} = 5 \cdot 10^4$ K·g/mol and M$= 100 * \left(\frac{180}{DE}\right)$ is the number average molecular weight.

5.3.5. Modelling single droplet drying

The single droplet drying model was based on heat and mass transfer theories similar to previous studies (Adhikari et al., 2007; Mezhericher et al., 2010; Perdana, Fox, Schutyser, et al., 2013; van der Sman, 2003). The droplet has a uniform temperature throughout drying (Biot number (Bi) < 0.4) (Patel & Chen, 2008). Bi represents the ratio of external and internal heat flux, with the external heat transfer coefficient h_{ext} (W·m^{-2}·K^{-1}), the droplet radius r (m) and the effective heat conductivity λ_{eff} (W·m^{-1}·K^{-1}). In this study, Bi is around 0.12.

$$Bi = \frac{h_{ext} r}{\lambda_{eff}} \quad 5.5$$

The numerical model is based on the following differential equations for mass and energy transport:

$$\partial_t c_w + \nabla \cdot c_w \overrightarrow{u_s} = \nabla \cdot D_m \nabla c_w \quad 5.6$$

$$\partial_t \rho_{eff} c_{p,eff} T + \nabla \cdot \rho_{eff} c_{p,eff} T \overrightarrow{u_s} = \nabla \cdot \lambda_{eff} \nabla T \quad 5.7$$

c_i is the mass concentration ($kg \cdot m^{-3}$), u_i is the velocity of the moving mass ($m \cdot s^{-1}$) ($i = w, s$ for water and solute), D_m is the mutual moisture diffusion ($m^2 \cdot s^{-1}$), ρ_{eff} is the effective density ($kg \cdot m^{-3}$), $c_{p,eff}$ is the effective heat capacity ($J \cdot kg^{-1} \cdot K^{-1}$), T is the droplet temperature (K). Note that the above equations hold in the Eulerian frame. We will solve the equations in the co-moving Lagrangian frame of the shrinking droplet. Using the definition of the convective derivative $D_t = \partial_t + \nabla \cdot \overrightarrow{u_s}$, where D_t is the time derivative in the Lagrangian reference frame, the equations can be rewritten in a familiar form of Fick's and Fourier's law:

$$D_t c_w = \nabla \cdot D_m \nabla c_w \quad 5.8$$

$$D_t \rho_{eff} c_{p,eff} T = \nabla \cdot \lambda_{eff} \nabla T \quad 5.9$$

We will solve the energy and mass balance in spherical coordinates with the cell-centered Finite Volume scheme, using central differencing, and simple Euler forward time integration. As said, the model is solved in the Lagrangian frame of the solid material, meaning that the amount of solids remains constant throughout the computation. Only water will be exchanged between control volumes, which will change the volume of spherical shells. At each time step new positions, volumes and surface areas of the control volumes are computed, which are used to compute the diffusive mass and energy fluxes. For the temperature of the droplet we integrate the energy balance over the whole volume of the droplet.

The initial and boundary conditions are as follows:

$$c_w(r, t = 0) = c_{w,0} \qquad T(r, t = 0) = T_0$$

$$\partial_r c_w(r = 0) = 0 \qquad \partial_r T(r = 0) = 0$$

$$-D_m \, \partial_r c_w(r = R) = J_{evap} \tag{5.10}$$

$$-\lambda_{eff} \, \partial_r T(r = R) = h_{ext}(T - T_{air}) - \left[\Delta H_{evap,0} + \left(c_{p,v} - c_{p,w}\right)(T - T_0) \right] J_{evap} \tag{5.11}$$

ρ_{eff} λ_{eff}, D_m are moisture dependent material properties, with relations shown in Table 5.1. r is the radial coordinate (m), R is the droplet radius (m), $c_{w,0}$ is the initial water concentration (kg·m^{-3}), T_0 is the reference temperature for the enthalpy for evaporation, being 0 °C, T_{air} is the temperature of the bulk air (K), $\Delta H_{evap,0}$ heat of vaporization of water at 0 °C (J·kg^{-1}), $c_{p,v}$ and $c_{p,w}$ (J·kg^{-1}·K^{-1}) the specific heat of vapour and water, respectively.

The evaporative mass flux J_{evap} (kg·s^{-1}) equals:

$$J_{evap} = f_{cap} 4\pi R^2 \beta_{ext} M_w \frac{p_0}{R_{gas} T_{avg}} \ln\left(\frac{p_0 - p_{air}}{p_0 - a_w p_{sat}(T)}\right) \tag{5.12}$$

f_{cap} is a factor correcting for the fact that the droplet is not spherical, but it is sessile. β_{ext} (m·s^{-1}) is the external mass transfer coefficient, M_w (kg·mol^{-1}) molecular weight of water, p_0 atmospheric pressure, p_{air} air pressure and p_{sat} (Pa) saturation pressure at drop temperature T (K), $T_{avg} = (T_{air} + 2T)/3$ (K) is the estimated average temperature of the boundary layer, a_w is the water activity (-). As we use the cell-centered Finite Volume method we have to estimate c_w and T at the outer surface of the droplet via solving the boundary conditions with an implicit solver (bisection method).

Table 5.1. Closure equations used in drying model. The values of the parameters are indicated in Table A.5.2 and for material specific parameters the values can be found in Table S.5.2.

Equation name	Equation	Reference
Diffusion coefficient of water (Free volume theory)	$D_w = D_0 \cdot exp\left(\frac{-dE}{R_{gas}T}\right) \cdot exp\left(\frac{y_w \cdot V_{c,w} + \xi_b \cdot (1-y_w) \cdot V_{c,s}}{B}\right)$ with $B = y_w \cdot K_{w,w} \cdot \left(K_{s,w} - T_{g,w} + T\right) + (1-y_w) \cdot K_{w,s}\left(K_{s,s} - T_{g,s} + T\right)$	Vrentas & Dudas (1991); Siemons et al. (2019); van der Sman & Meinders (2013)
Diffusion coefficient of solute (Generalized Stokes Einstein relation)	$D_{s,0} = \frac{k_B \cdot T}{6\pi \cdot \eta_w \cdot a_0}$ with a_0 as the hydrodynamic radius (m)	Einstein (1905); Sutherland (1905) van der Sman & Meinders (2013)
Effective diffusion coefficient	$D_{eff} = D_{s,0} \cdot \frac{\eta_w}{\eta_{eff}}$ with $\log\left(\frac{\eta_{eff}}{\eta_0}\right) = 4q + 11q^2 + 10q^3$ and $q = \frac{T_g}{T - 0.35}$	van der Sman & Mauer (2019)
Mutual diffusion coefficient Darken relation	$D_m = Q_D \cdot \left(\varphi_w D_{eff} + (1-\varphi_w) \cdot D_w\right)$ with $\varphi_w = \frac{V_w}{V_{tot}}$ volume fraction of water (-)	Darken (1948); Siemons et al. (2019); Perdana et al. (2014b)
Water activity Flory-Huggins theory	$a_w = \exp\left(\frac{\mu_w}{R_{gas}\,T}\right) = \exp\left(\ln(\varphi_w) + \left(1 - \frac{1}{N_s}\right) \cdot (1-\varphi_w) + \chi_{eff} \cdot (1-\varphi_w)^2\right)$ $\chi_{eff} = \begin{cases} \chi_{ws}, & \chi_{ws} \le \chi_0 \\ \chi_{ws} - (\chi_{ws} - \chi_0) \cdot (\varphi_w)^2, & \chi_{ws} > \chi_0 \end{cases}$ with N_s the ratio of molar volume of solvent and solute, χ_{eff} the effective interaction parameter (-), χ_{ws} the interaction parameter of maltodextrin	Fox & Flory (1950); (1953); van der Sman & Meinders (2011)
External mass transfer coefficient	$\beta_{ext} = f_\alpha \frac{Sh\, D_{air}}{2R}$	
Sherwood number (Ranz Marshall)	$Sh = 2 + 0.6Re^{0.5}Sc^{0.33} = 2 + 0.6\left(\frac{U2R}{\nu_{air}}\right)^{0.5}\left(\frac{\nu_{air}}{D_{air}}\right)^{0.33}$	Ranz & Marshall (1952); (2007)
Alpha correction factor (Film theory)	$f_\alpha = \frac{\ln\left(1 + \frac{a_w p_{sat}(T) - p_{air}}{p_0 - p_{air}}\right)}{\frac{a_w p_{sat}(T) - p_{air}}{p_0 - p_{air}}}$	Bird et al. (1960); Adhikari et al. (2007)
Heat transfer coefficients	$h_{eff} = \frac{1}{\frac{1}{h_{int}} + \frac{1}{h_{ext}}}$ with $h_{ext} = \frac{Nu\,\lambda_{air}}{2R}$ and $h_{int} = \frac{\lambda_{eff}}{0.5\,r}$	
Thermal conductivity	$\lambda_{eff} = \varphi_w \lambda_w + \varphi_s \lambda_s$	
Effective density	$\rho_{eff} = \frac{1}{vspec} = \frac{1}{\frac{y_w}{\rho_w} + \frac{1-yw}{\rho_s}}$	
Nusselt number Ranz Marshall	$Nu = 2 + 0.6Re^{0.5}Pr^{0.33} = 2 + 0.6\left(\frac{U2R}{\nu_{air}}\right)^{0.5}\left(\frac{\nu_{air}}{\alpha_{air}}\right)^{0.33}$ with α_{air} as thermal diffusivity of air ($m^2 \cdot s^{-1}$)	Adhikari et al. (2007)

To correct for the supporting plate and consequently the reduced surface area of the sessile single drop (Fig. 5.1), A_{drop} was calculated based on changing wall angles $\delta = \pi - \theta$ (rad), height of the cap $h_{cap} = r\left(1 - cos(\delta)\right)$ (m) and height of the drop $H_{drop} = r\left(1 + cos(\delta)\right)$ (m) (Soh et al., 2016):

$$A_{drop} = 4\,\pi R^2 - 2\,\pi R h_{cap} = 2\pi R H_{drop} \quad 5.13$$

$$f_{cap} = \frac{A_{drop}}{4\pi R^2} \quad 5.14$$

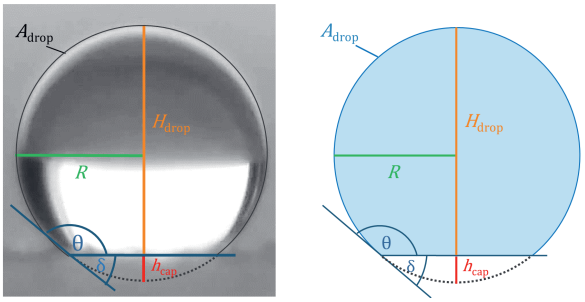

Figure 5.1. Geometry of sessile single drop as a sphere without cap with drop surface area A_{drop}, drop height H_{drop}, drop radius R, cap height h_{cap} as well as wall angle of droplet θ and of cap δ.

Non-uniform air flow and heat transfer were considered as the air flow pattern near the droplet is influenced by the supporting flat plate, although it is thin (Fig. 5.2) (Mosaad, 1999; Perdana, Fox, Schutyser, et al., 2013). For the thickness of the hydrodynamic boundary layer δ_U (m) the distance x_p=2.25 cm from start of the plate until where the droplet was located, the bulk air velocity $U_{air} = 0.3$ m·s^{-1} and the calculated kinematic viscosity of air $\upsilon_{air} = 2.2 \cdot 10^{-5}$ m^2·s^{-1} were used. The air velocity U and the air temperature T near the droplet were calculated using the height $z = R$.

$$\delta_U = 5\sqrt{\frac{\upsilon_{air} x_p}{U_{air}}} \quad 5.15$$

$$\frac{U}{U_{air}} = \frac{3}{2}\left(\frac{z}{\delta_U}\right) - \frac{1}{2}\left(\frac{z}{\delta_U}\right)^3 ; 0 \le z \le \delta_U \quad 5.16$$

For the thickness of the thermal boundary layer δ_t, the Prandtl Pr number is necessary. The temperature of the plate at distance x_p ($T_{p,x}$) was 70 °C (Table S.5.1).

$$\delta_t = \begin{cases} Pr^{-\frac{1}{3}}, & Pr \leq 1 \\ Pr, & Pr > 1 \end{cases} \quad 5.17$$

$$\frac{T - T_{air}}{T_{p,x} - T_{air}} = 1 - \frac{3}{2}\left(\frac{z}{\delta_t}\right) + \frac{1}{2}\left(\frac{z}{\delta_t}\right)^3 ; 0 \leq z \leq \delta_t \quad 5.18$$

The model was implemented in Python 3.8.3 with the programme Spyder 4.1.5 (Anaconda Inc., USA). Model parameters and material parameters are provided (Table A.5.2, Table S.5.1, S.5.2). The model was validated with single droplet drying experiments as described by Siemons et al. (2020, 2021). The experimental radius decrease and wall angles were obtained via image analysis toolbox from Matlab (Mathworks, USA) as described by Both et al. (2018a). Videos were analysed from the onset of drying until the mean locking point times for each DE as reported in previous work (Siemons et al., 2020). The locking point represents an indirect indication for the inception of the skin and from this point onwards the morphology starts to develop. Fits were obtained for three videos for the DE-values (Fig. S.5.7, S.5.8).

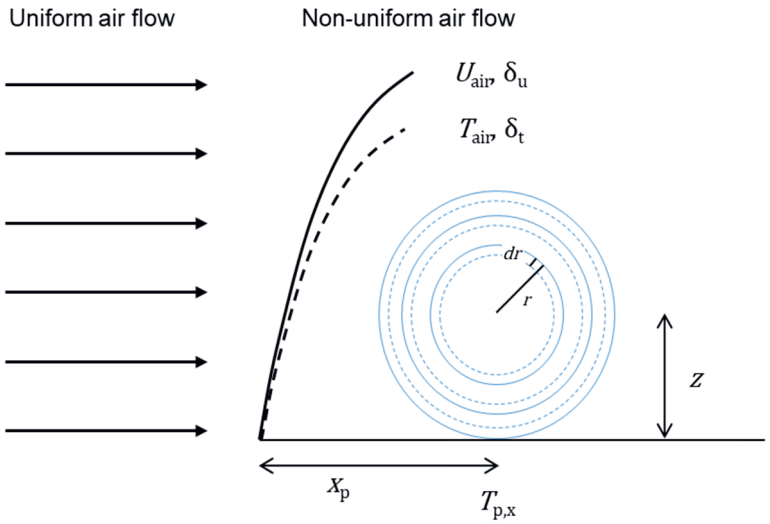

Figure 5.2. Schematic illustration of air flow distribution over flat plate with hydrodynamic boundary layer thickness δ_u with bulk air velocity U_{air} and thermal boundary layer thickness δ_t with bulk air temperature T_{air} as well as distance x_p, height z and temperature of plate $T_{p,x}$. The droplet is schematically illustrated with exemplary three different shells with radius decrease dr and outer radius r of each shell. The shells are calculated as spheres, the surface area and the radius of the whole droplet however are calculated as a reduced area and as the radius of a sphere without a cap, accounting for the sessile droplet. This is not shown in this figure.

5.3.6. Connecting rheological model and single droplet drying model

The connection of drying and rheological data was based on shear rates $\dot{\gamma}$ (s^{-1}) obtained from modelled radius decrease over time dr/dt ($m \cdot s^{-1}$). Therefore, the derivative of the modelled drop radius was obtained using the finite difference method with time step $dt = 0.001$ s (Fig. 5.2).

$$\dot{\gamma} = \frac{dr}{dt} \cdot \frac{1}{r} \tag{5.19}$$

According to the Cox-Merz rule, a shear rate can be directly translated into angular frequency ω ($rad \cdot s^{-1}$) in the linear viscoelastic range for certain materials, mostly linear homopolymers such as maltodextrins (Augusto et al., 2013; Cox & Merz, 1958; Dupas-Langlet et al., 2019; Ishii & Nakamura, 2020; Sillick & Gregson, 2009; Winter, 2009). Therefore, the calculated shear rate was directly translated to an equivalent angular frequency.

Besides shear rates, droplet temperature, glass transition temperature and accordingly horizontal shift factors (a_T) were calculated for each shell and drying time. The latter required fitting of log a_T values obtained from construction of master curves with a linear function of glass transition temperature and drop temperature $\left(\frac{T}{T_g} - 0.77\right)^{-1}$ with fitting parameter a and b (Liu et al., 2006).

$$\log a_T = a \left(\frac{T}{T_g} - 0.77\right)^{-1} + b \tag{5.20}$$

Note, that a and b are not independent parameters, as their relation is defined by the reference temperature for the shift factor. The calculated angular frequencies were multiplied with the calculated horizontal shift factors ($\omega \cdot a_T$) and with this G' and G'' could be obtained directly with the MG model.

5.4. Results and discussion

5.4.1. Dependence of viscoelastic behaviour of thin films on temperature

Small amplitude oscillatory shear data were first collected for maltodextrin thin films at a particular concentration as function of the temperature. The frequency dependence of the storage (G') and loss (G'') moduli at different temperatures between 20 to 70 °C of maltodextrin thin films varying in dextrose equivalence (DE) are shown in Fig. 5.3. The moduli of DE5 and DE12 films span roughly three orders of magnitude (Fig. 5.3A and C); at low temperatures elastic behaviour was observed, while at intermediate temperatures the films showed a transition from viscous behaviour at low frequencies to elastic behaviour at high frequencies. For the highest temperatures, a cross-over from elastic behaviour at low frequencies to viscous behaviour at higher frequencies was observed. DE21 and DE38 thin films showed viscous behaviour over the frequency and temperature range tested (Fig. 5.3E and G). Only at low temperatures did DE21 films exhibit a transition from viscous to elastic behaviour.

Master curves for G' and G'' were obtained by shifting the spectra horizontally along the frequency axis using the superposition algorithm (Fig. 5.3B, D, F and H). The master curves then describe the viscoelastic properties of the maltodextrin thin films over a broad frequency range. Especially, the sigmoidal transition found for DE5 (Fig. 5.3B) agrees well with a part of the universal master curve for entangled polymers (Groot & Agterof, 1995); indicating that the films are in a transition zone between rubber-like and glass-like behaviour. At low frequencies the storage modulus is the predominant response, followed by a sharp increase in moduli upon cooling the film. At high frequencies elastic behaviour is again dominant. Similar transition behaviour could be identified for DE12 (Fig. 5.3D) (G' ~ G''), although the sigmoidal shape is not as pronounced as for DE5. The rubber-like behaviour is likely the consequence of physical entanglements at sufficiently high concentration of long polymeric chains (Table A.5.3). According to Levine and Slade (1986) above a critical polymer concentration starch hydrolysis products with a DE≤6 should be capable of forming a gel network via entanglements, while Castro et al. (2016) state that entanglements may also be observed for DE≤12.

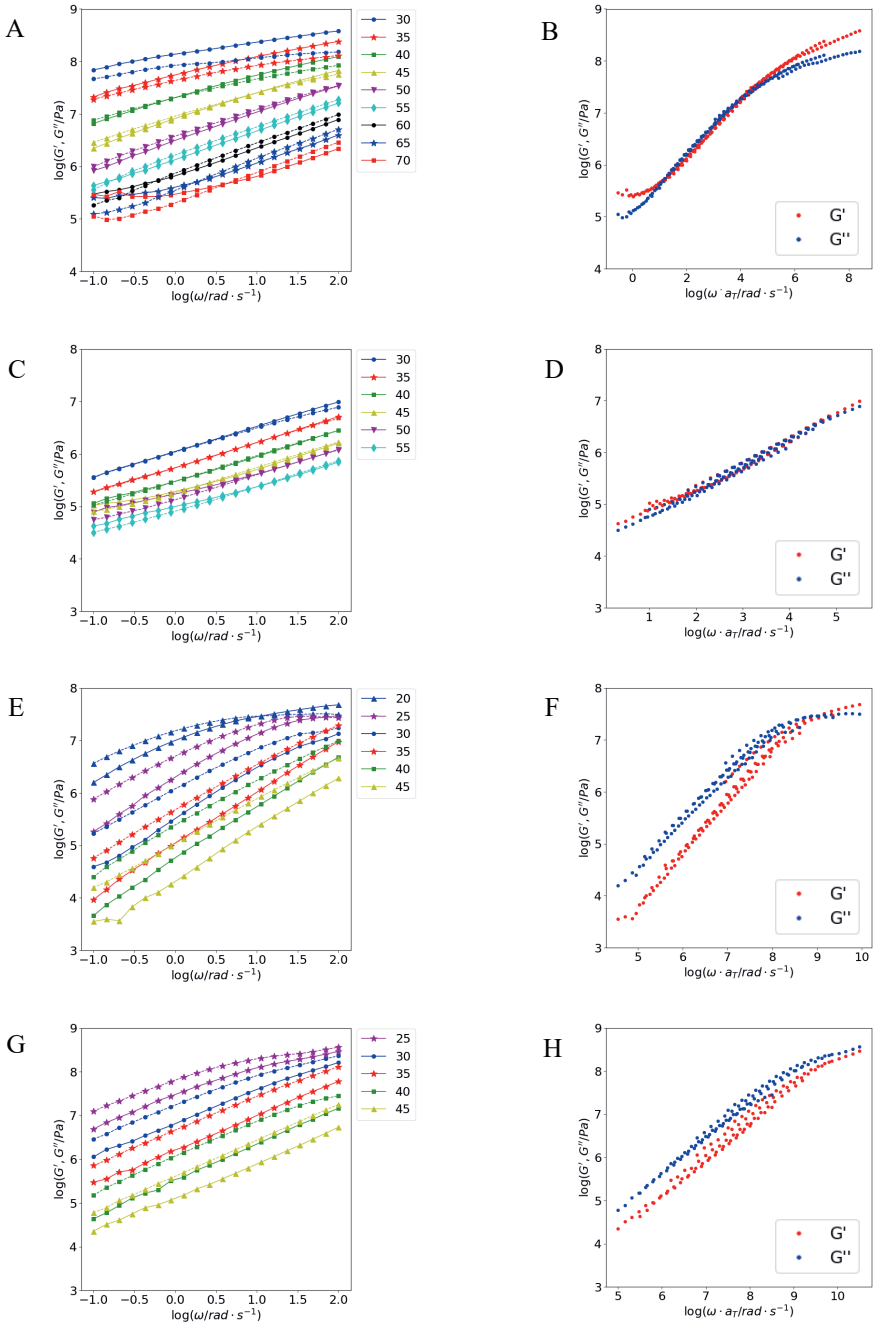

Figure 5.3. Left graphs are example mechanical spectra showing the frequency dependence of G' (straight lines) and G'' (dashed lines) of maltodextrin thin films at various temperatures (° C) and right graphs show the master curve (G' red diamonds and G'' blue circles) of maltodextrin thin films obtained by horizontal superposition along the frequency axis (A, B= DE5 at 84.1% (w/w), C, D= DE12 at 83.8% (w/w), E, F= DE21 at 85.1% (w/w), G, H= DE38 at 95.0% (w/w)).

The master curves of the DE21 and DE38 thin films (Fig. 5.3F and H) showed dominant viscous behaviour over a wide frequency window of roughly four decades. Above a DE of 20, maltodextrins mostly comprise of short oligomers and small sugars (Loret et al., 2004) (Table A.5.3). High DE maltodextrins are known to exhibit viscous behaviour even at relatively high solids concentrations, which is only changed to elastic behaviour upon approaching the glassy state (Siemons et al., 2020; Tsoga et al., 1999). The polysaccharides responsible for the entanglements and hence the rubber plateau for low DE maltodextrins are in high DE maltodextrins replaced by larger fractions of oligomers and small sugars that are more flexible and may reptate sufficiently fast, except in the vicinity of glassy state.

5.4.2. Dependence of viscoelastic behaviour on temperature and concentration

As moisture content and temperature are continuously evolving during drying, we further examined rheological behaviour of maltodextrins over a range of temperatures (10 °C - 70 °C) and concentrations (61.8% (w/w) - 95.0% (w/w) solids). From the data we constructed G' and G'' master curves as described by Marin-Graessley (MG) model (Fig. 5.4). The logarithm of the horizontal shift factors log (a_T) describes the combined effect of moisture concentration and temperature and is scaled with $(T/T_g\text{-}0.77)^{-1}$ (Fig. 5.5). Fitted model parameters are provided in Table 5.2.

For maltodextrin DE5 the master curve covers values from ~$10^{3.9}$ to $10^{8.7}$ Pa and a frequency range of twelve orders of magnitude (Fig. 5.4A and B). The master curves illustrate the presence of a rubbery plateau zone at low frequencies, followed by a remarkable rise in viscoelasticity, which is recognized as the transition region to glassy behaviour (Ferry et al., 1953; Groot & Agterof, 1995). The scaling exponent α was 0.65, resulting in dominating loss modulus in the transition zone. Similar scaling in the transition zone was reported by van der Sman (2021) for maltodextrin DE2 ($\alpha = 0.6$) (Table 5.2). As the frequency increases beyond the capability of the polysaccharides to respond, i.e. polysaccharides cannot attain their dynamic equilibrium configuration on the timescale of observation, the material glassifies and responds as a hard elastic solid (Ngai, 2011). In the glassy state the storage modulus may reach a maximum value of roughly 10^9 Pa and the loss modulus is expected to decrease (Sperling, 2001). This is however not clearly observed from Fig. 5.4, however it is more prominent in work reported by for instance Kasapis (2001) and van der Sman et al. (2021). The MG model describes the experimental data well, even though the experimental loss moduli deviate from the model at higher frequency values. This may be improved by obtain-

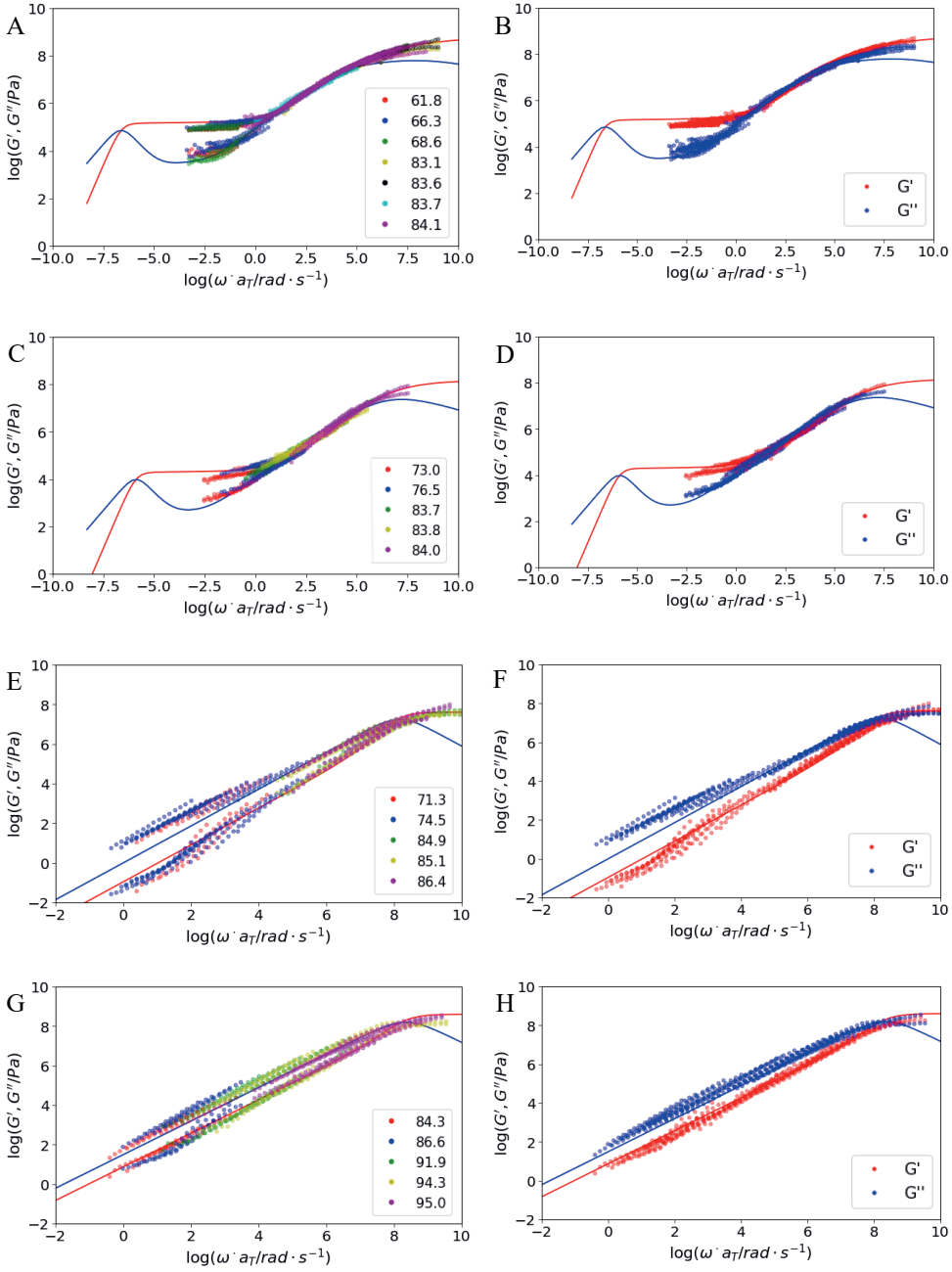

Figure 5.4. Master curve G' and G'' fitted to MG model for DE5 (A, B), DE12 (C, D), DE21 (E, F) and DE38 (G, H). The solids concentrations (% (w/w)) are indicated in different colours in the legends of A, C, E, G. Predicted G' and G'' are given in lines, red for G' and blue for G''.

ing the modulus in the glassy state, which in this model was based on roughly the highest G' value measured for thin films, even we know that the elastic modulus further increases as solids concentration increases or the temperature decreases beyond the range tested. The model also predicts the rheological behaviour at lower frequencies beyond the frequency range covered by the experimental data, where increased molecular motion as a consequence of increased temperature/decreased concentration may cause assemblies of polysaccharide chains to move in a coordinated manner and accordingly exhibit viscous flow (Sperling, 2001).

A similar viscoelastic pattern was observed for maltodextrin DE12 (Fig. 5.4C and D), with the scaling exponent α of 0.60 close to 0.65 for DE5 and similar as was found by van der Sman et al. (2021). Though the plateau modulus (G_N) differed from DE5 as the elastic modulus decreased from about 10^5 to roughly 10^4 Pa. We attribute this to a decreased concentration of long polymeric chains and hence a decreased crosslinking density of the polysaccharides (Ferry, 1980) (Fig. A.5.1 and Table A.5.3). Additionally, a higher DE (and thus lower average molecular weight) of the maltodextrins may result in decreasing plateau modulus as a consequence of decrease in molecular weight (Avaltroni et al., 2004; Marin & Graessley, 1977; Rong et al., 2009; Sunthar, 2012).

Master curves constructed for maltodextrins DE21 (Fig. 5.4E and F) and DE38 (Fig. 5.4G and H) show an analogous development in the moduli ranging over roughly eight orders of magnitude. For both maltodextrins G'' dominates G' over a broad range of frequencies, while at high frequencies the onset of a cross-over is visible which could signify the vicinity of the glass transition. The scaling exponent α approaches 1 and is 0.93 and 0.85 for DE21 and DE38, respectively. If the scaling exponent α is 1, following Cox-Merz, it suggests the system is behaving as a Newtonian fluid in the transition zone. Additionally, high DE maltodextrins did not exhibit rubber-like behaviour as may be explained by the absence of sufficiently high concentration polysaccharides to form an entangled network (Table A.5.3). High DE maltodextrins instead have a large fraction of small sugars present which may act as plasticizers, separating the polysaccharides from each other and making disentanglement easier. Due to the absence of a plateau region for high DE maltodextrins, the MG model is simplified by removing the third term of the model (which is required to broaden and flatten the response in the plateau zone) and k_α and τ_α are significantly increased (Marin & Graessley, 1977; van der Sman et al., 2021). This then results in such low G_N values that the

plateau zone is not involved in fitting of the model to the data. Practically, this implies fitting the model in absence of a plateau.

Table 5.2. Fitted model parameters for maltodextrins varying in dextrose equivalence (DE). DE2 data was obtained from van der Sman et al. (2021) *for comparison. Note that a and b are defined by the reference temperature for the shift factor, reference temperatures differ for the different DEs.*

Marin-Graessley parameters	DE5	DE12	DE21	DE38	DE2
τ_M (s)	10^3	10^2	10^3	10^3	10^3
τ_α (s)	0.5	0.5	$1 \cdot 10^{10}$	$1 \cdot 10^{12}$	0.5
τ_p (s)	$2 \cdot 10^3$	$6 \cdot 10^3$	-	-	-
k_α (-)	$3.5 \cdot 10^3$	$11 \cdot 10^3$	$8 \cdot 10^{16}$	$2 \cdot 10^{17}$	$3 \cdot 10^{-3}$
k_p (-)	$7 \cdot 10^2$	10^3	-	-	-
G_∞ (Pa)	$6 \cdot 10^8$	$1.5 \cdot 10^8$	$4 \cdot 10^7$	$4 \cdot 10^8$	$1 \cdot 10^9$
α (-)	0.65	0.60	0.93	0.85	0.60
p (-)	0.25	0.35	-	-	-
Linear fit shift factors					
a (-)	2.42	2.43	2.89	1.61	
b (-)	-6.64	-6.63	-5.30	-3.76	

The horizontal shift factors required for the construction of the master curves that capture both the effect of temperature and moisture concentration are shown in Fig. 5.5. Van der Sman et al. (2021) demonstrated that the horizontal shift factors for highly concentrated maltodextrins and starch are a function of T_g/T. Liu et al. (2006) also investigated the applicability of scaling the shift factors using T_g/T obtained by TTSP by comparing a variety of amorphous polymers and copolymers in the Arrhenius as well as non-Arrhenius regions (T_g/T from 0.5-1). They found a universal linear relation between log a_T and $T_g/(T-0.77T_g)$ with a slope of 3 in Arrhenius and non-Arrhenius regions. We indeed find a linear relation between log a_T and $T_g/(T-0.77T_g)$ for all the maltodextrins, where slopes vary from 1.6 to 2.9 depending on the DE. A universal slope of 3 was established for a variety of polymers by Liu et al., however as can be seen from the molecular weight distributions maltodextrins are

mixtures of polymers, oligomers and sugars which may have caused the slope to diverge from the universal value found for polymers (Fig. A.5.1).

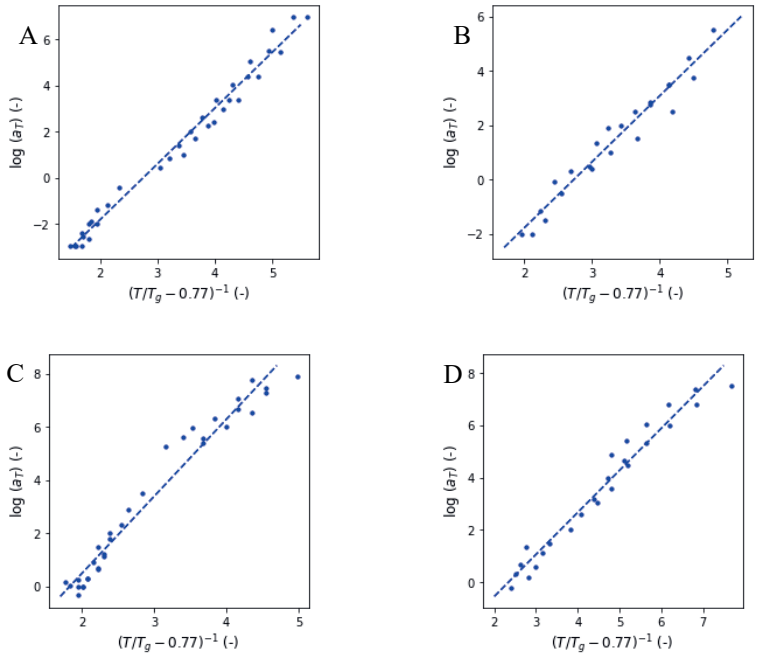

Figure 5.5. Horizontal shift factors (a_T) required to construct master curves as function of $(T/T_g\text{-}0.77)^{-1}$ for DE5 (A), DE12 (B), DE21 (C), DE38 (D). T_g is based on the moisture concentration of the sample as estimated with Couchman-Karasz and T is the experimental temperature of the mechanical spectra. Dotted lines are obtained by fitting with $\log a_T = a\left(\frac{T}{T_g} - 0.77\right)^{-1} + b$.

5.4.3. Linking rheological data to skin formation and morphology development

To illustrate the added value of the rheological data, we here discuss how rheological behaviour can be connected to morphology development during drying of solutions of maltodextrin DE5 (Fig. 5.6) and DE38 (Fig. 5.7). The drying kinetics could be described well with the model until inception of the skin, i.e. locking points (Fig. 5.6A, 5.7A, S.5.7, S.5.8). For DE38 the radius decreased a bit faster than the model predicted, which may be due to experimental variations in air and plate temperature. Based on the modelled drying kinetics, the shifted frequencies (shear rates) acting on the different droplet shells were predicted over drying time (Fig. 5.6B and 5.7B). The shifted frequencies evolved differently for the different shells of the droplet, accordingly resulting in a distinct evolution of the rheological properties for the different shells (Fig. 5.6C and 5.7C).

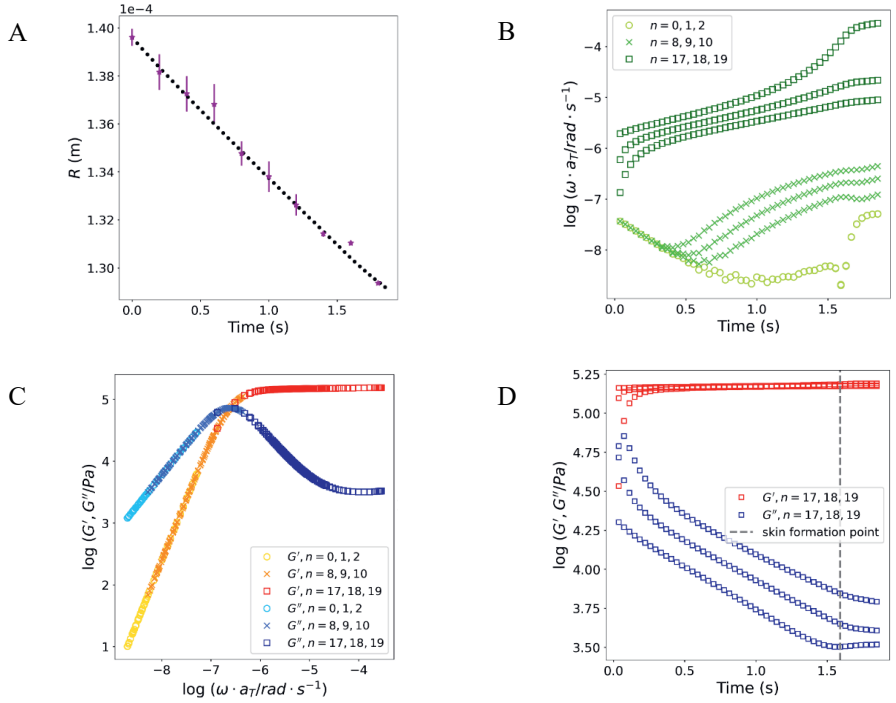

Figure 5.6. Radius decrease over time for single droplet drying of DE5 (30% (w/w) initial solids, air temperature 90 °C, air velocity 0.3 m/s) (A), SSE = $1.12 \cdot 10^{-12}$ m^2. Shifted frequency log $\omega \cdot a_T$ over drying time for different shells n (with n=0,1,2 for the inner shells, n=8,9,10 for middle shells and n=17,18,19 for outer shells) (B). G' and G'' as function of shifted frequency log $\omega \cdot a_T$ (C). G' and G'' as function of drying time for outer shells n=17,18,19 (D).

For the DE5 droplet, G'' is larger than G' for all inner shells, whereas middle and outer shells showed decreasing G'' for higher frequencies, eventually resulting in elastic behaviour (G' > G'') (Fig. 5.6C and D). The inner part of the droplet can therefore be characterised as viscoelastic liquid for the drying times investigated, while the middle and outer part showed a transition from a viscous material to an elastic material during drying. It is interesting to note that the elasticity of the skin is not caused by a strong increase of the storage moduli, but by a decrease of the loss moduli. For the DE38 droplet, G'' is always higher than G' (tan δ = G''/G' » 1) for all droplet shells, which suggests that both the interior and the skin remain viscous throughout the drying process (Fig. 5.7C and D). Other droplets studied for DE5 and DE38, confirmed the observed trends (Fig. S.5.9 and S.5.10).

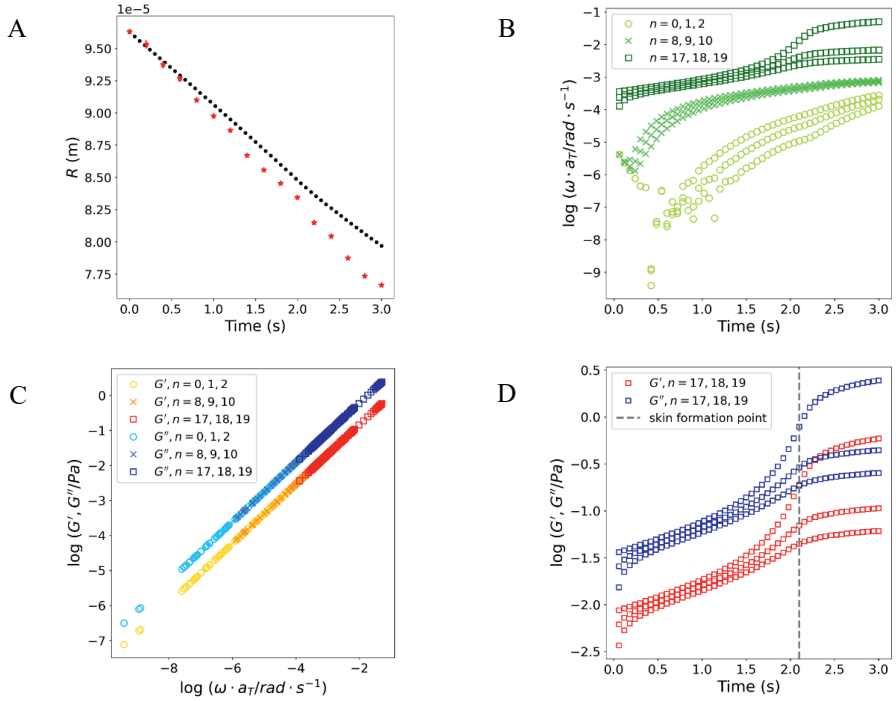

Figure 5.7. Radius decrease over time for single droplet drying of DE38 (30% (w/w) initial solids, air temperature 90 °C, air velocity 0.3 m/s) (A), SSE = 4.92·10^{-11} m^2. Shifted frequency log ω · a_T over drying time for different shells n (with n=0,1,2 for the inner shells, n=8,9,10 for middle shells and n=17,18,19 for outer shells) (B). G' and G'' as function of shifted frequency log ω · a_T (C). G' and G'' as function of drying time for outer shells n=17,18,19 (D).

Based on the rheological results as a function of the drying time, we attempted to define a skin formation moment. This was done as our hypothesis was that the rheological properties of the outer layers of the droplet at the skin formation moment can help explain the evolution of the surface during drying. For the skin formation moment, the point of steepest increase in log G' of the outer shell in combination with a characteristic change in tan δ was considered (Fig. 5.6D and 5.7D). For this, the derivative of log G' was determined by finite difference method and the maximal value of the derivative was selected as skin formation time; tan δ as function of drying time also showed a clear change in slope at this skin formation time (Fig. S.5.11). For DE5 this skin formation moment was roughly 0.5 s earlier than DE38 (1.6 s and 2.1 s, respectively). This earlier skin formation for low DE maltodextrins was previously suggested based on locking point analysis, where the locking points serve as an indirect indication for the inception of the skin (Siemons et al., 2020).

As previously mentioned, we consider the rheological properties of the outer layers at skin formation important in explaining the mechanical instabilities occurring later during drying. For maltodextrin DE5 at the defined skin formation point, dominant elastic behaviour is predicted for the outer shells of the droplet (Fig. 5.6D). This is likely the consequence of entanglements of the polysaccharides present. Elasticity is suggested important for explaining cavity formation (Bouman et al., 2016; Du et al., 2020). When an elastic/gelled skin is formed at the surface that is still permeable to moisture, ongoing evaporation of moisture from the core of the droplet will result in a skin with increased rigidity. At some point during drying the rigidification of the skin hampers further shrinkage, resulting in a decreasing pressure difference between the inside and outside of the droplet. This results in an inward elastic stress at the weakest point of the skin and consequently cavity formation (Fig. 5.8A). As soon as a cavity is formed, the pressure difference is eliminated, the compression stress on the skin is removed and wrinkling phenomena are repressed, eventually resulting in a smooth and hollow particle (Du et al., 2020). During skin formation moment for DE38, dominant viscous behaviour of all layers including the outer layers of the droplet is predicted. The droplet may therefore be considered a soft, viscous sphere and with increasing shrinkage, the pressure difference over the outer layers due to water evaporation leads to viscous deformation and wrinkle development (Fig. 5.8B) (Du et al., 2020; Li et al., 2011). The pressure/compressional energy is dissipated by viscous deformation and thus is not available to restore/retain the spherical shape as it is the case for the elastic skin of DE5 (Brinson & Brinson, 2015; Sperling, 2001).

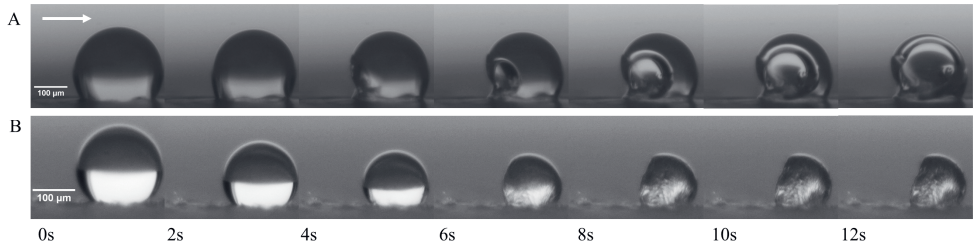

Figure 5.8. Particle morphology development (R_0 100 ± 40 µm) during single droplet dying at 90 °C of maltodextrin DE5 30% (w/w) (A), maltodextrin DE38 30% (w/w) (B). Air flow (0.3 m/s) came from the left as indicated in the figure by the arrow. Scale bars of 100 µm are provided.

5.5. Conclusions

Small amplitude oscillatory shear data of maltodextrins with different DE values as function of temperature and concentration could be mapped onto master curves for G' and G'' as described with a model for transient/entangled polymeric networks.

Low DE maltodextrins, containing a sufficiently large fraction of polysaccharides, showed a rubber-to-glass transition, whereas high DE maltodextrins mostly consisting of small sugars and oligomers exhibited viscous behaviour over a large range of frequencies. The presence of a rubber plateau zone for low DE maltodextrins is likely the consequence of physical entanglements at sufficiently high concentrations of polysaccharides. The logarithm of the horizontal shift factors for constructing the master curves could be linearly scaled with $T_g/(T-0.77T_g)$, therefore incorporating both the effect of moisture and temperature. We thus show a Time-Temperature-Concentration superposition principle for these systems.

Finally, we demonstrate that the rheological behaviour can be linked to droplet drying via a numerical model validated with single droplet drying experiments. The rheological properties of the skin formed at the surface of the droplet could indeed be related to the occurrence of mechanical instabilities i.e. cavitation or wrinkling.

Therefore, the morphology of the droplets for instance generated with spray drying can be predicted using the rheological properties of the materials. This will be a great help in guiding spray drying processes towards desired morphologies and powder properties.

5.6. Appendix

Table A.5.1. Thin films for rheology measurements were prepared by partial drying of the solutions in an oven set at 80 °C, followed by an equilibration step in a climate chamber. Sample volumes, oven times and relative humidity (RH) of the climate chamber are indicated. NA indicates no partial drying in an oven was required prior to the climate chamber. Range of dry matter contents are provided.

DE	Volume (mL)	Oven time (min)	RH (%)	D.M.% (w/w)
5	6-7	115	82-90	81-84
12	6-7	115	80-85	83-84
21	6-7	NA	65-71	84-86
38	5-6	NA	50-55	92-95

Table A.5.2. Parameter definitions, values and respective model symbols, sources of values are as indicated in the text.

Parameter	Definition	Value
a_{FF}	Flox-Flory fitting parameter ($J \cdot mol^{-1} \cdot K^{-1}$)	$5.00 \cdot 10^{4}$
$c_{p,s}$	Heat capacity of solute ($J \cdot kg^{-1} \cdot K^{-1}$)	1000
$c_{p,w}$	Heat capacity of vapour ($J \cdot kg^{-1} \cdot K^{-1}$)	1996
$c_{p,w}$	Heat capacity of water ($J \cdot kg^{-1} \cdot K^{-1}$)	4200
D_0	Diffusivity constant ($m^2 \cdot s^{-1}$)	$1.39 \cdot 10^{-7}$
D_{air}	Diffusion coefficient of air ($m^2 \cdot s^{-1}$)	$2.42 \cdot 10^{-7}$
$\Delta c_{p,s}$	Change in specific heat of solute ($J \cdot mol^{-1} \cdot K^{-1}$)	420
$\Delta c_{p,w}$	Change in specific heat of water ($J \cdot mol^{-1} \cdot K^{-1}$)	1910
dE	Activation energy to overcome neighbouring attraction ($kJ \cdot s^{-1}$)	1980
$dH_{evap,0}$	Heat of vaporisation of water at 0 °C ($J \cdot kg^{-1}$)	$2.50 \cdot 10^{6}$
dt	Iteration time step (s)	0.001
k_B	Boltzmann constant ($J \cdot K^{-1}$)	$1.38 \cdot 10^{23}$
$K_{s,s}$	Free volume parameter for solute (K)	69.21
$K_{s,w}$	Free volume parameter for water (K)	-19.73
$K_{w,s}$	Free volume parameter for solute ($m^3 \cdot kg^{-1} \cdot K^{-1}$)	$3.36 \cdot 10^{-4}$
$K_{w,w}$	Free volume parameter for water ($m^3 \cdot kg^{-1} \cdot K^{-1}$)	$1.95 \cdot 10^{-3}$
N	Total number of shells (-)	20
p_0	Atmospheric pressure (Pa)	$1.00 \cdot 10^{5}$
Q_D	Thermodynamic factor of Darken relation (-)	1.00
R_{gas}	Ideal gas constant ($J \cdot K^{-1} \cdot mol^{-1}$)	8.31

$T_{g,s}^{\infty}$	Glass transition of solute in infinity (K)	475
$T_{g,w}$	Glass transition temperature of water (K)	136
$V_{c,s}$	Specific critical free volume of solute ($m^3 \cdot kg^{-1}$)	0.59
$V_{c,w}$	Specific critical free volume of water ($m^3 \cdot kg^{-1}$)	0.91
x_p	Distance from droplet place on plate (m)	0.02
η_0	Zero viscosity of solute solution (Pas)	$2.20 \cdot 10^{-4}$
η_w	Viscosity of water (Pas)	$1.00 \cdot 10^{-3}$
λ_s	Thermal conductivity of solute ($W \cdot m^{-1} \cdot K^{-1}$)	0.33
ξ_b	Ratio of solvent and jumping units (-)	0.79
χ_0	Interaction parameter of water (-)	0.50

Molecular weight distributions

Molecular weight distributions of the different maltodextrins were determined by High Performance Liquid Chromatography (HPLC) using a Shodex KS-802 (7 µm) 8.0 × 300 (mm) + Guard column. The column is operated at 50 °C and connected to a refractive index (RI) detector (Shodex RI-501). Milli-Q water was used as eluent with a flow rate of 1 mL/min. The retention time of maltotridecaose, i.e. maltopolymer with degree of polymerization (DP) of 13, (Elicityl, France) was used to determine the fraction of sugars with a DP above and below 13.

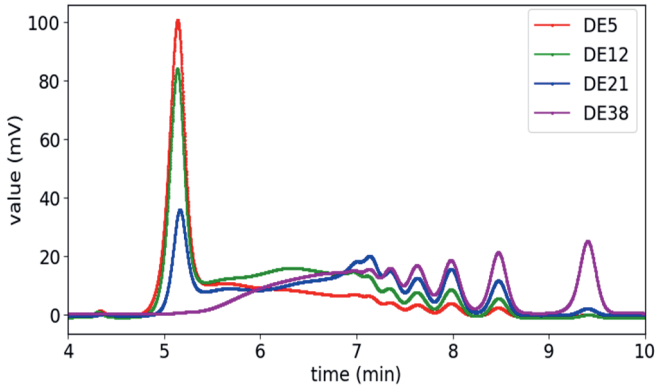

Figure A.5.1. Molecular weight distribution for maltodextrin DE5 (red), DE12 (green), DE21 (blue), DE38 (magenta). Molecules with higher molecular weight elute first, followed by low molecular weight components.

Table A.5.3. Relative sugar fractions (%) with degree of polymerization (DP) above and below 13 determined by relative peak areas.

DE	>DP13	<DP13
5	77.53	22.47
12	62.77	37.23
21	40.96	59.04
38	18.97	81.03

5.7. Supplementary data

Supplementary data will be made available online after publication. If needed it can be made available upon request by email to isabel.siemons@wur.nl/isabelsiemons006@gmail.com or ruud.vandersman@wur.nl.

Chapter 6

Protective effect of carrier matrices on survival of Lactobacillus plantarum WCFS1 during single droplet drying explained by particle morphology development

This chapter has been published as Siemons, I.[1], Vaessen, E.M.J.[1], Oosterbaan van Peski, S.E., Boom, R.M., Schutyser, M.A.I. Protective effect of carrier matrices on survival of *Lactobacillus plantarum* WCFS1 during single droplet drying explained by particle morphology development. *Journal of Food Engineering.* **2021**, 292. https://doi.org/10.1016/j.jfoodeng.2020.110263.

6.1. Abstract

Spray drying can be used to manufacture powder ingredients with lactic acid bacteria. Carrier matrices are used to increase survival of bacteria during drying; however, it is not exactly known why some matrices provide better protection than others. Depending on the carrier matrix and the drying conditions, different powder particle morphologies are obtained. Here, we employed single droplet drying to investigate the relation between particle morphology and survival of *Lactobacillus plantarum* WCFS1. Different carrier matrices with varying physicochemical properties were selected and dried at 90 °C (R_0 ~100 μm), yielding smooth, hollow or dented morphologies. A clear correlation was observed between the observed particle morphologies and the viabilities after drying. Highest survival (78-90%) was obtained for dense and smooth particles; low survival (2-8%) was obtained for dented particles. The relation between the morphology and survival is likely to be rooted in a complex interplay between matrix properties and dynamics, where a skin that hinders evaporation most resulted in the highest inactivation. The identified correlation between morphology development and bacterial survival will be important to identify the mechanisms of inactivation of bacteria during drying.

6.2. Introduction

Lactic acid bacteria are widely used in food production as starter cultures or probiotics. These bacterial food ingredients are often dried and stored in powder form to increase their shelf life (Broeckx et al., 2016; Huang et al., 2017; Peighambardoust et al., 2011). Freeze and spray drying are the main drying techniques that are used to industrially dry probiotics and starter cultures. Although during freeze drying the heat sensitive microorganisms are less exposed to heat as is the case during spray drying, spray drying is an interesting alternative since the drying time is shorter and the energy consumption is much smaller compared to freeze drying (Huang et al., 2017; Santivarangkna et al., 2007).

During spray drying, considerable inactivation of bacteria occurs due to thermal and dehydration stresses (Liu et al., 2018; Perdana, Bereschenko, et al., 2013). Therefore, bacteria are commonly dried in a protective matrix, consisting of for example carbohydrates, proteins or reconstituted skim milk to enhance their viability after drying (Broeckx et al., 2017; Perdana, Fox, Siwei, et al., 2014). The protective effect of these drying matrices, especially for sugars, is often explained by their ability to form a glassy matrix in which the cells are embedded and/or they may depress a phase change of the cellular membrane from liquid crystalline to gel phase (Broeckx et al., 2016; Leslie et al., 1995; Perdana, Fox, Siwei, et al., 2013). Additionally, the viability is also influenced by drying kinetics of the matrices, leading to a specific temperature-moisture content history of the droplets during drying (Ghandi et al., 2012b; Khem et al., 2015). In general, survival decreases considerably when the product is exposed to higher temperatures at higher moisture contents for a longer time (Liu et al., 2018; Perdana, Bereschenko, et al., 2013). The fact that some strategies lead to higher viability after spray drying shows that it is possible to increase the survival, though there is still a lack of insight in the reasons why some drying matrices result in better protection during spray drying compared to others.

Spray drying can yield entirely distinct particle morphologies depending on the carrier matrix and the applied drying conditions (e.g. smooth, hollow, dented) (Both, Karlina, et al., 2018; Siemons et al., 2020). Hitherto, particle morphology development during spray drying has been mainly studied with respect to physical powder properties such as bulk density and particle size (Both, Karlina, et al., 2018; Sadek et al., 2014; Schutyser et al., 2018). Some studies suggested that the development of the skin and the overall particle morphology during spray drying may also affect bacterial survival (Ghandi et al., 2012a; Khem et al., 2015, 2016;

Wang et al., 2016). However, it is not known whether the particle morphology and bacterial survival can be linked. We here therefore hypothesize that the particle morphology as influenced by the properties of the carrier materials and drying conditions also has a specific effect on the survival of bacteria during spray drying.

In this study we focused on drying of sessile single droplets to evaluate this hypothesis. Sessile single droplet drying allows for drying of small droplets which can provide insight into spray drying processes when dried under well-controlled conditions (Schutyser et al., 2018). This method allows us to visually monitor the particle morphology development and analyse bacterial survival for each droplet after drying. Different drying matrices were selected (trehalose, xylose, whey proteins, maltodextrins) that lead to distinct particle morphologies and have different physicochemical properties (e.g. different glass transition temperatures). *Lactobacillus plantarum* WCFS1 was used as a model probiotic bacterium. A systematic set of experiments was conducted to distinguish between the direct effect of the matrix on the survival of bacteria, and the effect of morphology, indirectly influenced via the rheological properties of the matrix (Siemons et al., 2020). The results may contribute to the development of spray drying processes leading to higher bacterial survival.

6.3. Materials and methods

6.3.1. Carrier materials

Five types of drying matrices were investigated for their protective effects during drying of *L. plantarum* WCFS1 cells, i.e. whey protein, trehalose, maltodextrin dextrose equivalence (DE) 19, maltodextrin DE5, and xylose. Whey proteins, purity 97.0-98.4% (BiPro®, Davisco, Switzerland), trehalose (Sigma Aldrich, USA), and xylose (Sigma Aldrich, USA) drying matrices were prepared at a dry matter concentration of 20% (w/w). The maltodextrin matrices (Roquette, France) had a dry matter concentration of 20% (w/w), 30% (w/w) or 40% (w/w) before drying. The protein matrices were stirred overnight at 4 °C to ensure complete hydration, while the carbohydrate matrices were stirred for a minimum of 30 min. All components were dissolved in demineralized water.

6.3.2. Microorganisms and pre-culture

Lactobacillus plantarum WCFS1 was obtained from the in-house strain collection. Pre-culture of this strain was performed according to the method described by Vaessen et al. (2018). *L. plantarum* WCFS1 was plated from a frozen stock on De Man, Rogosa and Sharpe

(MRS) agar. The plates were incubated micro-aerobically at 30 °C for 60-70 h. After incubation, the plates were stored at 4 °C until further use. From these plates a single colony was transferred into 10 ml MRS broth and grown for 24 ± 2 h at 30 °C. This culture was subsequently diluted 1:100 into fresh MRS broth and incubated overnight for 17 ± 1 h at 30 °C. This overnight culture was centrifuged at 13,500 × *g* for 10 min. The pH of the supernatant was measured to check the growth of the culture and was always 3.9 ± 0.1. The remaining pellet was washed once with a washing buffer (for composition see (Vaessen et al., 2018)) and centrifuged again using the same settings. After centrifugation the supernatant was discarded and the pellet was suspended in the carrier matrix. This culture in drying medium consisted of 3-4 · 10^9 CFU/ml.

6.3.3. Single droplet drying

The drying experiments were done using the single droplet drying equipment described earlier (Siemons et al., 2020). The droplets were dispensed by a PipeJet® NanoDispenser (BioFluidix, Germany) using 200-S PipeJet® Pipes (Biofluidix, Germany) on a flat hydrophobic membrane (Tetratex® ePTFE 3104 Polytetrafluoroethylene membrane, thickness 0.27 mm) (Donaldson Nederland B.V., The Netherlands). Droplets were dried for 20 s in a heated air flow from an insulated air feed tunnel (RH=0%) at 90 °C, at a flow velocity of 0.3 m/s. Deposited droplets had an initial radius (R_0) of 100 ± 20 µm, which is roughly in the upper part of the droplet size range in industrial spray dryers (Filková et al., 2014). The size and shape were recorded with a camera. A complete overview (including pictures) of the setup can be found in Siemons et al. (2020). The obtained sequences were analysed for the initial droplet size and locking point via image analysis using Image J software (National Institute of Health, USA). The locking point, which represents the onset of solidity and the morphology development, was defined as the first visual observation of shape deviation of the drying droplet during video analysis. The experiments were carried out in duplicate at least.

After drying, the particles were studied using scanning electron microscopy (SEM). For SEM analysis, samples were fixed on a sample holder using carbon adhesive tabs. SEM images were taken at 5 kV, 3.74 pA, using a Phenom G2 Pure SEM (Thermo Fischer Scientific, The Netherlands). For all droplets, a full image and a topographic image were made using a high sensitivity backscatter electron detector (Thermo Fischer Scientific, The Netherlands). The SEM analyses were performed at least in duplicate.

For each experiment with bacteria, first a droplet was dispensed and subsequently the membrane with the droplet was immediately transferred into a vial containing 1 ml phosphate buffered saline (PBS) for dissolution of the droplet. This was done at least in duplicate and these droplets served as the control, without drying. Additionally for each experiment two to six droplets were dried for 20 s at 90 °C. After drying, these droplets were kept on the membrane at room temperature for maximum 2 h until subsequent survival analysis. For each dispensed droplet the exact droplet volume was determined by stroboscopic images analysed by the Biofluidix Control Software V2.9 (BioFluidix, Germany) and used for the calculation of the survival.

6.3.4. Survival analysis

The dried droplets were rehydrated by transferring the membrane with the dried droplet into vials containing 1 ml PBS. After at least 10 min of rehydration, this culture was decimally diluted by pipetting 50 µl of this rehydrated culture into 450 µl PBS. The control droplets, which were dispensed but not dried, were also decimally diluted in the same way. Subsequently, the diluted cultures were plated in duplicate on MRS agar plates and incubated for 48-96 h at 30 °C under microaerobic conditions. After incubation, the plates were counted and subsequently these counts were used to calculate the survival. Firstly, for each droplet the average CFU of the duplicate plates was used to calculate the CFU/nl of the initial droplet by taking into account the dilutions and the exact volume of the dispensed droplet. Secondly, the survival was calculated by dividing the average CFU/nl of the dried droplet by the average CFU/nl of the control droplets.

6.3.5. Experimental setup

All drying experiments with bacteria were carried out at least in duplicate, with each replicate being a fully independent experiment performed with another pre-culture and on another day. Additionally, for each experiment, multiple non-dried control and dried droplets were taken into account, to minimize the experimental errors. The morphology development during single droplet drying was also evaluated for at least three droplets.

6.4. Results and discussion

6.4.1. Particle morphologies after single droplet drying

Trehalose, whey protein and maltodextrin DE19 solutions were dried at 90 °C using the sessile single droplet drying platform. In the initial phase of the drying process, the droplets decreased in size with similar rates, and remained spherical. After this initial drying phase, skin formation occurs due to an increased viscosity near the droplet surface. From the onset of the skin formation, often referred to as the locking point, the particle morphology starts to develop (Both, Karlina, et al., 2018; Siemons et al., 2020). In droplets with 20% (w/w) whey proteins we observed that an air vacuole started to develop shortly after the locking point (Fig. 6.1A). The final whey protein particle contained a large vacuole and had a smooth surface. The same morphology for whey protein particles was also observed in previous single droplet drying studies with droplets of a larger initial radius of ~500 µm at varying drying temperatures and whey protein concentrations (Both, Karlina, et al., 2018; Bouman et al., 2016; Sadek et al., 2013). Also Khem et al. (2016) observed this morphology after spray drying of *Lactobacillus plantarum* in the presence of whey proteins. The droplets with 20% (w/w) trehalose shrank continuously until a small, dense and spherical particle was obtained (Fig. 6.1B). For trehalose no clear onset of skin formation could be observed. Droplets with 20% (w/w) maltodextrin DE19 formed a dented morphology (Fig. 6.1C), which resembled the morphology of dried maltodextrin DE21 as was described before by Siemons et al. (2020). In a spray drying study, Paramita et al. (2010) also found dented particles with high maltodextrin concentrations and smoother particles with high trehalose concentrations for mixtures of gum arabic and these components. Overall, the different final particle morphology types that we observed were a smooth dense particle, a smooth particle with a large vacuole and a dented particle.

To link the microbial survival after single droplet drying to the particle morphology, we selected components with different properties but leading to similar morphologies. For this purpose, xylose, 20% (w/w) maltodextrin DE5 and 30% (w/w) maltodextrin DE5 were selected. Xylose is a monosaccharide that results in dense and smooth particles that are similar as those obtained with trehalose (Fig. 6.2). Drying of 20% (w/w) maltodextrin DE5 results in mostly dented particles, similar to maltodextrin DE19. However, maltodextrin DE19 had coarser edges and more smaller indentations, whereas maltodextrin DE5 had larger indentations with smoother edges (Fig. 6.2). Interestingly, when 30% (w/w) maltodextrin

DE5 was dried, a particle with a large vacuole was formed, similar to the morphology of whey protein. For almost all of the drying matrices, we observed consistent development of similar morphology for each dried particle; only in few cases for 20% (w/w) maltodextrin DE5 a vacuole was observed similar to our observations for drying of 30% (w/w) maltodextrin DE5 (Fig. 6.2). Therefore, both types of morphologies are displayed in Fig. 6.2. Additional time series for all components can be found in the Appendix (Fig. A.6.1).

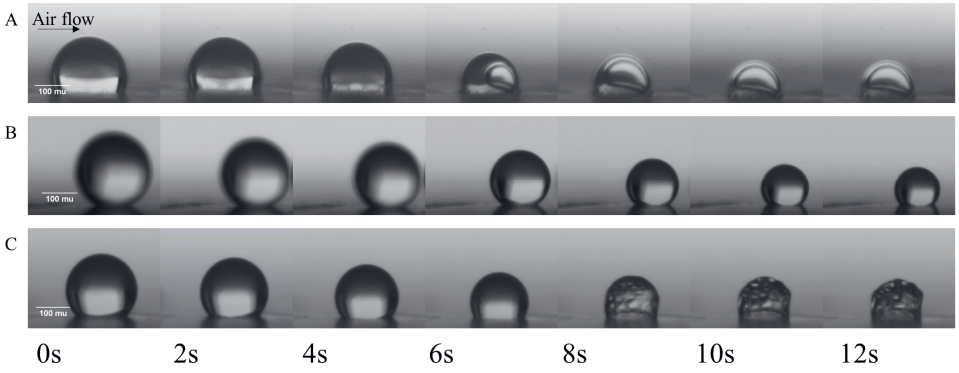

Figure 6.1. Particle morphology development during single droplet dying at 90 °C of whey proteins (A), trehalose (B) and maltodextrin DE19 (C) at 20% (w/w) initial solids concentration, R_0 100 ± 20 μm (mu indicates μm). Air flow came from the left as indicated in the figure by the arrow.

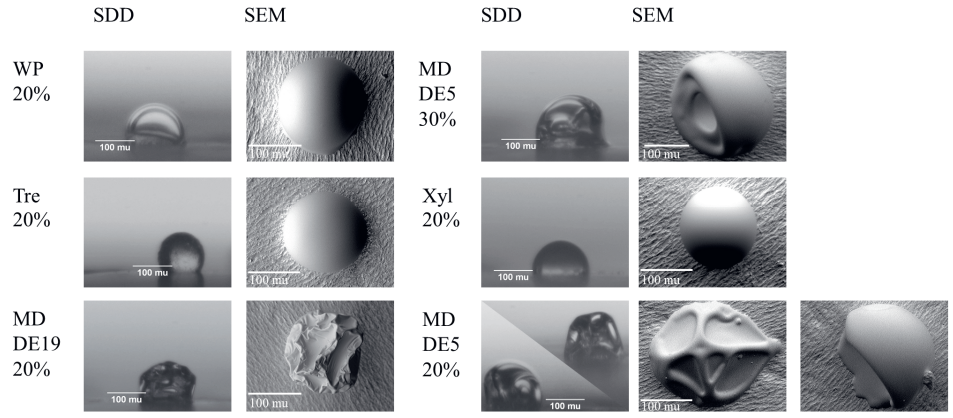

Figure 6.2. Final particle morphologies after single droplet drying at 90 °C of various drying matrices. WP=whey proteins, Tre= trehalose, MD DE19= maltodextrin DE19, Xyl= xylose, MD DE5= maltodextrin DE5. The initial solids concentrations are indicated in percentages and scale bars are indicated.

6.4.2. *Survival of L. plantarum WCFS1*

Survival of *Lactobacillus plantarum* WCFS1 after single droplet drying was evaluated for all drying matrices described in the previous section (Fig. 6.2). The survival was comparable for drying matrices that yielded similar particle morphologies (Fig. 6.3). The highest survival was observed with the matrices that yield dense smooth particles, namely xylose (90%) and trehalose (78%). The drying matrices that led to a smooth and hollow morphology resulted in moderate survival of 51% for whey proteins and 35% for 30% (w/w) maltodextrin DE5. Survival was lowest in drying matrices that resulted in dented particles, namely 2% for maltodextrin DE19 and 8% for 20% (w/w) maltodextrin DE5.

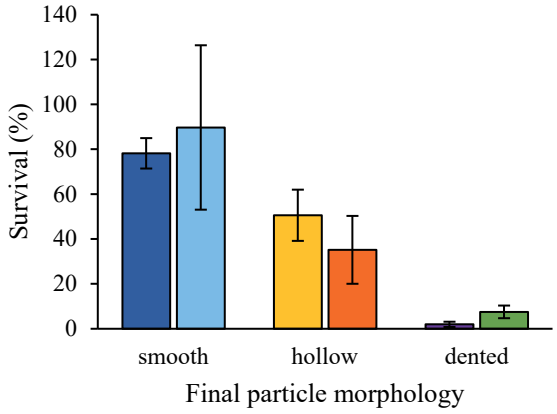

Figure 6.3. Survival of L. plantarum WCFS1 after single droplet drying at 90 °C in various drying matrices. The drying matrices were (from left to right): 20% (w/w) trehalose (dark blue), 20% (w/w) xylose (light blue), 20% (w/w) whey proteins (yellow), 30% (w/w) maltodextrin DE5 (orange), 20% (w/w) maltodextrin DE19 (purple) and 20% (w/w) maltodextrin DE5 (green). Error bars represent standard deviations of independent replicates (n≥2).

This lower survival for maltodextrin is in agreement with the study of Broeckx et al. (2017), who evaluated the survival of *L. rhamnosus* GG after spray drying, and found a higher survival with trehalose and lactose compared to maltodextrin DE6. Other studies reported a similar effect when comparing survival of *L. plantarum* WCFS1 in trehalose and maltodextrin (DE19, DE16 and 6) after spray drying (Perdana, Fox, Siwei, et al., 2014; Vaessen et al., 2020). On the other hand, Vaessen et al. (2020) found a similar survival of *L. plantarum* WCFS1 in whey protein and trehalose after spray drying and Khem et al. (2015) found a higher survival of *Lactobacillus plantarum* A17 after single droplet drying in whey proteins compared to trehalose as drying matrix. This latter study ascribes this to the high

temperature increase rates observed for trehalose droplets, while the temperature increase for whey protein droplets was more gradual. This is not in line with our observations. We speculate that the difference in drying conditions and drying time, e.g. 240 s in their study vs 20 s in our study, is relevant here.

The observed trends regarding survival of *L. plantarum* WCFS1 in the various drying matrices suggest that there is a relation between particle morphology development and survival of bacteria in this drying matrix. Though, before drawing further conclusions based on these observations, several aspects require further investigation. First of all, maltodextrin DE5 was used with two different concentrations; with a solids content of 20% (w/w) mainly a dented particle was formed, and with a solids content of 30% (w/w) a smooth particle with a large vacuole was formed. In line with the correlation that we found, the survival with 20% DE5 was low, while the survival with 30% was moderate. This means that the same type of drying matrix with different morphology gives different survival.

6.4.3. Effect of solids content and duration of constant rate period

We evaluated the survival of *L. plantarum* WCFS1 in maltodextrin DE19 and maltodextrin DE5 as drying matrices at various solids contents. Survival in maltodextrin DE5 increased from 8% to 35% with increasing solids content from 20% (w/w) to 30% (w/w) and changing morphology from predominantly dented to hollow (Fig. 6.2). For maltodextrin DE19 the increase in survival from 2% to 5% was not significant with the same increase in solids content (Fig. 6.4A). Further increasing the solids content to 40% (w/w) resulted in a slightly higher survival of 13%. For all of these matrices we found dented particle morphologies (Fig. 6.4B), where only the edges and indentations of the particles became less coarse upon increasing the initial solids content. Unfortunately, it was not possible to dry maltodextrin DE5 at 40% (w/w) as the viscosity was already too high for dispensing.

In literature, different effects of solids content have been reported for survival of bacteria after drying. For example, Perdana et al. (2014a) found that 2% (w/w) trehalose was sufficient to protect *L. plantarum* WCFS1 during drying, and found no further increase in survival by increasing the trehalose content further. Another study reported that increasing the content of gelatin, gum arabic or soluble starch from 10 to 20 and 30% (w/w) resulted in a lower survival of Bifidobacteria compared to 10% (w/w) (Lian et al., 2002). On the other hand, Ghandi et al. (2012a) reported an increase in survival of *Lacotococcus lactis* when this

strain was dried at higher solids contents. For example, the survival increased from 9 to 22% when increasing the solids content of a lactose-sodium caseinate carrier from 10 to 35% (w/w). Würth et al. (2018) described a decrease in survival of *L. paracasei* when increasing the solids content of a skim milk concentrate from 12.5% (w/w) to 35% (w/w). Important to note is that all the previous authors kept the amount of bacteria in the feed solution constant, whereas Würth et al. (2018) kept the biomass to solids ratio constant. Additionally, they found a strong correlation between the particle size of the spray-dried particle and bacterial survival; a smaller particle resulted in better survival. They relate this to the solids content, with lower solids contents leading to a smaller final particle and a prolonged constant rate period (Würth et al., 2018). To evaluate whether the duration of this constant rate drying period can be linked to survival, we used the locking point as measure for the duration of the constant rate drying period (Fig. 6.5).

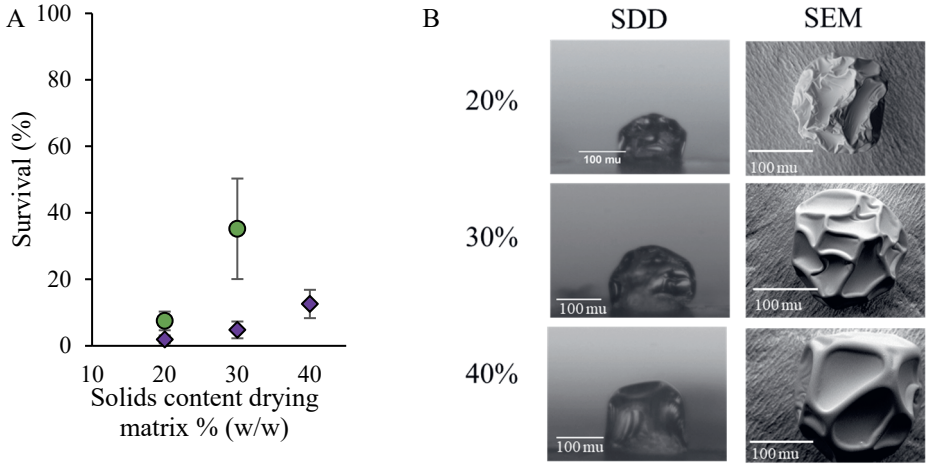

Figure 6.4. Effect of solids content on survival of L. plantarum WCFS1 (A) and particle morphology (B). (A) Survival of L. plantarum WCFS1 in maltodextrin DE19 (purple diamonds) and maltodextrin DE5 (green circles). Error bars indicate standard deviations of independent replicates (B) Final particle morphologies after single droplet drying at 90 °C of maltodextrin DE19 at various solids content, i.e. 20,30 and 40% (w/w).

The determination of the locking point was based on the visual analysis of droplet drying videos. At the locking point, the spherical shape of the droplet becomes distorted and shows first signs of cavity formation or denting (Siemons et al., 2020). The droplets with trehalose and xylose did not exhibit a clear locking point. These droplets have a longer constant rate period (Fig. A.6.2), and did not show any distortions from spherical shape, eventually resulting in small spherical particles. This was expected as for these small sugars the solute

diffusivity is faster or comparable to the drying rate (Vehring, 2008; Vehring et al., 2007). Therefore, the saturation at the droplet surface is reached late in the drying process with relatively homogeneous distribution of these sugars in the droplet. Overall, we did not observe a consistent relation between the locking point time, i.e. the duration of the constant rate period and the survival of *L. plantarum* WCFS1 after drying (Fig. 6.5).

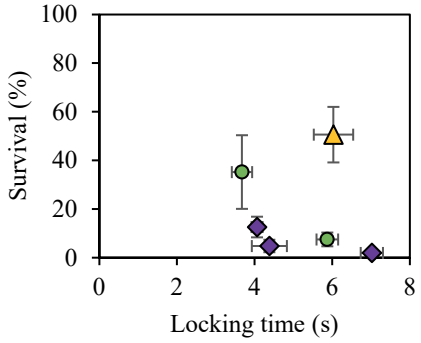

Figure 6.5. Survival of L. plantarum WCFS1 after single droplet drying in several drying matrices as a function of the locking time. The drying matrices are whey proteins (yellow triangles), maltodextrin DE5 (green circles) and maltodextrin DE19 (purple diamonds). Horizontal error bars represent the standard error of the locking point analysis and vertical error bars represent the standard deviation of bacterial survival. The matrices with trehalose and xylose did not exhibit a clear locking point.

Several single droplet drying studies described that the inactivation during the constant rate period is limited, probably due to the low droplet temperature (wet bulb temperature) during this period. These studies show that most inactivation took place during the second, falling rate period of drying (Khem et al., 2015; Zheng et al., 2015). In this period, diffusion limitation is dominant and the droplet temperature increases gradually towards the air temperature. If this happens when the droplet is still high in water internally, this will result in strong thermal inactivation. Therefore, it is expected that the microbial survival rate is more strongly coupled to the processes in the falling rate period, than it is to processes in the constant rate period.

6.4.4. Effect of physicochemical matrix properties

The physical state of the matrix during drying, i.e. glassy or non-glassy, is considered important to the survival of probiotics during and after drying (Santivarangkna et al., 2011). As the evaporation of water progresses during drying, the viscosity of the droplet surface will increase until the surface reaches a critical temperature and moisture content, at which the matrix will behave as a glass. The extremely high viscosity of amorphous glassy matrices ($\geq 10^{12}$ Pa·s) effectively halts diffusion-controlled deterioration reactions, improving the chemical and physical stability of the embedded bacterial cells (Aschenbrenner et al., 2012; Schutyser et al., 2012).

Carrier materials with a high glass transition temperature (T_g) are expected to provide a glassy matrix earlier during droplet drying or soon after drying upon cooling (Perdana et al., 2012; Perdana, Fox, Siwei, et al., 2014). We estimated the T_g as function of moisture content for every component studied in this work using the Couchman-Karasz theory (Fig. 6.6A). This theory is further explained in the Appendix.

Maltodextrin DE5 has the highest T_g for moisture contents below 0.3 kg water/kg, followed by maltodextrin DE19 and trehalose, whey proteins and xylose (Fig. 6.6A). In Fig. 6.6B the survival is given as function of the T_g of the anhydrous matrix. Fig. 6.6B indicates that a higher T_g of a matrix is not directly correlated to higher retention of viability after drying. In particular, the survival percentages found for *L. plantarum* WCFS1 after drying in maltodextrin and xylose matrices contradict the hypothesis that matrices with high T_g offer higher degree of survival after drying.

While entering the glassy state at an early stage during drying in principle should offer better survival, it also halts the drying process itself by reducing the water diffusivity (Ribeiro et al., 2002; Zobrist et al., 2011). For maltodextrin matrices, it is expected that the skin that is formed upon concentration will quickly move towards the glass transition, where the viscosity increases dramatically, and water diffusivity is strongly reduced. The decreased water diffusivity causes the droplet temperature to increase, while the viscosity of the skin remains high due to ongoing evaporation. The relatively fast skin formation followed by a quick approach of the glassy state may result in a short constant rate period, and a quickly rising droplet temperature, while the droplet interior may still have relatively high water content. Especially the combination of elevated temperature and high moisture content may lead to extensive microbial inactivation.

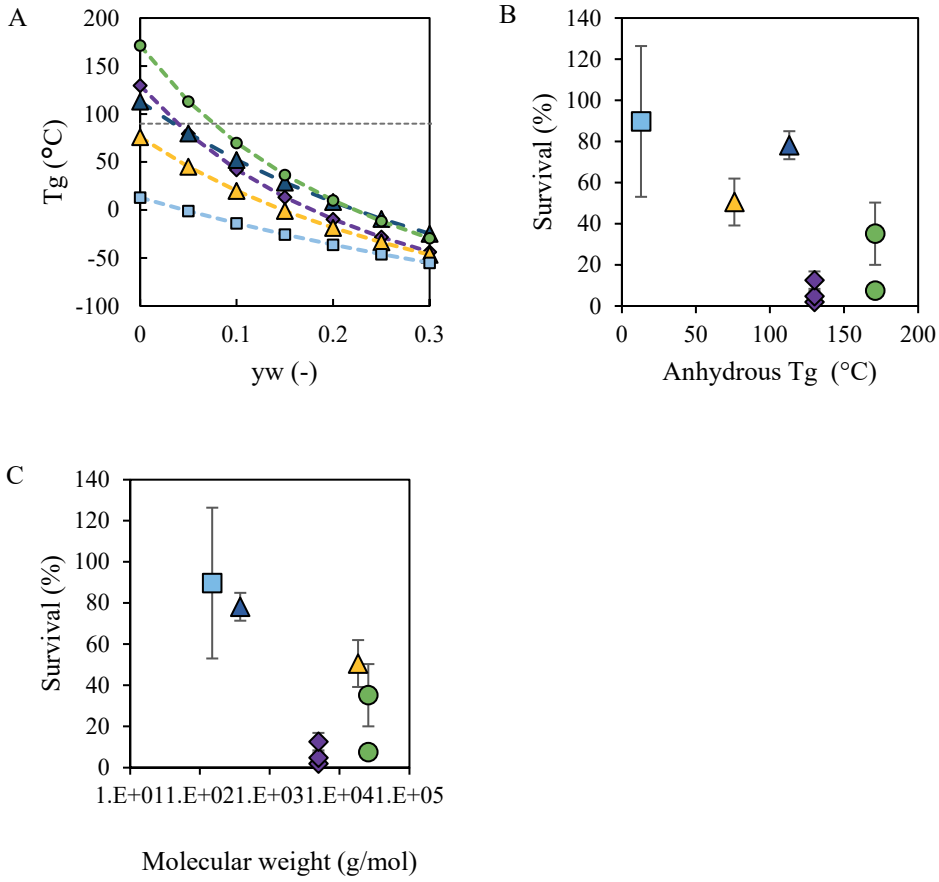

Figure 6.6. (A) Glass transition temperatures as function of moisture content (yw) as calculated with Couchman-Karasz. The drying air temperature of 90 °C is indicated with a dotted line. (B) Survival of L. plantarum WCFS1 after single droplet drying as function of anhydrous glass transition temperature and (C) as a function of the molecular weight. The components are trehalose (blue triangles), xylose (light blue squares), whey proteins (yellow triangles), maltodextrin DE5 20 and 30% (w/w) (green circles) and maltodextrin DE19 20, 30 and 40% (w/w) (purple diamonds).

Whey proteins undergo a colloidal glass transition already above a solids concentration of 50% (w/w) (Both, Siemons, et al., 2019; Both, Tersteeg, et al., 2019). This transition is based on jamming, leading to elasticity, and not just an increase in viscosity. Therefore, as soon as the skin is formed, it will withstand the surface stresses and retains its shape, while at the same time lower internal pressures develop due to the ongoing evaporation (Both, Karlina, et al., 2018; Bouman et al., 2016). At some point, a weak point in the skin will yield, and a cavity is formed. In this case, the glassy colloidal skin does not directly result in quickly rising droplet temperatures, since the cavity serves as an evaporation vent (Bouman et al.,

2016). Hence, bacteria may be better protected against heat and high moisture content due to prolonged constant drying via the cavity. It may even be that the vacuole formation causes a longer constant rate period than what was predicted based on locking point analysis. The latter might also explain higher survival for maltodextrin DE5 at 30% (w/w).

Trehalose is a disaccharide, while xylose is a monosaccharide. These molecules have relative high diffusivities compared to oligo- or polysaccharides (van der Sman & Meinders, 2013). Therefore, these components will accumulate more slowly below the surface, and the droplet will lose more of its moisture in the constant rate regime, where the temperature is low and microbial inactivation is therefore limited. Indeed, we observed via image analysis that the constant rate regime continued for a longer time with these matrices (Fig. A.6.2). These droplets only come into the falling rate period at a later stage, when the concentration of water has reduced strongly. The latter implies that the period of microbial inactivation has shortened, and the lower water content at the start of the falling rate period may additionally slow down the inactivation.

On the cellular level, the protective effect of low molecular weight carbohydrates such as trehalose and xylose is often explained by their ability to depress the phase transition of the bacterial cell membrane due to interactions with the phospholipids (Bryant et al., 2001; Huang et al., 2017). Indeed, the low molecular weight components in our experiments provided the best protection during survival (Fig. 6.6C). However, at higher molecular weights no relationship is observed between molecular weight and bacterial survival in this matrix. This differs from Perdana et al. (2014a), who observed a decreasing residual viability with increasing molecular weight if the molecular weight was higher than $2 \cdot 10^3$ g/mol. A complication in this comparison of survival and molecular weight is that maltodextrins are mixtures of smaller and larger carbohydrates, especially maltodextrin DE19 contains a considerable amount of low molecular weight components (Avaltroni et al., 2004). In addition to the importance of low molecular weight, the combination of low molecular weight and glass transition is also often described as an important aspect for the stabilization of bacterial cell membranes. Glass transition close to the membrane phospholipids might reduce the compressive stresses that force the membrane lipids from a fluid phase into a gel phase causing loss of membrane integrity (Bryant et al., 2001). For this effect components should be small enough to enter the spacing between membranes and have a high T_g. Actually, this is not in agreement with the high survival of xylose, which has a very low glass transition

temperature (Fig. 6.6A and B). Despite the possible capability of xylose to enter the intermembrane spacing due to its low molecular weight, it is still likely that xylose does not vitrify during drying as the T_g values are far below the drying air temperature. This might also affect survival during storage after drying, which is of great importance for dried bacterial ingredients and requires further investigation since it has not been considered in our study.

We demonstrate that the clear relation that we found between the morphology and the microbial survival, is likely rooted in a complex interplay between matrix properties (glass transition) and drying dynamics (diffusion rates). However, they are both the consequence of the same process; hence the strong correlation between these two resultants. This implies that the investigation of the morphologies may well offer a route towards better microbial survival during spray drying.

6.5. Conclusions and outlook

Drying of droplets having different matrices resulted in smooth, hollow or dented particles. Dented or folded particles were developed for maltodextrin DE19 and 20% (w/w) maltodextrin DE5; hollow particles were observed for whey protein and 30% (w/w) maltodextrin DE5, while smooth spherical and dense particles were obtained for trehalose and xylose. The survival of *Lactobacillus plantarum* WCFS1 that was embedded in these matrices showed clear correlation with these morphologies, with the smooth particles giving high survival, dented particles low survival, and hollow particles in between.

This strong correlation can be explained by a combination of drying dynamics and the glass transition, with high-molecular weight components like maltodextrins giving fast formation of a viscous shell, which folds into a dented geometry, allowing significant inactivation due to the long falling rate period at elevated temperatures. Small components such as xylose and trehalose exhibit a much longer constant rate period, and significant protection against inactivation during the shorter falling rate period. The hollow particles are the result of an elastic shell that resists folding, but offer a prolonged constant evaporation due to cavity formation allowing fast evaporation and therefore a longer low temperature period than the high-molecular weight maltodextrins.

Our results suggest that the morphology development is strongly correlated to the microbial survival, because it is fundamentally related to the same underlying mechanisms. Therefore, it is an excellent phenomenon to use for optimizing microbial survival during spray drying.

Other bacterial strains and different drying matrices, including mixes of carbohydrates and proteins, should be tested to further support our findings. Single sessile droplet drying experiments offer the opportunity to probe many bacterial drying formulations and drying conditions to find promising particle morphologies leading to higher bacterial survival.

6.6. Appendix

Glass transition temperatures and molecular weights

In our study, the glass transition temperature T_g of the different components was estimated as a function of moisture content. The relation was described using the theory of Couchman and Karasz (1978):

$$T_g = \frac{y_w \Delta C_{P,w} T_{g,w} + y_s \Delta C_{p,s} T_{g,s}}{y_w \Delta C_{p,w} + y_s \Delta C_{p,s}} \quad \text{A.6.1}$$

Here y_i is the mass fraction ($i = w, s$ for water and solute), $T_{g,i}$ is the glass transition temperature for the pure component ($T_{g,w}$=139 K), $\Delta C_{p,i}$ is the change in the specific heat at the glass transition. For $\Delta C_{p,w}$ a value of 1.91 kJ/kg·K was used. Glass transition temperatures of maltodextrins were determined as described by Siemons et al. (2020). The anhydrous glass transition temperature and the heat capacities of the solutes and the molecular weights of the components are provided in Table A.6.1.

Table A.6.1. Overview of materials and their anhydrous glass transition temperature, specific heat capacity and molecular weight.

Pure components	T_g (°C)	ΔC_p ($J \cdot g^{-1} K^{-1}$)	Mw ($g \cdot mol^{-1}$)	Reference
Trehalose	113	0.65	342	(Kawai et al., 2005)
Xylose	13	0.95	150	(Kalichevsky et al., 1993)
Whey proteins	76	0.58	18200	(Nicolai et al., 2011; Yang et al., 2010)
Maltodextrin DE19	130	0.43	4978	(Castro et al., 2016; van der Sman & Meinders, 2011)
Maltodextrin DE5	171	0.43	25847	(Castro et al., 2016; van der Sman & Meinders, 2011)

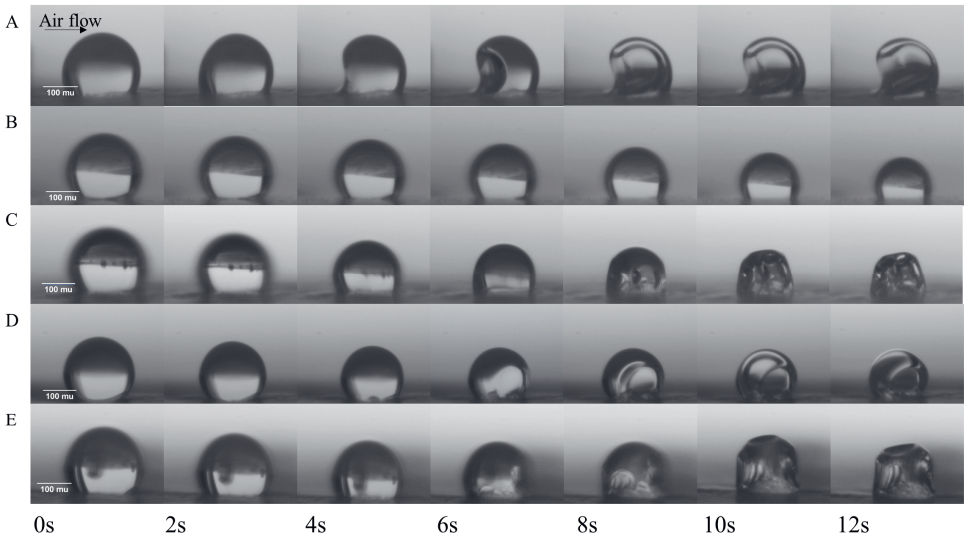

Figure A.6.1. Particle morphology development (R0 100 ± 20 µm, mu indicates µm) during single droplet dying at 90 °C of maltodextrin DE5 30% (w/w) (A), xylose 20% (w/w) (B), maltodextrin DE5 20% (w/w) (C), maltodextrin DE5 20% (w/w) (D), maltodextrin DE19 40% (w/w) (E). Air flow came from the left as indicated in the figure by the arrow.

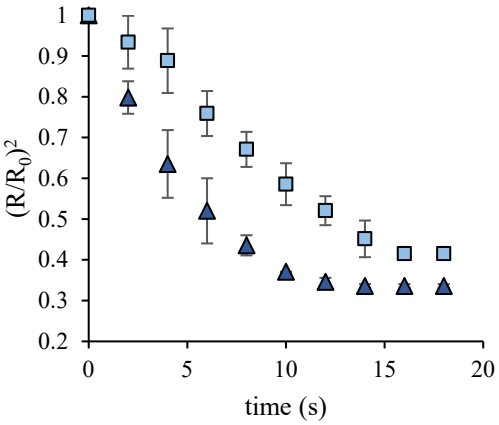

Figure A.6.2. Normalized squared radius as function of drying time for xylose (light blue squares) and trehalose (blue triangles). A linear decrease indicates a constant drying rate as described by Bouman et al. (2016). The data were obtained from videos via image analysis.

Chapter 7

General discussion

7.1. Introduction

The particle morphologies resulting from drying droplets containing food components represent fascinating study objects. Predicting the morphological evolution of primary particles during drying is considered important for steering the final characteristics of spray-dried powders. Tailoring the morphology evolution may for instance be desired for achieving superior bulk properties of the final powder, but it may also be crucial for the protection and controlled release of active ingredients. The morphology development of drying droplets is intrinsically complex as it involves amongst others diffusion, flow, gelling, glass transition, and the interplay between these processes will determine the final structure of the dried particle. Effective control of this process therefore asks for a mechanistic interpretation of this interplay.

The overall objective of this thesis was to relate the fundamental properties of the drying materials to the dynamics and skin properties of drying single droplets. For this, we aimed to predict the skin properties during drying and the final particle morphology, from the rheological properties of the constituents depending on concentration and change in temperature. This chapter discusses the main findings of the previous chapters. To put the main findings into a broader perspective, we will further investigate the rheology of concentrated whey proteins as an important model system and test the applicability of superposition principles for explaining the morphology evolution during drying. We will discuss and combine the results for whey proteins and maltodextrins and accordingly, we attempt to arrive at a more generic description of the mechanisms governing the morphology development. Finally, we examine if this generalized description may also be used to interpret the particle morphology developed at a larger scale. For this, we perform pilot-scale drying experiments for maltodextrins. We conclude this chapter with an outlook towards future research.

7.2. Main findings

The rheological properties of drying materials are expected to be important for understanding morphology development during drying. In **Chapter 2**, we therefore investigated the role of viscosity in morphology development. We analysed the viscosity of maltodextrins, whey proteins and their mixtures at increasing concentrations. The measured viscosities were modelled as a function of concentration using well-known viscosity models for polymer solutions and colloidal dispersions. We demonstrated that the viscosity of whey proteins progressively increases with increasing concentrations and that jamming of these proteins may be expected at around 50% (w/w) solids. With increasing the fraction of maltodextrins in a mixture of whey proteins and maltodextrins, the jamming of whey proteins becomes hindered. Maltodextrin rich solutions in contrast gradually increase in viscosity upon concentration. By relating the viscosity to the morphology development, we hypothesised that whey protein droplets form a rigid and elastic skin as a consequence of the jamming of whey proteins, eventually resulting in a smooth and hollow morphology. For drying of maltodextrin rich solutions, however, the more gradual increase in viscosity will result in a weaker, deformable skin, susceptible to wrinkling. The viscosity of concentrated solutions in combination with viewing the drying conditions applied is important in evaluating the properties of the skin developed.

For understanding and accurate modelling of droplet drying processes, moisture diffusion data as a function of the water content and temperature are critical. However, limited data on moisture diffusivity over a wide range of water contents and temperatures are available for food systems. In **Chapter 3**, we therefore systematically investigated the moisture diffusivity in concentrated protein and carbohydrate systems which were of potential interest for later single droplet drying experiments. Thin film drying experiments were carried out for these systems to extract moisture diffusion data at elevated temperatures. Moisture diffusion of protein/carbohydrate-water systems showed universal behaviour at low moisture concentrations, which may be attributed to random coil behaviour leading to similar water-solute interactions. The Darken relation described the moisture diffusion reasonably well, however, measured mutual moisture diffusion may be lower due to fast skin formation as a consequence of jamming. In complex mixed systems of carbohydrates and proteins, the moisture diffusivity was strongly affected by the presence of caseins as a consequence of their high voluminosity. In addition, for these complex mixed systems, a sharper decrease in

moisture diffusivity was found in the dry regime when compared to binary systems. We hypothesised that this phenomenon may be ascribed to a denser, random molecular packing in the dry/glassy regime or that it may be caused by water trapping due to skin formation.

In **Chapter 4**, we studied the morphology development during drying of maltodextrins varying in dextrose equivalence (DE) value. To be more precise, for these systems we aimed to obtain experimental data on the skin formation and mechanical instabilities induced by the drying. For this, a new sessile single droplet drying system was developed for drying small droplets (~200 μm) at relatively high initial solids concentrations (30% (w/w)). Molecular weight distributions, glass transition temperatures and rheological properties at various solids concentrations were determined for all maltodextrins to support explaining the observations during single droplet drying. Low DE maltodextrins had a broad molecular weight distribution and exhibited higher glass transition temperatures and viscosities than higher DE maltodextrins. We demonstrated that the DE value of maltodextrins can be used as an indicator for particle morphology development when viewed in the context of the applied drying conditions. For low DE maltodextrins, the onset of morphology development started relatively early during drying. We hypothesised based on rheological measurements at high solids concentrations that the skin formed can withstand the compression stresses developed due to dominant elastic behaviour, resulting in a hollow sphere morphology. High DE maltodextrins, in contrast, were expected to develop elastic behaviour later during drying in the vicinity of the glass transition. Rheological measurements suggested that the droplet skins developed for these systems become mostly viscous, yielding wrinkled, folded or creased morphologies.

The rheological properties at high concentrations were relevant for understanding the morphology development of particles (**Chapter 4**). In **Chapter 4**, valuable insights were obtained by performing thin film rheology experiments at one concentration and with a fixed temperature. During drying, however, the moisture content and temperature are continuously evolving. For better evaluating the rheological properties of the particle and in particular the skin formed, we hypothesised that it would be important to characterise the rheological properties over a wider range of concentrations and temperatures. Therefore, in **Chapter 5**, we continued with investigating the rheological behaviour of maltodextrins varying in DE as a function of frequency, temperature and concentration. Rheological data obtained at different concentrations and temperatures in the linear viscoelastic regime could be mapped

onto master curves for storage and loss moduli using a superposition algorithm. Low DE maltodextrins exhibited rubber-to-glass-like behaviour, where the rubber behaviour was suggested to be the consequence of entanglements at sufficiently high concentrations of longer-chain polysaccharides. High DE maltodextrins showed predominantly viscous behaviour at high concentrations, which changed to elastic behaviour upon approaching the glass transition. The absence of rubber-like behaviour was explained by the larger fractions of oligomers and small sugars that may inhibit the formation of a network based on entanglements. Rheological behaviour was also connected to the morphology development during drying by modelling the temperature and moisture evolution profiles during single droplet drying and connecting the local and momentary concentrations and temperatures to the local rheology. For modelling droplet drying, we also employed theories from **Chapter 3**. Eventually, the rheological properties during droplet skin formation could be estimated and accordingly the occurrence of mechanical instabilities could be described. The elastic behaviour of the low DE maltodextrin skin could be related to cavitation and the viscous behaviour of high DE maltodextrin skin to wrinkling.

The morphology development may be important for protecting components during drying, like heat-sensitive probiotics. In **Chapter 6**, we therefore examined the drying of different food matrices incorporating lactic acid bacteria and studied the bacterial survival after drying. More specifically, we investigated if the particle morphology observed during single droplet drying could be related to the survival of *Lactobacillus plantarum* WCFS1 after drying. By systematically varying the drying matrices, we could distinguish between a direct effect of the matrix on the survival of the bacteria and the effect of morphology. The survival of *L. plantarum* WCFS1 showed a strong correlation with the final particle morphology generated: survival in smooth, spherical and dense particles was highest, followed by hollow and smooth particles and the survival was lowest in dented particles. The relation between survival and particle morphology was explained by a combination of matrix properties and drying dynamics of the drying droplets.

7.3. Translation to whey proteins

In this thesis, we established that the rheological properties of concentrated food systems are important for the prediction of the skin properties and accordingly the occurrence of deformations during droplet drying (Chapter 2, 4 and 5). By following the constructed master curves for concentrated maltodextrins and predicting the evolution of viscoelasticity during droplet drying, we were able to understand cavitation or wrinkling phenomena taking place after skin formation (Chapter 5). The study in Chapter 5 raises the question of whether a similar approach of investigating the rheology over a wide range of concentrations and temperatures followed by construction of master curves may also be used for interpreting the morphology development of other solutes. It would be expected plausible that other polymers/random coil-like components, including carbohydrates such as starch, exhibit viscoelastic behaviour comparable to maltodextrins, rendering similar explanations for the deformations occurring during droplet drying. In practice, however, many food formulations that are dried consist of a large fraction of proteins or a mixture of proteins and carbohydrates. For some elastomeric proteins, including elastin, gluten and resilin superposition principles like proposed in Chapter 5 may be possible (Gosline & French, 1979; Khandaker et al., 2017; Tatham & Shewry, 2000; Tsiami et al., 1997), likely due to their polymer-like structure. Some proteins have a more compact globular structure in their native state, including whey proteins (Haque, 2015). It would be of interest to investigate if the approach of Chapter 5 may also work for these globular protein systems. In the next sections, we will therefore focus on investigating the rheological properties of concentrated globular whey proteins. We have selected whey proteins as an important model system as they are used extensively as functional and nutritional ingredients in pharmaceutical and food products, including infant formula, health foods and drinks, and high gel product applications (Dissanayake et al., 2012; Morr & Ha, 1993). Besides, these proteins are often used as ingredients in powder form, obtained by spray drying (Abdul-Fattah et al., 2007; Chávez & Ledeboer, 2007).

In the next section, a brief review of the morphology development of whey proteins is provided. Next, we will investigate if a similar approach as reported in Chapter 5 can be used to investigate the rheology of concentrated whey proteins and accordingly support the explanation of the morphology development. For this, we will study the effects of frequency, temperature and concentration on the rheological behaviour of concentrated whey proteins using a similar method as employed in Chapter 5. We again investigate whether single master

curves for storage (G') and loss (G'') moduli can be constructed. Finally, we compare the rheological properties of highly concentrated maltodextrins and whey proteins and attempt to establish a more general explanation for the occurrence of mechanical instabilities during the drying of food droplets.

7.3.1. Morphology development of whey proteins

In many applications involving whey proteins, control of the characteristic features of whey protein powders is desired, including the size and the morphology of the particles. These can for instance affect the foaming and gel-forming ability and rehydration dynamics of the powder (Anandharamakrishnan et al., 2008; Dissanayake et al., 2012; Walton, 2000). Hence, the monitoring and analysis of the evolution of the morphology during droplet drying has received considerable attention (Both, Karlina, et al., 2018; Bouman et al., 2016; Lanotte et al., 2018; Malafronte et al., 2019; Sadek et al., 2014; Yu et al., 2021).

Similar to other droplets, whey protein droplets first undergo homogeneous shrinkage in the initial drying phase (Fig. 7.1) (Both, Karlina, et al., 2018; Bouman et al., 2016; Sadek et al., 2014). At the initial stage, the protein distribution in the droplet is still homogeneous. As the droplet shrinks during evaporation, whey proteins accumulate at the interface. At a critical protein concentration, these proteins form an elastic but moisture-permeable skin that does not bend under pressure (Bouman et al., 2016; Sadek et al., 2014; Yu et al., 2021). After a certain period of drying, the elastic skin solidifies further; the characteristic relaxation times become longer than the drying time and further shrinkage of the droplet is inhibited. Further moisture evaporation will then result in a pressure difference between the inside and outside of the droplet, leading to the formation of a cavity or vacuole. This cavitation during drying of WPI droplets was also observed in Chapter 6.

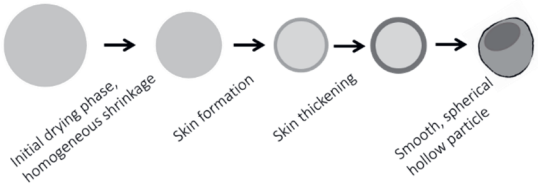

Figure 7.1. Schematic illustration of drying of whey protein droplet.

Malafronte et al. (2019) further extended the explanation for the morphology development of whey protein droplets during drying based on the drying of colloidal particles. They

investigated the morphology development of native and aggregated whey protein dispersions during single droplet drying and accordingly used structure-mechanical parameters to predict the final morphology. Important structure-mechanical parameters used to explain the morphology development, include the Péclet number, the critical buckling pressure and Darcy's pressure. The Péclet number was for all whey protein droplets larger than 1, which indicates that whey protein particles accumulate at the surface of the droplet leading to skin formation. Under the Darcy pressure, whey protein molecules are forced onto each other and may undergo a sol-gel transition, leading to an elastic skin. The skin formed will buckle if the pressure in the skin exceeds a critical value, which is referred to as critical buckling pressure. The critical buckling pressure depends on the thickness of the skin, if the skin forms instantaneously, the thickness may be large enough to prevent buckling and a hollow sphere is obtained. When the pressure exerted on the skin exceeds the critical buckling pressure, buckling is expected. The degree of buckling depends on the presence or absence of an inner gel layer, in absence the wavelength selected by buckling is the largest possible. All the aforementioned research supposes a sol-gel transition during drying of whey protein droplets, leading to the formation of an elastic skin. In the next sections, we will investigate how the rheological properties of whey proteins as measured using SAOS experiments corroborate the previous descriptions given for the morphology development.

7.3.2. The influence of concentration and temperature on the rheology of whey proteins

The rheological properties of proteins are governed by their composition, molecular mass, size, shape, flexibility, degree of hydration and intermolecular interactions (De Wit & Van Kessel, 1996). These factors may in turn be influenced by concentration, temperature, pH, ionic strength and processing history (Tung, 1978). The influence of these conditions on the rheological properties of whey protein dispersions has been investigated before at lower concentrations (Dissanayake et al., 2013; Ikeda et al., 2000; Loveday et al., 2007; Lupi et al., 2020; Saĝlam et al., 2013; Tung, 1978; Vardhanabhuti & Foegeding, 1999). However, in the more concentrated states relevant to the drying process, the rheological picture is still rather incomplete.

Whey proteins are compact globular proteins in their native state. Hence there are analogies between the rheological behaviour of hard-sphere colloidal suspensions and concentrated globular protein solutions (Brownsey et al., 2003; Loveday et al., 2007; Parker et al., 2005).

Hard-sphere colloids are considered rigid spherical particles with no interparticle forces other than infinite repulsion at contact (Genovese, 2012). The viscosity of a suspension of such particles increases progressively with the concentration, i.e. with increasing volume fraction of particles (Genovese, 2012; Parker et al., 2005). This increase in viscosity is commonly described with the Krieger-Dougherty relation (Krieger & Dougherty, 1959). Although whey proteins are not perfectly hard spherical particles and are mixtures of differently sized, shaped and charged molecules, the viscosity of their solutions is well approximated by the Krieger-Dougherty relation (Brownsey et al., 2003; Parker et al., 2005). In Chapter 2 of this thesis, we demonstrated this for whey protein isolate (WPI) solutions below 50% (w/w) solids. For investigating the drying of WPI droplets it would be of interest to further characterise the rheological properties of WPI at higher concentrations and different temperatures. Therefore, we extend our investigation of WPI systems with small amplitude oscillatory tests using a similar approach as described in Chapter 5. We hypothesise that considering rheological data over a wide range of concentrations and temperatures and interpreting the results by analogy with the behaviour of colloidal systems, we will likely obtain a more complete view on the behaviour of whey proteins during drying.

At concentrations below 50% (w/w) solids, WPI solutions behave as predominantly viscous liquids at the temperature range investigated (Fig. 7.2A). Increasing the temperature resulted in decreased moduli, which may be caused by the added thermal energy which increases molecular mobility (Quevedo et al., 2021). The solutions showed Newtonian behaviour at 20 °C, which is in agreement with the viscosity data as obtained in Chapter 2 (Fig. 7.2B). At this concentration range (~20-50% (w/w)), whey protein solutions are likely in the dilute or semi-dilute regime going towards the concentrated regime. In the dilute regime, whey protein molecules are practically isolated from each other and are free to move independently and their interaction is predominantly with the solvent and not with other whey protein molecules (Maron et al., 1959). As the concentration of whey proteins increases, the space available for each whey protein decreases and the molecules begin to also interact with other protein molecules. The viscosity of the matrix will then rise very quickly on increasing the concentration (Krieger & Dougherty, 1959) (Fig. 7.2C).

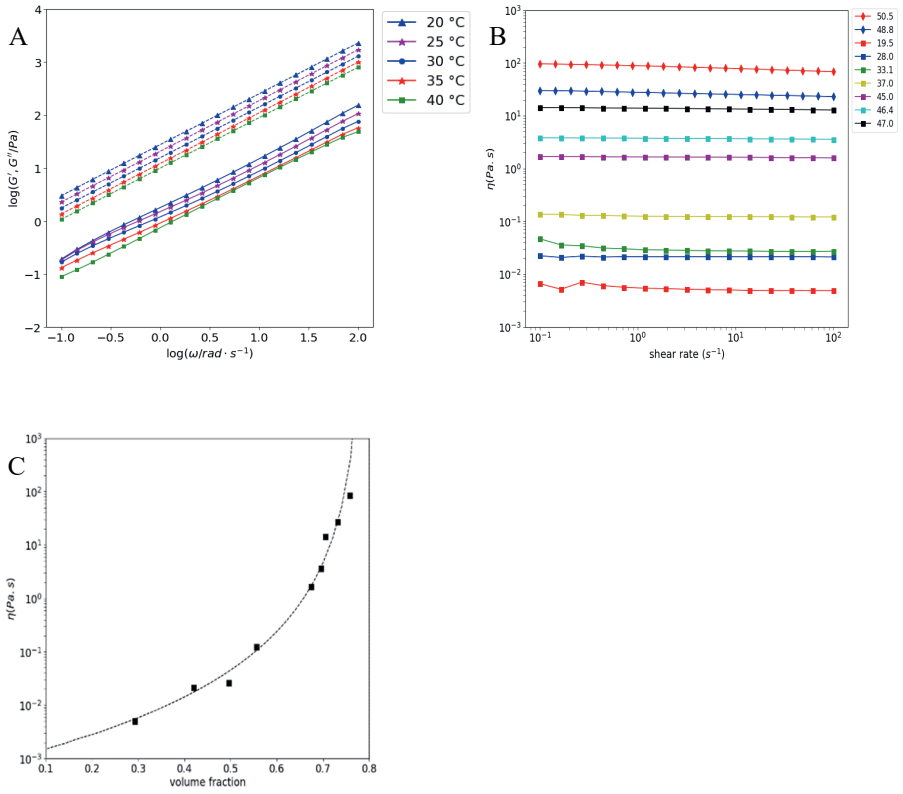

Figure 7.2. Exemplary mechanical spectra as measured with small amplitude oscillatory shear tests showing the frequency dependence of G' (straight lines) and G'' (dashed lines) of a WPI solution at 48.8% (w/w) solids at various temperatures (A). The method for obtaining the spectra is explained in Chapter 5. Viscosity data as obtained from shear ramps (squares) as collected in Chapter 2 of this thesis and oscillatory tests (diamonds) for different solids concentrations % (w/w) at 20 °C (B). The oscillatory frequency range is converted into an equivalent shear rate range based on assuming Cox-Merz holds for concentrations below 50% (w/w) for the frequencies tested. Viscosity data as described by the Krieger-Dougherty relation with fitting parameters from Chapter 2 (C).

Increasing the concentration beyond 50% (w/w) solids resulted in gel-like or hard-solid structures, with a clear change in the rheological behaviour, from mainly viscous to mainly elastic (Fig. 7.3). The moduli decreased with increasing temperatures to 40 °C, which was also observed by Quevedo et al. for concentrated β-lactoglobulin and WPI systems (2019, 2021). The viscosity changed from Newtonian to shear thinning (data not shown). At these high concentrations, there is no longer sufficient fluid to lubricate the relative motion of the proteins and hence there is a slowing of the particle dynamics (Mason & Weitz, 1995). Protein particles become confined within an increasingly crowded network, and essentially become trapped in cages formed by their nearest neighbours (Mason & Weitz, 1995; Pusey

& Megen, 1986). The result is a jammed structure that can become stress bearing such that for small applied stresses the material will exhibit predominantly elastic behaviour (Brownsey et al., 2003; Parker et al., 2005). Deformation can now only come from deformation of the cages, or of the molecules themselves. Larger deformation will cause the cages to break down and restructure, resulting in a drop of the elasticity.

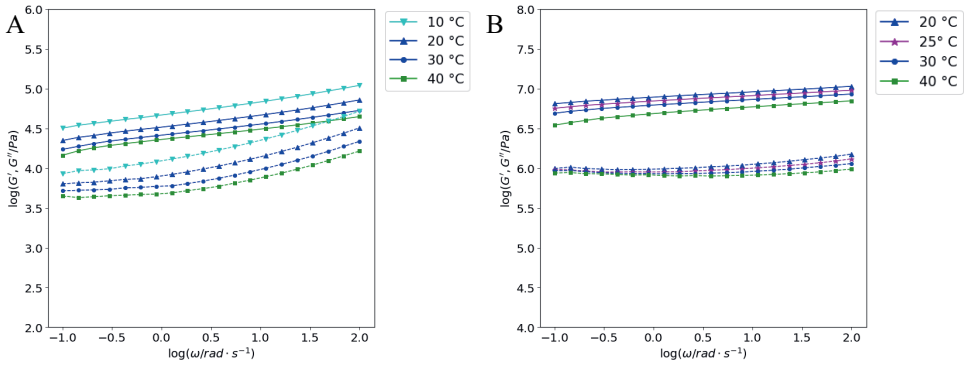

Figure 7.3. Example mechanical spectra as measured with small amplitude oscillatory shear tests (plate-plate) showing the frequency dependence of G' (straight lines) and G'' (dashed lines) of a WPI solution at 58.0% (w/w) (A) and 67.2% (w/w) (B) solids at various temperatures. Samples are prepared using the thin film approach as described in Chapters 4 and 5.

Parker and others (2005) already demonstrated this change from viscous to elastic behaviour upon increasing the concentration of β-lactoglobulin dispersions. With increasing volume fraction of β-lactoglobulin, the viscosity increased and resulted in a slowing of structural rearrangement. For the concentrations, 45% and 52% (w/w) β-lactoglobulin dispersions at pH 5.1, G'' dominated G' over a frequency range of 0.02-30 Hz. The viscous liquid-like response was changed however to dominant elastic behaviour at 54% (w/w) solids. Brownsey et al. (2003) studied bovine serum albumin (BSA) solutions in the concentration range 40-52% (w/w) by oscillatory rheometry and demonstrated dominant viscous behaviour for concentrations below 50% (w/w) for a frequency range of 0.01-10 Hz. When increasing the concentration to 50% (w/w), a crossover to elastic behaviour was observed. The crossover to solid-like behaviour is in both cases compared to a colloidal glass transition, where particle motions become inhibited in their cages (Mason & Weitz, 1995). The dominant elasticity is attributed to the resistance to distortion of the average particle configurations (Parker et al., 2005; Prasad et al., 2003).

In order to further understand at which concentrations these crowding effects may start to take place for WPI systems, the effect of the WPI concentration on the complex viscosity can be investigated as proposed by Quevedo et al. (2021). They investigated WPI solutions over a range of concentrations from 17 to 70% (w/w) and analysed the complex viscosity at 30 °C. By analysing the complex viscosity and representing the viscosity by two straight lines, Quevedo et al. (2021) found a critical concentration at around ~40% (w/w) solids. Using this approach of investigating the complex viscosity, a better approximation can be made at which concentration the system changes from the dilute region to the semi-dilute overlap region and the concentrated region. Our data are in close agreement with Quevedo et al. (2021) (Fig. 7.4A) and following a similar approach resulting in a critical concentration of ~42% (w/w) based on our measurements (Fig. 7.4B). Below this critical concentration, the whey proteins are free to move independently. Around the critical concentration, the proximity of the protein molecules increases, resulting in a steep increase in viscosity. Upon further increasing the concentration, proteins become confined in a crowded network in the concentrated region, where the rheological behaviour of the system changes from mainly viscous to mainly elastic (Maron et al., 1959; Quevedo et al., 2019).

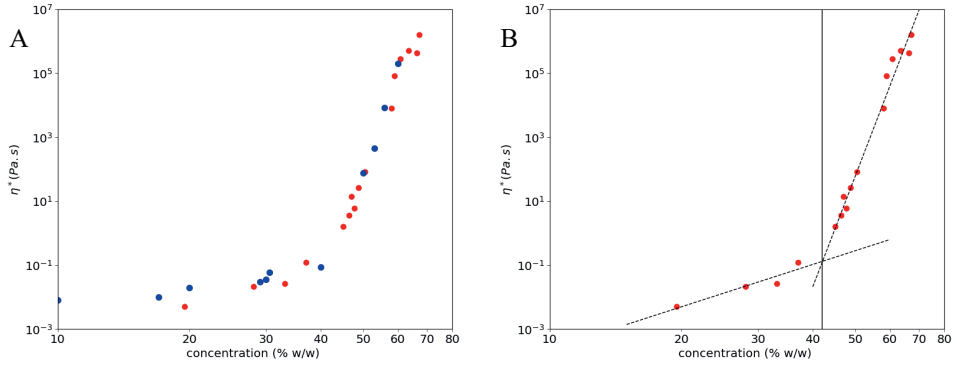

Figure 7.4. Viscosity as a function of whey protein isolate concentration. Complex viscosity data in blue is obtained from (Quevedo et al., 2021), measured viscosity data in red is obtained with shear ramps and oscillatory rheology as selected at 5.46 rad/s at 20-25 °C (A). Viscosity curves are represented by two straight lines showing the critical concentration around ~42% (w/w) as indicated by the vertical line (B).

7.3.3. Application of superposition principles for whey protein systems

We demonstrated in Chapter 5 that master curves for G' and G'' moduli for various maltodextrins could be constructed based on superposing oscillatory data measured at different temperatures and concentrations. While the use of superposition principles in polymeric systems is widespread, there has been much less use of such superposition principles in colloidal systems, including for globular proteins. The time-temperature superposition (TTS) principle has been used to investigate the viscoelastic behaviour of BSA and whey protein concentrate suspensions (Ikeda & Nishinari, 2000; Meza et al., 2010). TTS was successfully applied in whey protein concentrate suspensions with a protein content of 5% (w/v) in the range of 30 to 50 °C (Meza et al., 2010). For BSA solutions at 10% (w/w), TTS master curves could also be generated for frequency curves measured at 10 to 40 °C (Ikeda & Nishinari, 2000). Apparently, for these conditions, no morphological changes occurred in the material and hence the moduli displayed similar temperature dependence, resulting in the successful application of TTS (Ferry, 1980). Superposition may however fail upon increasing protein concentrations, treatment or temperatures as this may lead to profound morphological changes of the system. Meza et al. (2010) for example showed a failure of the TTS for heat-treated suspensions with 9% (w/v), which was attributed to the formation of aggregates that are susceptible to morphological changes during rheological measurements at different temperatures.

We tested if the superposition principle as reported in Chapter 5 could be applied to construct master curves for concentrated WPI systems. It should be noted that differential scanning calorimetry (DSC) experiments were performed before rheological tests (Table A.7.1). This was done on the one hand to determine whether the proteins were still native after sample preparation (i.e. after rotary evaporation or climate chamber), and on the other to determine the denaturation temperature of the proteins. Protein denaturation temperatures of WPI significantly increased for high concentrations (~70% (w/w)), which may be explained by lower water activities, increased conformational stability of proteins at higher concentrations due to higher viscosities, increased excluded volume and hydration effects (Mittal et al., 2015; Quevedo et al., 2021). All rheological tests were performed at temperatures below the measured protein denaturation temperatures. This was done as during spray drying the loss of whey proteins due to denaturation should be limited. Additionally, testing below

denaturation temperatures limits the morphological changes due to measurement temperatures (Meza et al., 2010).

Time-temperature superposition (TTS) was successfully applied to construct master curves at different concentrations from the rheological spectra as measured at 10 to 40 °C for frequencies from 0.1 to 100 rad/s using the superposition algorithm of Chapter 5 (Fig. 7.5). WPI solutions below 50% (w/w) showed dominant viscous behaviour over a frequency window of four decades (Fig. 7.5A, B and C). The slopes of the master curves were close to 1, implying that the rheological behaviour of WPI solutions below 50% (w/w) is Newtonian, agreeing with the viscosity data (Fig. 7.2B). When increasing the concentration further, WPI exhibited elastic behaviour, which is suggested to be caused by caging as aforementioned. For these higher concentrations superposition could be applied, albeit for WPI at 58.0% (w/w) a small vertical shift could have improved the superposition as checked with the van Gurp-Palmen plot (data not shown). The separate master curves imply that a cross-over from viscous to elastic behaviour should occur above the critical concentration of ~42% (w/w) in the concentrated region, between 48.8% (w/w) and 58.0% (w/w) solids. This is in agreement with the cross-overs found for β-lactoglobulin and BSA, 54% (w/w) and 50% (w/w), respectively (Brownsey et al., 2003; Parker et al., 2005). The cross-over indicates a dynamic transition which can be compared to the colloidal glass transition (Mason & Weitz, 1995). At a concentration of 67.2% (w/w), G' and G'' did not increase significantly anymore over a frequency range of roughly five decades and the system behaves as a hard elastic solid with moduli around 1-10 MPa (Fig. 7.5G, H and I). Similar rheological behaviour of WPI was found by Both et al. (2019b) around 70% (w/w). The limited change in rheological properties of the WPI systems at these concentrations signifies glass-like behaviour. Brownsey et al. (2003) also demonstrated that at higher concentrations (62-86% (w/w)) BSA showed solid-like characteristics (tensile moduli ~10 MPa to 1.0 GPa) with relaxation times in the order of 100 s, indicative of glass-like behaviour.

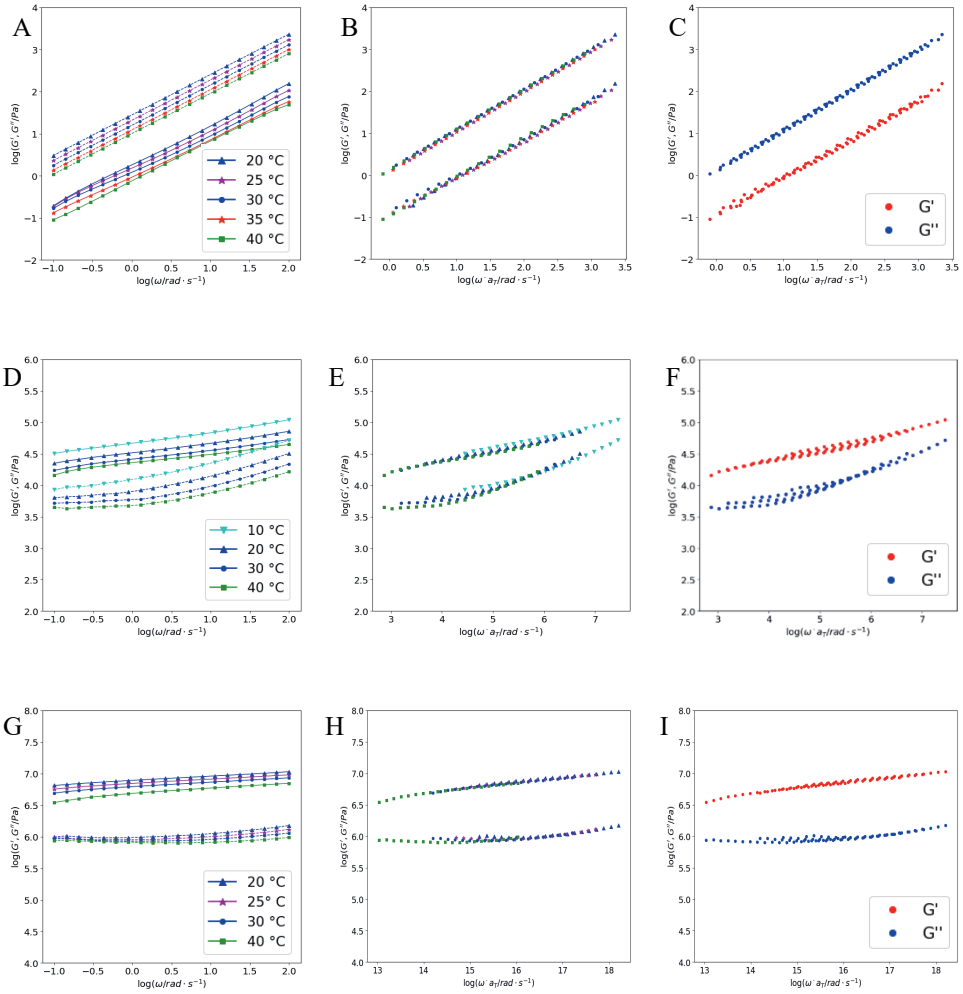

Figure 7.5. Example mechanical spectra of G' and G'' with master curves constructed (A, B, C = 48.8% (w/w), D, E, F =58.0% (w/w), G, H, I = 67.2% (w/w) solids). Fitting parameters are provided in Table A.7.2.

The applicability of time-temperature-concentration superposition (TTCS) was also tested for WPI systems to investigate if a single master curve could be composed. Even though TTS could be applied for the samples at different solids concentrations (Fig. 7.5), the TTCS failed over the complete concentration range, implying no transient network is formed. Failure may be due to the limited data in the range of 48.0% to 58% (w/w) solids, which was experimentally a difficult regime to reach with the used methods as described in Chapter 5. However, TTCS could also not be applied for rheological data in the concentration range from 58% to 67.2% (w/w), as was checked with the van Gurp-Palmen plots. Failure of TTCS

may be explained by various aspects that are not directly evident from only our rheological experiments. The superposition may fail due to concentration-induced transitions in morphology/structure of the system, causing sudden changes in molecular mobility, and/or the presence of very different relaxation processes which follow other temperature or concentration dependencies (Dealy & Plazek, 2009; Simon & Ploehn, 1999; van Gurp & Palmen, 1998). To our knowledge, literature lacks studies investigating TTCS for hard-sphere colloidal systems, even though time-concentration superposition (TCS) showed that the experimental modulus values for colloidal glasses at different volume fractions can be collapsed onto a master curve (Cicuta et al., 2003; Mattsson et al., 2009; Wen et al., 2015). Peng et al. (2018) later demonstrated that the TCS principle fails for concentrated soft-sphere and near hard-sphere colloidal dispersions near the glass transition region, because of the emergence of a strong β-relaxation process which overlaps with the α-relaxation. The α- and β-relaxation mechanisms show different volume fraction dependences, which results in the breakdown of TCS. Sundaravadivelu Devarajan et al. (2020) showed by using molecular dynamics simulations for nano-colloidal systems that TCS fails at high volume fractions (>0.40) near the glass transition.

A single G' and G'' master curve for WPI could not be constructed over the entire concentration range studied and thus the approach for predicting the rheology of the skin at the start of morphology development as proposed in Chapter 5 cannot be directly translated to globular whey proteins. The globular configuration of whey proteins, combined with its complex dynamics, i.e. caging and consequent sol-gel transition, at increasing concentrations asks for a different rheological modelling approach, possibly describing the moduli as function of particle volume fraction (Genovese, 2012). Even though we could not model the time-temperature-concentration rheology evolution of WPI, the rheological data and the separate TTS master curves are useful in supporting the description of the morphology development during drying (section 7.3.1). The master curves imply that a sol-gel transition takes place upon concentration: at low concentrations, whey proteins are still free to move in the system and the system is purely viscous and as the concentration increases beyond a critical concentration, the whey proteins eventually become confined in a network, leading to an elastic system. Hence, the data confirm the previous description of the morphology development, stating that as whey proteins concentrate at the droplets' surface during drying, caging of the particles and a sol-gel transition will result in an elastic skin. As the evaporation

progresses, the skin rigidifies and becomes more elastic, the droplet shrinkage is halted and the compression/pressure stresses developed are relieved by the formation of a cavity.

7.3.4. Learnings for other food systems

When comparing the discussions in this chapter with those in Chapter 5, it is evident that the rheology of concentrated whey proteins differs substantially from concentrated maltodextrins. Whey proteins, when in a globular state, can be viewed as colloidal particles. Within the examined range of concentrations, whey protein samples varied from fluids to gels and eventually glasses. Upon increasing the concentration of proteins beyond a critical concentration, whey proteins undergo crowding effects, eventually leading to jammed structures that will result in a change of viscous behaviour to dominant elastic behaviour. Maltodextrins are glucose polymers and their rheological behaviour depends on the distribution of chain lengths (i.e. DE). Maltodextrins with a considerable fraction of high chain length polymers show rubber to glass-like behaviour at high concentrations, while maltodextrins consisting mostly of small chain glucose polymers exhibit viscous behaviour up to the glass transition. Although differences in rheological behaviour are observed between maltodextrins and whey proteins, both systems eventually show signs of glassy states. Around or below the glass transition, structural relaxation is slowing down strongly and the system behaves as a hard elastic solid.

In this thesis, we demonstrated that superposition principles can be powerful methods of data treatment. For maltodextrins, simple horizontal shifting of the rheological data as measured at different temperatures and concentrations permits the construction of master curves, mapping the data beyond the range obtainable by single experiments. Hence, all contributing relaxation mechanisms of the maltodextrin systems have the same temperature and concentration dependence and all stress magnitudes at all frequencies have the same temperature and concentration dependence (Dealy & Plazek, 2009). The reason for the successful application of the TTCS principle for maltodextrins may be explained based on the free volume of the polymer (Krauklis et al., 2019). The free volume is the space that allows movement of the polymer chains and a change in free volume directly affects the viscoelastic properties of the polymer. Temperature and plasticization have a similar effect on the free volume of the polymer, increasing temperature or the concentration of plasticizer (in this case water) will result in increased free volume, and therefore the TTCS principle can be established. The glass transition temperature (T_g), being a threshold in chain mobility, is

also related to the free volume. Therefore, we found that the T_g is an important parameter describing the master curves and hence its importance for the rheology of maltodextrins (Chapter 5). The TTCS principle can probably also be applied for other systems that have a random coil-like configuration. Globular proteins do not have a random-coil like configuration, but TTS could be applied for shifting the spectra uniformly along the frequency axis (Fig. 7.5). The partial successful application of TTS for whey protein, suggests that no morphological changes occur in the material upon changing temperature and moduli thus display similar temperature dependence at the specific concentration measured (Ferry, 1980). However, the superposition failed when shifting data with changing temperature and concentration, i.e. TTCS over the complete concentration range failed. The underlying reason for the failure of this principle is not obvious. Peng et al. (2018) suggested that this may be caused by the different volume fraction dependencies of the relaxation mechanisms. Interpreting dynamic rheology data with molecular dynamic simulations may contribute to further development of the understanding, as was demonstrated by Sundaravadivelu Devarajan et al. (2020).

Despite the observed differences in the evolution of the rheological properties between maltodextrins and whey proteins, we do recognize that similar mechanisms govern cavity formation during drying in both systems. Cavitation requires dominant elastic behaviour of the droplets' skin. The close connection between the elastic behaviour of the droplet skin and cavitation can be further confirmed with other systems, for instance drying of starch. During single droplet drying of starch solutions at 30% (w/w) cavitation takes place, resulting in smooth, hollow and spherical particles (Gouaou et al., 2016) due to the elastic behaviour of the skin as is likely generated by entanglements of the polysaccharides (Gouaou et al., 2016; Kasapis et al., 2000; van der Sman et al., 2021). The elastic behaviour of the skin may well have different origins, where maltodextrins and starch acquire elastic behaviour via physical entanglements, whereas whey proteins in their native state acquire this via caging and jamming. Alternatively, the elastic behaviour for whey proteins during drying may also result from non-covalent or covalent bonds, due to conformational changes and even unfolding of their initial globular structure, especially at the interface of the droplets (deWit & Klarenbeek, 1984; Dickinson, 2001; Haque, 2015; Mulvihill & Donovan, 1987; Quevedo et al., 2019).

Even though elastic behaviour of the skin may be critical for cavitation to occur, it is not necessarily a guarantee that smooth and hollow particles develop. To illustrate, caseins,

which are more random coil-like colloids, show a clear sol-gel transition due to close packing, where at low concentrations the system behaves as a viscoelastic liquid, while at a critical concentration of ~20% (w/w) the system exhibits elastic behaviour (Bouchoux et al., 2009; Guo & Wang, 2016). During drying, these caseins quickly absorb on the droplets' interface due to their flexible structure, high surface activity and limited self-diffusivity and once they reach the critical concentration they form an elastic skin (Dickinson, 2001; Sadek, Pauchard, et al., 2015; Yu et al., 2021). However, different than for globular whey proteins, caseins are still able to deform and deswell at high concentrations, resulting in an elastic skin that is still flexible enough to deform in response to drying stresses (Both, Nuzzo, et al., 2018; Dahbi et al., 2010; Sadek, Pauchard, et al., 2015; Yu et al., 2021). This elastic and flexible skin yields twisted and wrinkled particles after single droplet drying, sometimes including a vacuole. Similarly, for drying of skim milk droplets containing ~30% casein, caseins concentrate at the surface causing eventually elastic behaviour of the skin (Alexander et al., 2002; Both, Nuzzo, et al., 2018; Chew et al., 2014; Karlsson et al., 2005). However, also for single droplet drying of skim milk diverse morphologies have been found, including wrinkled particles comparable with casein particles or hollow and spherical particles depending on the drying conditions applied (Both, Nuzzo, et al., 2018; Rogers et al., 2012). Another example where elastic behaviour of the skin is expected, yet no hollow and smooth particles are obtained, is for single droplet drying of maltodextrin DE12 30% (w/w) droplets at 90 °C (Chapter 4 and 5). In this case, the formation of wrinkles ahead of the formation of a large cavity was observed.

To better discriminate between the pathways leading to hollow and spherical particles without wrinkles and those resulting in wrinkled and hollow or only wrinkled particles from elastic skins, one needs to include the skin thickness and the droplet weight loss. Du et al. (2020) investigated how the morphology of a drying soft matter droplet can evolve with time based on a pseudo-dynamic analysis. For cavitation to result in a hollow and smooth particle, the ratio of the elastic length (inversely related to the elastic modulus) over the shell thickness should be sufficiently low, i.e. the skin should have a relatively high elastic modulus and should be thick. Once cavitation takes place, the pressure difference between the outside and the droplet will decrease, the stress is relieved and therefore no wrinkling will be observed after cavity formation. For particles to be amenable to wrinkling, a large elastic length is required with a limited shell thickness, which requires a low elastic modulus and a thin skin.

If after wrinkling the weight loss exceeds a critical value, cavitation may still be observed. The authors explain that the decreasing pressure difference between the outside and inside, with the increase of the weight loss upon cavitation, could flatten the wrinkles. However, in practice, the wrinkles formed may become more rigid by e.g. turning glassy. Wrinkling in the absence of cavitation may also be observed for viscous skins, which was demonstrated for high DE maltodextrins in this thesis (Chapter 4 and 5). The viscous skin gradually form wrinkles on the experimental time scale, relieving the compression/pressure stresses. The occurrence of different wrinkling patterns is strongly related to the shrinkage evolution of the droplet, combined with the ratio between the shear moduli of the skin and the core (Li et al., 2011). First, the skin buckles into periodic wrinkles to release the compression in the skin when the shrinkage reaches a critical shrinkage factor. The wrinkle pattern will evolve into a pattern consisting of regular pentagons and hexagons with increasing shrinkage. With further increasing the shrinkage, a wrinkle-to-fold transition may take place and at sufficiently large shrinkage this transforms into a labyrinthine pattern, yielding creased particles (Chapter 4). Folds increase in thickness when the modulus ratio between the skin and the core increases (Li et al., 2012).

In short, our results in conjunction with literature show that the rheological properties of the skin formed at the surface of the droplet are critical for explaining the instabilities during drying, and accordingly the final particle morphology. Characterisation of the rheological behaviour over a range of temperatures and concentrations, possible through constructed master curves, help to estimate the rheological behaviour of the skin. If during drying a skin develops exhibiting viscous behaviour, wrinkling phenomena will likely occur and depending on the shrinkage as caused by the mass loss of the droplet due to evaporation different wrinkling patterns may be observed (Fig. 7.6) (Li et al., 2011). In the case the skin exhibits elastic behaviour, yet the skin has a low elastic modulus and limited thickness, wrinkling morphologies may also develop with cavitation as soon as the weight loss exceeds a critical value. Note that in the latter case also different wrinkling patterns may develop depending on the shrinkage induced. Skins that exhibit elastic behaviour and have high elastic modulus and sufficient thickness will be amenable to cavitation, where the formation of the cavity reduces the pressure difference during drying, impeding the occurrence of wrinkling.

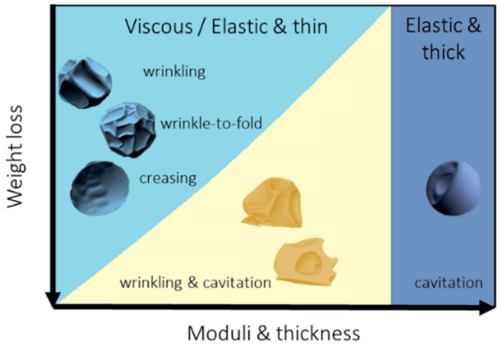

Figure 7.6. Schematic overview of the particle morphology evolution from skin formation onwards. The morphology evolution depends on the weight loss of the droplet and the evolution of the rheological behaviour and thickness of the skin (Du et al., 2020; Li et al., 2011).

7.4. Pilot-scale spray drying of maltodextrins

Single droplet drying in combination with investigating the rheological properties of drying materials at different concentrations and temperatures has helped to capture the essential mechanisms underlying the morphology evolution of a drying food droplet. The question remains if these mechanisms derived from single droplet drying studies are also useful in interpreting the particle morphology developed for large scale dryers. Translating the knowledge as obtained at a single droplet scale to large scale spray dryers may for instance be more intricate due to the wide droplet size distribution combined with the different particle trajectories entailing droplet-droplet interactions, droplet-wet particle interactions and droplet-drying chamber wall collisions. Additionally, for large scale dryers, the drying rate is relatively faster and the drying time is relatively shorter by several magnitudes when compared to single droplet dryers, which may further complicate the interpretation of the morphology evolution (Fu, Woo, Chen, et al., 2012). These differences are mostly ascribed to the smaller initial droplet sizes obtained during spray drying when compared to single droplet drying, resulting in a reduced timescale of the drying process ($t \sim d^2$). Despite these difficulties, several researchers already compared the morphologies obtained at different scales (Both et al., 2020; Gouaou et al., 2019; Nuzzo et al., 2015, 2017; Ullum et al., 2010). For example, Both et al. (2020) demonstrated by comparing pilot-scale to single droplet drying experiments that overall the particle morphologies observed after pilot-scale drying for mixtures of maltodextrins and whey proteins could be deduced from single droplet drying experiments. Nuzzo et al. (2015) showed that the morphology of polymer-lactose particles prepared by spray drying was well reproduced with single droplet drying. A later study by

Nuzzo et al. (2017) concluded that the morphology of whole milk particles dried at single droplet, laboratory and spray drying scale is quite similar despite differences in physical scale and time scale. Similarly, Ullum et al. (2010) found that the particle morphology from single levitated droplet drying experiments agreed well with the morphology of spray-dried particles if processed under conditions similar to the outlet conditions of the spray drying process. These studies suggest that regardless of differences in drying scale, similar mechanisms govern the morphology development.

Hence it is of interest to investigate the translation of our proposed mechanisms for morphology development to powder morphologies as obtained at larger drying scales. For this, pilot-scale spray drying experiments were performed at different process conditions for 30% (w/w) maltodextrin DE6 and maltodextrin DE21 using a single-stage pilot-scale spray dryer (DW350 Spray dry work, Netherlands). To assess the effect of drying rate on the developed morphology, we varied the inlet drying air temperatures (160, 180 and 200 °C), while the outlet air temperature was kept constant at 80 °C by adjusting the feed flow rate. The inlet air temperature was selected as a parameter of interest for morphology development as this is a key parameter during the initial drying, where most evaporation takes place and skin formation is initiated (Both et al., 2020). The outlet air temperature is more important at the final stage of drying, where most water has already evaporated and the morphology has already been developed. The produced powder morphologies were analysed with scanning electron microscopy (SEM) and microscopic imaging using a Malvern Morphologi 4 system as explained by Both et al. (2020). The Morphologi 4 particle characterization was used for morphology characterization of more than 10,000 individual particles per powder sample from 2D images. The filters applied to classify the particles are described in Table A.7.3.

When viewing the quantitative morphology results as obtained with the Morphologi 4 using the applied filters, it can be noted that the majority of the larger particles produced (between 20 and 100 μm) were classified as wrinkled for all drying conditions applied and for both DE values. Increasing the inlet temperature resulted in less wrinkled particles and more spherical and hollowed particles (Fig. 7.7), similar as observed by Both et al. (2020) and Gouaou et al. (2019). Alamilla-Beltrán et al. (2005) state that at lower drying temperatures, the mechanisms allowing for droplet shrinkage and deformations are more pronounced. Higher drying air temperature is associated with higher drying rates resulting in faster stable skin formation which decreases the residence time for particle deformation and therefore leading to an

increase in particles with spherical and hollow morphologies (El-Sayed et al., 1990; Gouaou et al., 2019; Hassan & Mumford, 1993; Walton, 2000). Small size droplets also have a higher rate of evaporation, therefore this also could explain an increase in the fraction of particles classified as spherical and hollow for smaller particles (between 5 and 20 µm) compared to larger particles at the same processing conditions. In contrast to the larger particles, the smaller particles generally had a dominant spherical and hollow morphology.

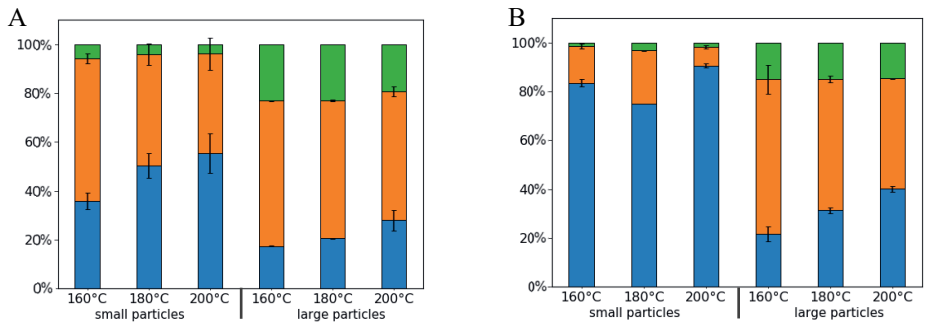

Figure 7.7. Morphologi 4 results with % spherical and hollow (blue), % wrinkled (orange) and % other (green) for maltodextrin DE6 (A) and maltodextrin DE21 (B) as dried at different inlet air temperatures with an outlet air temperature of 80 °C. Results are divided into two size groups: small particles (between 5 and 20 µm) and large particles (between 20 and 100 µm). Morphology categorization can be found in the Appendix. Other morphologies indicate particles that were fragmented or agglomerated without a distinctive morphology. The error bars represent the absolute error.

The quantitative morphological results, especially when viewing the larger particles, suggested that both maltodextrins yield quite similar particle morphologies regardless of the DE value. However, 3D visualization using SEM revealed more morphological details which were not detected using the Morphologi 4 analysis. SEM imaging did show morphological differences between maltodextrin DE6 and DE21 powders (Fig. 7.8 and A.7.1). The majority of DE21 particles showed wrinkled morphologies with coarser edges than maltodextrin DE6 particles. Maltodextrin DE6 particles were more spherical and featured smooth surface dents. The fact that the Morphologi 4 analysis could not detect these differences can be explained as even small surface distortions for spherical particles can cause protuberances leading to reduced HS circularity in 2D analysis. Therefore, the DE6 particles that are more spherical on SEM images are still characterized as wrinkled by the Morphologi 4 analysis using the applied filters.

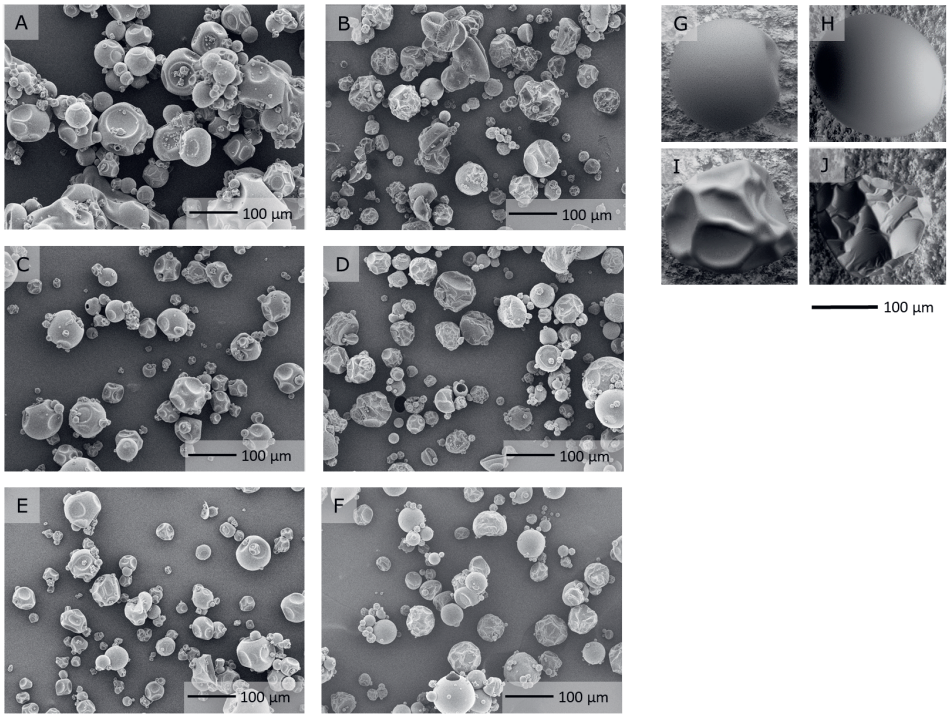

Figure 7.8. SEM images of maltodextrin particles after pilot-scale spray drying: (A) 200/80 °C DE6, (B) 200/80 °C DE21, (C) 180/80 °C DE6, (D) 180/80 °C DE21, (E) 160/80 °C DE6, (F) 160/80 °C DE21. SEM images of maltodextrin particles after single droplet drying from Chapter 4: (G) 60 °C DE5, (G) 90 °C DE5, (I) 60 °C DE21, (J) 90 °C DE21, 0.3 m/s, 30% (w/w).

Particle morphologies that we observed with DE6 powders were also found for spray drying of hydroxypropylated pea starch (15-30 wt%), where spherical particles with undulated particle surfaces were observed for different drying conditions. For maltodextrin DE21, wrinkled morphologies after spray drying were confirmed by Turchiuli et al. (2011). Alamilla-Beltrán et al. (2005) and Ullum et al. (2010) reported comparable wrinkled morphologies for drying of maltodextrin DE20 and DE18, respectively. Additionally, from the SEM images, it can be observed that the wrinkled morphologies obtained for DE21 after pilot-scale drying resemble the morphologies obtained after single droplet drying. When comparing single droplet dried particles of maltodextrin DE5 with pilot-spray-dried particles of maltodextrin DE6, single particles have fewer surface deformations when compared to the pilot-scale dried particles. Besides, for drying of maltodextrin DE5, cavitation was observed during single droplet drying, rendering spherical and hollow particles. It may be speculated that especially the more spherical particles produced with DE6 are also hollow, but this is hard to conclude from our results only. However, analysis of cross-cut structures for spray-

dried powders with different DE values revealed that in particular low DE maltodextrins typically have large vacuoles (Ghani et al., 2017; Gharsallaoui et al., 2012).

Despite the different time and length scales for single droplet drying and pilot-scale spray drying, the majority of maltodextrin DE21 droplets developed a wrinkled particle morphology. This can be explained by the viscous behaviour of the skin as expected based on rheological measurements (Chapter 5). The compressive stress elicited by the shrinkage of the droplet during drying triggers the formation of wrinkling patterns as was previously explained (section 7.3.4). The DE21 pilot-scale powder particles showed both wrinkled structures with periodic surface undulations and wrinkle-to-fold patterns with polygons narrowing into deeper surface valleys (Li et al., 2012). Although the majority of the larger DE21 particles showed wrinkled surfaces, we also found small spherical and smooth particles, especially at the higher inlet air temperatures tested (Fig. 7.7, 7.8 and A.7.1). Similar smooth and spherical morphologies were found alongside wrinkled morphologies by Alfons et al. (2021) for pilot-scale spray drying of maltodextrin DE21 at 30% (w/w) at an inlet air temperature of 220 °C and an outlet temperature of 100 °C. Small droplets at high drying temperatures experience high drying rates, resulting in fast evaporation and in turn fast concentration of the outer layers of the droplet leading to rapid skin formation. If in this case, the viscous skin formed also quickly reaches a high glass transition temperature to drop temperature ratio (T_g/T_{drop}), the moduli of the skin may significantly increase (Chapter 5). When the moduli of the skin increase sufficiently fast during drying and reach for example the vicinity of glass transition (~10^8 Pa), further shrinkage of the particle may be hampered such that the critical shrinkage factor for inducing surface wrinkling is not exceeded. The lower drying rates that larger DE21 droplets experience result in viscous skins which approach high T_g/T_{drop} and consequently high moduli later during drying, allowing more time for structures to shrink and consequently wrinkling patterns may be observed.

Maltodextrin DE6 yielded predominantly spherical particles with smooth surface dents. Some pilot-scale dried particles resembled the morphologies observed after single droplet drying of 30% (w/w) maltodextrins DE5, however, most of the powder particles showed more surface dents than obtained after single droplet drying. For low DE maltodextrins during drying, elastic behaviour of the skin is expected based on rheological measurements (Chapter 5). The disparity in morphology between single droplet scale and pilot-scale

morphologies may be ascribed to the skin thickness of the particles. The skins developed for DE5 during drying of larger single droplets exhibit elastic behaviour and likely have sufficient thickness to result in smooth and hollow particles (section 7.3.4). The higher drying rates in smaller droplets or with higher drying air temperatures during pilot-scale spray drying may result in earlier skin formation with a skin of limited thickness when compared to single droplet drying scale. This effect of the development of a thin skin upon fast skin formation was already suggested by Gouaou et al. (2019), who demonstrated that the skin thickness was reduced at higher air temperature due to increased evaporation rates, leading to an early locking point, and a thin skin. A similar picture is sketched by Archer et al. (2020) for drying aerosol droplets containing nanosilica particles, where increasing drying rate (i.e. higher Péclet number) results in earlier locking and a thin skin. Although the skins developed for DE6 during pilot drying may exhibit elastic behaviour at an early stage of drying, the skin may have been too thin to prevent denting before cavitation (section 7.3.4). If, however, the skin moves very quickly to high T_g/T_{drop}, again the skin may be less susceptible to deformations, yielding more spherical and smooth particles. For testing if the skin thickness varies between the drying scales, it would already be relevant to compare the morphologies developed for similar sized droplets after single droplet drying at moderate temperature (e.g. 60/90 °C, as we have used) with the morphologies after single droplet drying with an air temperature-time profile resembling that of pilot-scale drying (e.g. from 200 °C going to 80 °C in a very short time). The latter may allow for rapid initial drying and faster skin formation, rendering an elastic skin with a limited thickness which may make them more susceptible to denting than the skins formed for single droplets dried at moderate temperatures.

Overall, these findings demonstrate that pilot-scale drying yields a distribution in particle morphologies for both maltodextrins likely owing to the diversity in skin properties developed throughout drying. Our previously proposed mechanisms for the morphology development of single droplets helped to interpret the final morphologies developed after pilot-scale spray drying. Hence, this corroborates that single droplet drying is a valuable method to arrive at a deeper understanding of the mechanisms governing morphology development. The proposed mechanisms may be further tested with single droplet drying techniques that can simulate the temperature profile of (industrial) large scale dryers, allowing for higher drying rates. Pilot-scale spray drying experiments also suggest the importance of viewing the rheological properties of the skin together with the skin thickness.

7.5. Conclusions and future directions

This thesis reports on the morphology development of drying food droplets aiming at unravelling the mechanisms governing the morphology development. Although the particle morphology is the result of a complex interplay of matrix properties and drying dynamics, a more mechanistic understanding of this interplay was obtained by investigating sessile drying droplets, moisture diffusion, rheological properties of materials, molecular weight distributions and glass transition temperatures of model food components. We addressed the importance of the rheological behaviour of the droplet skin for explaining the mechanical instabilities triggered during drying and accordingly the final morphology. The rheological properties of the skin were interpreted or predicted from the time-temperature-concentration evolution of the rheological properties of the drying material. For maltodextrins we could describe this rheological evolution with a model that we coupled with a single droplet drying model to predict the rheological behaviour of the skin at the onset of morphology development.

For obtaining the rheological properties, we measured small deformation shear moduli of the drying systems; important for describing cavitation in soft matter spheres (Hong et al., 2009; Wang & Cai, 2015) and useful in explaining wrinkling and cavitation during single droplet drying (Both, Tersteeg, et al., 2019). Other techniques offer great potential to assess the rheological properties of the skin developed, including indentation techniques on concentrated thin films at room temperature (Sadek, Pauchard, et al., 2015) and drop tensiometry at room temperature for relatively low concentrations (Andersson et al., 2018; Yu et al., 2021). All these techniques offer insights into the rheological properties of the skin but only provide offline measurements. Ideally, though, the development of inline techniques allowing for time-resolved measurements of the rheological properties of drying materials experiencing evaporation at realistic drying temperatures is highly desired. These techniques should also be capable of dealing with the development of spatial gradients.

Besides methods to better assess the rheological properties of the skin, it would also be relevant to study the evolution of the skin thickness during drying as both codetermine the morphological evolution followed. The skin thickness is usually based on predictions as it is difficult to experimentally assess the thickness of the droplet skin in situ during drying. Only after drying, data on the skin thickness may be obtained by analysis of cross-cut structures. It would be desirable if non-destructive microscopy techniques with high spatial and temporal

resolution could be used in combination with single droplet drying techniques to monitor the skin thickness development, possibly confocal Raman microscopy or other laser illumination techniques could be applied for serving this purpose (Both, Nuzzo, et al., 2018; Nuzzo et al., 2015; Nuzzo et al., 2017; Schutyser et al., 2018).

A next step to advance our understanding of morphology development would be to further develop numerical models for predicting morphology development. In this work, we could predict the rheological properties of the skin and accordingly the morphology developed for maltodextrins by integrating rheology and drying kinetics. This modelling approach relied on using TTCS. This TTCS approach is expected to work for solutes with random coil-like configuration, however, its application is limited for whey proteins. It would therefore be relevant to develop alternative models which can be tuned with rheological data to describe the rheology as a function of concentration, temperature and relevant time. Ideally, morphological models are developed that integrate the mechanical stress and strain functions and drying kinetics, and accordingly predict the conditions under which cavitation/wrinkling phenomena occur. For practical use, the results may be captured in morphology maps, as was for instance already proposed by Du et al. (2020). These models could first be optimized for important model food systems, like whey proteins, caseins and maltodextrins and mixtures thereof and then be generalised to more complex food formulations, including milk. Preferably however, a database is developed containing important material parameters of different systems to tune the morphological model for drying of various food systems. Since the mechanisms proposed for the morphology evolution of a single droplet were also valuable for explaining pilot-scale particle morphologies, it may be expected that the model developed may eventually be useful for establishing guidelines for steering spray drying processes towards desired morphologies.

7.6. Appendix

Table A.7.1. Denaturation onset temperatures and denaturation peak temperatures of WPI samples at different concentrations heated from 20 to 100 °C. Samples were measured at least in duplicate and standard deviations are shown in superscript.

Sample	T_{onset} (°C)	T_d (°C)
WPI rotary evaporation (~50% (w/w))	$61.9^{\pm 1.49}$	$68.0^{\pm 0.47}$
WPI climate chamber (~60% (w/w))	$63.2^{\pm 0.54}$	$67.9^{\pm 0.10}$
WPI climate chamber (~70% (w/w))	$75.7^{\pm 0.50}$	$88.2^{\pm 1.25}$

Table A.7.2. Fitted model parameters for WPI systems at different concentration (% (w/w)).

Marin-Graessley parameters	48.2	58.0	67.2
τ_M (s)	10^3	10^3	10^3
τ_α (s)	10^{10}	0.5	0.5
τ_p (s)	-	$1 \cdot 10^3$	10^3
k_α (-)	$8 \cdot 10^{16}$	$7 \cdot 10^3$	$3 \cdot 10^3$
k_p (-)	-	$8 \cdot 10^3$	$6 \cdot 10^3$
G_∞ (Pa)	$4 \cdot 10^7$	10^7	10^7
α (-)	0.93	0.26	0.26
p (-)	-	0.32	0.25

Table A.7.3. Filter settings used in the Morphologi 4 analyzer software to discriminate spherical and hollow, wrinkled and other particles.

		HS Circularity**		
		<0.85	0.85≤ x <0.98	≥0.98
Intensity mean*	<50	Other	Wrinkled	Spherical & hollow
	≥50		Spherical & hollow	Spherical & hollow

* Intensity mean: the average of the pixel greyscale levels in the object ranging from 0 (black) to 255 (white)

** HS Circularity: $\frac{4*\pi*Area}{Perimeter^2}$

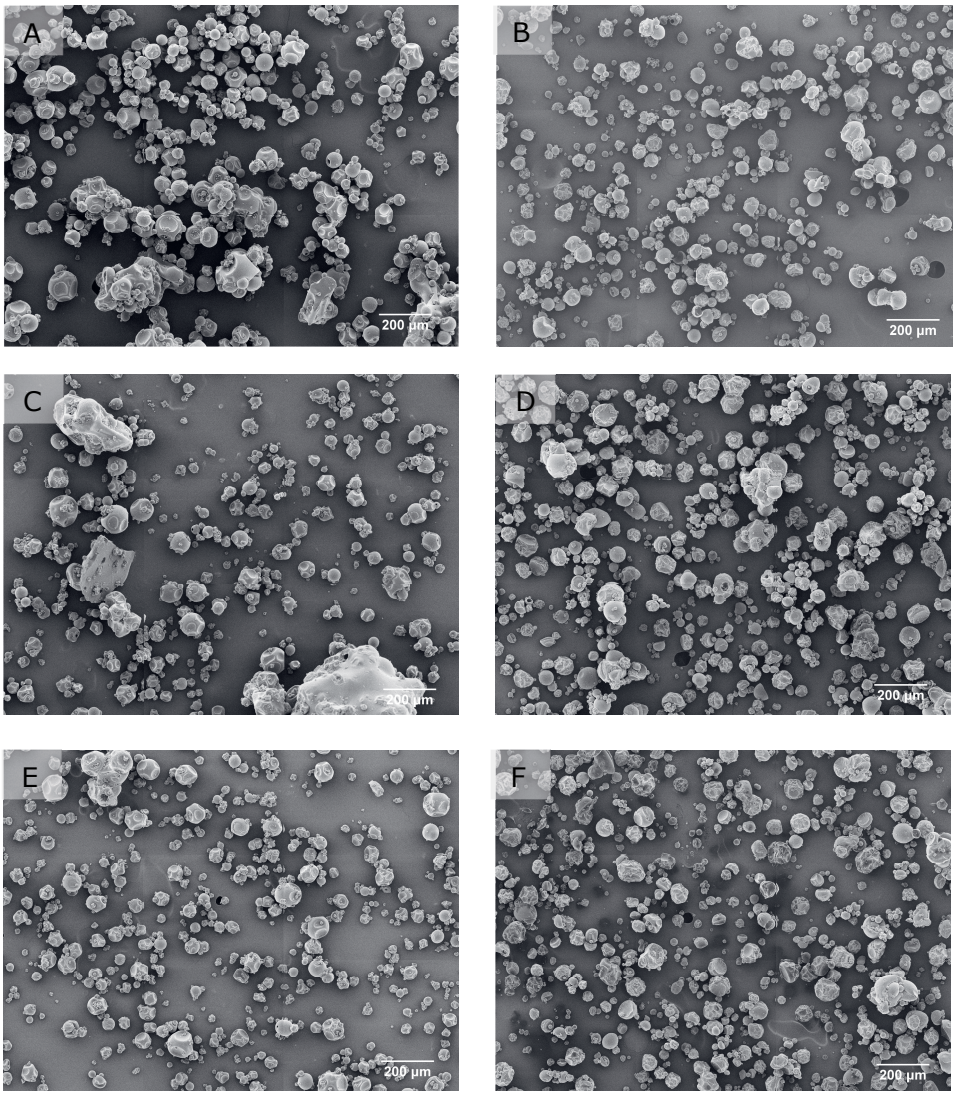

Figure A.7.1. SEM montage images of maltodextrin particles after pilot-scale spray drying: (A) 200/80 °C DE6, (B) 200/80 °C DE21, (C) 180/80 °C DE6, (D) 180/80 °C DE21, (E) 160/80 °C DE6, (F) 160/80 °C DE21. Scale bars are provided.

R

References

Abdul-Fattah, A. M., Kalonia, D. S., & Pikal, M. J. (2007). The challenge of drying method selection for protein pharmaceuticals: Product quality implications. *Journal of Pharmaceutical Sciences*, *96*(8), 1886–1916. https://doi.org/10.1002/jps.20842

Adhikari, B., Howes, T., & Bhandari, B. R. (2007). Use of solute fixed coordinate system and method of lines for prediction of drying kinetics and surface stickiness of single droplet during convective drying. *Chemical Engineering and Processing: Process Intensification*, *46*(5), 405–419. https://doi.org/10.1016/j.cep.2006.06.018

Adhikari, B., Howes, T., Bhandari, B. R., & Troung, V. (2004). Effect of addition of maltodextrin on drying kinetics and stickiness of sugar and acid-rich foods during convective drying: Experiments and modelling. *Journal of Food Engineering*, *62*(1), 53–68. https://doi.org/10.1016/S0260-8774(03)00171-7

Adhikari, B., Howes, T., Bhandari, B. R., & Truong, V. (2000). Experimental studies and kinetics of single drop drying and their relevance in drying of sugar rich foods : A review. *International Journal of Food Properties, 3*(3). https://doi.org/10.1080/10942910009524639

Akkerman, J. C. (1992). *Drainage of curd*. Wageningen University.

Alamilla-Beltrán, L., Chanona-Pérez, J. J., Jiménez-Aparicio, A. R., & Gutiérrez-Lopez, G. F. (2005). Description of morphological changes of particles along spray drying. *Journal of Food Engineering*, *67*(1–2), 179–184. https://doi.org/10.1016/j.jfoodeng.2004.05.063

Alexander, M., Rojas-Ochoa, L. F., Leser, M., & Schurtenberger, P. (2002). Structure, dynamics, and optical properties of concentrated milk suspensions: An analogy to hard-sphere liquids. *Journal of Colloid and Interface Science*, *253*(1), 35–46. https://doi.org/10.1006/jcis.2002.8452

Alfons, J., Valentin, T., Hinrichs, J., & Kohlus, R. (2021). Nozzle zone agglomeration in spray dryers : In fl uence of total solid content on agglomerate properties. *Powder Technology*, *390*, 292–302. https://doi.org/10.1016/j.powtec.2021.05.094

Anandharamakrishnan, C., Rielly, C. D., & Stapley, A. G. F. (2008). Loss of solubility of α-lactalbumin and β-lactoglobulin during the spray drying of whey proteins. *LWT - Food Science and Technology*, *41*(2), 270–277. https://doi.org/10.1016/j.lwt.2007.03.004

Andersson, I. M., Glantz, M., Alexander, M., Millqvist-Fureby, A., Paulsson, M., & Bergenståhl, B. (2018). Impact of surface properties on morphology of spray-dried milk serum protein/lactose systems. *International Dairy Journal*, *85*, 86–95. https://doi.org/10.1016/j.idairyj.2018.04.011

Anese, M., Shtylla, I., Torreggiani, D., & Maltini, E. (1996). Water activity and viscosity—relations with glass transition temperatures in model food systems. *Thermochimica Acta*, *275*(1), 131–137. https://doi.org/10.1016/0040-6031(95)02712-2

Archer, J., Walker, J. S., Gregson, F. K. A., Hardy, D. A., & Reid, J. P. (2020). Drying kinetics and particle formation from dilute colloidal suspensions in aerosol droplets. *Langmuir*, *36*(42), 12481–12493. https://doi.org/10.1021/acs.langmuir.0c01830

Aschenbrenner, M., Kulozik, U., & Foerst, P. (2012). Evaluation of the relevance of the glassy state as stability criterion for freeze-dried bacteria by application of the Arrhenius and WLF model. *Cryobiology*, *65*(3), 308–318. https://doi.org/10.1016/j.cryobiol.2012.08.005

Atkins, P., & De Paula, J. (2010). *Physical Chemistry* (9th). Oxford University Press.

Augusto, P. E. D., Falguera, V., Cristianini, M., & Ibarz, A. (2013). Viscoelastic Properties of Tomato Juice: Applicability of the Cox-Merz Rule. *Food and Bioprocess Technology*, *6*(3), 839–843. https://doi.org/10.1007/s11947-011-0655-y

Avaltroni, F., Bouquerand, P. E., & Normand, V. (2004). Maltodextrin molecular weight distribution influence on the glass transition temperature and viscosity in aqueous solutions. *Carbohydrate Polymers*, *58*(3), 323–334. https://doi.org/10.1016/j.carbpol.2004.08.001

Baulin, V. A., & Halperin, A. (2002). Concentration dependence of the flory χ parameter within two-state models. *Macromolecules*, *35*(16), 6432–6438. https://doi.org/10.1021/ma020296o

Bird, R. B., Stewart, W. E., & Lightfoot, E. N. (1960). *Transport Phenomena*. John Wiley & Sons.

Boel, E., Koekoekx, R., Dedroog, S., Babkin, I., Vetrano, M. R., Clasen, C., & Van den Mooter, G. (2020). Unraveling particle formation: From single droplet drying to spray drying and electrospraying. *Pharmaceutics*, *12*(7), 1–58. https://doi.org/10.3390/pharmaceutics12070625

Both, E. M. (2019). *Powder morphology development during spray drying*. Wageningen University & Research.

Both, E. M., Boom, R. M., & Schutyser, M. A. I. (2020). Particle morphology and powder properties during spray drying of maltodextrin and whey protein mixtures. *Powder Technology*, *363*, 519–524. https://doi.org/10.1016/j.powtec.2020.01.001

Both, E. M., Karlina, A. M., Boom, R. M., & Schutyser, M. A. I. (2018a). Morphology development during sessile single droplet drying of mixed maltodextrin and whey protein solutions. *Food Hydrocolloids*, *75*, 202–210. https://doi.org/10.1016/j.foodhyd.2017.08.022

Both, E. M., Nuzzo, M., Millqvist-Fureby, A., Boom, R. M., & Schutyser, M. A. I. (2018b). Morphology development during single droplet drying of mixed component formulations and milk. *Food Research International*, *109*(April), 448–454. https://doi.org/10.1016/j.foodres.2018.04.043

Both, E. M., Siemons, I., Boom, R. M., & Schutyser, M. A. I. (2019a). The role of viscosity in morphology development during single droplet drying. *Food Hydrocolloids*, *94*, 510–518.

Both, E. M., Tersteeg, S. M. B., Boom, R. M., & Schutyser, M. A. I. (2019b). Drying kinetics and viscoelastic properties of concentrated thin films as a model system for spray drying. *Colloids and Surfaces A: Physicochemical and Engineering Aspects*, *585*.

Bouchoux, A., Debbou, B., Gésan-Guiziou, G., Famelart, M. H., Doublier, J. L., & Cabane, B. (2009). Rheology and phase behavior of dense casein micelle dispersions. *Journal of Chemical Physics*, *131*(16). https://doi.org/10.1063/1.3245956

Bouchoux, A., Gésan-Guiziou, G., Pérez, J., & Cabane, B. (2010). How to squeeze a sponge: Casein micelles under osmotic stress, a SAXS study. *Biophysical Journal*, *99*(11), 3754–3762. https://doi.org/10.1016/j.bpj.2010.10.019

Bouchoux, A., Schorr, D., Daffé, A., Cambert, M., Gésan-Guiziou, G., & Mariette, F. (2012). Molecular mobility in dense protein systems: An investigation through 1H NMR Relaxometry and Diffusometry. *Journal of Physical Chemistry B*, *116*(38), 11744–11753. https://doi.org/10.1021/jp306078k

Bouman, J., Venema, P., de Vries, R. J., van der Linden, E., & Schutyser, M. A. I. (2016). Vacuole and hole formation during drying of sessile whey protein droplets. *Food Research International*, *84*, 16. https://doi.org/10.1016/j.foodres.2016.03.027

Brindle, L. P., & Krochta, J. M. (2008). Physical properties of whey protein-hydroxypropylmethylcellulose blend edible films. *Journal of Food Science*, *73*(9). https://doi.org/10.1111/j.1750-3841.2008.00941.x

Brinson, H. F., & Brinson, L. C. (2015). *Polymer Engineering Science and Viscoelasticity: An Introduction*. Springer. https://doi.org/10.1007/978-1-4899-7485-3

Broeckx, G., Vandenheuvel, D., Claes, I. J. J., Lebeer, S., & Kiekens, F. (2016). Drying techniques of probiotic bacteria as an important step towards the development of novel pharmabiotics. *International Journal of Pharmaceutics*, *505*(1–2), 303–318. https://doi.org/10.1016/j.ijpharm.2016.04.002

Broeckx, G., Vandenheuvel, D., Henkens, T., Kiekens, S., van den Broek, M. F. L., Lebeer, S., & Kiekens, F. (2017). Enhancing the viability of *Lactobacillus rhamnosus* GG after spray drying and during storage. *International Journal of Pharmaceutics*, *534*(1–2), 35–41. https://doi.org/10.1016/j.ijpharm.2017.09.075

Brownsey, G. J., Noel, T. R., Parker, R., & Ring, S. G. (2003). The glass transition behavior of the globular protein bovine serum albumin. *Biophysical Journal*, *85*(6), 3943–3950. https://doi.org/10.1016/S0006-3495(03)74808-5

Bryant, G., Koster, K. L., & Wolfe, J. (2001). Membrane behaviour in seeds and other systems at low water content: The various effects of solutes. *Seed Science Research*, *11*(1), 17–25. https://doi.org/10.1079/SSR200056

Buma, T. J. (1965). The true density of spray milk powders and of certain constituents. *Neth. Milk Dairy J.*, *19*, 249–265.

Bumiller, M., Carson, J., & Prescott, J. (2002). A Preliminary Investigation Concerning The Effect Of Particle Shape On a Powder's Flow Properties. *World Congress on Particle Technology*, *July*. https://doi.org/10.1017/CBO9781107415324.004

Cangialosi, D., Schut, H., Van Veen, A., & Picken, S. J. (2003). Positron annihilation lifetime spectroscopy for measuring free volume during physical aging of polycarbonate. *Macromolecules*, *36*(1), 142–147. https://doi.org/10.1021/ma021214z

Castro, N., Durrieu, V., Raynaud, C., & Rouilly, A. (2016). Influence of DE-value on the physicochemical properties of maltodextrin for melt extrusion processes. *Carbohydrate Polymers*, *144*, 464–473. https://doi.org/10.1016/j.carbpol.2016.03.004

Chávez, B. E., & Ledeboer, A. M. (2007). Drying of probiotics: Optimization of formulation and process to enhance storage survival. *Drying Technology*, *25*(7–8), 1193–1201. https://doi.org/10.1080/07373930701438576

Chen, X. D. (2007). Moisture diffusivity in food and biological materials. *Drying Technology*, *25*(7–8), 1203–1213. https://doi.org/10.1080/07373930701438592

Chew, J. H., Liu, W., Fu, N., Gengenbach, T., Chen, X. D., & Selomulya, C. (2014). Exploring the drying behaviour and particle formation of high solids milk protein concentrate. *Journal of Food Engineering*, *143*, 186–194. https://doi.org/10.1016/j.jfoodeng.2014.07.004

Chronakis, I. S. (1998). On the molecular characteristics, compositional properties, and structural-functional mechanisms of maltodextrins: A review. *Critical Reviews in Food Science and Nutrition*, *38*(7), 599–637. https://doi.org/10.1080/10408699891274327

Cicuta, P., Stancik, E. J., & Fuller, G. G. (2003). Shearing or compressing a soft glass in 2D: time-concentration superposition. *Physical Review Letters*, *90*(23), 236101.

Colsenet, R., Mariette, F., & Cambert, M. (2005). NMR relaxation and water self-diffusion studies in whey protein solutions and gels. *Journal of Agricultural and Food Chemistry*, *53*(17), 6784–6790. https://doi.org/10.1021/jf050162k

Couchman, P. R., & Karasz, F. E. (1978). A Classical Thermodynamic Discussion of the Effect of Composition on Glass-Transition Temperatures. *Macromolecules*, *11*(1), 117–119. https://doi.org/10.1021/ma60061a021

Coumans, W. J. (2000). Models for drying kinetics based on drying curves of slabs. *Chemical Engineering and Processing: Process Intensification*, *39*(1), 53–68. https://doi.org/10.1016/S0255-2701(99)00084-7

Cox, W. P., & Merz, E. H. (1958). Correlation of dynamic and steady flow viscosities. *Journal of Polymer Science*, *28*(118), 619–622.

Dahbi, L., Alexander, M., Trappe, V., Dhont, J. K. G., & Schurtenberger, P. (2010). Rheology and structural arrest of casein suspensions. *Journal of Colloid and Interface Science*, *342*(2), 564–570. https://doi.org/10.1016/j.jcis.2009.10.042

Darken, L. S. (1948). Diffusion, mobility and their interrelaton through free energy in binary metallic systems. *Transactions of the American Institute of Mining, Metallurgical and Petroleum Engineers*, *175*, 184–201.

Dauphas, S., Mouhous-Riou, N., Metro, B., MacKie, A. R., Wilde, P. J., Anton, M., & Riaublanc, A. (2005). The supramolecular organisation of β-casein: Effect on interfacial properties. *Food Hydrocolloids*, *19*(3), 387–393. https://doi.org/10.1016/j.foodhyd.2004.10.005

De Freitas, R. A., Spier, V. C., Sierakowski, M. R., Nicolai, T., Benyahia, L., & Chassenieux, C. (2015). Transient and quasi-permanent networks in xyloglucan solutions. *Carbohydrate Polymers*, *129*, 216–223. https://doi.org/10.1016/j.carbpol.2015.04.066

De Kruif, C. G., Huppertz, T., Urban, V. S., & Petukhov, A. V. (2012). Casein micelles and their internal structure. *Advances in Colloid and Interface Science*, *171–172*, 36–52. https://doi.org/10.1016/j.cis.2012.01.002

De Wit, J. N., & Van Kessel, T. (1996). Effects of ionic strength on the solubility of whey protein products. A colloid chemical approach. *Food Hydrocolloids*, *10*(2), 143–149. https://doi.org/10.1016/S0268-005X(96)80028-2

Dealy, J., & Plazek, D. (2009). Time-temperature superposition-a users guide. *Rheology Bulletin*, *78*(2), 16–31.

deWit, J. N., & Klarenbeek, G. (1984). Effects of Various Heat Treatments on Structure and Solubility of Whey Proteins. *Journal of Dairy Science*, *67*(11), 2701–2710. https://doi.org/10.3168/jds.S0022-0302(84)81628-8

Dhanalakshmi, K., Ghosal, S., & Bhattacharya, S. (2011). Agglomeration of food powder and applications. *Critical Reviews in Food Science and Nutrition*, *51*(5), 432–441. https://doi.org/10.1080/10408391003646270

Dickinson, E. (2001). Milk protein interfacial layers and the relationship to emulsion stability and rheology. *Colloids and Surfaces B: Biointerfaces*, *20*(3), 197–210. https://doi.org/10.1016/S0927-7765(00)00204-6

Dissanayake, M., Liyanaarachchi, S., & Vasiljevic, T. (2012). Functional properties of whey proteins microparticulated at low pH. *Journal of Dairy Science*, *95*(4), 1667–1679. https://doi.org/10.3168/jds.2011-4823

Dissanayake, M., Ramchandran, L., & Vasiljevic, T. (2013). Influence of pH and protein concentration on rheological properties of whey protein dispersions. *International Food Research Journal*, *20*(5), 2167–2171.

Dobry, D. E., Settell, D. M., Baumann, J. M., Ray, R. J., Graham, L. J., & Beyerinck, R. A. (2009). A model-based methodology for spray-drying process development. *Journal of Pharmaceutical Innovation*, *4*(3), 133–142. https://doi.org/10.1007/s12247-009-9064-4

Dokic, P., Jakovljevic, J., & Dokic-Baucal, L. (1998). Molecular characteristics of maltodextrins and rheological behaviour of diluted and concentrated solutions. *Colloids and Surfaces A: Physicochemical and Engineering Aspects*, *141*(3), 435–440. https://doi.org/10.1016/S0927-7757(97)00118-0

Donev, A., Cisse, I., Sachs, D., Variano, E. A., Stillinger, F. H., Connelly, R., Torquato, S., & Chaikin, P. M. (2004). Improving the Density of Jammed Disordered Packings Using Ellipsoids. *Science*, *303*(5660), 990 LP – 993. https://doi.org/10.1126/science.1093010

Dormidontova, E. E. (2002). Role of competitive PEO-water and water-water hydrogen bonding in aqueous solution PEO behavior. *Macromolecules*, *35*(3), 987–1001. https://doi.org/10.1021/ma010804e

Dörr, A., Sadiki, A., & Mehdizadeh, A. (2013). A discrete model for the apparent viscosity of polydisperse suspensions including maximum packing fraction. *Journal of Rheology*, *57*(3), 743–765. https://doi.org/10.1122/1.4795746

Du, G., Ye, F., Doi, M., & Meng, F. (2020). Drying Pathways of an Evaporating Soft Matter Droplet. *ArXiv*.

Dupas-Langlet, M., Meunier, V., Pouzot, M., & Ubbink, J. (2019). Influence of blend ratio and water content on the rheology and fragility of maltopolymer/maltose blends. *Carbohydrate Polymers*, *213*(November 2018), 147–158. https://doi.org/10.1016/j.carbpol.2019.02.066

Einstein, A. (1905). No Title. *Ann. Physics*, *17*(4), 549.

El-Sayed, T. M., Wallack, D. A., & King, C. J. (1990). Changes in particle morphology during drying of drops of carbohydrate solutions and food liquids. 1. Effect of composition and drying conditions. *Industrial & Engineering Chemistry Research*, *29*(12), 2346–2354.

Fäldt, P., Bergenståhl, B., & Carlsson, G. (1993). The surface coverage of fat on food powders analyzed by ESCA (electron spectroscopy for chemical analysis). *Food Structure*, *12*(2), 225–234.

Ferrari, G., Meerdink, G., & Walstra, P. (1989). Drying kinetics for a single droplet of skim-milk. *Food Engineering*, *10*(3), 215–230.

Ferry, J. D. (1980). *Viscoelastic properties of polymers*. John Wiley & Sons.

Ferry, J. D., Grandine, L. D., & Fitzgerald, E. R. (1953). The relaxation distribution function of polyisobutylene in the transition from rubber-like to glass-like behavior. *Journal of Applied Physics*, *24*(7), 911–916. https://doi.org/10.1063/1.1721401

Filková, I., Huang, L. X., & Mujumdar, A. S. (2014). Industrial spray drying systems. In *Handbook of industrial drying*.

Filková, I., & Mujumdar, A. S. (1995). Industrial Spray Drying Systems. In *Handbook of industrial drying* (pp. 263–308).

Finotello, G., Padding, J. T., Deen, N. G., Jongsma, A., Innings, F., & Kuipers, J. A. M. (2017). Effect of viscosity on droplet-droplet collisional interaction. *Physics of Fluids*, *29*(6), 067102.

Flory, P. J. (1953). *Principles of Polymer Chemistry*. Cornell University Press.

Foerster, M., Woo, M. W., & Selomulya, C. (2016). Single Droplet Drying. In *Reference Module in Food Science*. Elsevier. https://doi.org/10.1016/b978-0-08-100596-5.21154-2

Fox, T. G., & Flory, P. J. (1950). Second order transition temperature and related properties of PS. *Journal of Applied Physics*, *21*(6), 581–591.

Frossling, N. (1938). Uber die Verdunstung Fallender Tropfen. *Gerlands Beitr. Geophys*, *52*, 107–216.

Fu, N., Xiao, J., Woo, M. & Chen, X.D. (2020). *Frontiers in spray drying*. CRC press.

Fu, N., Woo, M. W., & Chen, X. D. (2012). Single Droplet Drying Technique to Study Drying Kinetics Measurement and Particle Functionality: A Review. *Drying Technology*, *30*(February 2015), 1771–1785. https://doi.org/10.1080/07373937.2012.708002

Fu, N., Woo, M. W., Moo, F. T., & Chen, X. D. (2012). Microcrystallization of lactose during droplet drying and its effect on the property of the dried particle. *Chemical Engineering Research and Design*, *90*(1), 138–149. https://doi.org/10.1016/j.cherd.2011.06.016

Fu, X., Huck, D., Makein, L., Armstrong, B., Willen, U., & Freeman, T. (2012). Effect of particle shape and size on flow properties of lactose powders. *Particuology*, *10*(2), 203–208. https://doi.org/10.1016/j.partic.2011.11.003

Fuchs, N. (1934). Concerning the velocity of evaporation of small droplets in a gas atmosphere. *Physikalische Zeitschrift der Sowjetunion*, *6*.

Genovese, D. B. (2012). Shear rheology of hard-sphere, dispersed, and aggregated suspensions, and filler-matrix composites. *Advances in Colloid and Interface Science*, *171–172*, 1–16. https://doi.org/10.1016/j.cis.2011.12.005

Ghandi, A., Powell, I. B., Chen, X. D., & Adhikari, B. (2012a). The Effect of Dryer Inlet and Outlet Air Temperatures and Protectant Solids on the Survival of Lactococcus lactis during Spray Drying. *Drying Technology*, *30*(14), 1649–1657. https://doi.org/10.1080/07373937.2012.703743

Ghandi, A., Powell, I., Chen, X. D., & Adhikari, B. (2012b). Drying kinetics and survival studies of dairy fermentation bacteria in convective air drying environment using single droplet drying. *Journal of Food Engineering*, *110*(3), 405–417. https://doi.org/10.1016/j.jfoodeng.2011.12.031

Ghani, A., Adachi, S., Shiga, H., Neoh, T. L., Adachi, S., & Yoshii, H. (2017). Effect of different dextrose equivalents of maltodextrin on oxidation stability in encapsulated fish oil by spray drying. *Bioscience, Biotechnology and Biochemistry*, *81*(4), 705–711. https://doi.org/10.1080/09168451.2017.1281721

Gharsallaoui, A., Saurel, R., Chambin, O., & Voilley, A. (2012). Pea (Pisum sativum, L.) Protein Isolate Stabilized Emulsions: A Novel System for Microencapsulation of Lipophilic Ingredients by Spray Drying. *Food and Bioprocess Technology*, *5*(6), 2211–2221. https://doi.org/10.1007/s11947-010-0497-z

Ghosh, V., Ziegler, G. R., & Anantheswaran, R. C. (2002). Fat, moisture, and ethanol migration through chocolates and confectionary coatings. *Critical Reviews in Food Science and Nutrition*, *42*(6), 583–626. https://doi.org/10.1080/20024091054265

Gianfrancesco, A., Vuataz, G., Mesnier, X., & Meunier, V. (2012). New methods to assess water diffusion in amorphous matrices during storage and drying. *Food Chemistry*, *132*(4), 1664–1670. https://doi.org/10.1016/j.foodchem.2011.06.058

Giorgiutti-Dauphiné, F., & Pauchard, L. (2018). Drying drops: Drying drops containing solutes: From hydrodynamical to mechanical instabilities. *European Physical Journal E*, *41*(3). https://doi.org/10.1140/epje/i2018-11639-2

Gosline, J. M., & French, C. J. (1979). Dynamic mechanical properties of elastin. *Biopolymers: Original Research on Biomolecules*, *18*(8), 2091–2103.

Gouaou, I., Koutchoukali, M. S., & Kharaghani, A. (2016). Experimental study of drying conditions effect on starch single droplet shrinkage and morphology during drying. *Proceedings of the Third International Conference on Energy, Materials, Applied Energetics and Pollution*, 326–332.

Gouaou, I., Shamaei, S., Koutchoukali, M. S., Bouhelassa, M., Tsotsas, E., & Kharaghani, A. (2019). Impact of operating conditions on a single droplet and spray drying of hydroxypropylated pea starch: Process performance and final powder properties. *Asia-Pacific Journal of Chemical Engineering*, *14*(1), 1–18.

Griesing, M., Grosshans, H., Hellwig, T., Sedelmayer, R., Gopireddy, S. R., Pauer, W., Gutheil, E., & Moritz, H. U. (2016). Influence of Air Humidity on the Particle Formation of Single Mannitol-Water Droplets during Drying. *Chemie-Ingenieur-Technik*, *88*(7), 929–936. https://doi.org/10.1002/cite.201500087

Groot, R. D., & Agterof, W. G. M. (1995). Dynamic Viscoelastic Modulus of Associative Polymer Networks: Off-Lattice Simulations, Theory and Comparison to Experiments. *Macromolecules*, *28*(18), 6284–6295. https://doi.org/10.1021/ma00122a041

Guo, M., & Wang, G. (2016). Milk protein polymer and its application in environmentally safe adhesives. *Polymers*, *8*(9), 1–12. https://doi.org/10.3390/polym8090324

Haene, P. D., & Liederkerke, B. Van. (1996). Viscosity Prediction of Starch Hycirolysates from Single Point Measurements. *Starch-Stärke*, *48*(9), 327-334.

Handscomb, C. S., & Kraft, M. (2010). Simulating the structural evolution of droplets following shell formation. *Chemical Engineering Science*, *65*(2), 713–725. https://doi.org/10.1016/j.ces.2009.09.025

Haque, M. (2015). *Study on denaturation of whey protein isolate and its control in convective and spray drying processes.* RMIT University.

Haque, M. A., Chen, J., Aldred, P., & Adhikari, B. (2015). Drying and denaturation characteristics of whey protein isolate in the presence of lactose and trehalose. *Food Chemistry*, *177*, 8–16. https://doi.org/10.1016/j.foodchem.2014.12.064

Hassan, H. M., & Mumford, C. J. (1993). Mechanisms of drying of skin-forming materials. III. Droplets of natural products. *Drying Technology*, *11*(7), 1765–1782.

He, X. (2006). Water activity and mobility in solutions of glycerol and small molecular weight sugars: implication for cryo- and lyopreservation. *Journal of Applied Physics*, *100*(7), 074702.

Hecht, J. P., & King, C. J. (2000). Spray drying: Influence of developing drop morphology on drying rates and retention of volatile substances. 1. Single-drop experiments. *Industrial and Engineering Chemistry Research*, *39*(6), 1756–1765. https://doi.org/10.1021/ie9904652

Hong, W., Liu, Z., & Suo, Z. (2009). Inhomogeneous swelling of a gel in equilibrium with a solvent and mechanical load. *International Journal of Solids and Structures*, *46*(17), 3282–3289. https://doi.org/10.1016/j.ijsolstr.2009.04.022

Horne, D. S. (2008). Casein Micelle Structure and Stability. In *Milk Proteins* (Second Edi). Elsevier Inc. https://doi.org/10.1016/B978-0-12-374039-7.00005-2

Huang, S., Vignolles, M.-L., Chen, X. D., Loir, Y. Le, Jan, G., Schuck, P., & Jeantet, R. (2017). Spray drying of probiotics and other food-grade bacteria : A review. *Trends in Food Science & Technology*, *63*, 1–17. https://doi.org/10.1016/j.tifs.2017.02.007 0924-2244/©

Ikeda, S., & Nishinari, K. (2000). Intermolecular forces in bovine serum albumin solutions exhibiting solidlike mechanical behaviors. *Biomacromolecules*, *1*(4), 757–763. https://doi.org/10.1021/bm005587o

Ikeda, S., Nishinari, K., & Foegeding, E. A. (2000). Mechanical characterization of network formation during heat-induced gelation of whey protein dispersions. *Biopolymers*, *56*(2), 109–119. https://doi.org/10.1002/1097-0282(2000)56:2<109::AID-BIP1056>3.0.CO;2-U

Ishii, M., & Nakamura, H. (2020). Applicability of Modified Cox-Merz Rule to Concentrated Suspensions. *Journal of Non-Newtonian Fluid Mechanics*, *282*(November 2019). https://doi.org/10.1016/j.jnnfm.2020.104322

Iskandar, F., Gradon, L., & Okuyama, K. (2003). Control of the morphology of nanostructured particles prepared by the spray drying of a nanoparticle sol. *Journal of Colloid and Interface Science*, *265*(2), 296–303. https://doi.org/10.1016/S0021-9797(03)00519-8

Kalichevsky, M. T., Jaroszkiewicz, E. M., & Blanshard, J. M. V. (1993). A study of the glass transition of amylopectin-sugar mixtures. *Polymer*, *34*(2), 346–358. https://doi.org/10.1016/0032-3861(93)90088-R

Karlsson, A. O., Ipsen, R., Schrader, K., & Ardö, Y. (2005). Relationship Between Physical Properties of Casein Micelles and Rheology of Skim Milk Concentrate. *Journal of Dairy Science*, *88*(11), 3784–3797. https://doi.org/10.3168/jds.S0022-0302(05)73064-2

Kasapis, S. (2001). Advanced topics in the application of the WLF/free volume theory to high sugar/biopolymer mixtures: A review. *Food Hydrocolloids*, *15*(4–6), 631–641. https://doi.org/10.1016/S0268-005X(01)00048-0

Kasapis, S., Sablani, S. S., & Biliaderis, C. G. (2000). Dynamic oscillation measurements of starch networks at temperatures above 100°C. *Carbohydrate Research*, *329*(1), 179–187. https://doi.org/10.1016/S0008-6215(00)00161-0

Kawai, K., Hagiwara, T., Takai, R., & Suzuki, T. (2005). Comparative investigation by two analytical approaches of enthalpy relaxation for glassy glucose, sucrose, maltose, and trehalose. *Pharmaceutical Research*, *22*(3), 490–495. https://doi.org/10.1007/s11095-004-1887-6

Keshani, S., Daud, W. R. W., Nourouzi, M. M., Namvar, F., & Ghasemi, M. (2015). Spray drying: An overview on wall deposition, process and modeling. *Journal of Food Engineering*, *146*, 152–162. https://doi.org/10.1016/j.jfoodeng.2014.09.004

Khandaker, M. S. K., Dudek, D. M., Beers, E. P., & Dillard, D. A. (2017). Expression, crosslinking, and developing modulus master curves of recombinant resilin. *Journal of the Mechanical Behavior of Biomedical Materials*, *69*, 385–394.

Khem, S., Small, D. M., & May, B. K. (2016). The behaviour of whey protein isolate in protecting *Lactobacillus plantarum*. *Food Chemistry*, *190*, 717–723. https://doi.org/10.1016/j.foodchem.2015.06.020

Khem, S., Woo, M. W., Small, D. M., Chen, X. D., & May, B. K. (2015). Agent selection and protective effects during single droplet drying of bacteria. *Food Chemistry*, *166*, 206–214. https://doi.org/10.1016/j.foodchem.2014.06.010

Krauklis, A. E., Akulichev, A. G., Gagani, A. I., & Echtermeyer, A. T. (2019). Time-temperature-plasticization superposition principle: Predicting creep of a plasticized epoxy. *Polymers*, *11*(11). https://doi.org/10.3390/polym11111848

Krieger, I. M., & Dougherty, T. J. (1959). A mechanism for non-Newtonian flow in suspensions of rigid spheres. *Transactions of the Society of Rheology*, *3*(1), 137–152.

Krishna, R., & Van Baten, J. M. (2005). The darken relation for multicomponent diffusion in liquid mixtures of linear alkanes: An investigation using Molecular Dynamics (MD) simulations. *Industrial and Engineering Chemistry Research*, *44*(17), 6939–6947. https://doi.org/10.1021/ie050146c

Kristiansen, K. R., Otte, J., Ipsen, R., & Qvist, K. B. (1998). Large-scale preparation of β-lactoglobulin A and B by ultrafiltration and ion-exchange chromatography. *International Dairy Journal*, *8*(2), 113–118. https://doi.org/10.1016/S0958-6946(98)00028-4

Labuza, T. P., & Hyman, C. R. (1998). Moisture migration and control in multi-domain foods. *Trends in Food Science & Technology*, *9*(2), 47–55.

Langstroth, G. O., Diel, C. H. H., & Winhold, E. (1950). The evaporation of drops in still air. *Can.J.Res.*, *28A*(574).

Lanotte, L., Boissel, F., Schuck, P., Jeantet, R., & Le Floch-Fouéré, C. (2018). Drying-induced mechanisms of skin formation in mixtures of high protein dairy powders. *Colloids and Surfaces A: Physicochemical and Engineering Aspects*, *553*(May), 20–27. https://doi.org/10.1016/j.colsurfa.2018.05.020

Le Floch-Fouéré, C., Lanotte, L., Jeantet, R., & Pauchard, L. (2019). The solute mechanical properties impact on the drying of dairy and model colloidal systems. *Soft Matter*, *15*(30), 6190–6199. https://doi.org/10.1039/c9sm00373h

Leslie, S. B., Israeli, E., Lighthart, B., Crowe, J. H., & Crowe, L. M. (1995). Trehalose and sucrose protect both membranes and proteins in intact bacteria during drying. *Applied and Environmental Microbiology*, *61*(10), 3592–3597.

Levine, H., & Slade, L. (1986). A polymer physico-chemical approach to the study of commercial starch hydrolysis products (SHPs). *Carbohydrate Polymers*, *6*(3), 213–244. https://doi.org/10.1016/0144-8617(86)90021-4

Li, B., Cao, Y. P., Feng, X. Q., & Gao, H. (2012). Mechanics of morphological instabilities and surface wrinkling in soft materials: A review. *Soft Matter*, *8*(21), 5728–5745. https://doi.org/10.1039/c2sm00011c

Li, B., Jia, F., Cao, Y. P., Feng, X. Q., & Gao, H. (2011). Surface wrinkling patterns on a core-shell soft sphere. *Physical Review Letters*, *106*(23), 2–5. https://doi.org/10.1103/PhysRevLett.106.234301

Lian, W. C., Hsiao, H. C., & Chou, C. C. (2002). Survival of bifidobacteria after spray-drying. *International Journal of Food Microbiology*. https://doi.org/10.1016/S0168-1605(01)00733-4

Lin, S. X. Q., & Chen, X. D. (2004). Changes in milk droplet diameter during drying under constant drying conditions investigated using the glass-filament method. *Food and Bioproducts Processing*, *82*(3 C), 213–218. https://doi.org/10.1205/fbio.82.3.213.44178

Lintingre, E., Lequeux, F., Talini, L., & Tsapis, N. (2016). Control of particle morphology in the spray drying of colloidal suspensions. *Soft Matter*, *12*(36), 7435–7444. https://doi.org/10.1039/c6sm01314g

Littringer, E. M., Noisternig, M. F., Mescher, A., Schroettner, H., Walzel, P., Griesser, U. J., & Urbanetz, N. A. (2013). The morphology and various densities of spray dried mannitol. *Powder Technology*, *246*, 193–200. https://doi.org/10.1016/j.powtec.2013.05.004

Liu, B., Fu, N., Woo, M. W., & Chen, X. D. (2018). Heat stability of *Lactobacillus rhamnosus* GG and its cellular membrane during droplet drying and heat treatment. *Food Research International*, *112*(May), 56–65. https://doi.org/10.1016/j.foodres.2018.06.006

Liu, C., He, J., Keunings, R., & August, R. V. (2006). *New Linearized Relation for the Universal Viscosity - Temperature Behavior of Polymer Melts*. 8867–8869. https://doi.org/10.1021/ma061969w

Loret, C., Meunier, V., Frith, W. J., & Fryer, P. J. (2004). Rheological characterisation of the gelation behaviour of maltodextrin aqueous solutions. *Carbohydrate Polymers*, *57*(2), 153–163. https://doi.org/10.1016/j.carbpol.2004.03.026

Loveday, S. M., Creamer, L. K., Singh, H., & Rao, M. A. (2007). Phase and rheological behavior of high-concentration colloidal hard-sphere and protein dispersions. *Journal of Food Science*, *72*(7). https://doi.org/10.1111/j.1750-3841.2007.00452.x

Lupi, F. R., Franco, G., Baldino, N., & Gabriele, D. (2020). The effect of operating conditions on the physicochemical characteristics of whey protein–based systems. *Rheologica Acta*, *59*(4), 227–238. https://doi.org/10.1007/s00397-020-01197-6

Malafronte, L., Ahrné, L., Kaunisto, E., Innings, F., & Rasmuson, A. (2015). Estimation of the effective diffusion coefficient of water in skim milk during single-drop drying. *Journal of Food Engineering*, *147*, 111–119. https://doi.org/10.1016/jjfoodeng.2014.09.032

Malafronte, L., Ruoff, D., Gunes, D. Z., Lequeux, F., Schmitt, C., & Windhab, E. J. (2019). Morphology development in single drop drying for native and aggregated whey protein dispersions. *Colloids and Surfaces A: Physicochemical and Engineering Aspects*, *578*(April). https://doi.org/10.1016/j.colsurfa.2019.06.015

Marcone, M. F., Wang, S., Albabish, W., Nie, S., Somnarain, D., & Hill, A. (2013). Diverse food-based applications of nuclear magnetic resonance (NMR) technology. *Food Research International*, *51*(2), 729–747. https://doi.org/10.1016/j.foodres.2012.12.046

Mariette, F., Topgaard, D., Jönsson, B., & Soderman, O. (2002). 1H NMR diffusometry study of water in casein dispersions and gels. *Journal of Agricultural and Food Chemistry*, *50*(15), 4295–4302. https://doi.org/10.1021/jf0115948

Marin, G., & Graessley, W. W. (1977). Viscoelastic properties of high molecular weight polymers in the molten state. *Rheologica Acta*, *16*(5), 527–533. https://doi.org/10.1007/bf01525652

Maron, S. H., Nakajima, N., & Krieger, I. M. (1959). Study of entanglement of polymers in solution by viscosity measurments. *Journal of Polymer Science*, *37*(131), 1–18.

Mason, T. G., & Weitz, D. A. (1995). Linear viscoelasticity of colloidal hard sphere suspensions near the glass transition. *Physical Review Letters*, *75*(14), 2770–2773. https://doi.org/10.1103/PhysRevLett.75.2770

Masters, K. (1985). *Spray Drying*. John Wiley & Sons, Inc. https://doi.org/10.1002/0471743984.vse6665

Mattsson, J., Wyss, H. M., Fernandez-Nieves, A., Miyazaki, K., Hu, Z., Reichman, D. R., & Weitz, D. A. (2009). Soft colloids make strong glasses. *Nature*, *462*(7269), 83–86. https://doi.org/10.1038/nature08457

McSweeney, P. L., & Fox, P. F. (2009). *Advanced Dairy Chemistry: volume 3: lactose, water, salts and minor constituents*. Springer Science & Business Media.

Meerdink, G., & van't Riet, K. (1995). Modeling segregation of solute material during drying of liquid foods. *AIChE Journal*, *41*(3), 732–736. https://doi.org/10.1002/aic.690410331

Meng, F., Doi, M., & Ouyang, Z. (2014). Cavitation in drying droplets of soft matter solutions. *Physical Review Letters*, *113*(9), 1–5. https://doi.org/10.1103/PhysRevLett.113.098301

Meza, B. E., Verdini, R. A., & Rubiolo, A. C. (2010). Effect of freezing on the viscoelastic behaviour of whey protein concentrate suspensions. *Food Hydrocolloids*, *24*(4), 414–423. https://doi.org/10.1016/j.foodhyd.2009.11.008

Mezhericher, M., Levy, A., & Borde, I. (2010). Theoretical models of single droplet drying kinetics: A review. *Drying Technology*, *28*(2), 278–293. https://doi.org/10.1080/07373930903530337

Miller, C. C. (1924). The Stokes-Einstein law for diffusion in solution. *Proceedings of the Royal Society of London. Series A, Containing Papers of a Mathematical and Physical Character*, *106*(740), 724–749.

Mittal, G. S. (1999). Mass diffusivity of food products. *Food Reviews International*, *15*(1), 19–66. https://doi.org/10.1080/87559129909541176

Mittal, S., Chowhan, R. K., & Singh, L. R. (2015). Macromolecular crowding: Macromolecules friend or foe. *Biochimica et Biophysica Acta - General Subjects*, *1850*(9), 1822–1831. https://doi.org/10.1016/j.bbagen.2015.05.002

Molinero, V., Çağin, T., & Goddard, W. A. (2003). Sugar, water and free volume networks in concentrated sucrose solutions. In *Chemical Physics Letters* (Vol. 377, Issues 3–4, pp. 469–474). https://doi.org/10.1016/S0009-2614(03)01170-9

Morr, C. V., & Ha, E. Y. W. (1993). Whey Protein Concentrates and Isolates: Processing and Functional Properties. *Critical Reviews in Food Science and Nutrition*, *33*(6), 431–476. https://doi.org/10.1080/10408399309527643

Mosaad, M. (1999). Laminar forced convection conjugate heat transfer over a flat plate. *Warme- Und Stoffubertragung Zeitschrift*, *35*(5), 371–375. https://doi.org/10.1007/s002310050338

Mujumdar, A. S. (2015). *Handbook of industrial drying* (4th ed.). CRC press.

Mulvihill, D., & Donovan, M. (1987). Whey proteins and their thermal denaturation- a review. *Irish Journal of Food Science and Technology*, *11*(1), 43–75.

Nandiyanto, A. B. D., & Okuyama, K. (2011). Progress in developing spray-drying methods for the production of controlled morphology particles: From the nanometer to submicrometer size ranges. *Advanced Powder Technology*, *22*(1), 1–19. https://doi.org/10.1016/j.apt.2010.09.011

Nesmelova, I. V., Skirda, V. D., & Fedotov, V. D. (2002). Generalized concentration dependence of globular protein self-diffusion coefficients in aqueous solutions. *Biopolymers*, *63*(2), 132–140. https://doi.org/10.1002/bip.10023

Ngai, K. L. (2011). *Relaxation and diffusion in complex* systems. Springer Science & Business Media.

Nicolai, T., Britten, M., & Schmitt, C. (2011). β-Lactoglobulin and WPI aggregates: Formation, structure and applications. *Food Hydrocolloids*, *25*(8), 1945–1962. https://doi.org/10.1016/j.foodhyd.2011.02.006

Novikov, V. N., & Rössler, E. A. (2013). Correlation between glass transition temperature and molecular mass in non-polymeric and polymer glass formers. *Polymer*, *54*(26), 6987–6991. https://doi.org/10.1016/j.polymer.2013.11.002

Nuzzo, M;, Sloth, J., Brandner, B., Bergenstahl, B., & Millqvist-Fureby, A. (2015). Confocal Raman microscopy for mapping phase segregation in individually dried particles composed of lactose and macromolecules. *Colloids and Surfaces A: Physicochemical and Engineering Aspects*, *481*, 229–236. https://doi.org/10.1016/j.colsurfa.2015.04.044

Nuzzo, M., Sloth Overgaard, J., Bergenståhl, B., & Millqvist-Fureby, A. (2017). The morphology and internal composition of dried particles from whole milk—From single droplet to full scale drying. *Food Structure*, *13*, 35–44. https://doi.org/10.1016/j.foostr.2017.02.001

Nuzzo, Marine, Millqvist-Fureby, A., Sloth, J., & Bergenstahl, B. (2015). Surface Composition and Morphology of Particles Dried Individually and by Spray Drying. *Drying Technology*, *3937*(February 2015), 141217112010003. https://doi.org/10.1080/07373937.2014.990566

Palzer, S. (2010). The relation between material properties and supra-molecular structure of water-soluble food solids. *Trends in Food Science and Technology*, *21*(1), 12–25. https://doi.org/10.1016/j.tifs.2009.08.005

Palzer, S. (2005). The effect of glass transition on the desired and undesired agglomeration of amorphous food powders. *Chemical Engineering Science*, *60*(14), 3959–3968. https://doi.org/10.1016/j.ces.2005.02.015

Paramita, V., Iida, K., Yoshii, H., & Furuta, T. (2010). Effect of additives on the morphology of spray-dried powder. *Drying Technology*, *28*(3), 323–329. https://doi.org/10.1080/07373931003627098

Parker, R, Noel, T. R., Brownsey, G. J., Laos, K., & Ring, S. G. (2005). The Nonequilibrium Phase and Glass Transition Behavior of β-Lactoglobulin. *Biophysical Journal*, *89*(2), 1227–1236. https://doi.org/10.1529/biophysj.105.064246

Patel, K. C., & Chen, X. D. (2008). Surface-center temperature differences within milk droplets during convective drying and drying-based biot number analysis. *AIChE Journal*, *54*(12), 3273–3290. https://doi.org/10.1002/aic

Pauchard, L., & Allain, C. (2003). Stable and unstable surface evolution during the drying of a polymer solution drop. *Physical Review E - Statistical Physics, Plasmas, Fluids, and Related Interdisciplinary Topics*, *68*(5), 1–4. https://doi.org/10.1103/PhysRevE.68.052801

Pauchard, Ludovic, & Allain, C. (2003). Mechanical instability induced by complex liquid desiccation. *Comptes Rendus Physique*, *4*(2), 231–239. https://doi.org/10.1016/S1631-0705(03)00027-6

Peighambardoust, S. H., Golshan Tafti, A., & Hesari, J. (2011). Application of spray drying for preservation of lactic acid starter cultures: A review. In *Trends in Food Science and Technology*. https://doi.org/10.1016/j.tifs.2011.01.009

Peng, X., Wang, J. G., Li, Q., Chen, D., Zia, R. N., & McKenna, G. B. (2018). Exploring the validity of time-concentration superposition in glassy colloids: Experiments and simulations. *Physical Review E*, *98*(6), 1–11. https://doi.org/10.1103/PhysRevE.98.062602

Perdana, J., Fox, M. B., Schutyser, M. A. I., & Boom, R. M. (2011). Single-droplet experimentation on spray drying: Evaporation of a sessile droplet. *Chemical Engineering and Technology*, *34*(7), 1151–1158. https://doi.org/10.1002/ceat.201100040

Perdana, J., Bereschenko, L., Fox, M. B., Kuperus, J. H., Kleerebezem, M., Boom, R. M., & Schutyser, M. A. I. (2013). Dehydration and thermal inactivation of Lactobacillus plantarum WCFS1: Comparing single droplet drying to spray and freeze drying. *Food Research International*, *54*(2), 1351–1359. https://doi.org/10.1016/j.foodres.2013.09.043

Perdana, J., Bereschenko, L., Roghair, M., Fox, M. B., Boom, R. M., Kleerebezem, M., & Schutyser, M. A. I. (2012). Novel method for enumeration of viable Lactobacillus plantarum WCFS1 cells after single-droplet drying. *Applied and Environmental Microbiology*, *78*(22), 8082–8088. https://doi.org/10.1128/AEM.02063-12

Perdana, J., Fox, M. B., Schutyser, M. A. I., & Boom, R. M. (2013). Mimicking Spray Drying by Drying of Single Droplets Deposited on a Flat Surface. *Food and Bioprocess Technology*, *6*(4), 964–977. https://doi.org/10.1007/s11947-011-0767-4

Perdana, J., Fox, M. B., Siwei, C., Boom, R. M., & Schutyser, M. A. I. (2014a). Interactions between formulation and spray drying conditions related to survival of lactobacillus plantarum WCFS1. *Food Research International*, *56*, 9–17. https://doi.org/10.1016/j.foodres.2013.12.007

Perdana, J., van der Sman, R. G. M., Fox, M. B., Boom, R. M., & Schutyser, M. A. I. (2014b). Measuring and modelling of diffusivities in carbohydrate-rich matrices during thin film drying. *Journal of Food Engineering*, *122*(1), 38–47. https://doi.org/10.1016/j.jfoodeng.2013.08.033

Porfirio, T., Galindo-Rosales, F. J., Campo-Deaño, L., Vicente, J., & Semião, V. (2020). Rheological characterization of polymeric solutions used in spray drying process. *European Journal of Pharmaceutical Sciences*, *158*(May 2020), 105650. https://doi.org/10.1016/j.ejps.2020.105650

Prasad, V., Trappe, V., Dinsmore, A. D., Segre, P. N., Cipelletti, L., & Weitz, D. A. (2003). Rideal Lecture Universal features of the fluid to solid transition for attractive colloidal particles. *Faraday Discussions*, *123*(1), 1–12. https://doi.org/10.1039/b211107c

Pusey, P. N., & Megen, W. van. (1986). Phase behaviour of concentrated suspensions of nearly colloidal spheres. *Nature*, *320*, 340–342. https://www.nature.com/articles/320340a0

Quevedo, M., Jandt, U., Kulozik, U., Karbstein, H. P., & Emin, M. A. (2019). Investigation on the influence of high protein concentrations on the thermal reaction behaviour of β-lactoglobulin by experimental and numerical analyses. *International Dairy Journal*, *97*, 99–110. https://doi.org/10.1016/j.idairyj.2019.06.004

Quevedo, M., Karbstein, H. P., & Emin, M. A. (2021). Concentration-dependent changes in the reaction behavior of whey proteins: Diffusion-controlled or transition state-controlled reactions? *Food Hydrocolloids*, *118*(October 2020), 106745. https://doi.org/10.1016/j.foodhyd.2021.106745

Räderer, M., Besson, A., & Sommer, K. (2002). A thin film dryer approach for the determination of water diffusion coefficients in viscous products. *Chemical Engineering Journal*, *86*(1–2), 185–191. https://doi.org/10.1016/S1385-8947(01)00288-1

Ranz, W. E., & Marshall, W. R. J. (1952). Evaporation from drops. *American Institute of Chemical Engineers Journal*, *48*(3), 141–146&173–180.

Ratti, C. (2001). Hot air and freeze-drying of high-value foods: A review. *Journal of Food Engineering*, *49*(4), 311–319. https://doi.org/10.1016/S0260-8774(00)00228-4

Renzetti, S., Voogt, J. A., Oliver, L., & Meinders, M. B. J. (2012). Water migration mechanisms in amorphous powder material and related agglomeration propensity. *Journal of Food Engineering*, *110*(2), 160–168. https://doi.org/10.1016/j.jfoodeng.2011.07.005

Ribeiro, C., Zimeri, J. E., Yildiz, E., & Kokini, J. L. (2002). Estimation of effective diffusivities and glass transition temperature of polydextrose as a function of moisture content. *Carbohydrate Polymers*, *51*(3), 273–280. https://doi.org/10.1016/S0144-8617(02)00182-0

Rogers, S., Wu, W. D., Lin, S. X. Q., & Chen, X. D. (2012). Particle shrinkage and morphology of milk powder made with a monodisperse. *Biochemical Engineering Journal*, *62*, 92–100. https://doi.org/10.1016/j.bej.2011.11.002

Rong, Y., Sillick, M., & Gregson, C. M. (2009). Determination of dextrose equivalent value and number average molecular weight of maltodextrin by osmometry. *Journal of Food Science*, *74*(1), 33–40. https://doi.org/10.1111/j.1750-3841.2008.00993.x

Roos, Y. H., & Karel, M. (1991). Phase Transitions of Mixtures of Amorphous Polysaccharides and Sugars. *Biotechnology Progress*, *7*(1), 49–53. https://doi.org/10.1021/bp00007a008

Ruan, R., Long, Z., Chen, P., Huang, V., Almaer, S., & Taub, I. (1999). Pulse NMR study of glass transition in maltodextrin. *Journal of Food Science*, *64*(1), 6–9. https://doi.org/10.1111/j.1365-2621.1999.tb09850.x

Sadek, C., Li, H., Schuck, P., Fallourd, Y., Pradeau, N., Le Floch-Fouéré, C., & Jeantet, R. (2014). To What Extent Do Whey and Casein Micelle Proteins Influence the Morphology and Properties of the Resulting Powder? *Drying Technology*, *32*(13), 1540–1551. https://doi.org/10.1080/07373937.2014.915554

Sadek, C., Pauchard, L., Schuck, P., Fallourd, Y., Pradeau, N., Le Floch-Fouéré, C., & Jeantet, R. (2015a). Mechanical properties of milk protein skin layers after drying: Understanding the mechanisms of particle formation from whey protein isolate and native phosphocaseinate. *Food Hydrocolloids*, *48*, 8–16. https://doi.org/10.1016/j.foodhyd.2015.01.014

Sadek, C., Schuck, P., Fallourd, Y., Pradeau, N., Jeantet, R., & Le Floch-Fouéré, C. (2016). Buckling and collapse during drying of a single aqueous dispersion of casein micelle droplet. *Food Hydrocolloids*, *52*, 161–166. https://doi.org/10.1016/j.foodhyd.2015.06.016

Sadek, C., Schuck, P., Fallourd, Y., Pradeau, N., Le Floch-Fouéré, C., & Jeantet, R. (2015b). Drying of a single droplet to investigate process–structure–function relationships: a review. *Dairy Science and Technology*, *95*(6), 771–794. https://doi.org/10.1007/s13594-014-0186-1

Sadek, C., Tabuteau, H., Schuck, P., Fallourd, Y., Pradeau, N., Le Floch-Fouéré, C., & Jeantet, R. (2013). Shape, shell, and vacuole formation during the drying of a single concentrated whey protein droplet. *Langmuir*, *29*(50), 15606–15613. https://doi.org/10.1021/la404108v

Saĝlam, D., Venema, P., de Vries, R., Shi, J., & van der Linden, E. (2013). Concentrated whey protein particle dispersions: Heat stability and rheological properties. *Food Hydrocolloids*, *30*(1), 100–109. https://doi.org/10.1016/j.foodhyd.2012.05.005

Salami, S., Rondeau-Mouro, C., van Duynhoven, J., & Mariette, F. (2013). PFG-NMR self-diffusion in casein dispersions: Effects of probe size and protein aggregate size. *Food Hydrocolloids*, *31*(2), 248–255. https://doi.org/10.1016/j.foodhyd.2012.10.020

Santivarangkna, C., Aschenbrenner, M., Kulozik, U., & Foerst, P. (2011). Role of Glassy State on Stabilities of Freeze-Dried Probiotics. *Journal of Food Science*, *76*(8). https://doi.org/10.1111/j.1750-3841.2011.02347.x

Santivarangkna, C., Kulozik, U., & Foerst, P. (2007). Alternative drying processes for the industrial preservation of lactic acid starter cultures. *Biotechnology Progress*, *23*(2), 302–315. https://doi.org/10.1021/bp060268f

Schiffter, H., & Lee, G. (2007). Single-Droplet Evaporation Kinetics and Particle Formation in an Acoustic Levitator. Part 1: Evaporation of Water Microdroplets Assessed Using Boundary-Layer and Acoustic Levitation Theories. *Journal of Pharmaceutical Sciences*, *96*(9), 2274–2283. https://doi.org/10.1002/JPS.20860

Scholte, T. G., Meijerink, N. L. J., Schoffeleers, H. M., & Brands, A. M. G. (1984). Mark–Houwink equation and GPC calibration for linear short-chain branched polyolefines, including polypropylene and ethylene–propylene copolymers. *Journal of Applied Polymer Science*, *29*(12), 3763–3782. https://doi.org/10.1002/app.1984.070291211

Schutyser, M.A.I., Both, E. M., Siemons, I., Vaessen, E. M. J., & Zhang, L. (2018). Gaining insight on spray drying behavior of foods via single droplet drying analyses. *Drying Technology*, *0*(0), 1–10. https://doi.org/10.1080/07373937.2018.1482908

Schutyser, M.A.I., Perdana, J., & Boom, R. M. (2012). Single droplet drying for optimal spray drying of enzymes and probiotics. *Trends in Food Science and Technology*, *27*(2), 73–82. https://doi.org/10.1016/j.tifs.2012.05.006

Selvamuthukumaran, M. (2019). *Handbook on spray drying applications for food industries*. CRC press.

Sherbon, J. W. (1988). Physical properties of milk. In *Fundamentals of Dairy Chemistry* (pp. 409–460). Springer.

Siemons, I., Boom, R. M., van der Sman, R. G. M., & Schutyser, M. A. I. (2019). Moisture diffusivity in concentrated and dry protein-carbohydrate films. *Food Hydrocolloids*, *97*(June), 105219. https://doi.org/10.1016/j.foodhyd.2019.105219

Siemons, I., Politiek, R. G. A., Boom, R. M., Sman, R. G. M. Van Der, & Schutyser, M. A. I. (2020). Dextrose equivalence of maltodextrins determines particle morphology development during single sessile droplet drying. *Food Research International*, *131*(November 2019), 108988. https://doi.org/10.1016/j.foodres.2020.108988

Siemons, I., Vaessen, E. M. J., Oosterbaan van Peski, S. E., Boom, R. M., & Schutyser, M. A. I. (2021). Protective effect of carrier matrices on survival of *Lactobacillus plantarum* WCFS1 during single droplet drying explained by particle morphology development. *Journal of Food Engineering*, *292*(August 2020), 110263. https://doi.org/10.1016/j.jfoodeng.2020.110263

Sillick, M., & Gregson, C. M. (2009). Viscous fragility of concentrated maltopolymer/sucrose mixtures. *Carbohydrate Polymers*, *78*(4), 879–887. https://doi.org/10.1016/j.carbpol.2009.07.015

Simon, P. P., & Ploehn, H. J. (1999). Investigating time-temperature superpositioning in crosslinked polymers using the tube-junction model. *Journal of Polymer Science Part B: Polymer Physics*, *37*(2), 127–142.

Sobolewska-Zielińska, J., & Fortuna, T. (2010). Retrogradation of starches and maltodextrins of origin various. *Acta Scientiarum Polonorum, Technologia Alimentaria*, *9*(1), 71–81.

Soesanto, T., & Williams, M. C. (1981). *Volumetric Interpretation of Viscosity for Concentrated and Dilute Sugar Solutions*. 3338–3341. https://doi.org/10.1021/j150622a026

Soh, G. Y., Yeoh, G. H., & Timchenko, V. (2016). An algorithm to calculate interfacial area for multiphase mass transfer through the volume-of-fluid method. *International Journal of Heat and Mass Transfer*, *100*, 573–581. https://doi.org/10.1016/j.ijheatmasstransfer.2016.05.006

Soltanizadeh, N., Mirmoghtadaie, L., Nejati, F., Najafabadi, L. I., Heshmati, M. K., & Jafari, M. (2014). Solid-state protein-carbohydrate interactions and their application in the food industry. *Comprehensive Reviews in Food Science and Food Safety*, *13*(5), 860–870. https://doi.org/10.1111/1541-4337.12089

Sopade, P. a, Halley, P., Bhandari, B., D'Arcy, B., Doebler, C., & Caffin, N. (2002). Application of the Williams – Landel – Ferry model to the viscosity – temperature relationship of Australian honeys. *Journal of Food Engineering*, *56*, 67–75. https://doi.org/10.1016/S0260-8774(02)00149-8

Speedy, R. J. (1987). Diffusion in the hard sphere fluid. *Molecular Physics*, *62*(2), 509–515.

Sperling, L. H. (2001). *Introduction to physical polymer science* (3rd ed.). John Wiley & Sons, Ltd.

Spurlin, H. M., Martin, A. F., & Tennent, H. G. (1946). Characterization of cellulose derivatives by solution properties: plasticizers as solvents. *Journal of Polymer Science Part A: Polymer Chemistry*, *1*(2), 63–74.

Sugiyama, Y., Larsen, R. J., Kim, J. W., & Weitz, D. A. (2006). Buckling and crumpling of drying droplets of colloid-polymer suspensions. *Langmuir*, *22*(14), 6024–6030. https://doi.org/10.1021/la053419h

Sundaravadivelu Devarajan, D., Nourian, P., McKenna, G. B., & Khare, R. (2020). Molecular simulation of nanocolloid rheology: Viscosity, viscoelasticity, and time-concentration superposition. *Journal of Rheology*, *64*(3), 529–543. https://doi.org/10.1122/1.5125142

Sunthar, P. (2012). Polymer Rheology. *Robust Process Development and Scientific Molding*, 27–41. https://doi.org/10.3139/9783446433427.003

Sutherland, W. (1905). LXXV. A dynamical theory of diffusion for non-electrolytes and the molecular mass of albumin. *The London, Edinburgh, and Dublin Philosophical Magazine and Journal of Science*, *9*(54), 781–785.

Takeiti, C. Y., Kieckbusch, T. G., & Collares-Queiroz, F. P. (2008). Morphological and physicochemical characterization of commercial maltodextrins with different degrees of dextrose-equivalent. *International Journal of Food Properties*, *13*(2), 411–425. https://doi.org/10.1080/10942910802181024

Tanford, C. (1968). Protein denaturation. In *Advances in protein chemistry* (Vol. 23, pp. 121–282). Academic press.

Tatham, A. S., & Shewry, P. R. (2000). Elastomeric proteins: Biological roles, structures and mechanisms. *Trends in Biochemical Sciences*, *25*(11), 567–571. https://doi.org/10.1016/S0968-0004(00)01670-4

Thirunathan, P., Perdana, J., Gianfrancesco, A., Husny, J., & Arnz, P. (2017). Thermogravimetric analysis for rapid assessment of moisture diffusivity in polydisperse powder and thin film matrices. *Food Chemistry*, *242*, 519–526. https://doi.org/10.1016/j.foodchem.2017.09.089

Tokuyama, M., & Oppenheim, I. (1995). On the theory of concentrated hard-sphere suspensions. *Physica A: Statistical Mechanics and Its Applications*, *216*(1–2), 85–119. https://doi.org/10.1016/0378-4371(94)00280-7

Townrow, S., Roussenova, M., Giardiello, M., Alam, A., & Ubbink, J. (2010). Specific volume− hole volume correlations in amorphous carbohydrates: Effect of temperature, molecular weight, and water content. *The Journal of Physical Chemistry B*, *114*(4), 1568–1578.

Tran, T. T. H., Avila-Acevedo, J. G., & Tsotsas, E. (2016). Enhanced methods for experimental investigation of single droplet drying kinetics and application to lactose/water. *Drying Technology*, *34*(10), 1185–1195. https://doi.org/10.1080/07373937.2015.1100202

Tsapis, N., Dufresne, E. R., Sinha, S. S., Riera, C. S., Hutchinson, J. W., Mahadevan, L., & Weitz, D. A. (2005). Onset of buckling in drying droplets of colloidal suspensions. *Physical Review Letters*, *94*(1), 1–4. https://doi.org/10.1103/PhysRevLett.94.018302

Tsiami, A. A., Bot, A., Agterof, W. G. M., & Groot, R. D. (1997). Rheological properties of glutenin subfractions in relation to their molecular weight. *Journal of Cereal Science*, *26*(1), 15–27. https://doi.org/10.1006/jcrs.1996.0104

Tsoga, A., Kasapis, S., & Richardson, R. K. (1999). The rubber-to-glass transition in high sugar agarose systems. *Biopolymers*, *49*(4), 267–275.

Tung, M. A. (1978). Rheology of protein dispersions. *Journal of Texture Studies*, *9*(1–2), 3–31.

Turchiuli, C., Gianfrancesco, A., Palzer, S., & Dumoulin, E. (2011). Evolution of particle properties during spray drying in relation with stickiness and agglomeration control. *Powder Technology*, *208*(2), 433–440. https://doi.org/10.1016/j.powtec.2010.08.040

Ubbink, J. (2016). Structural and thermodynamic aspects of plasticization and antiplasticization in glassy encapsulation and biostabilization matrices. *Advanced Drug Delivery Reviews*, *100*, 10–26. https://doi.org/10.1016/j.addr.2015.12.019

Ubbink, J., Burbidge, A., & Mezzenga, R. (2008). Food structure and functionality: a soft matter perspective. *Soft Matter*, *4*(8), 1569–1581.

Ubbink, J., & Dupas-Langlet, M. (2020). Rheology of carbohydrate blends close to the glass transition: Temperature and water content dependence of the viscosity in relation to fragility and strength. *Food Research International*, *138*(PB), 109801. https://doi.org/10.1016/j.foodres.2020.109801

Ullum, T., Sloth, J., Brask, A., & Wahlberg, M. (2010). Predicting spray dryer deposits by CFD and an empirical drying model. *Drying Technology*, *28*(5), 723–729.

Vaessen, E. M. J., den Besten, H. M. W., Patra, T., van Mossevelde, N. T. M., Boom, R. M., & Schutyser, M. A. I. (2018). Pulsed electric field for increasing intracellular trehalose content in *Lactobacillus plantarum* WCFS1. *Innovative Food Science & Emerging Technologies*, *47*, 256–261. https://doi.org/10.1016/J.IFSET.2018.03.007

Vaessen, E. M. J., Leito, K., den Besten, H. M. W., & Schutyser, M. A. I. (2020). Pulsed electric field pre-treatment for enhanced bacterial robustness during drying: Effect of carrier matrix and strain variability. *Manuscript in Preparation*.

van der Sman, R. G. M. (2003). Simple model for estimating heat and mass transfer in regular-shaped foods. *Journal of Food Engineering*, *60*(4), 383–390. https://doi.org/10.1016/S0260-8774(03)00061-X

van der Sman, R. G. M. (2012a). Thermodynamics of meat proteins. *Food Hydrocolloids*, *27*(2), 529–535. https://doi.org/10.1016/j.foodhyd.2011.08.016

van der Sman, R. G. M. (2015). Biopolymer gel swelling analysed with scaling laws and Flory-Rehner theory. *Food Hydrocolloids*, *48*, 94–101. https://doi.org/10.1016/j.foodhyd.2015.01.025

van der Sman, R. G. M. (2012b). Soft matter approaches to food structuring. *Advances in Colloid and Interface Science*, *176–177*, 18–30. https://doi.org/10.1016/j.cis.2012.04.002

van der Sman, R. G. M. (2013). Predictions of glass transition temperature for hydrogen bonding biomaterials. *Journal of Physical Chemistry B*, *117*(50), 16303–16313. https://doi.org/10.1021/jp408184u

van der Sman, R. G. M., Ubbink, J., Dupas-Langlet, M., Siemons, I., & Kristiawan, M. (2021). Scaling relations in rheology of concentrated starches and maltodextrins. *Food Hydrocolloids*, *in press*.

van der Sman, R. G. M., Jin, X., & Meinders, M. B. J. (2013). A Paradigm Shift in Drying of Food Materials via Free-Volume Concepts. *Drying Technology*, *31*(15), 1817–1825. https://doi.org/10.1080/07373937.2013.829089

van der Sman, R. G. M., & Mauer, L. J. (2019). Starch gelatinization temperature in sugar and polyol solutions explained by hydrogen bond density. *Food Hydrocolloids*, *94*(March), 371–380. https://doi.org/10.1016/j.foodhyd.2019.03.034

van der Sman, R. G. M., & Meinders, M. B. J. (2011). Prediction of the state diagram of starchwater mixtures using the Flory–Huggins free volume theory. *Soft Matter*, *7*(2), 429–442. https://doi.org/10.1039/C0SM00280A

van der Sman, R. G. M., & Meinders, M. B. J. (2013). Moisture diffusivity in food materials. *Food Chemistry*, *138*(2–3), 1265–1274. https://doi.org/10.1016/j.foodchem.2012.10.062

van Gurp, M., & Palmen, J. (1998). Time-temperature superposition for polymeric blends. *J Rheol Bull*, *65*, 5–8.

Vardhanabhuti, B., & Foegeding, E. A. (1999). Rheological properties and characterization of polymerized whey protein isolates. *Journal of Agricultural and Food Chemistry*, *47*(9), 3649–3655. https://doi.org/10.1021/jf981376n

Vasbinder, A. J., & De Kruif, C. G. (2003). Casein-whey protein interactions in heated milk: The influence of pH. *International Dairy Journal*, *13*(8), 669–677. https://doi.org/10.1016/S0958-6946(03)00120-1

Vehring, R. (2008). Pharmaceutical particle engineering via spray drying. *Pharmaceutical Research*, *25*(5), 999–1022. https://doi.org/10.1007/s11095-007-9475-1

Vehring, R., Foss, W. R., & Lechuga-Ballesteros, D. (2007). Particle formation in spray drying. *Journal of Aerosol Science*, *38*(7), 728–746. https://doi.org/10.1016/j.jaerosci.2007.04.005

Vicente, J., Pinto, J., Menezes, J., & Gaspar, F. (2013). Fundamental analysis of particle formation in spray drying. *Powder Technology*, *247*, 1–7. https://doi.org/10.1016/j.powtec.2013.06.038

Vrentas, J. S., & Duda, J. L. (1977). Diffusion in polymer—solvent systems. I. Reexamination of the free-volume theory. *Journal of Polymer Science: Polymer Physics Edition*, *15*(3), 403–416. https://doi.org/10.1002/pol.1977.180150302

Vrentas, J. S., & Vrentas, C. M. (1991). Sorption in Glassy Polymers. *Macromolecules*, *24*(9), 2404–2412. https://doi.org/10.1021/ma00009a043

Walstra, P. (1979). The voluminosity of bovine casein micelles and some of its implications. *Journal of Dairy Research*, *46*(2), 317–323. https://doi.org/10.1017/S0022029900017234

Walstra, P., Jenness, R., & Badings, H. T. (1984). *Dairy chemistry and physics*. Wiley.

Walton, D. E. (2000). The morphology of spray-dried particles a qualitative view. *Drying Technology*, *18*(9), 1943–1986. https://doi.org/10.1080/07373930008917822

Walton, D. E., & Mumford, C. J. (1999). Spray Dried Products - Characterization of Particle Morphology. *Trans IChemE*, *77*(January), 21–38. https://doi.org/10.1205/026387699525846

Wang, H., & Cai, S. (2015). Cavitation in a swollen elastomer constrained by a non-swellable shell. *Journal of Applied Physics*, *117*(15), 1–5. https://doi.org/10.1063/1.4918278

Wang, J., Huang, S., Fu, N., Jeantet, R., & Chen, X. D. (2016). Thermal aggregation of calcium-fortified skim milk enhances probiotic protection during convective droplet drying. *Journal of Agricultural and Food Chemistry*, *64*(30), 6003–6010. https://doi.org/10.1021/acs.jafc.6b02205

Wen, Y. H., Schaefer, J. L., & Archer, L. A. (2015). Dynamics and rheology of soft colloidal glasses. *ACS Macro Letters*, *4*(1), 119–123. https://doi.org/10.1021/mz5006662

Werner, S. R. L., Edmonds, R. L., Jones, J. R., Bronlund, J. E., & Paterson, A. H. J. (2008). Single droplet drying: Transition from the effective diffusion model to a modified receding interface model. *Powder Technology*, *179*(3), 184–189. https://doi.org/10.1016/j.powtec.2007.06.009

Williams, M. L., Landel, R. F., & Ferry, J. D. (1955). The Temperature Dependence of Relaxation Mechanisms in Amorphous Polymers and Other Glass-forming Liquids. *Journal of the American Chemical Society*, *77*(14), 3701–3707. https://doi.org/10.1021/ja01619a008

Winter, H. H. (2009). Three views of viscoelasticity for Cox-Merz materials. *Rheologica Acta*, *48*(3), 241–243. https://doi.org/10.1007/s00397-008-0329-5

Wu, W. D., Liu, W., Gengenbach, T., Woo, M. W., Selomulya, C., Chen, X. D., & Weeks, M. (2014). Towards spray drying of high solids dairy liquid: Effects of feed solid content on particle structure and functionality. *Journal of Food Engineering*, *123*, 130–135. https://doi.org/10.1016/j.jfoodeng.2013.05.013

Würth, R., Foerst, P., & Kulozik, U. (2018). Effects of skim milk concentrate dry matter and spray drying air temperature on formation of capsules with varying particle size and the survival microbial cultures in a microcapsule matrix. *Drying Technology*, *36*(1), 93–99. https://doi.org/10.1080/07373937.2017.1301952

Yamamoto, S. (1999). Effects of Glycerol on the Drying of Gelatin and Sugar Solutions. *Drying Technology*, *17*(7–8), 1681–1695. https://doi.org/10.1080/07373939908917645

Yang, Z., Peng, H., Wang, W., & Liu, T. (2010). Crystallization behavior of poly(ε-caprolactone)/layered double hydroxide nanocomposites. *Journal of Applied Polymer Science*, *116*(5), 2658–2667. https://doi.org/10.1002/app

Yapel, R. A., Duda, J. L., Lin, X., & von Meerwall, E. D. (1994). Mutual and self-diffusion of water in gelatin: experimental measurement and predictive test of free-volume theory. *Polymer*, *35*(11), 2411–2416. https://doi.org/10.1016/0032-3861(94)90780-3

Yu, M., Le Floch-Fouéré, C., Pauchard, L., Boissel, F., Fu, N., Chen, X. D., Saint-Jalmes, A., Jeantet, R., & Lanotte, L. (2021). Skin layer stratification in drying droplets of dairy colloids. *Colloids and Surfaces A: Physicochemical and Engineering Aspects*, *620*(February). https://doi.org/10.1016/j.colsurfa.2021.126560

Zhang, Y., Qian, Y., Liu, Z., Li, Z., & Zang, D. (2014). Surface wrinkling and cracking dynamics in the drying of colloidal droplets. *European Physical Journal E*, *37*(9), 1–7. https://doi.org/10.1140/epje/i2014-14084-3

Zheng, X., Fu, N., Duan, M., Woo, M. W., Selomulya, C., & Chen, X. D. (2015). The mechanisms of the protective effects of reconstituted skim milk during convective droplet drying of lactic acid bacteria. *Food Research International*, *76*(Part 3), 478–488. https://doi.org/https://doi.org/10.1016/j.foodres.2015.07.045

Ziaee, A., Albadarin, A. B., Padrela, L., Femmer, T., O'Reilly, E., & Walker, G. (2019). Spray drying of pharmaceuticals and biopharmaceuticals: Critical parameters and experimental process optimization approaches. *European Journal of Pharmaceutical Sciences*, *127*(November), 300–318. https://doi.org/10.1016/j.ejps.2018.10.026

Zobrist, B., Soonsin, V., Luo, B. P., Krieger, U. K., Marcolli, C., Peter, T., & Koop, T. (2011). Ultra-slow water diffusion in aqueous sucrose glasses. *Physical Chemistry Chemical Physics*, *13*(8), 3514–3526. https://doi.org/10.1039/c0cp01273d

S

Summary

Spray drying is a widely used process providing powders with long shelf lives which can easily be transported and readily reconstituted. During spray drying, droplets generated by atomization of the feed are converted into particles with a particular size, surface composition, and morphology depending on both the material properties and the process parameters. The morphology of primary particles greatly determines the characteristics of a powder formed from these particles or from agglomerates of primary particles. Therefore, tailoring the primary particle morphology is desired for producing powders with superior bulk properties. Morphology development may also be critical for the protection and controlled release of active ingredients or retention of volatile substances. Despite the widespread use of spray dryers, it is still a difficult task to adapt the primary particle morphology during spray drying towards desired applications as there is limited understanding of the key factors responsible for the morphology development. Lack of understanding and accordingly inefficient control of the morphology evolution of particles may result in material losses when the product fails to meet the required quality standards.

A more thorough understanding of morphology development is required to advance particle engineering during spray drying. In the present work, we improved our understanding of morphology development by relating the fundamental properties of the drying materials to the dynamics and skin properties of drying single food droplets. To do this, we aimed to predict the skin properties during drying and the final particle morphology, from the rheological properties of the constituents depending on concentration and temperature. The insights obtained in this work may offer a route towards multi-scale understanding and better control of spray drying processes.

In **Chapter 2** we investigated the role of viscosity in morphology development for maltodextrins, whey proteins, and their mixtures. Viscosity data as function of concentration were modelled with viscosity models for polymer solutions and colloidal dispersions. Whey proteins showed a steep increase in viscosity due to jamming of the proteins around 50% (w/w) solids, while the viscosity of maltodextrins only increased gradually. The jamming of the proteins was hindered in the mixtures when increasing the fraction of maltodextrins. Droplet drying experiments revealed that morphology development of the whey protein-maltodextrin solutions could be well related to the rheological behaviour of the mixtures. However, the final morphology appeared also dependent on drying conditions, such as initial droplet size and initial dry matter content.

For understanding and modelling drying processes, an accurate and full description of moisture diffusivity as a function of water content and temperature is important. In **Chapter 3**, we focussed on measuring and describing moisture diffusivity in concentrated protein and carbohydrate systems for a wide range of moisture contents at elevated temperatures. Diffusion data were extracted from controlled thin film drying experiments. At low water contents, the diffusion of water showed universal behaviour for different binary systems, which was attributed to random coil behaviour. Moisture diffusion in mixed systems of carbohydrates and proteins was strongly influenced by the presence of caseins. Additionally, these complex systems showed a sharper decrease in moisture diffusivity in the dry regime when compared to binary systems, which may be due to a denser, random molecular packing. Alternatively, this sharper decrease may be caused by water trapping or promoted protein-carbohydrate interactions.

In **Chapter 4**, we studied the morphology development during drying of maltodextrins varying in dextrose equivalence (DE) value. Single droplet drying experiments with a new custom-built sessile single droplet dryer demonstrated that the DE value of maltodextrins can be used as an indicator for particle morphology development. Low DE maltodextrins developed a skin at an earlier stage during drying than droplets with higher DE and remained fairly spherical while developing a large cavity. The smooth morphology observed combined with the rheological properties at high solids concentrations, suggested that low DE droplets reach a critical skin stability relatively early during drying. High DE maltodextrins showed dominant viscous behaviour and after drying various surface wrinkling patterns were found. Visual observations were successfully related to data from rheological experiments on thin films at several high concentrations and a fixed temperature. However, because moisture content and temperature are continuously evolving during drying, it was considered worthwhile to study the rheological properties of materials over a much wider range of concentrations and temperatures. Therefore, in **Chapter 5**, we studied the rheological behaviour of maltodextrins varying in DE as a function of frequency, temperature and concentration. Storage and loss moduli at different temperatures and concentrations obtained within linear viscoelastic regime were mapped onto master curves using superposition principles. Low DE maltodextrins exhibited rubber-to-glass-like behaviour, where the rubber behaviour was proposed to be the consequence of polysaccharide entanglements. High DE maltodextrins demonstrated predominantly viscous behaviour even at high concentrations.

Rheological data were linked to droplet drying based on modelling of temperature and moisture evolution using an effective diffusion model validated with single droplet drying experiments. This modelling approach allowed for estimating the rheological properties of the skin developed. The elastic behaviour of the low DE maltodextrin skin was related to cavitation and the viscous behaviour of high DE maltodextrin skin to wrinkling.

In **Chapter 6** we evaluated the impact of the droplet morphology development on the protection of probiotic components. More specifically, we investigated if the particle morphology could be related to the survival of probiotic *Lactobacillus plantarum* WCFS1 after drying. The survival of *L. plantarum* WCFS1 showed a strong correlation with the final particle morphology generated: survival in smooth, spherical and dense particles was highest, followed by hollow and smooth particles and the survival was lowest in dented particles. The relation between survival and particle morphology was explained by a combination of matrix properties, including glass transition, and drying dynamics, including diffusion, of the drying droplets.

Finally, in **Chapter 7** we placed our findings into a broader context to arrive at a more generic description of the mechanisms governing the morphology development. For this, we first examined the rheological behaviour of concentrated whey proteins at different concentrations and temperatures and compared these to the earlier results of maltodextrins (**Chapter 5**). Different from maltodextrins, which are glucose polymers, whey proteins showed analogy with hard-sphere colloids. At low concentrations (<50% (w/w) solids), whey proteins exhibited dominant viscous behaviour. When the concentration was increased >50% (w/w), dominant elastic behaviour was observed which was explained by the formation of an increasingly crowded network leading to stress bearing jammed structures. For whey proteins the modelling approach established in **Chapter 5** could not directly be applied for estimating the rheological properties of the skin developed, yet rheological data appeared highly informative for the morphology development during drying. Pilot-scale drying experiments demonstrated that the mechanisms proposed for the morphology development of drying single droplets were also valuable for explaining pilot-scale particle morphologies. Insights obtained in this work may offer a route towards building models for predicting morphology development and accordingly constructing morphological maps offering better practical understanding and control of the final powder quality.

Appendices

Acknowledgments

Kōin ya no gotoshi - time flies like an arrow- as they would say in Japan! I still vividly remember the start of these amazing four years, it sometimes feels as if I have just begun. A PhD project cannot be done alone. I consider myself very fortunate to have been surrounded by a group of supportive, intelligent, and kind people. The completion of this thesis would not have been possible without this group. Therefore, I would like to express my gratitude to those who have helped me in completing this work.

First of all, I would like to sincerely thank *Maarten*, *Ruud*, and *Remko* for their supervision and guidance during the past four years. *Maarten*, I consider you the "drying guru". I have learned so much from your interesting talks about spray drying and single droplet drying during group meetings and conferences. It also inspired me to continue research in the drying field. I could always walk into your office for advice and even during these strange COVID times I could easily discuss my ideas and problems with you. I must say I was also very impressed with your rapid and useful feedback on manuscripts, thank you for this. *Ruud*, I would have never thought that after four years I would be so interested in soft matter science, you were a great motivator to dive into this rather difficult topic. You always took the time to help me further understand theories and models. I also very much enjoyed investigating the rheology of concentrated maltodextrins together. *Remko*, your enthusiasm, and innovative research ideas greatly helped me throughout my PhD. I hope you enjoyed diving back into your old study topics while reading my work.

Throughout my PhD project I received a lot of support also in the lab. *Jos*, you were always there to help me with my experiments. I would come to your office if I struggled with experimental protocols or if I just wanted to have somebody capable of discussing ideas with me. You also helped during all pilot-scale spray drying trials, which were intensive though a lot of fun. I will never forget that hair can turn into cotton candy during cleaning of the spray dryer! *Maurice*, thank you for your technical support with the DSC and HPLC and the fun chats. *Martin*, thank you for helping with the single droplet drying experiments and the fun chats as well. I would also like to acknowledge my MSc and BSc students *Regina, Sabien, Tobias, Sietske, Rutger, Laura, Rick, Julia, Guus, and Timo* for their help in gathering data and insights needed for this thesis. It was a pleasure to supervise all of you. *Regina, Sietske,* and *Julia* thank you for your significant contribution to some of my publications.

I would also like to thank all project partners from the consortium. The discussions we had during our user meetings were always very inspiring and interesting to me. I enjoyed all the company and university visits, traveling from Wageningen to Utrecht, Delft, and Sweden. *Stefan* and *Erik*, I enjoyed our meetings and I wish you both success.

Without FPE my work would not have nearly been as pleasant as it turned out to be. I would like to thank all of my FPE colleagues for creating a very enjoyable working environment! *Evelien*, *Eline,* and *Anja* you encouraged me to start this PhD adventure. I always enjoyed working with you, but perhaps more importantly I could always have a nice chat with you whether it was at Axis or outside during our walks or dinners. *Evelien* and *Eline*, thank you for helping me out especially during the first and last struggles of the PhD project. *Sicong,* we were office mates at the start of our projects, soon we could not do without our weekly chats. I very much enjoyed our conversations and hope to still visit you and your family regularly in Sweden. *Yu*, I think you are one of the most positive persons I have ever had the pleasure of meeting. I will certainly visit you in China and we will keep in touch via WeChat! *Floor, Emma,* and *Nynke,* I think we really got to know one another in Canada during our PhD trip. Soon after, most people of FPE probably noticed that we could not stop chatting in our offices, often we were laughing and FPE knew we were there. *Jan-Eise*, during COVID times I was happy that you were often at Axis and that we could go for a nice and inspiring lunch walk. *Pina, Eric, Luc,* thanks for being great office mates, I hope our plants will finally thrive after poor treatment by me. *Julia* and *Regina,* as my former MSc students, I am happy and kind of proud that I could partly motivate you to join our great FPE team. *Anneloes,* I also want to thank you for supporting me with the spray drying trials and all of the fun chats we had via Teams. *Nienke* and *Anneloes,* I wish you the best of luck with your PhD projects, I hope to read all of your single droplet drying and spray drying work.

Of course, friends and family have always been there to support me mentally. I would like to thank my close friends, *Renée, Viviënne, Jarno,* and my *Utrecht Goedestraat* friends for time away from my project when I needed it most! Our borrels, chats, festivals, sleep overs and random activities have always made me happy and I hope that we will continue these activities on a regular basis! The biggest thank you I owe to my boyfriend, *Daan,* and my family. I do not know how I would have finished this work without the everlasting support from you. I actually get very emotional when thinking about this. Lieve *Sabrina,* jouw telefoontjes en je knuffels had ik en heb ik altijd nodig om gelukkig te zijn en gemotiveerd

te blijven. Lieve *mama* en *papa*, ik kan me niet voorstellen dat ik dit had volgehouden zonder jullie onvoorwaardelijke steun, aanmoediging en betrokkenheid. Ook al is het niet een onderwerp dat dichtbij jullie staat, jullie hebben je altijd ingeleefd en geholpen waar kon. Ik hoop jullie met dit boekje ook een beetje trots te mogen maken. Lieve *Daan*, iedere week vanaf het begin van mijn PhD, keek ik al uit naar de weekenden om naar Utrecht te kunnen komen. Je hebt me enorm gesteund, veel gelezen en veel gekookt, maar nog belangrijker ik heb genoten van al onze weekenden vol activiteiten en gezelligheid. Ik verheug me op de volgende stappen samen met jou in Utrecht of waar dan ook ter wereld. Lieve *Charlotte*, mijn tweelingzus, ik eindig met jou omdat ik samen met jou dit PhD traject ben begonnen. Jouw onvoorwaardelijke, motiverende, inspirerende steun hebben mij gebracht waar ik nu ben. Zonder jouw aanwezigheid had ik dit niet kunnen doen. Ik beloof je dezelfde steun te geven bij het afronden van jouw promotieonderzoek. Ik had me geen fijnere tijd in Wageningen kunnen wensen dan samen met jou, dank je.

About the author

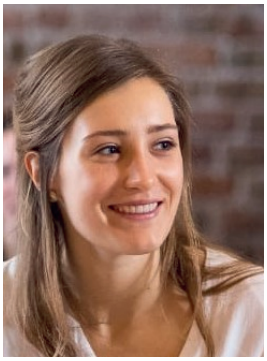

Isabel Siemons was born in June 1994 in Tokyo, Japan. Her family moved from Yoyogi in Tokyo to Leerdam. She attended high school at "O.R.S. Lek en Linge" in Culemborg with a major in Nature and Technology and Nature and Health.

In 2012, Isabel started the study Biotechnology at Wageningen University & Research. She finished her bachelor studies in 2015 with distinction (*cum laude*). In the same year Isabel continued with her master studies in Biotechnology, with a specialization in Process Technology. During her master thesis she investigated the survival of lactic acid bacteria after single droplet drying at the Laboratory of Food Process Engineering and Food Microbiology. Based on her interest in drying, she moved to Utrecht and continued an internship at Danone Nutricia Research on pilot-scale spray drying of fermented infant formula. She obtained her master's degree in 2017.

Isabel started as a PhD candidate at the Laboratory of Food Process Engineering in 2017 in collaboration with the Technical University of Delft. She investigated morphology development during drying of foods, and results of this research are described in this thesis.

Contact: isabelsiemons006@gmail.com

Publications

M.A.I. Schutyser, E.M. Both, **I. Siemons**, E.M.J. Vaessen, L. Zhang, Gaining insight on spray drying behavior of foods via single droplet drying analyses, *Drying Technology, 37, (2018).* https://doi.org/10.1080/07373937.2018.1482908.

E.M. Both, **I. Siemons**, R.M. Boom, M.A.I. Schutyser, The role of viscosity in morphology development during single droplet drying, *Food Hydrocolloids, 94, (2019).* https://doi.org/10.1016/j.foodhyd.2019.03.023.

I. Siemons, R.M. Boom, R.G.M. van der Sman, M.A.I. Schutyser, Moisture diffusivity in concentrated and dry protein-carbohydrate films, *Food Hydrocolloids, 97, (2019).* https://doi.org/10.1016/j.foodhyd.2019.105219.

I. Siemons, R.G.A. Politiek, R.M. Boom, R.G.M. van der Sman, M.A.I. Schutyser, Dextrose equivalence of maltodextrins determines particle morphology development during single sessile droplet drying. *Food Research International, 131, (2020).* https://doi.org/10.1016/j.foodres.2020.108988.

I. Siemons[1], E.M.J. Vaessen [1], S.E. Oosterbaan van Peski, R.M. Boom, M.A.I. Schutyser, Protective effect of carrier matrices on survival of *Lactobacillus plantarum* WCFS1 during single droplet drying explained by particle morphology development. *Journal of Food Engineering, 292, (2021).* https://doi.org/10.1016/j.jfoodeng.2020.110263.

I. Siemons, J. Veser, R.M. Boom, M.A.I. Schutyser, R.G.M. van der Sman, Rheological behaviour of concentrated maltodextrins describes skin formation and morphology development during droplet drying, *submitted.*

R.G.M. van der Sman, J. Ubbink, M. Dupas-Langlet, **I. Siemons**, M. Kristiawan, Scaling relations in rheology of concentrated starches and maltodextrins. *Food Hydrocolloids, in press.*

Overview of completed training activities

Discipline specific activities

Courses

Physical Chemistry, Han-sur-Lesse, Belgium	2018
Spray drying and atomisation of formulations, Leeds, UK	2018
Physical Chemistry, Han-sur-Lesse, Belgium	2019
Rheology school, Leuven, Belgium	2019
Rheology: the do's and the don'ts	2020

Conferences

NWGD symposium, Wageningen, The Netherlands*	2017
International drying symposium, Valencia, Spain*	2018
NWGD symposium, Wageningen, The Netherlands*	2019
International Symposium on Food Rheology and Structure, Zürich, Switzerland*	2019
Effost, Rotterdam, The Netherlands*	2019
NWG symposium, Rheden, The Netherlands	2019
Sorption Technology symposium, Wageningen, The Netherlands*	2020
NWGD symposium, Wageningen, The Netherlands*	2021

General courses

VLAG PhD week, Baarlo, The Netherlands	2018
Scientific publishing, Wageningen, The Netherlands	2018
Presenting with impact, Wageningen, The Netherlands	2018
Scientific writing, Wageningen, The Netherlands	2019
Career perspectives, Wageningen, The Netherlands	2021

Other activities

Preparation of research proposal	2017
PhD study tour to Canada	2018
FPE weekly group meetings	2017-2021
PhD trip committee UK	2020

**Oral or poster presentation*

The studies presented in this thesis were performed within the framework of the Netherlands Organisation for Scientific Research (NWO) (grant number 15459 “Multi-scale understanding and control of spray drying processes”).

Cover design by Simone Golob

Printed by Proefschriftmaken ‖ www.proefschriftmaken.nl